INFORMATION TO USERS

This manuscript has been reproduced from the microfilm master. UMI films the text directly from the original or copy submitted. Thus, some thesis and dissertation copies are in typewriter face, while others may be from any type of computer printer.

The quality of this reproduction is dependent upon the quality of the copy submitted. Broken or indistinct print, colored or poor quality illustrations and photographs, print bleedthrough, substandard margins, and improper alignment can adversely affect reproduction.

In the unlikely event that the author did not send UMI a complete manuscript and there are missing pages, these will be noted. Also, if unauthorized copyright material had to be removed, a note will indicate the deletion.

Oversize materials (e.g., maps, drawings, charts) are reproduced by sectioning the original, beginning at the upper left-hand corner and continuing from left to right in equal sections with small overlaps.

ProQuest Information and Learning
300 North Zeeb Road, Ann Arbor, MI 48106-1346 USA
800-521-0600

DISSERTATION

THE REACTIVITY OF ALKYL RADICALS CONTAINING LEAVING GROUPS IN THE β-POSITION AND THE MECHANISM OF COPPER PHENANTHROLINE INDUCED DNA STRAND SCISSION

Submitted by
Brian Christopher Bales
Department of Chemistry

In partial fulfillment of the requirements
For the Degree of
Doctor of Philosophy

Colorado State University
Fort Collins, Colorado
Summer 2002

ProQuest Information and Learning Company
300 North Zeeb Road
P.O. Box 1346
Ann Arbor, MI 48106-1346

COLORADO STATE UNIVERSITY

May, 29, 2002

WE HEREBY RECOMMEND THAT THE DISSERTATION PREPARED UNDER OUR SUPERVISION BY BRIAN CHRISTOPHER BALES ENTITLED THE REACTIVITY OF ALKYL RADICALS CONTAINING LEAVING GROUPS IN THE β-POSITION AND THE MECHANISM OF COPPER PHENANTHROLINE INDUCED DNA STRAND SCISSION BE ACCEPTED AS FULFILLING IN PART REQUIREMENTS FOR THE DEGREE OF DOCTOR OF PHILOSOPHY.

Committee on Graduate Work

Adviser

Department Chair

Abstract of Dissertation

THE REACTIVITY OF ALKYL RADICALS CONTAINING LEAVING GROUPS IN THE β-POSITION AND THE MECHANISM OF COPPER PHENANTHROLINE INDUCED DNA STRAND SCISSION.

The reactivity of alkoxy substituted alkyl radicals containing bromide (**96**) and diphenylphosphate (**97**) as leaving groups in the β-position has been studied in 4:1 methanol/acetonitrile solution with a hydrogen atom donor (1,4-cyclohexadiene) and a proton scavenger (2,6-di-*t*-butylpyridine). Product and laser flash photolysis studies provide evidence for the formation of olefin cation radical **103**. Subsequent reaction of **103** forms dimethylketal **102** and vinyl ether **105**. Olefin cation radical **103** is proposed to arise from heterolytic cleavage of the β-leaving group in radicals **96** and **97**.

The rate constants for heterolytic loss of the leaving group to form **103** in acetonitrile are 8.0×10^7 s^{-1} for the loss of bromide and $> 1 \times 10^8$ s^{-1} for loss of diphenylphosphate. The rate constants for reaction of **103** with 1,4-cyclohexadiene and methanol are 6.0×10^5 M^{-1} s^{-1} and $< 1 \times 10^3$ M^{-1} s^{-1} respectively. Dimethylketal **102** is proposed to arise from hydrogen atom transfer to the benzylic carbon in **103** followed by trapping with methanol or through trapping of **103** with methanol followed by hydrogen atom transfer. The reaction of **103** with 1,4-cyclohexadiene is proposed to occur through

hydrogen atom transfer to the ether oxygen in **103** followed by deprotonation to generate **105**. This is the first example of this reaction motif in solution.

Evidence for a copper 1,10-phenanthroline induced β-elimination of the 2-deoxyribonolactone (**1**) lesion has been obtained. Through the use of copper phenanthroline conjugates coupled with site specific incorporation of (**1**) in DNA, rate constants for this process have been measured. Comparison of the rate of cleavage of independently prepared **1** (k_{21} = (5.63 ± 0.69) x 10^{-4} s^{-1}) to the rate of decay of alkali labile lesions (k_{decay} = (4.70 ± 0.90) x 10^{-4} s^{-1}) indicates that **1** is the major alkali labile lesion generated from reaction of the conjugates with DNA. The rate of DNA oxidation (k_{OX}) by the CuOP conjugates is slower than k_{decay} ($k_{OX} < k_{decay}$). Similar ratios of direct strand breaks to alkali labile lesions are observed for the conjugates and $Cu(OP)_2$, indicating that k_{decay}:k_{OX} is similar. This leads to the conclusion that $Cu(OP)_2$ produces direct strand breaks through a $Cu(OP)_2$ induced cleavage of **1**.

Brian Christopher Bales
Chemistry Department
Colorado State University
Fort Collins, CO 80523
Summer, 2002

Table of Contents

Part 1.

Appendices

List of Figures

Part 1.

Part 2.

List of Tables

Part 1.

Part 2.

List of Abbreviations

A_{Bz}	benzoyl protected adenine
AcN	acetonitrile
dATP	deoxyadenosine triphosphate
ATP	adenosine triphosphate
BME	2-mercaptoethanol (β-mercaptoethanol)
Bpy	2,2'-bipyridine
BSA	bovine serum albumin
AIBN	2,2'-azobis-(2-methylpropionitrile)
CAN	cerric amonium nitrate
CHD	1,4-cyclohexadiene
Cu(OP)	copper 1,10-phenanthroline
$Cu(OP)_2$	bis(1,10-phenanthroline) copper
DCC	N,N'-dicyclohexyldicarbodiimide
DMAP	4-N,N-dimethylaminopyridine
DMEDA	N,N'-dimethylethylendiamine
DMF	N,N-dimethylformamide
DNA	deoxyribonucleic acid
DTT	dithiothreitol
E. coli	*Escherichia coli*

EDTA	ethylenediamine tetraacetate
ESR	electron spin resonance spectroscopy
EtOAc	ethyl acetate
GC	gas chromatography
HEPES	4-(2-hydroxyethyl)-1-piperazine-ethanesulfonic acid
HFIP	1,1,1,3,3,3-hexafluoroisopropanol
HPLC	high pressure liquid chromatography
KIE	kinetic isotope effect
LDA	lithium diisopropylamide
LFP	laser flash photolysis
MOPS	3-(N-morpholino)propane sulfonic acid
MPA	3-mercaptopropionic acid
MPE	methidiumpropyl-ethylenediamine tetraacetate
MS	mass spectroscopy
OAc	acetate
OP	1,10-phenanthroline
PAGE	polyacrylamide gel electrophoresis
PDC	pyridinium dichromate
PSET	photoinduced single electron transfer
PTOC	pyridine-2-thione carbonyl
PyBOP	benzotriazole-1-yl-oxy-tris-pyrrolidino-phosphonium hexafluorophosphate
RNA	ribonucleic acid
SCE	saturated calomel electrode

SIM	selective ion monitoring
TBP	2,6-di-*t*-butylpyridine
TBS	tertbutyldimethylsilyl
THF	tetrahydrofuran
T_M	DNA melting temperature
TRIS	tris(hydroxymethyl)amino methane
Tpy	2,2',2"-terpyridine
trp	*L*-tryptophan

Part 1.

The Reactivity of Alkyl Radicals Containing Leaving Groups in the β-Position.

1 Introduction.

The history of cation radicals in organic chemistry began with the isolation Wurster's Red and Blue salts in 1879.[1,2] Interestingly, this predates the isolation of carbon centered radicals by Gomberg in 1900 and carbocations by von Baeyer in 1902.[3,4] However, while the significance of radicals and carbocations in organic chemistry was realized almost immediately, the true nature of Wurster's Red and Blue salts was not recognized for another 50 years. It was not until Weitz's report of the isolation of triarylaminium perchlorates in 1926 that the true nature of these salts as monomeric species, containing both an unpaired electron and a single unit of positive charge was finally appreciated.[5] Michaelis provided the first accurate theoretical description for the bonding and delocalization of these types of compounds in 1935, with a model that is still reasonably accurate today.[6] Recognition of cation radicals as reactive intermediates in

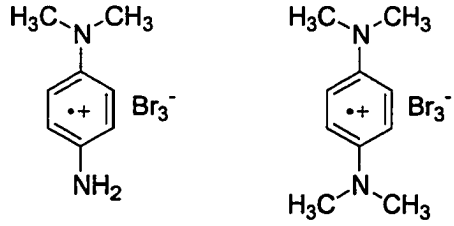

Wurster's Salts

(Red) (Blue)

organic reactions by Weiss in 1946 was predated by the recognition of carbocations by Meerwein (1922) and radicals by Paneth and Hofeditz (1929) as reaction intermediates.[7-9] Moreover, the mechanistic chemistry of both carbocations and radical species has been much more appreciated and thoroughly explored than that of cation radicals.

1.1 Significance of Olefin Cation Radicals.

Cation radicals are becoming increasingly more significant in organic chemistry due to their utility in organic synthesis and their observation as intermediates in biological systems.[10-12] Within the field of organic chemistry, olefin cation radicals are one of, if not the most common type of cation radical. The utility of these highly reactive intermediates in organic synthesis stems from their ability to react through either cationic or radical manifolds.[10,13,14] This, coupled with the high rates of reactions with alkenes, dienes, and nucleophiles (bimolecular rate constants can approach the diffusional limit) typically exhibited by olefin cation radicals, makes this class of reactive intermediates especially attractive for synthetic and physical-organic chemists alike.[15,16]

The enhanced reactivity of olefin cation radicals, relative to their charge and spin free counterparts contributes to these compounds' usefulness as synthetic intermediates. For example, addition of tris(*p*-bromophenyl)aminium hexachloro-antimonate to a solution of 1,3-cyclohexadiene (**1**) affords the Diels-Alder cycloaddition products **2** and **3** with a rate enhancement of 10^{15} relative to the same reaction carried out using thermal conditions (Figure 1).[11,17] Mechanistic studies have shown this process to occur via one electron oxidation of the π-system of 1,3-cyclohexadiene, generating the corresponding olefin cation radical which reacts by rapid cycloaddition with an uncharged molecule of

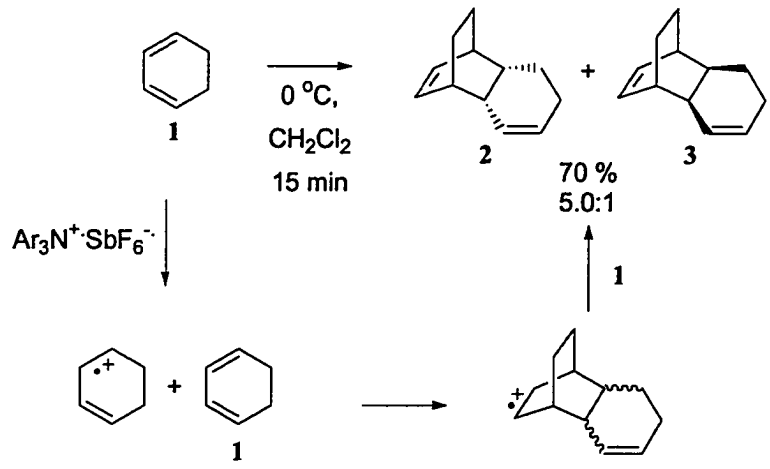

Figure 1. Reaction Pathway for the Cation Radical induced Diels-Alder Reaction.[17]

1,3-cyclohexadiene.[17,18] The chain is propagated when the cation radical of the Diels-Alder adduct is reduced by another molecule of 1,3-cyclohexadiene or by the triarylamine generated from the initial oxidation step.

The ability of olefin cation radicals to react initially through either the unpaired electron or the cation can provide access to compounds not easily prepared through other means.[13,14] Generation of the highly strained *trans* 5,6-ring fusion with greater than 20:1 selectivity over the more stable *cis*-5,6-ring fusion has been demonstrated by Snider and co-workers through the use of olefin cation radicals (Figure 2).[14] Single electron oxidation of the silyl enol ether (**4**) by copper generates the stabilized olefin cation radical (**5**) which undergoes a 5-*exo*-trig cyclization with the pendant olefin coupled with loss of the silyl group. The stereochemical determining step occurs during the 5-*exo* trig cyclization, resulting in a *trans* orientation of the hydrogen atoms across the single bond. Cyclization of the resulting γ-radical with the pendant phenyl ring followed reduction of

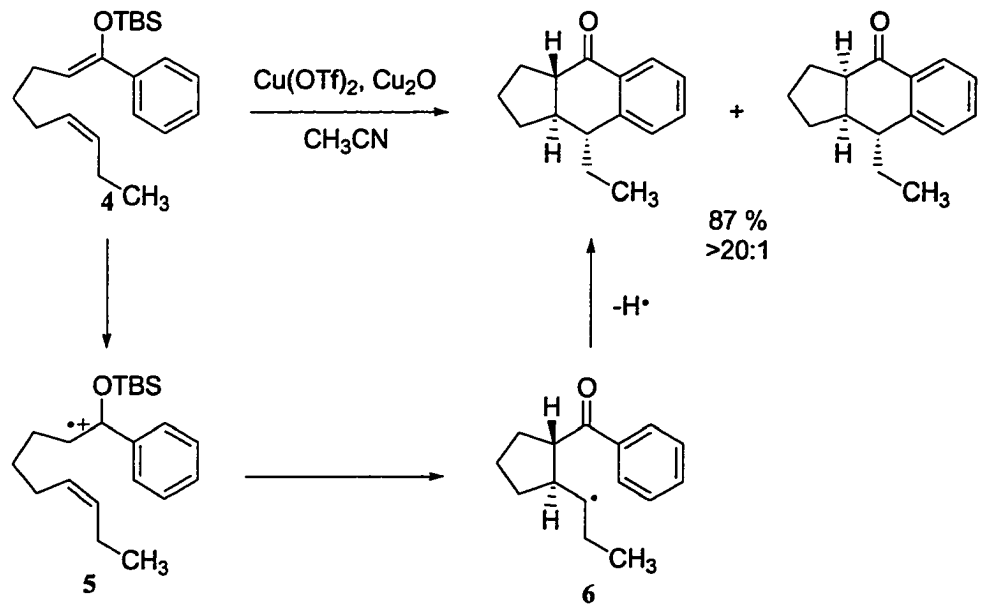

Figure 2. Sequential reactivity of olefin cation radicals.[14]

the resulting radical by either another silyl enol ether or the copper species generated in the initial oxidation step generates the observed products.

The relevance of olefin cation radicals in biological processes such as DNA damage has also been realized. As early as 1975, it was proposed by Dizdaroglu, von Sonntag, and Schulte-Frohlinde that generation of a radical in DNA at the C4'-position could lead to olefin cation radical formation *via* cleavage of the DNA phosphate backbone (Eq 1).[19] Early studies using tetrahydrofuran model systems performed by Schulte-Frohlinde and co-workers established the feasibility of this process.[20] Trapping

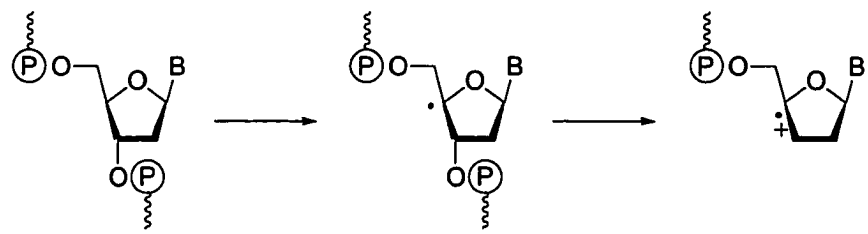

(1)

studies performed by Giese and co-workers confirmed that C4' radicals were capable of generating olefin cation radicals in modified nucleosides.[21] Subsequent studies using both single and duplex DNA under physiological conditions have shown that this elimination occurs with a rate constant of 1×10^3 s^{-1} in single strand DNA and 1×10^2 s^{-1} in duplex DNA.[22,23]

1.2 Methods of Generation.

Several methods have been developed for the generation of olefin cation radicals. Perhaps the most straight forward of these is photoionization. This process involves the removal of an electron from the olefin π-system by a photon of light. Studies carried out by Johnston and co-workers have shown the photochemical ionization of styrene type molecules to be a biphotonic process.[15] The first photon excites a π-electron in the olefin moiety and the second photon is responsible for ejection of the electron, generating the olefin cation radical. The primary drawback of photochemical ionization arises from the fact that not all olefins have similar oxidation potentials. Olefins with high oxidation potentials require high energy photons for ionization, which can potentially lead to undesired side reactions such as molecular fragmentation.

Generation of olefin cation radicals through photochemically induced single electron transfer (PSET) is a common method for the generation of olefin cation radicals which does not require that photochemistry be done directly with the olefin to be oxidized.[10,11] PSET involves electron transfer from the π-system of the olefin, commonly referred to as the donor, to a photochemically excited acceptor molecule such as dicyanoanthracene or chloranil.[11] Since the products of the electron transfer process are

the olefin cation radical of the donor and the anion radical of the acceptor, a competition exists between diffusion of the cation radical away from the acceptor anion radical and back electron transfer to regenerate starting material. However, this is typically not a problem since the process is photochemical, and absorption of another photon by the acceptor molecule repeats the process until the free olefin cation radical is generated. Reaction between the newly formed olefin cation radical and the anion radical generated can also occur prior to diffusion out of the solvent cage.[10] This method requires that the system be energetically "matched" in order to be an effective method of olefin oxidation. The ground state energy of the acceptor molecule must be lower in energy than the ground state of the olefin to be oxidized. Furthermore, the excited state energy of the acceptor molecule be lower in energy than the energy of the π^* orbital of donor compound (Figure 3).

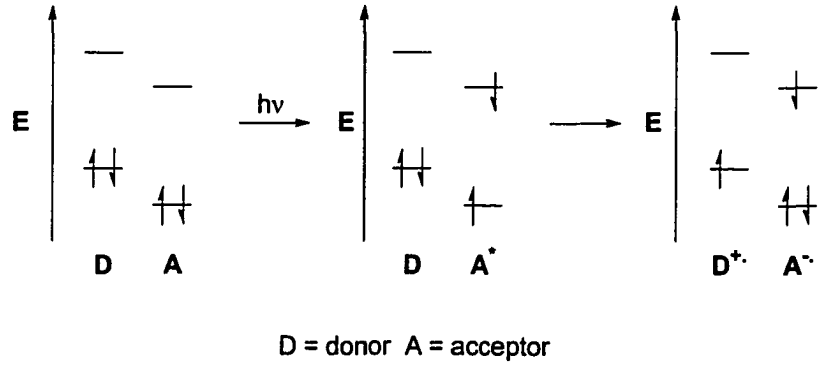

Figure 3. Relative electronic energies required for photoinduced single electron transfer (PSET).

Oxidation by either electrochemical or chemical methods provides a non-photochemcial method for the generation of olefin cation radicals. These methods are also limited by the oxidation potential of the olefin to be oxidized with respect to oxidation of other functional groups which may be present in the molecule. These methods are further hampered by the fact that many organic substrates are not readily soluble in the electrolyte systems required for electrochemical oxidation. Oxidation by chemical means is a commonly used method for the generation of olefin cation radicals.[10,11,13,14] Examples of such chemical oxidants include cerric ammonium nitrate (CAN) and the ferricinium ion. However, chemical oxidation suffers from the inability to oxidize olefins which have high oxidation potentials due to the fact that strongly oxidizing species can be difficult to prepare and/or isolate. In addition, functional group tolerance can also be an issue with respect to oxidation.

The newest method of olefin cation radical generation involves the heterolytic cleavage of a leaving group β to a radical center (Eq 2). A variety of olefin cation

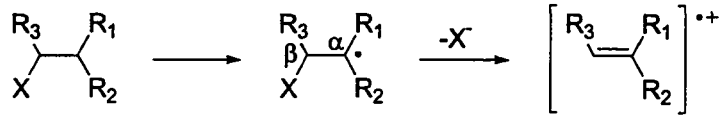

(2)

radicals have been generated in this manner ranging from substituted styrene compounds to alkyl vinyl ether olefin cation radicals which do not contain aryl substitutents.[24,25] While this method is also limited by the oxidation potential of the olefin, the rate of heterolysis of the leaving group can be easily affected by both the nature of the leaving group and solvent polarity, with more polar solvents favoring a faster heterolysis rate. As

a result, this method provides a potentially very attractive and much more universal method for the generation of olefin cation radicals than those presented above.

In addition to olefin cation radical formation, radicals with leaving groups in the β-position can undergo other reactions such as $S_{RN}2'$ substitution and [1,2]-migrations.[26,27] Recent studies have provided spectroscopic evidence for the formation of olefin cation radicals as common intermediates for both of the [1,2]-migration and $S_{RN}2'$ reactions. The focus of this research project was to provide chemical evidence for the formation of olefin cation radicals in radical systems containing leaving groups β to the radical center, and to probe for the presence of reaction intermediates other than olefin cation radicals in these systems through the use of radical precursors with different leaving groups at the β-position.

2 Background.

The chemistry of alkyl radicals containing leaving groups in the β-position relative to the radical center has been of considerable interest for some time. This interest stems from the wide range of reactions available to this type of radical. These pathways include heterolytic cleavage of the leaving group to form the olefin cation radical (Figure 4, pathway a), and migration of the leaving group from the β to α position (Figure 4,

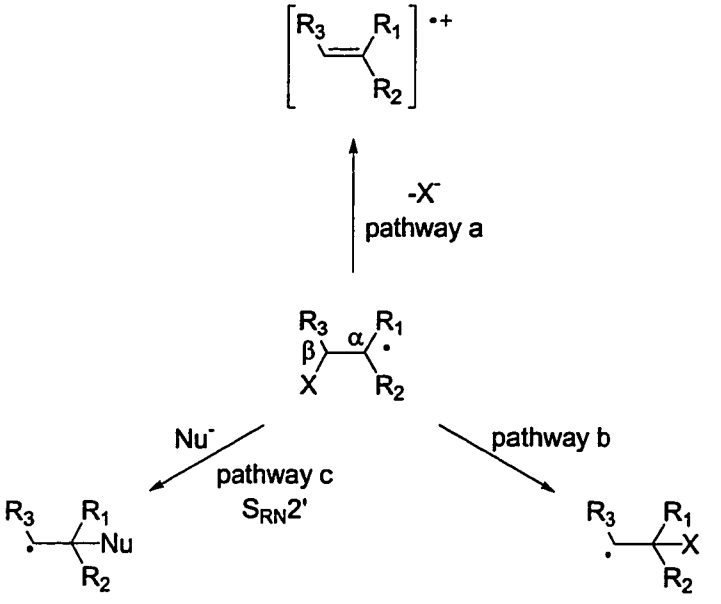

Figure 4. Reaction pathways for radicals with β-leaving groups.

pathway b).[24,27] Computational experiments predict that the radical can participates in $S_{RN}2'$ substitution.[26] This radical analogue of the S_N2' reaction involves nucleophilic attack at the radical center coupled with heterolytic loss of the leaving group and migration of the radical to the β-position (Figure 4, pathway c). The focus of this research is to provide insight into the mechanism(s) by which radicals with β-leaving

groups react with respect to the reaction pathways discussed below through the use of product and laser flash photolysis studies.

2.1 Formation of Olefin Cation Radicals.

2.1.1 Olefin Cation Radical Formation in DNA Model Systems.

The initial proposal that alkyl radicals with leaving groups in the β-position could fragment to form olefin cation radicals by heterolytic scission of the leaving group was put forth in 1975 by Schulte-Frohlinde and co-workers.[19] This reaction motif was proposed as an explanation for the observation of direct strand scission resulting from γ-irradiation of DNA in aqueous solution. Analysis of isolated sugars by GC-MS showed the presence of 2,5-dideoxypentos-4-ulose (**7**) and 2,3-dideoxypentos-4-ulose (**8**). These sugars were proposed to arise through generation of the C4'-DNA radical (**9**) by a reactive species generated from the γ-irradiation of H_2O (Figure 5). Subsequent heterolytic cleavage of the 5'-phosphate was proposed, generating olefin cation radical **10**. Nucleophilic attack by H_2O on **10** and subsequent hydrolysis of the nucleobase, followed by β-elimination of the C3'-phosphate group was proposed to account for the formation of **7**. A similar mechanism involving heterolysis of the 3'-phosphate in **9** rather than heterolysis of the 5'-phosphate was proposed to account for the formation of **8**.

In order to provide evidence for the intermediacy of the proposed olefin cation radicals in the degradation of C4' DNA radicals, Schulte-Frohlinde and co-workers carried out model studies using radicals generated from 1,1-dimethoxy-2-chloroethane (**11**).[28,29] Radical **12** was generated by hydrogen atom abstraction from the acetal carbon using either triplet acetone, hydroxyl radicals, or $SO_4^{\bullet-}$. Heterolytic loss of chloride ion

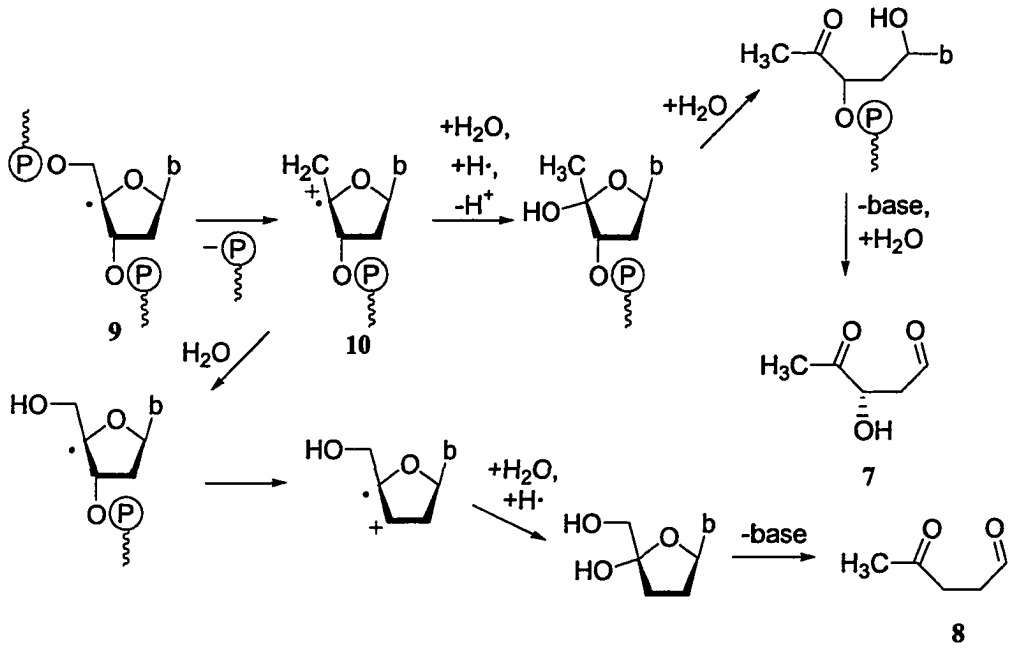

Figure 5. Proposed mechanism for the formation of **7** and **8** from γ-radiolysis of DNA.[19]

from radical **12** was proposed to account for the observation of olefin cation radical **13** by electron spin resonance spectroscopy (ESR) (Figure 6). While radicals attributable to

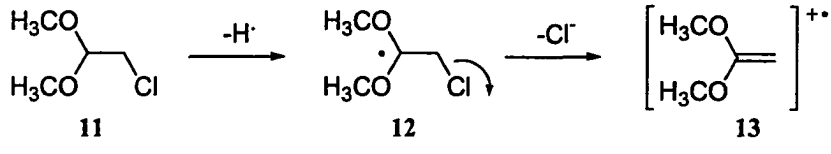

Figure 6. Proposed pathway for the formation of **13**.[28]

hydrogen atom abstraction at positions other than the acetal carbon were detected during the ESR experiments, only **12** was shown to give rise to the spectrum attributable to **13**.

Several leaving groups including chloride, bromide, and acetate were successfully employed in the generation of **13**.

The observation that oxygen did not inhibit the formation of olefin cation radicals allowed determination of a lower limit of 2×10^5 s^{-1} for the rate of heterolytic cleavage of the leaving group from the acetal radicals in aqueous solutions with a pH < 5.[28] The kinetics of reaction of olefin cation radical **13** with hydroxide and phosphate were also determined in aqueous solution at pH ≥ 8.5.[30] A rate of 9×10^5 M^{-1} s^{-1} was directly measured for the reaction of phosphate with **13**, and a rate constant of 1.8×10^9 M^{-1} s^{-1} for reaction of **7** with hydroxide was determined using competitive kinetic methods.

Further evidence for the intermediacy of olefin cation radicals was obtained using substituted tetrahydrofuran compounds as analogues for the sugar moiety in deoxyribonucleic acids.[20] Generation of radical **14** in aqueous solution via pulse radiolysis resulted in observation of radical **15** by ESR (Eq 3). Reaction of **16** in aqueous

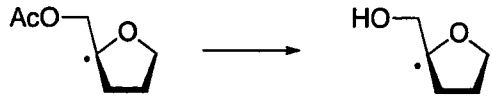

14 **15** (3)

solution generated radicals **17** and **18**, which were also observed by ESR (Eq 4). The

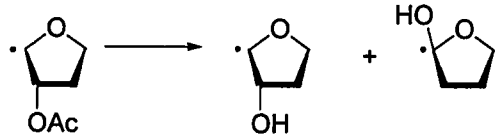

16 **17** **18** (4)

presence of oxygen in the reaction mixture did not show any effect on the rate of reaction of **14** or **16**, or the resulting distribution of products in aqueous solutions. Unfortunately, direct observation of radicals **14** and **16** was not possible in aqueous solution due their rapid rate of reaction. However, **14** and **16** were observed by ESR spectroscopy when generated by pulse radiolysis in acetone solution, suggesting that these radicals were also generated in aqueous solutions.

The formation of olefin cation radicals from the solvolysis of **14** and **16** is supported by the increased stability of **14** and **16** in acetone. This is consistent with the formation of ionic intermediates. This is consistent with the increase in solvent polarity as measured by the $E_T(30)$ scale which gives a value of 42.2 kcal mol^{-1} and 63.1 kcal mol^{-1} for acetone and H_2O respectively.[31,32] The presence of ionic intermediates in these types of systems is also supported by the fact that 2-methoxyethyl-2-yl acetate (**19**) showed a 350 fold increase in the rate of hydrolysis upon substitution of the hydrogen atom α to the radical center with a methyl group (**20**).[20] A decrease, or little change, in

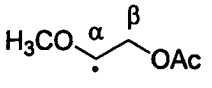

19

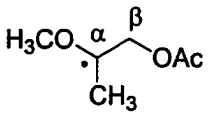

20

the rate of solvolysis of **19** upon substitution with a methyl group would be predicted for S_N2 type reactivity on the basis of sterics. The compilation of data suggesting the involvement of a polar intermediate in the hydrolysis of **14** and **16** coupled with the ESR observation of olefin cation radicals in systems with leaving groups β to dialkyloxy substituted radicals led Schulte-Frohlinde and co-workers to propose the formation of

olefin cation radicals as the polar intermediate in the observed hydrolysis reactions of **14** and **16**.

The model systems studied by Schulte-Frohlinde and co-workers provided spectroscopic evidence that simple systems with leaving groups β to alkoxy substituted radicals undergo heterolytic cleavage to generate olefin cation radicals. However, while chloride, bromide, and acetate were shown to be effective leaving groups in model studies, the extension of this reaction motif to duplex DNA with phosphate diesters as leaving groups was not straight forward. To this end, Giese and co-workers undertook a series of studies aimed at elucidating the decay pathways for the C4' radical in model systems, as well as in single stranded and duplex DNA.

The initial report by Giese and co-workers involved product studies carried out using a modified dinucleotide (**21**) designed to allow the generation of the desired C4' radical (**22**) by addition of the phenylthiyl radical to the C4'-C5' double bond of **21** (Figure 7).[33] The isolated products were shown to be the C3',C4'-dehydrosugar moiety (**23**), and the C5'-phosphate of the adjacent base (**24**). Similar products were isolated from identical experiments carried out using a similarly modified thymidine dinucleotide. To account for the observed products, Giese and co-workers proposed heterolytic cleavage of the C3'-phosphate in **22** to generate the olefin cation radical **25**. Reduction of the olefin cation radical with thiophenol by electron transfer was proposed to account for the formation of **23**.

In order to gain insight into the rate of the heterolysis reaction, competitive kinetic experiments were carried out using a diphenylphosphate substituted mononucleotide (**26**).[33] The C4' radical (**27**) was generated in the manner described above, by addition of

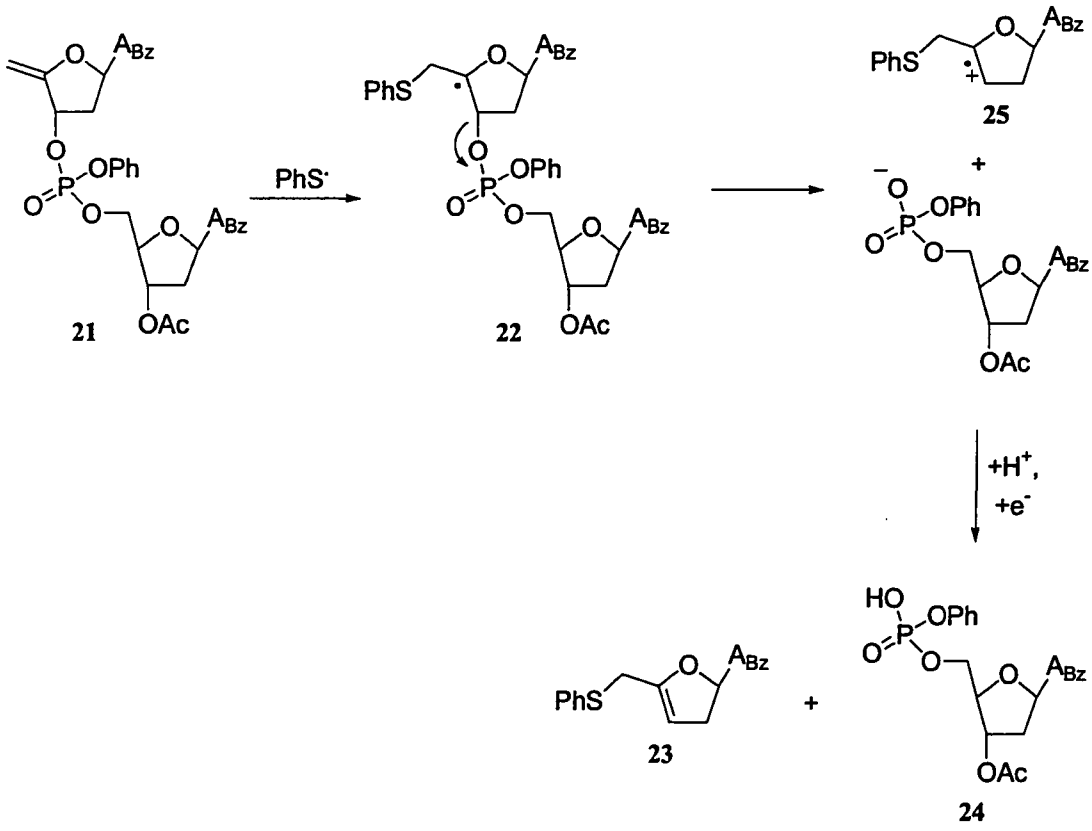

Figure 7. Proposed reactivity of **21** with phenylthiyl.[33]

phenylthiyl to the exocyclic double bond of **26**, and the ratio of **23** to trapped product (**28**) was measured under pseudo first order conditions with respect to thiophenol (Figure 8). Using the known rate of reaction of thiophenol with alkyl radicals (8×10^6 M^{-1} s^{-1}), a rate of heterolysis of $> 10^8$ s^{-1} was estimated in 10:1 methanol:H_2O.[34] It was also observed that the analogous compound with a benzoate functionality in place of the diphenylphosphate moiety did not produce any product attributable to degradation of the initial radical by heterolysis. This indicates that the ionizing ability of the leaving group is important in determining the reaction pathway for these types of radicals.

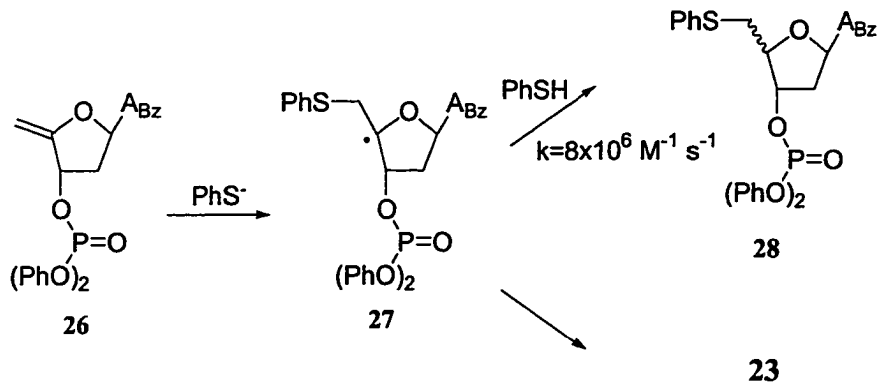

Figure 8. Competition between H-atom abstraction and β-heterolysis for **27**.[33]

Evidence for the intermediacy of charged intermediates in the decay pathway for DNA C4'-radicals was obtained through the use of photocurrent experiments.[35] Using a thymidine C4'-phenylselenide radical precursor (**29**), the intermediacy of cation radical **30** was inferred from the rise of current upon decay of the C4'-radical (**31**). Generation of **31** was accomplished by photolysis of **29** (Figure 9, pathway a). Unfortunately, the detection of current in these systems does not provide direct evidence for the formation of olefin cation radicals, only for the presence of ions in solution.

When the C4'-radical is generated in thymidine, the possibility of phosphate loss due to anchimeric assistance from the C2 carbonyl to form **32** cannot be ruled out (Figure 9, pathway b). In order to gain evidence for or against anchimeric assistance in the formation of free phosphate, Giese and co-workers examined model compounds containing a phenyl group in place of the nucleobase.[36] The C4'-radicals **34** and **35** were independently generated by Norish type I photocleavage of the C4'-*t*-butyl ketones **36** and **37** respectively. Photolysis of either **36** or **37** in methanol in the presence of tributyltin hydride yielded an identical product distribution regardless of the

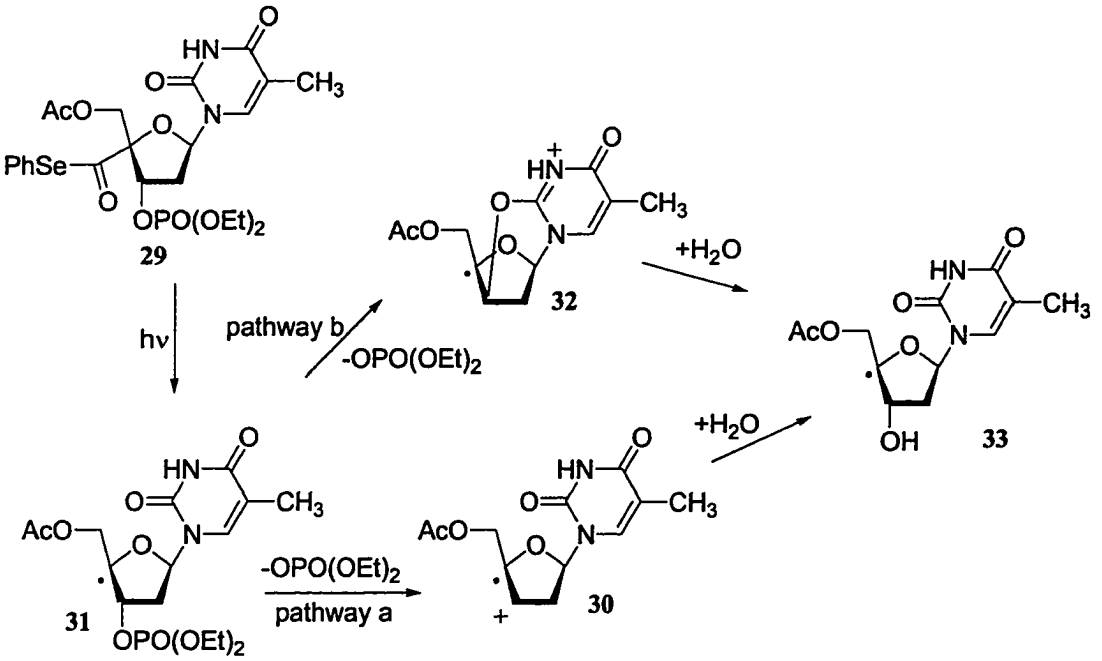

Figure 9. Possible pathways for the formation of **33**.

stereochemistry at C3', indicating the presence of a common intermediate (Figure 10). All of the observed products can be accounted for assuming olefin cation radical **38** is the common intermediate with products **39** – **42** arising from nucleophilic trapping of the olefin cation radical by the methanol solvent. Enol ether **43** was proposed to arise from reduction of the olefin cation radical by electron transfer, most likely from the Bu_3SnH. The product ratios show a stereochemical preference for nucleophilic trapping of the olefin cation radical by methanol *trans* to the phenyl group. This stereoselectivity is lower than that observed in the case of thymidine, where substitutions *trans* to the nucleobase account for all of the observed products.[37] This observation was rationalized by the decreased steric bulk of a phenyl group relative to that of thymine. While these results do not allow exclusion of anchimeric assistance in the formation of the free phosphate when the C2 carbonyl is present or the involvement of anchimeric assistance

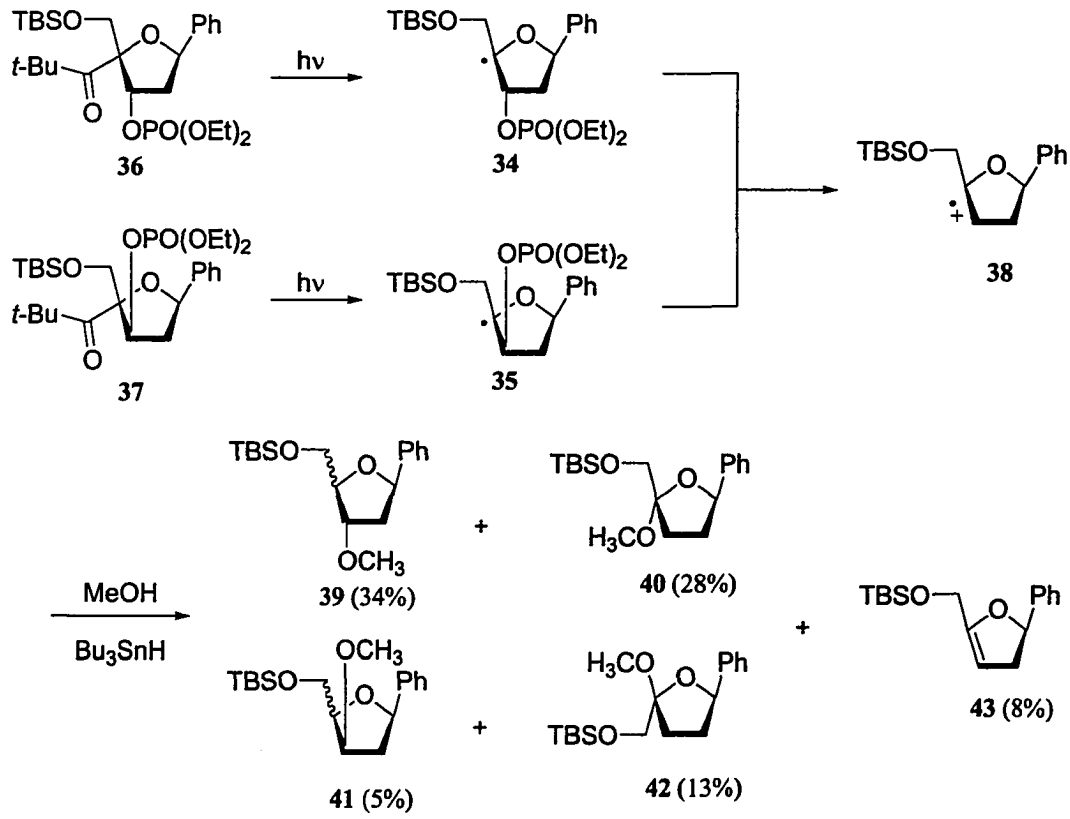

Figure 10. Products resulting from the photolysis of **36** and **37**.[36]

in the stabilization of the intermediate olefin cation radical, they do indicate that anchimeric assistance is not required for heterolysis of a C3'-phosphate.

Detailed study of the reactivity of C4'-radicals in both single stranded and duplex DNA was first reported by Giese and co-workers.[23,38] Measurement of the rate of heterolysis of the C3'-phosphate from C4'-DNA radicals was carried out in both single stranded and duplex DNA by comparing the ratio of products resulting from trapping of the C4' radical with a hydrogen atom donor to those resulting from phosphate elimination. Interestingly, the measured rates of heterolysis, 1×10^3 s^{-1} and 1×10^2 s^{-1} in single stranded and duplex DNA respectively, are significantly slower than the rates reported for the model systems discussed above. While the exact reason for the

decreased rate of heterolysis in oligonucleotides remains unclear, a hypothesis has been put forward that the higher ordered structure of both single stranded and duplex DNA orients the C4' radical in such a position to prevent heterolytic cleavage of the C3'-phosphate. Along these lines, it has been proposed that in order to maintain the strongest hydrogen bonding orientation in DNA the C4'-radical must remain sp^3 hybridized.[39] In this conformation, the C3'-phosphate heterolysis would have to occur via a *cis*-elimination pathway, and as a result the rate of heterolysis may be significantly reduced. However, comparison of the rates of heterolysis in duplex DNA to those observed using the model studies described above are not straight forward. The phosphate containing model systems discussed above all make use of phosphate diester leaving groups rather than the phosphate monoester groups present in duplex DNA. This structural difference is a possible reason for the observed decreased rate of heterolysis in the biopolymer.

2.1.2 Olefin Cation Radical Generation in Small Molecules.

All of the experiments discussed above provide evidence for the intermediacy of olefin cation radicals generated through heterolysis of a β-leaving group. However, no direct evidence for the intermediacy of olefin cation radicals was obtained from these studies. To this end, several reports have recently appeared in which the formation of olefin cation radicals by heterolysis of β-leaving groups has been directly observed by laser flash photolysis (LFP) experiments. The advantage of this spectroscopic method is that it allows direct observation of olefin cation radicals containing suitable chromophores. Because the technique allows rate measurements to be made for processes with rates in the range of 1×10^3 s^{-1} to 1×10^8 s^{-1}, direct measurement of the

kinetics for the heterolysis reaction can be made without the need for competitive kinetic studies. The primary drawback to LFP is that only freely diffusible species can be detected. Thus, olefin cation radicals generated from heterolysis reactions that react at the caged or solvent separated ion pair stage are not observable.

In late 1997, Cozens and co-workers reported the observation (by LFP) of styrene type olefin cation radicals that were generated from heterolysis of either chloride or bromide β to a benzylic radical (Figure 11).[40] As would be expected for the formation of

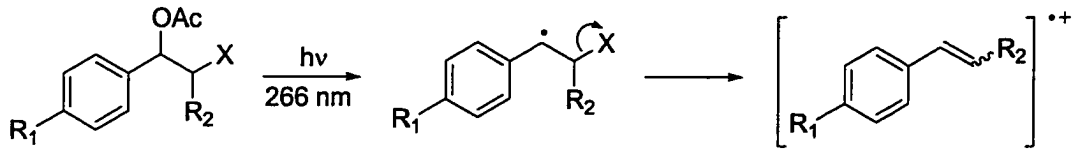

44a, X = Cl, R_1 = OCH_3, R_2 = CH_3
44b, X = Cl, R_1 = H, R_2 = Ph
45a, X = Br, R_1 = OCH_3, R_2 = CH_3
45b, X = Br, R_1 = H, R_2 = Ph

46a, X = Cl, R_1 = OCH_3, R_2 = CH_3
46b, X = Cl, R_1 = H, R_2 = Ph
47a, X = Br, R_1 = OCH_3, R_2 = CH_3
47b, X = Br, R_1 = H, R_2 = Ph

48a, R_1 = OCH_3, R_2 = CH_3
48b, R_1 = H, R_2 = Ph

Figure 11. Proposed pathway for the formation of **48** from **44** and **45**.[40]

a polar intermediate, the measured rate constants for the heterolysis reactions were affected by the polarity of the solvent, analogous to the solvent effects observed for S_N1 type substitution reactions.[41] For example, radical **44a** did not show any signs of decay to olefin cation radical **48a** in acetonitrile ($E_T(30)$ = 45.6 kcal mol^{-1}), but did undergo heterolysis in neat 1,1,1,3,3,3-hexafluoroisopropanol (HFIP) ($E_T(30)$ = 65.3 kcal mol^{-1}) with a rate of 1.1 x 10^7 s^{-1}.[32]

The effect of the leaving group ability of the β-substituent was also probed through the comparison of the rates of heterolysis of **44a** and **45a** as a function of solvent

polarity. Plots of the ionizing ability of the solvent as a function of the log of the rate of heterolysis showed less dependence on the rate of ionization of the bromine substituted compounds as a function of solvent polarity than the chlorine substituted compounds. Comparison of compounds with and without alkyl substituents at the β-position showed faster rates of heterolysis for the compounds with alkyl substituents at the β-position, consistent with a faster rate of heterolysis for compounds with lower oxidation potentials.

Comparison of the rates constant for heterolysis for **44a** (1×10^7 s^{-1}) and **44b** (8.5×10^7 s^{-1}) with the oxidation potentials of the corresponding alkenes of 0.92 V and 1.5 V respectively, indicates that the rate of heterolysis is not solely dictated by the oxidation potential of the corresponding olefin.[42,43] The same trend was observed for **45a** and **45b** with rate constant for heterolysis of 5×10^7 s^{-1} and approximately 1×10^8 s^{-1} respectively. These observations indicate that the factors governing the rate of heterolysis of leaving groups β to radical centers is a complex interplay of solvent polarity, ionizing ability of the leaving group, and the ability of the compound to stabilize the buildup of positive charge at the site of heterolysis.

The observation of freely diffusible olefin cation radicals using phosphate leaving groups was a result of mechanistic studies carried out regarding the reactivity of β-(phosphatoxy)alkyl radicals. After generation of the homobenzylic radical **49** by photolysis of pyridine-2-thionecarbonyl (PTOC) ester **50**, growth of a U.V. signal with maxima at 360 and 600 nm was observed.[24] This spectrum was attributed to the β-dimethyl-*p*-methoxystyrene cation radical (**51**) on the basis of comparison to the previously reported spectrum.[36] Cation radical **51** was proposed to arise from heterolytic cleavage of the diethylphosphate moiety in **49** (Figure 12). The rate of heterolysis was

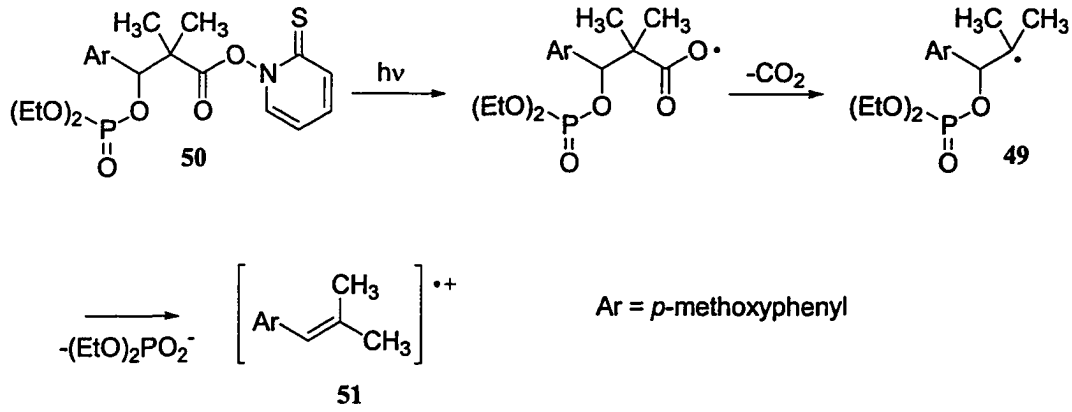

Figure 12. Formation of **51** from photolysis of **50**.[24]

again strongly affected by ionizing ability of the solvent, with **51** not observable in THF ($E_T(30)$ = 37.4 kcal mol^{-1}). A 25% yield of **51** was generated in butanone ($E_T(30)$ = 41.3 kcal mol^{-1}) and quantitative formation of **51** was observed in 10% H_2O/Acetonitrile ($E_T(30)$ = 53.1 kcal mol^{-1}) solutions. The observation of olefin cation radicals by LFP in this system provided the first direct evidence that β-(phosphatoxy)alkyl radicals such as those formed by hydrogen atom abstraction at the C4'-position in DNA could fragment to generate olefin cation radicals.

Recently, β-heterolysis of phosphate diesters from α-alkoxyalkyl radicals which do not contain aryl groups has been reported.[25,44] Photolysis of PTOC ester (**52**) with 355 nm light resulted in the generation of radical **53** which underwent heterolytic cleavage of the phosphate moiety acetonitrile ($E_T(30)$ = 45.6 kcal mol^{-1}) to generate olefin cation radical **54** (Figure 13).[32,44] Because **54** does not contain a chromophore to allow detection through LFP experiments, (p-$BrC_6H_4)_3N$ was used as a reporter compound. Since the triarylamine is easier to oxidize than the corresponding olefin of **54** and the aminium cation radical of (p-$BrC_6H_4)_3N$ contains an effective chromophore, the

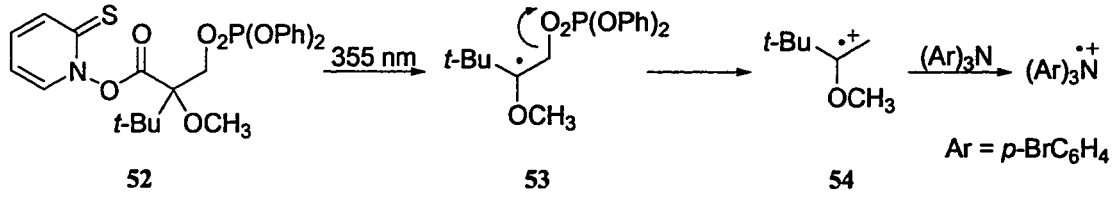

Figure 13. Mechanism for the formation of **54** upon photolysis of **52**.[44]

formation of **54** was detected through the generation of the triaryl aminium cation radical of (p- $BrC_6H_4)_3N$. The rate of heterolysis of **53** to generate **54** was determined to be (9 ± 1) x 10^6 s^{-1} in acetonitrile based on the rate of growth of the aminium cation radical.

This class of olefin cation radicals has recently been used in the formation of pyrrolizidines using the ability of olefin cation radicals to undergo sequential reactions first as cations and then as radicals.[45] Reaction of **55** with triphenyltin hydride and AIBN in refluxing benzene yielded a 1:1 mixture of **56** and **57**. Reaction of the nitro moiety in **55** with triphenyltin hydride and AIBN generates **58** which undergoes heterolytic

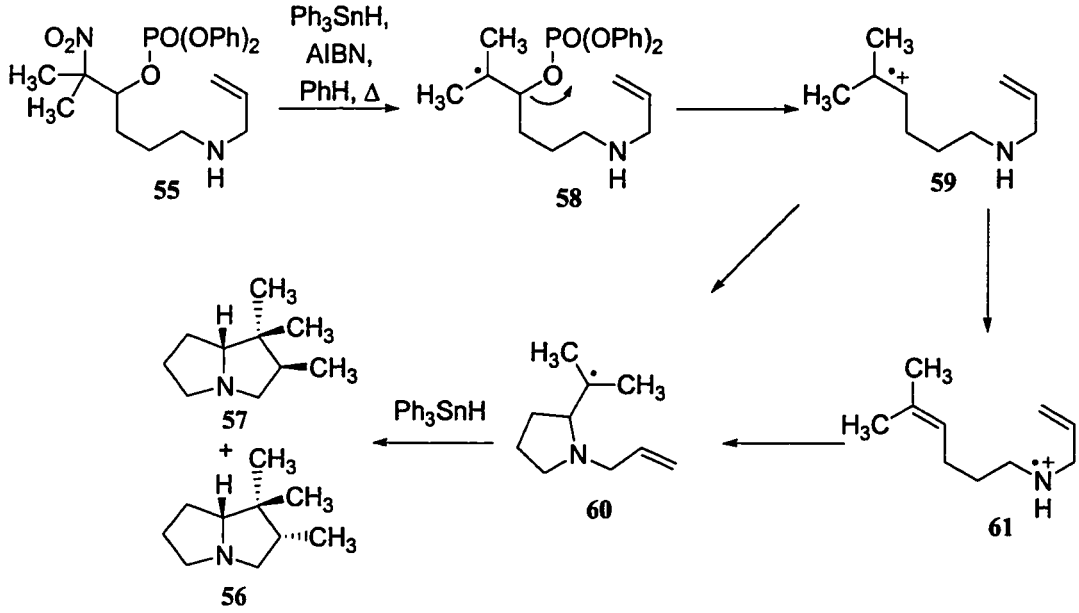

Figure 14. Possible pathways for the formation of **56** and **57** from **55**.[45]

cleavage of the β-phosphate group to form olefin cation radical **59** (Figure 14). The olefin cation radical **59** then either reacts as an electrophile with the nitrogen functionality to generate **60**, or more likely is reduced by the intramolecular nitrogen to form the corresponding aminium cation radical **61**. Reaction of the aminium cation radical with the pendant olefin generates **60** which can then undergo a 5-exo cyclization followed by hydrogen atom transfer from the triphenyltin hydride to generate the product and propagate the radical chain. The formation of freely diffusible olefin cations in this reaction is not clear for two reasons. First, the low solvent polarity of benzene ($E_T(30)$ = 34.3 kcal mol^{-1}) is not expected to favor the formation of freely diffusible ions. Second, either nucleophilic attack or electron transfer on the part of the amine at the contact ion pair stage cannot be ruled out.

These experiments indicate that this method of olefin cation radical generation is very general with respect to the oxidation potential of the corresponding alkene. The fact that rapid rates of heterolysis in relatively low polarity solvents such as acetonitrile in the case of **53** provides further support to the conclusions of Cozens and co-workers with respect to the dependence of the rate of heterolysis on the oxidation potential of the corresponding alkene.[40] This indicates that formation of olefin cation radicals through heterolytic cleavage of leaving groups in the β-position does suffer as greatly from many of the limitations associated with other methods of olefin cation radical formation.

2.2 Migration of the Leaving Group.

2.2.1 β-(Acyloxy)alkyl Radical Migrations.

The first example of β-(acyloxy)alkyl radical rearrangements was reported in 1967 by Surzur and Teisser.[46] While investigating the dibenzoyl peroxide initiated addition of ethyl cyanoacetate (**62**) to isoprenyl acetate (**63**), both the expected addition product (**64**) and the product resulting from a 1,2-migration of the ester moiety (**65**) were observed (Figure 15). The facility of this reaction has since been shown to be governed

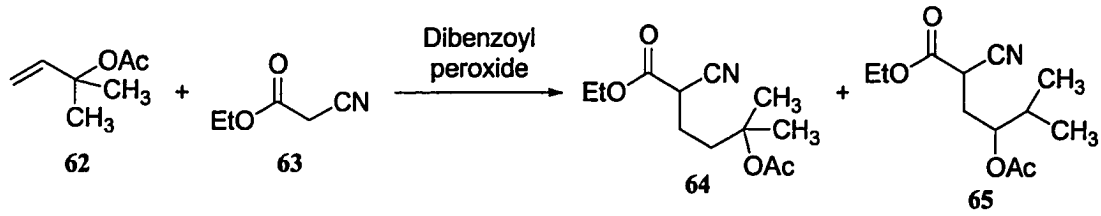

62 63 64 65

Figure 15. Formation of non-migrated product **64** and migrated product **65**.[46]

primarily by the stability of the resulting radical. Measured rates for acyloxy migrations have ranged from 10^2 - 10^6 s^{-1} with the majority of the observed rates in the 10^4 s^{-1} range.[27]

Elucidation of the mechanism of the β-ester migration has proven to be a difficult challenge, and as a result a significant body of mechanistic data has been gathered. At the outset, a wide range of mechanisms were proposed. These were (a) fragmentation to an ester radical and an alkene followed by recombination (either within the solvent cage, or as freely diffusible species) (Figure 16, pathway a), (b) fragmentation to an olefin cation radical and an ester anion followed by recombination (either within the solvent

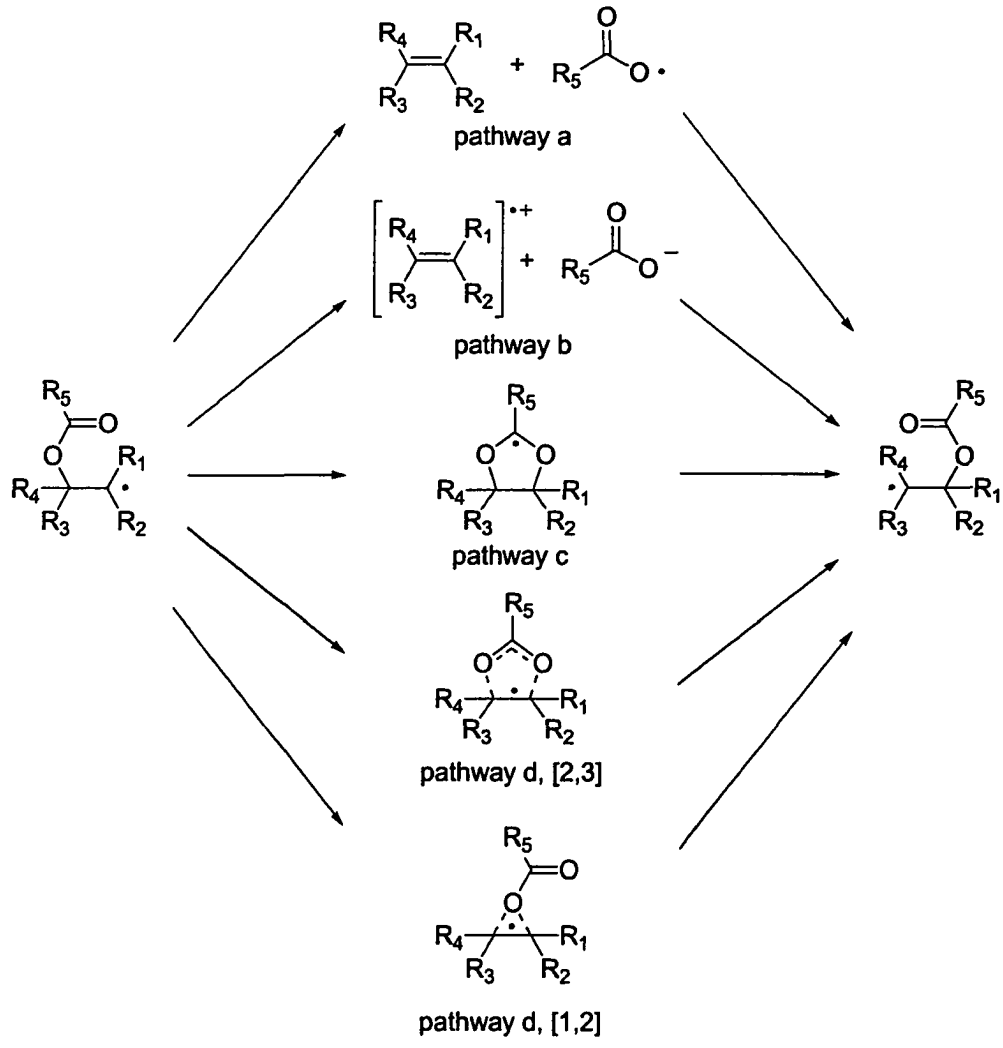

Figure 16. Proposed pathways for the β-(acyloxy)alkyl radical migration.[27]

cage, or as freely diffusible species) (Figure 16, pathway b), (c) ring closure to a five-membered cyclic ring radical followed by ring opening (Figure 16, pathway c), and (d) concerted reaction via either a [2,3] or a [1,2] mechanism (Figure 16, pathway d).

β-Ester migration involving the formation of a freely diffusible olefin and an acyloxy radical (Figure 16, pathway a) has been ruled out on the basis of kinetics as the rate of decarboxylation of the acyloxy radical exceeds the observed rates of ester

migration.[47] The formation of freely diffusible olefin cation radicals and an acyloxy anion has also been ruled out due to the high stereoselectivity observed from β-ester migration in steroidal and acyclic systems.[48,49] In addition, attempts to trap olefin cation radical intermediates in these migration reactions have been unsuccessful.[50] However, the high degree of stereoselectivity and the inability to trap the olefin cation radical with nucleophiles observed in these systems does not rule out heterolytic fragmentation of the ester group to form a contact ion pair followed by recombination.

Cyclization of the β-ester functionality to form a five-membered cyclic ring radical followed by ring opening (Figure 16, pathway c) has also been ruled out. The intermediacy of the dioxolanyl radical (**66**) was probed for using the cyclopropylcarbinyl radical ring opening reaction (Figure 17).[51] Generation of radical **67** was carried out by

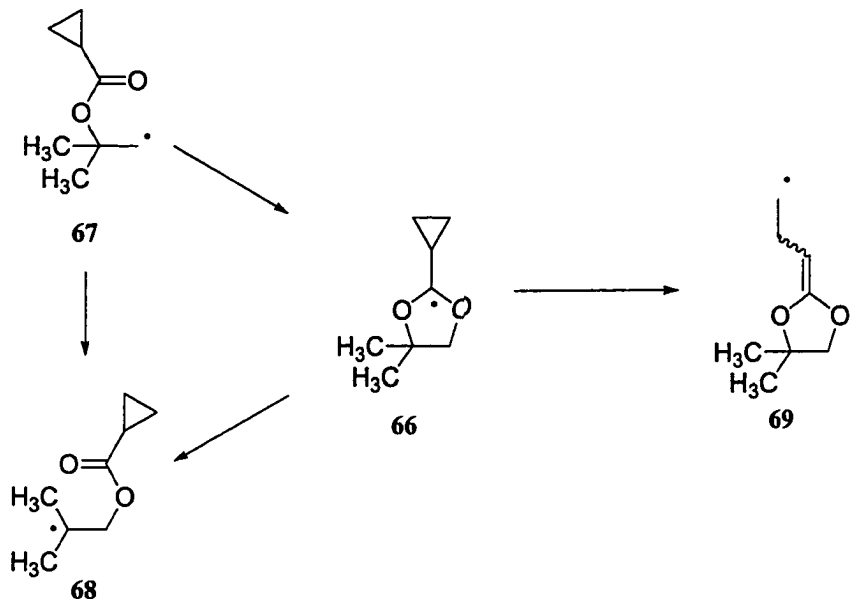

Figure 17. Use of the cyclopropylcarbinyl radical rearrangement to probe for the intermediacy of **66**.[51]

photolysis of the appropriate diacylperoxide, and the reaction was monitored by electron paramagnetic resonance spectroscopy (EPR). Migration of the ester functionality in **67** to the β-position to give radical **68** was observed to proceed with a rate constant of 1.2×10^2 s^{-1}. During the course of the reaction, no spectroscopic evidence was obtained for the presence of the product from the cyclopropylcarbinyl radical ring opening (**69**) which was independently shown to open with a rate of 8.7×10^5 s^{-1}. The fact that radical **69** was not observed as a byproduct of the rearrangement of **67** to **68** indicates that the dioxolanyl radical (**66**) is not an intermediate the migration reaction since the cyclopropylcarbinyl radical undergoes ring opening 10^3 times faster than the rate of migration.

The most complete mechanistic study of the β-(acyloxy)alkyl radical migration has been carried out by Beckwith and co-workers, and probes the effects of solvent polarity, electronic effects within the β-(acyloxy)alkyl radical, and the oxygen connectivity in the migrated product through the use of labeling studies.[50] The rate of migration of radical **70** to radical **71** was measured as a function of solvent polarity as well as a function of the substituents on the aryl ring (Eq 5). An increase of over an order

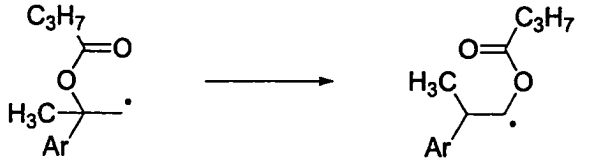

(5)

70
a Ar = Ph
b Ar = *p*-H_3COPh
c Ar = *p*-NCPh

71
a Ar = Ph
b Ar = *p*-H_3COPh
c Ar = *p*-NCPh

of magnitude for the rate of migration was observed upon changing the solvent polarity from cyclohexane to methanol, indicating a polarized transition state for the migration reaction (Table 1). Substituent effects on the aryl ring showed an increase in the rate of migration upon increasing the donor ability of the aryl group (**70b** $k_{rearr.} = 1.7 \times 10^5\ s^{-1}$; **70c** $k_{rearr.} = 1.6 \times 10^4\ s^{-1}$).

Table 1. Effect of increasing solvent polarity on the migration of **70a** to **71a** at 75 °C.

Solvent	Polarity[a]	Migration Rate (s^{-1})
Cyclohexane	30.9	3.7×10^4
Benzene	34.5	6.4×10^4
Dimethylether	38.2	5.8×10^4
Dimethylformamide	43.8	8.4×10^4
Ethanol	51.9	1.3×10^5
Methanol	55.5	1.6×10^5

[a] $E_T(30)$ solvent polarity scale (see ref 31).

In order to gain evidence for or against a mechanism shift from a concerted [1,2] or [2,3] migration to heterolytic fragmentation to generate either a caged or diffusibly free olefin cation radical and an ester anion upon increasing solvent polarity, Beckwith and co-workers undertook an ^{17}O labeling study.[50] The ^{17}O label was incorporated into the carbonyl oxygen in **70a-c** and the location of the label after migration was determined by ^{17}O NMR. Under conditions that do not favor a highly polarized transition state (**70a** and **70c** in benzene), complete transposition of the ^{17}O label was observed, indicating that the migration occurred through a concerted [2,3]-pathway (Eq 6). However, under conditions that favor a polarized transition state (**70a** and **70b** in methanol), scrambling of the ^{17}O label was observed (Eq 7). This observation implies that when a more polar transition state is favored, the migration occurs by a mix of [2,3] and [1,2] pathways or

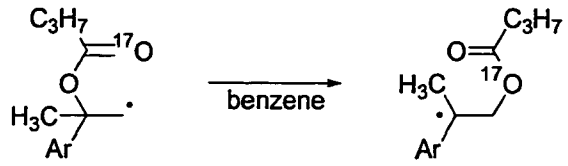

70a or **70c** **71a** or **71c** (6)

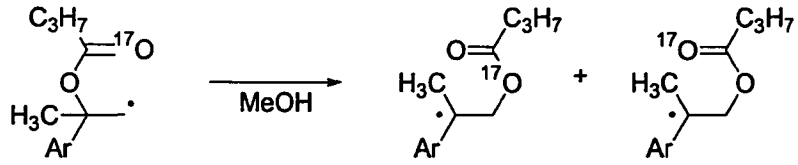

70a or **70b** **71a** or **71b** **71a** or **71b** (7)

through the formation of an ion radical pair followed by recombination. Attempts to trap the olefin cation radical with nucleophiles were unsuccessful, indicating that if olefin cation radicals are formed, they most likely react within the solvent cage.

Computational studies carried out in the gas phase using **72** - **74** by Zipse indicate that the [2,3] migration pathway is the most favorable of the mechanisms studied.[52] Similar substituent effects to those discussed above were also observed, albeit to a lesser degree. Computations also indicate a significant amount of positive charge build up in the alkane during migration coupled with a build up of negative charge in the migrating ester functionality. Evidence for the build up of positive charge in the transition state was also obtained from calculations comparing the relative reaction barriers for the migration in **73** and **74** where **74** showed a 1.8 kcal/mol lower barrier to migration. Including the effect of protonation of the carbonyl oxygen in **72** in order to model high polarity solvents resulted in reduction of the barrier for [1,2] migration by 10.1 kcal mol^{-1}. While protonating the carbonyl in **72** is an extreme method to model the effect of high polarity solvents, the results are consistent with Beckwith's and co-worker's study where oxygen

scrambling was observed in systems with the ability to stabilize the build up of positive charge during the migration.[50]

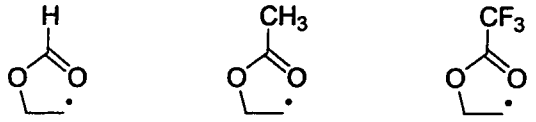

72 73 74

2.2.2 β-(Phosphatoxy)alkyl Radical Migrations.

As a result of the mechanistic studies carried out by Crich and co-workers regarding the β-(acyloxy)alkyl radical migration, the question was posed as to whether or not structurally similar β-(phosphatoxy)alkyl radicals would undergo migration reactions. In 1993, Crich and co-workers reported the migration of **75** to **76** (Eq 8) concurrently

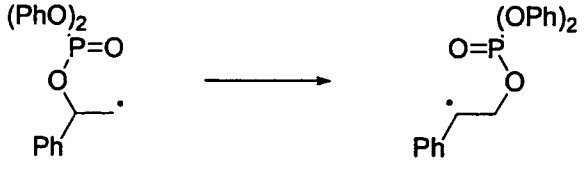

75 76 (8)

with the report of the migration of **77** to **78** by Giese and co-workers (Eq 9).[53,54] Giese and co-workers measured a rate of 8 x 10^6 s^{-1} for the migration of **77** to **78** which is approximately two orders of magnitude faster than the average rate of β-(acyloxy)alkyl radical migration.[54,55] Subsequently, this reaction motif has been shown to be quite general and has been subjected to a high level of mechanistic scrutiny.

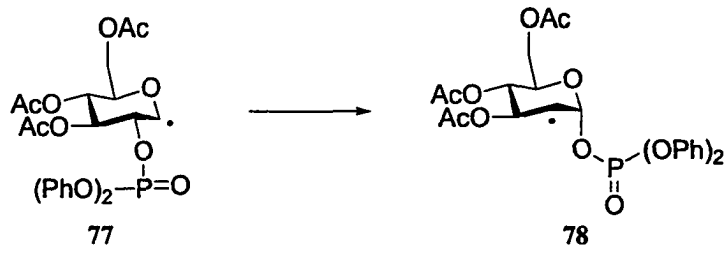

77 78 (9)

Mechanisms identical to those initially proposed for the β-(acyloxy)alkyl radical migration were originally put forward to account for the phosphatoxy migration. The observation of a high degree of stereoselectivity in the phosphate migration reaction in carbohydrate systems led to dismissal of mechanisms involving fragmentation to generate diffusibly free intermediates.[35,49,54] Migration by homolytic cleavage of the C-O bond to form an oxygen centered phosphate radical and an alkene within the solvent cage followed by recombination is ruled out as a feasible mechanism due to the high energy of the generated oxygen centered phosphate radicals.[55]

The possibility of a stepwise migration occurring through a cyclic phosphoranyl radical was ruled out through studies aimed at detecting the intermediacy of **79** through fragmentation products (Figure 18).[49] Generation of **80** by treatment of the corresponding bromide with Bu_3SnH and AIBN in refluxing benzene yielded the migrated product **81** as well as **82**, the product resulting from hydrogen atom transfer to **80**. The cyclic phosphate triester (**83**) which was expected to result from fragmentation of **79** was not observed, and as a result, the intermediacy of cyclic phosphoranyl radicals in the β-(phosphatoxy)alkyl radical migration was eliminated from consideration.

Labeling studies carried out in a manner similar to those described above for the β-(acyloxy)alkyl radical rearrangement were carried out using **75** with an ^{18}O label

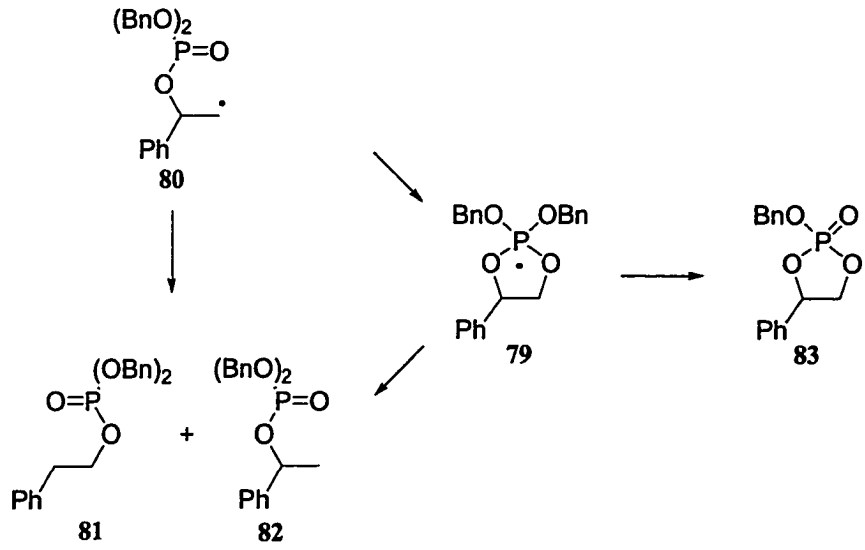

Figure 18. Proposed pathway for the formation of **83** from **80**.[49]

incorporated at the benzylic C-O bond and showed a 1.5/1 ratio of retention over inversion at phosphorous.[49] This data is consistent with the phosphate migration occurring through either a concerted pathway involving a mixture of both the [1,2] and the [2,3] pathways with the activation energy for the former being slightly lower, or through heterolytic fragmentation to form an olefin cation radical phosphate anion contact ion pair followed by rapid recombination. Computational studies carried out by Zipse on **84** - **86** support the hypothesis of a lower barrier to activation for the concerted [1,2] migration over both the [2,3] pathway and heterolytic fragmentation followed by in cage recombination.[56] The explanation for the preference of the [1,2] pathway over the [2,3] pathway is due to a greater degree of charge separation in the transition state in the [2,3]-migration. This implies that the [2,3] pathway may become the predominate mechanism of migration in more strongly ionizing solvents.

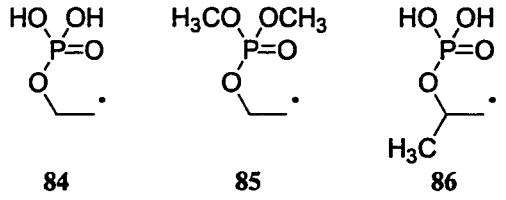

84 85 86

In order to resolve the question as to whether or not the β-(phosphatoxy)alkyl radical migration involved heterolytic cleavage of the phosphate moiety followed by rapid recombination, Crich, Newcomb, and co-workers undertook a series of laser flash photolysis studies aimed at probing for the intermediacy of olefin cation radicals in these systems.[57,58] Generation of homobenzylic radical **87** was carried out by photolysis of PTOC **88**, and the subsequent reactivity of **87** was monitored using LFP (Figure 19). In low polarity solvents such as THF and acetonitrile, only the benzylic radical **89** was observed. However, in aqueous acetonitrile solutions, a UV signal attributable to olefin cation radical **90** was detected. Similar pre-exponential factor values for migration

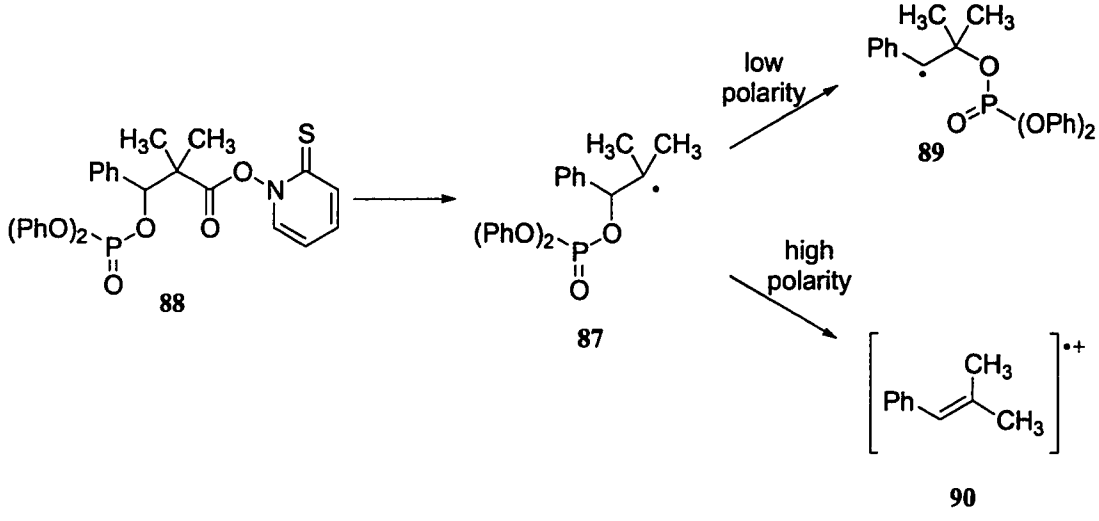

88 87 89 90

Figure 19. Reactivity of **87** as a function of solvent polarity.[58]

reactions measured in low polarity solvents and for the formation of olefin cation radical **90** in higher polarity solvents indicate that both processes occur through a common mechanism, heterolytic cleavage to from a solvent caged olefin cation radical phosphate anion pair which then either recombines to form the migrated products or in higher polarity solvents forms freely diffusible olefin cation radicals.

The dependence of solvent polarity on the formation of olefin cation radicals from **88** is somewhat different than that of the structurally similar **50**. Generation of freely diffusible olefin cation radicals occurs at lower solvent polarity for **48** (acetonitrile) than for **88** (aqueous acetonitrile) which is somewhat unexpected considering the diphenylphosphate moiety in **87** should be a better leaving group than the diethylphosphate present in **49**. This is a result of the presence of the *p*-methoxy group in **49** which leads to more stable olefin cation radical.

2.3 $S_{RN}2'$ Substitution.

As an extension of computational studies regarding S_N2 substitution by nucleophiles β to a radical center, Zipse reported computational evidence for a radical analogue of the S_N2' substitution ($S_{RN}2'$).[26,59,60] Studies were carried out using the degenerate substitution of 2-chloroethan-1-yl (**91**) with chloride ion. It was shown that nucleophilic substitution at the site of the radical coupled with heterolytic loss of the leaving group and migration of the radical to the β-position has a barrier approximately 5 kcal/mol lower than for direct S_N2 substitution of the chloride ($S_{RN}2$) (Figure 20). The reduced barrier for this process was attributed to mixing of the homolytic and heterolytic character of the dissociation process.

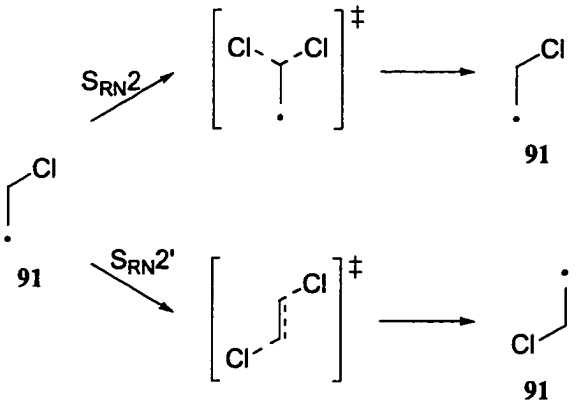

Figure 20. The $S_{RN}2$ and the $S_{RN}2'$ reactions.[62]

Substitution of the alcohol moiety of protonated alcohols containing radicals in the β-position by neutral nucleophiles has been observed in the gas phase.[61] For example, radical **92** has been shown (by mass spectroscopy) to react with $H_2{}^{18}O$ to generate the corresponding ^{18}O substituted radical (**93**) in the gas phase.[62] This reaction is only observed in the case of the cation radical as the reaction of protonated ethanol with H_2O results in deprotonation in the gas phase. The two proposed mechanisms to account for the observed substitution are either the $S_{RN}2$ or the $S_{RN}2'$ pathways. However, the experimental details needed to differentiate between these two pathways have not been obtained to date.

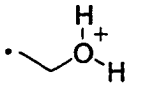

92

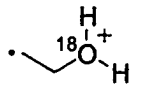

93

Similar reactivity in the solution phase has also been observed. Generation of **87** in THF in the presence of 1-octanol resulted in the observation of benzylic radical **94** by

LFP.[51] The rate of growth of **94** was shown to have a first order dependence on the concentration of 1-octanol and the intermediacy of olefin cation radical **90** was not observed. Experiments performed on a preparative scale using *t*-BuSH as a hydrogen atom donor gave a 60% yield of the alcohol substituted product **95**. Even though **90** was not observed by LFP, this does not provide conclusive evidence for the formation of **94** by the $S_{RN}2'$ pathway as reaction of 1-octanol with a solvent caged olefin cation radical phosphate anion pair cannot be ruled out (Figure 21).

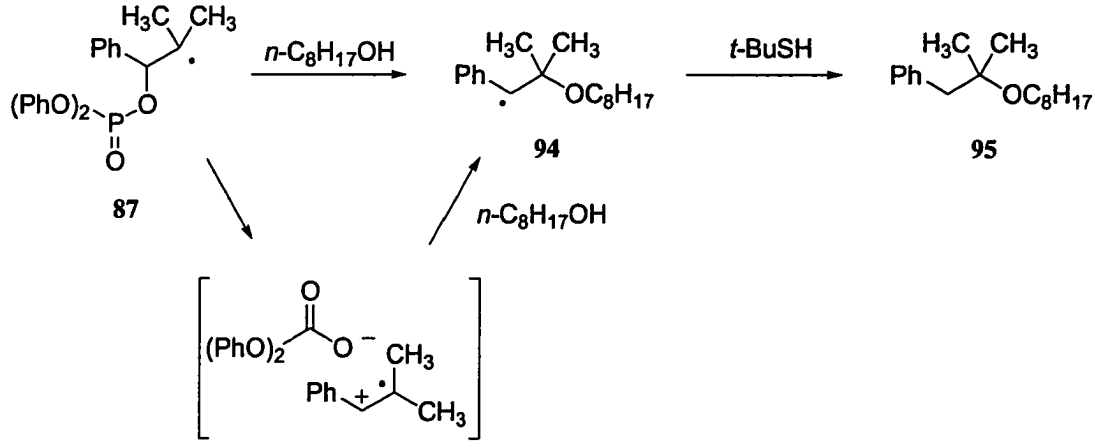

Figure 21. Proposed pathways for the formation of **95**.[51]

2.4 Statement of Research Objectives.

From the mechanistic studies outlined above several conclusions can be made with regard to the reactivity of alkyl radicals containing leaving groups in the β-position:

1) The factors governing the rate of heterolytic cleavage to generate olefin cation radicals are dependent on the interplay of solvent polarity,

the ability to stabilize the build up of positive charge in the heterolysis transition state, and the stability of the resulting olefin cation radical.

2) Activation parameters for the β-(acyloxy)alkyl and β-(phosphatoxy)alkyl radical rearrangements and for heterolysis of β-phosphatoxy groups show similar log A values, indicating that these intermediates undergo heterolysis to form a contact ion pair followed by either recombination to yield migrated products or diffusion out of the solvent cage to generate free olefin cation radicals.

3) Extension of the mechanistic studies carried out for the migration reactions implies that the direct reaction of radicals with leaving groups in the β-position with nucleophiles occurs through a caged olefin cation radical anion pair rather than through the $S_{RN}2'$ pathway.

The mechanistic studies described above are consistent with the formation of olefin cation radicals as common intermediates in both migration and substitution reactions of radicals with β-leaving groups. However, product studies supporting or contradicting the spectroscopic studies described above are lacking. Furthermore, mechanistic studies aimed at providing chemical evidence for the intermediacy of reactive intermediates other than olefin cation radicals in systems favoring olefin cation radical formation have not been carried out to date.

The goal of this research is the mechanistic investigation a series of compounds which will allow the following questions to be addressed through the use of spectroscopic and product studies:

1) Can chemical evidence for the intermediacy of olefin cation radicals arising from heterolytic cleavage of β-leaving groups be obtained through the use of product studies?

2) If olefin cation radicals are generated by β-heterolysis, what are the decay pathways available in the presence of nucleophiles and hydrogen atom donors?

3) Can chemical evidence be obtained for the formation of products through intermediates other than olefin cation radicals in high polarity solvents?

3 Results and Discussion.

Radicals **96** and **97** were chosen for study for several reasons. It was anticipated

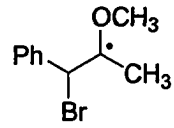

96

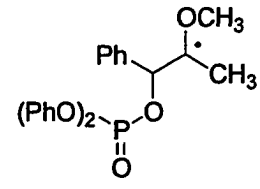

97

that the use of two distinct leaving groups would provide a probe for multiple reaction intermediates through the comparison of product ratios. The advantage of the use of the β-bromo radical (**96**) arises from the fact that the bromide was not expected to undergo migration reactions as has been shown to be the case for β-(phosphatoxy)alkyl radicals similar to **97**.[35,53,54,57,58] However, it is possible that **96** could degrade by homolysis of the carbon bromine bond.[63-65] The primary advantage of using β-phosphate radical **85** arises from the fact that the phosphate will not undergo homolysis due to the high energy of oxygen centered phosphorous radicals.[55] It was hoped that the α-methoxy substituent would enhance the stability of radical **97** to the point that phosphate migration would not be observed.

In order to avoid the possibility of product decomposition due to the need for forcing conditions to generate radicals **96** and **97**, pyridine-2-thionecarbonyl (PTOC) esters **98** (bromo-PTOC) and **99** (phospho-PTOC) were chosen as radical precursors to **96** and **97** respectively. This type of radical precursor has been used extensively in LFP studies and has been shown to afford the desired alkyl radicals in a very clean and rapid

manner.[34,66] Upon exposure to long wavelength U.V. irradiation, PTOC esters undergo rapid N-O bond homolysis. The resulting carboxyl radical then decarboxylates on the sub-microsecond time scale (Eq 10).

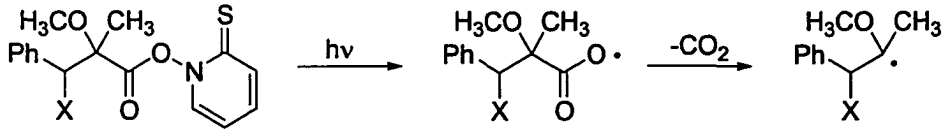

(10)

98 X = Br
99 X = $(PhO)_2PO_2$

96 X = Br
97 X = $(PhO)_2PO_2$

A wide range of products can be expected from the reaction of radical **96** or **97** in the presence of hydrogen atom donors and methanol as a nucleophile (Figure 20). Hydrogen atom abstraction by **96** or **97** will give rise to **100** or **101** respectively. Reaction of radicals **96** or **97** with methanol by $S_{RN}2'$ substitution followed by hydrogen atom abstraction gives rise to dimethylketal **102**. Cleavage of the bromide in the case of **96** or diphenylphosphate in the case **97** will form olefin cation radical **103**, which can be expected to react through several pathways. Reaction of **103** with methanol followed by hydrogen atom transfer will generate **102** and/or vicinal ether **104**, depending on the regiochemistry of methanol addition. Vinyl ethers **105** and **106** will be formed from deprotonation of **103** to form allylic radical **107**, followed by hydrogen atom transfer. Finally, phenylacetone (**108**) was expected to arise from any decomposition of vinyl ethers **105** and **106**. Vinyl ether **105** can also be formed by homolytic loss of bromine in the case of **96** or the phosphate moiety in the case of **97**. Methyl ether **109** was expected to arise from photochemical decomposition of **100** or **101** through the intermediacy of the corresponding benzylic radical.

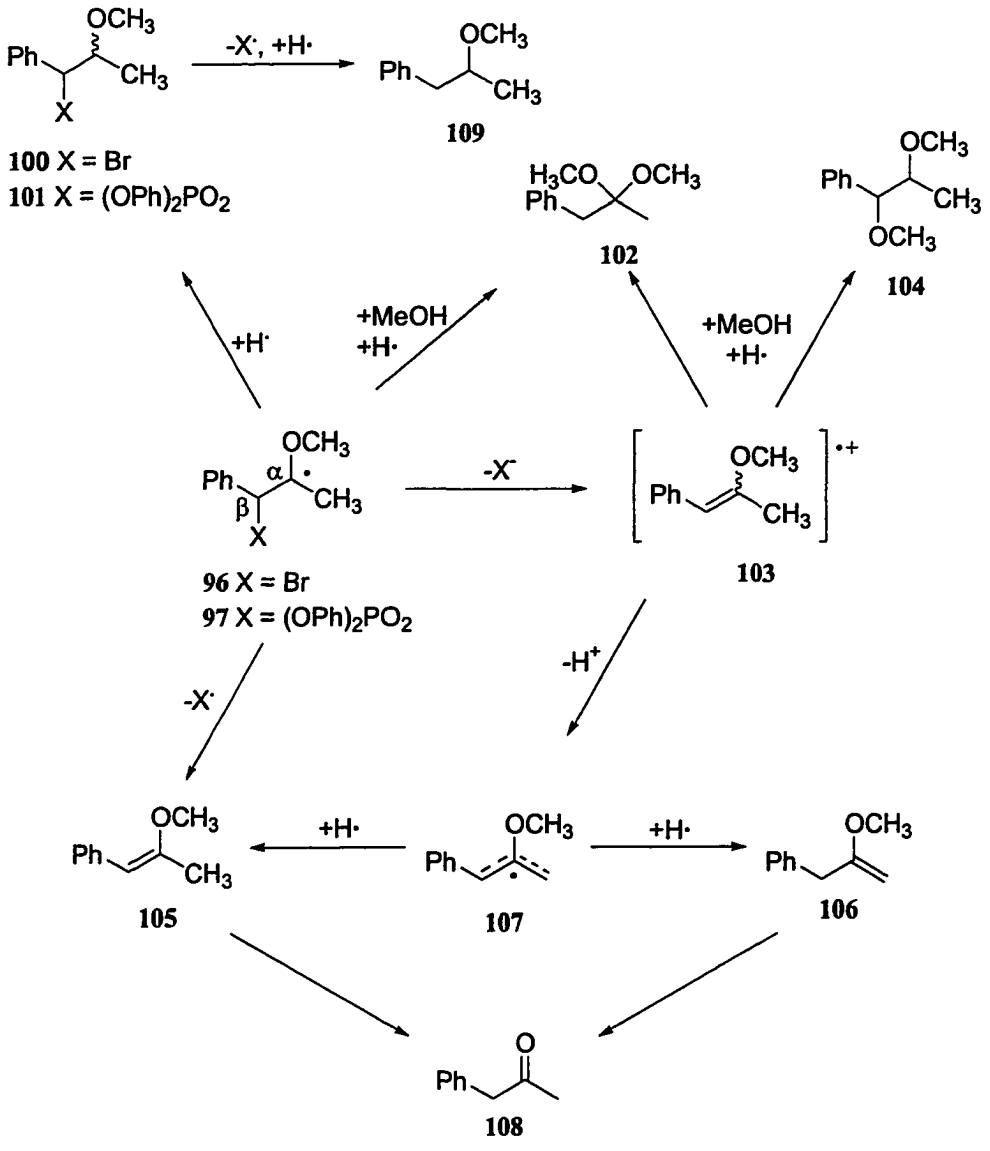

Figure 22. Anticipated products from the reaction of **96** or **97** in MeOH/AcN.

The study of **96** and **97** should provide the ability to differentiate between several of the possible reaction mechanisms. Since the leaving groups in **96** and **97** are different, different product ratios are expected from the two radicals for processes not involving a common reactive intermediate. Thus, reaction of **96** and **97** by $S_{RN}2'$ substitution was anticipated to give different yields on the basis of the fact that the rate of the substitution

reaction should be different for compounds containing different leaving groups. As mentioned above, homolytic scission of the leaving group is only expected to take place in **96**, while products attributable to migration are only expected in the case of **97**. In addition, products resulting from the formation of **107** are also expected to form in different yields from **96** and **97** as a result of the different basicity of bromide and diphenylphosphate. Thus, the use of radicals which differ only by the leaving group should provide a useful mechanistic probe for the reactions of alkoxy radicals containing leaving groups in the β-position.

3.1 Synthesis of Radical Precursors.

Initial synthetic studies toward **98** were aimed at the conversion of benzylic alcohol **110** to the desired β-bromo acid, followed by PTOC formation. To this end, ethyl (*S*)-(-)-lactate (**111**) was methylated using NaH and MeI to give ethyl 2-methoxypropionate (**112**) (Scheme 1).[67] Saponification of **112** was followed by an aldol condensation between benzaldehyde and 2-methoxypropionic acid (**113**) to give both diastereomers of **110** in a 1:1 ratio.[68,69] Treatment of **110** with CBr_4 and PPh_3 gave lactone **114** rather than the desired benzylic bromide.

It was thought that protecting the carboxylic acid as an ester would prevent lactone formation upon activation of the benzylic alcohol. However, the ester functionality needed to be removable using mild conditions in order to prevent hydrolysis of the benzylic bromide. The 2-trimethylsilylethyl ester was chosen due to its instability to mild fluoride conditions. Treatment of acid **110** with 2-trimethylsilylethanol and DCC gave lactone **114** rather than the desired ester (Scheme 1). The facile cyclization

Scheme 1.[a]

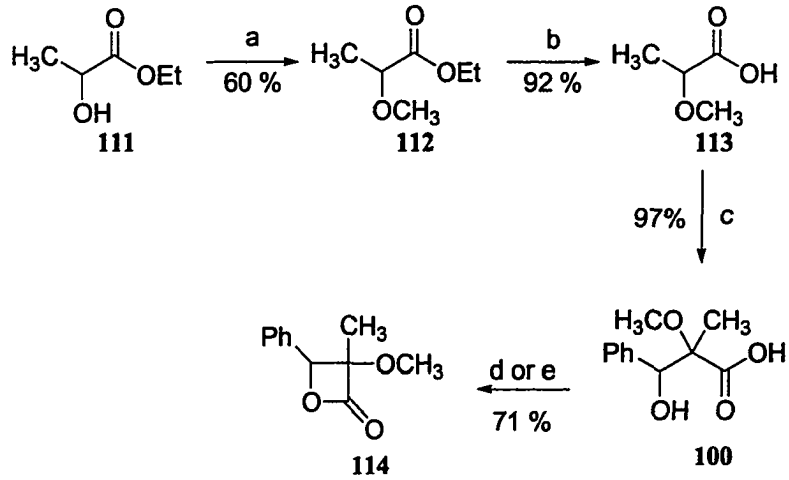

[a] Key: (a) NaH, MeI, THF. (b) KOH, EtOH. (c) LDA, PhCHO, THF. (d) CBr_4, PPh_3, Et_2O. (e) 2-trimethylsilylethanol, DCC, CH_2Cl_2:EtOAc (7:1).

observed upon activation of either the alcohol or acid functionality in **110** is most likely due to the Thorp-Ingold effect which decreases the bond angle between the carbonyl carbon and the benzylic carbon, allowing the system to more easily adopt the conformation required for cyclization.[70,71]

In order to avoid lactone formation, the synthesis was redesigned to allow incorporation of the desired bromide through a radical based benzylic bromination. Alkylation of **112** with benzylbromide yielded ethyl 2-methoxy-2-methyl-3-phenylpropionate (**115**) and subsequent saponification of the ester functionality gave the desired acid (**116**) in good yield (Scheme 2). Benzylic bromination of the free acid (**116**) with NBS and AIBN gave the PTOC precursor (**117**) as 1:1 a mixture of diastereomers. Due to the propensity of **117** to undergo rapid decarboxylation and loss of bromide under mildly basic conditions, **117** was carried on crude. Using Mitsonobu conditions, **117** was

reacted with 2,2'-dithiopyridine-1,1'-dioxide in the presence of PPh_3 to give an equal ratio of both diastereomers of bromo-PTOC **98**.[72]

Scheme 2.[a]

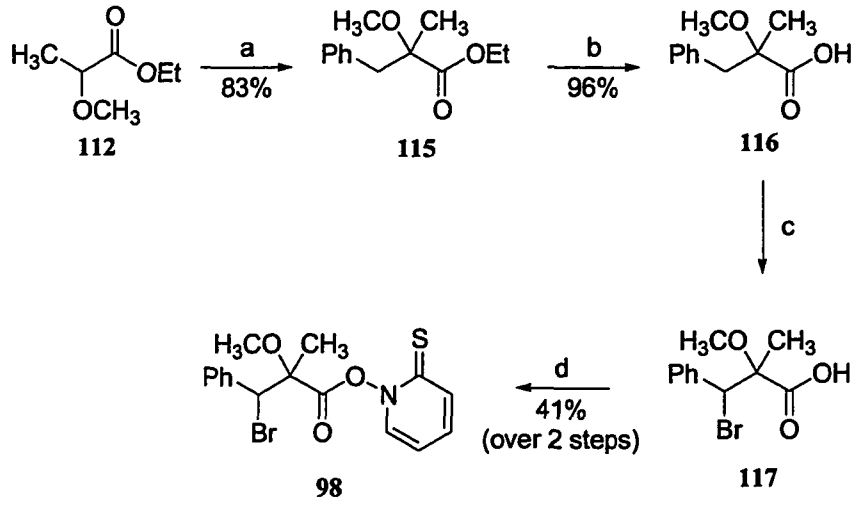

[a] Key: (a) LDA, BnBr, THF. (b) KOH, EtOH. (c) NBS, CCl4. (d) PPh_3, 2,2'-dithiopyridine-1,1'-dioxide, CH_2Cl_2.

Preparation of **99** was carried out in a similar manner to the synthesis reported by Crich and co-workers for the preparation of **50**.[24] Coupling of 2,4-dimethoxybenzyl alcohol with **113** gave ester **118** which was subsequently reacted by aldol condensation with benzaldehyde to afford β-hydroxyester **119** as a 2:1 mixture of diastereomers (Scheme 3). Phosphate triester formation was carried out using diphenylchloro-phosphate to give the desired β-diphenylphosphate ester **120**. In order to avoid the expected facile decarboxylation of the carboxylate upon alkaline saponification of **120**, the 2,4-dimethoxybenzyl moiety was removed using oxidative conditions. Reaction of **120** with CAN afforded both diastereomers of acid **121** in a ratio of 3:1. Reaction of

Scheme 3.[a]

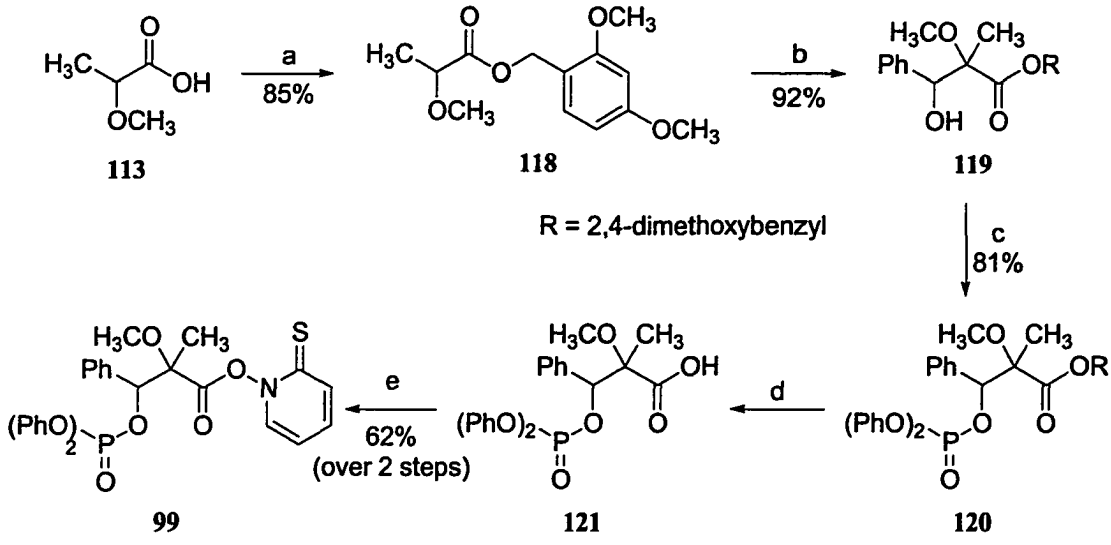

[a] Key: (a) 2,4-dimethoxybenzyl alcohol, PyBOP, Hünig's Base, CH_2Cl_2. (b) LDA, PhCHO, THF. (c) $(PhO)_2P(O)Cl$, DMAP, CH_2Cl_2. (d) CAN, H_2O:CH_3CN (10:1). (e) PPh_3, 2,2'-dithiopyridine-1,1'-dioxide, CH_2Cl_2.

crude **121** under the Mitsonobu conditions described above gave a 3:1 ratio of diastereomers of phospho-PTOC **99**.[72]

3.2 Synthesis of Possible Products.

Dimethoxy-PTOC **122** was prepared as it was the expected product arising from solvolysis of **98** and **99**, and an authentic sample was required to determine the stability of **98** and **99** to the sample preparation conditions. Aldol condensation between **112** and benzaldehyde provided β-hydroxy ethyl ester **123** as a 6:1 mixture of diastereomers 92% (Scheme 4). Alkylation of the benzylic hydroxyl in **123** followed by saponification provided the PTOC precursor **125**. PTOC formation was carried out in the manner

Scheme 4.[a]

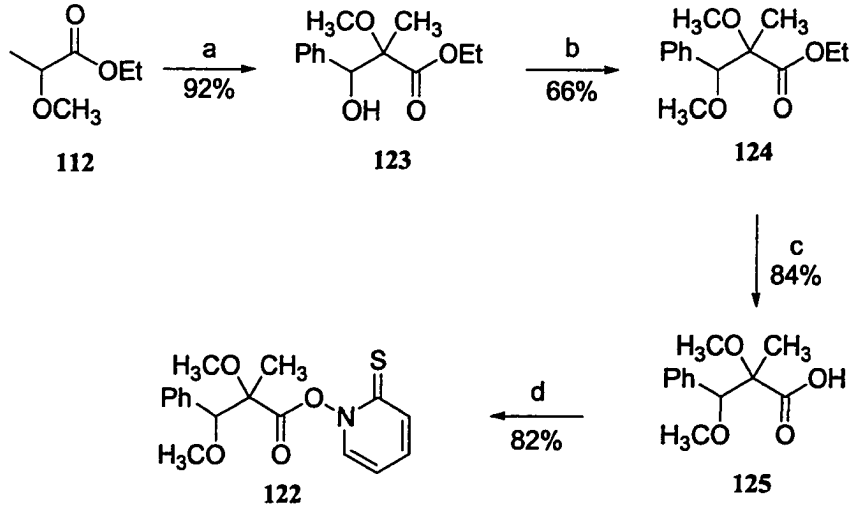

112 123 124 125 122

[a] Key: (a) LDA, PhCHO, THF. (b) NaH, MeI, THF. (c) KOH, EtOH. (d) PPh_3, 2,2'-dithiopyridine-1,1'-dioxide, CH_2Cl_2.

described for the preparation of both **98** and **99** to give the desired dimethoxy-PTOC (**122**) as a 3:2 mixture of diastereomers.[72]

Preparation of reduction products **100** and **101** was carried out using a common intermediate, 2-methoxy-1-phenyl-1-propanol (**126**). To this end, 2-methoxy-acetophenone (**127**) was alkylated with MeI to give **128** which was reduced with $NaBH_4$ to give a 3:2 mixture of diastereomers of **126** (Scheme 5). Treatment of **126** with PBr_3 yielded both diastereomers as a 5:4 mixture of the desired bromide (**100**). An equal mixture of both diastereomers of **101** was prepared by treatment of **126** with diphenylchlorophosphate.

Dimethylketal **102** was prepared from phenylacetone.[73] Preparation of a 1:1 mixture of diastereomers of vicinal ether **104** was carried out by osmium mediated dihydroxylation of β-methylstyrene followed by alkylation with NaH and MeI.[74]

Scheme 5.[a]

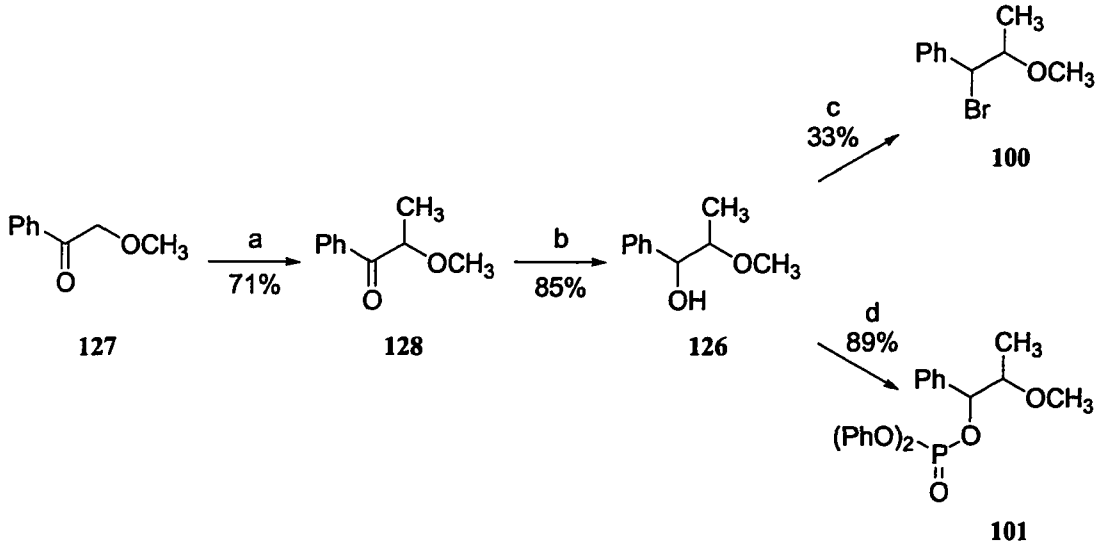

127 128 126 100 101

[a] Key: (a) LDA, MeI, THF. (b) $NaBH_4$, MeOH. (c) PBr_3, Et_2O. (d) $(PhO)_2P(O)Cl$, DMAP, CH_2Cl_2.

Phenylacetone (**108**) was prepared through PDC mediated oxidation of 1-phenylisopropanol. Ether **109** was prepared by reaction of 1-phenylisopropanol with NaH and MeI.

Preparation of vinyl ether **105** was carried out using by taking advantage of the propensity of **117** to decarboxylate. To this end, **117** was treated with Hünig's base to afford a 1:1 mixture of both *E* and *Z* isomers of **105** which were separable by column chromatography. Structural assignments of the *E* and *Z* configuration were made using ^{1}H-NMR through comparison to calculated shift tables, which predict that the vinyl proton in the *E*-isomer will resonate downfield of the corresponding proton in the *Z*-isomer.[75] This prediction is consistent with values previously reported for the two isomers of **105**.[76] Preparation of vinyl ether **106** was carried out by a titanocene

methyleneation of methyl phenylactetate using bis(cyclopentadienyl)dimethyl titanium.[76,77]

3.3 U.V. Irradiation of Bromo-PTOC (98) and Phospho-PTOC (99).

3.3.1 Radical Precursor and Product Stability.

Irradiation of **98** or **99** in Pyrex vessels was carried out under anaerobic conditions (freeze-pump-thaw degassed solutions) in a Rayonet photochemical reactor using λ_{max} = 350 nm lamps for 20 min. Photolyses were performed in 4:1 methanol/acetonitrile solutions, employing methanol as the nucleophile. While varying the concentration of the nucleophile could serve as a useful mechanistic probe, the solvent composition was not changed in order to avoid complications resulting from the strong dependence of diffusively free olefin cation radical formation on solvent polarity.[24,32,40,58,78] Both the bromo-PTOC (**98**) and the phospho-PTOC (**99**) were shown to be stable at room temperature in the dark during the period of sample preparation. However, some decomposition was observed in the presence Hünig's base, as an acid scavenger, upon standing at room temperature for 12 h (Table 2).

Table 2. Decomposition of **98** and **99** in the presence of Hünig's base in 4:1 MeOH/AcN as a function of time.[a]

PTOC	Time (h)	% Decomp.[b]
98	0.5	3.0
98	12	30.0
99	2	0
99	4	5.0
99	11	5.0

[a] [PTOC] = 26 mM, [Hünig's Base] = 53 mM, 4:1 d_4-MeOH/d_3-AcN. [b] Relative to hexamethyldisilane as internal standard.

The sole decomposition product was shown to be the dimethoxy-PTOC (**122**) by ^{1}H NMR through comparison to an authentic sample. Photolysis of **122** in the presence of a hydrogen atom donor was shown to only generate **104** by GC analysis (Eq 11). The

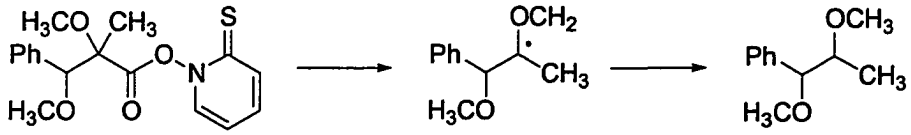

122 **104** (11)

lack of production of **104** upon photolysis of either bromo-PTOC **98** or phospho-PTOC **99** provides further indication that both radical precursors do not undergo decomposition during the period of sample preparation.

Photolysis of **102**, **104** – **106**, **108** and **109** in the presence of **98** or **99** in 4:1 methanol/acetonitrile showed that only products **104**, **108**, and **109** were stable to the photolysis conditions, and that dimethyl ketal **102**, and vinyl ethers **105** and **106** decomposed to phenylacetone (**108**). The observed product instability was attributed to acid catalyzed decomposition. Generation of HBr in the case of **98** can arise as the result of either heterolytic or homolytic cleavage of the leaving group from **96** to generate either bromide or bromine respectively, followed by proton or hydrogen atom transfer respectively. A similar pathway in the case of **97** can account for the formation of diphenylphosphoric acid from photolysis of **99**. As a result, all subsequent photolyses were carried out in the presence of an acid scavenger.

2,6-Di-*t*-butylpyridine (TBP) was chosen as the acid scavenger for several reasons. First, it was believed that trialkylamines could easily reduce olefin cation

radical **103** if it were formed during photolysis by electron transfer. The reduction potential of **103** was approximated by estimating the oxidation potential of **105**. An upper limit for the oxidation potential ($E_{1/2}$) of **105** was estimated to be 1.33 V (versus SCE) by comparison to structurally related styrenes. For example, the oxidation potential of β-methyl-4-methoxystyrene has been measured to be 1.33 V vs. SCE and a value of 1.32 V vs. SCE has been measured for the oxidation potential of α-trimethylsilyloxystyrene.[79,80] The oxidation potential of triethylamine has been measured at 0.78 V vs. SCE, 0.5 V lower than the estimated reduction potential of **103**.[81,82] Thus, reduction of **103** by alkyl amines could be favored by as much as 12.6 kcal mol^{-1}. Conversely, pyridine has an oxidation potential of 2.12 V vs. SCE and will not be able to reduce **103** as this process is disfavored by 17.8 kcal mol^{-1}.[83] Due to the propensity of pyridine to react nucleophilically with olefin cation radicals ($k \approx 10^9$ M^{-1} s^{-1}), a hindered pyridine was chosen in order to reduce the rate of nucleophilic attack.[84]

The choice of the hydrogen atom donor was governed by limitations similar to those discussed above for the proton scavenger. Electron transfer from alkyl thiols to olefin cation radical **103** was expected to be energetically favorably by approximately 5.3 kcal mol^{-1}, as alkyl thiols have oxidation potentials on the order of 1.1 V.[85] The use of tributyltin hydride was avoided as products attributable to reduction of similar olefin cation radicals by tributyltin hydride have been observed previously, and it was anticipated that the presence of tin species could provide difficulties with respect to product analysis by GC.[21] 1,4-Cyclohexadiene (CHD) was chosen as the hydrogen atom donor on the basis of its oxidation potential in acetonitrile of 1.74 V vs. SCE.[86] Thus, electron transfer from CHD to **103** is disfavored by 9.5 kcal mol^{-1}.

3.3.2 Photolysis of 98 and 99 in the Presence of 1,4-Cyclohexadiene and 2,6-Di-*t*-butylpyridine.

Analysis of the products produced upon photolysis of **98** or **99** under the conditions described above by GC showed *Z*-2-methoxy-1-phenylpropene (**105**) to be the major product (Table 3). The opposite vinyl ether isomer, *E*-2-methoxy-1-phenyl-propene, was not observed. Preferential formation of the *Z*-isomer is consistent with molecular modeling at the AM1 level of theory which predicts a 2.17 kcal/mol lower $\Delta\Delta H_f$ for the *Z*-isomer. Both **98** and **99** generated low yields of dimethylketal **102**, while vicinal ether **104** was not observed from either precursor. Photolysis of **98** also generated a low yield of methyl ether **109**. The product yields from photolysis of **98** were consistently lower than the yields obtained from the photolysis of **99**.

Table 3. Product distribution in the presence of 1,4-cyclohexadiene (CHD) and 2,6-di-*t*-butylpyridine (TBP).[a]

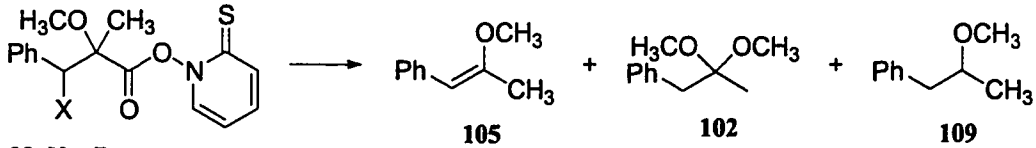

98, X = Br
99, X = $O_2P(OPh)_2$

	% Yield		
PTOC	**105**	**102**	**109**
98	22.4 ± 1.2	3.7 ± 0.3	3.2 ± 0.2
99	38.3 ± 2.2	4.4 ± 0.7	–[b]

[a] [PTOC] = 5 mM, [TBP] = 10 mM, [CHD] = 500 mM, 4:1 MeOH:AcN (by volume), [MeOH] = 19.75 M. [b] Not observed.

In order to ascertain the stability of **102, 105, 106,** and **109** to the photolysis conditions in the presence of TBP and CHD, photolysis experiments were carried out in the presence of the independently synthesized products and amount of decomposition was determined by GC analysis. The primary mode of decomposition was expected to be acid catalyzed, and as HBr is a stronger acid than diphenylphosphoric acid, product stabilities were carried out using the bromo-PTOC (**98**). These experiments showed that vinyl ether **105** underwent less than 2% decomposition to form phenylacetone (**108**) during the course of the photolytic reaction (Table 4). Similar experiments indicated that dimethylketal **102** was also stable to the photolysis conditions (Table 5).

Table 4. Product yields obtained from photolysis of bromo-PTOC **98** as a function of added **105**.[a]

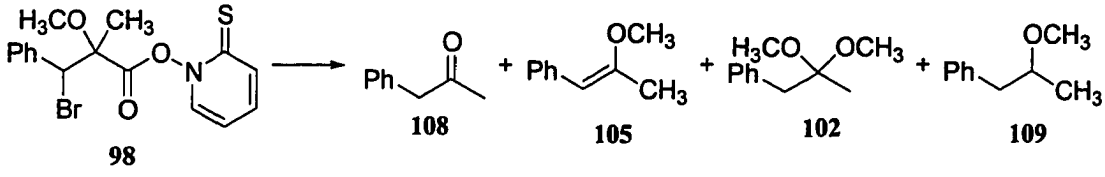

	% Yield[b]			
Composition	**108**	**105**	**102**	**109**
98	1.4 ± 0.1	20.5 ± 0.8	2.9 ± 0.2	2.0 ± 0.1
105	0.5 ± 0.3	6.0 ± 0.4[c]	-[d]	-[d]
98 +105	2.0 ± 0.1	24.5 ± 1.1[c]	2.3 ± 0.1	2.0 ± 0.1

[a] [PTOC] = 5 mM, [TBP] = 10 mM, [CHD] = 500 mM, 4:1 MeOH:AcN (by volume), [MeOH] = 19.75 M. [b] Yield based on [PTOC]. [c] [**105**] = 0.325 mM. [d] Not observed.

Table 5. Product yields obtained from photolysis of bromo-PTOC **98** as a function of added **102**.[a]

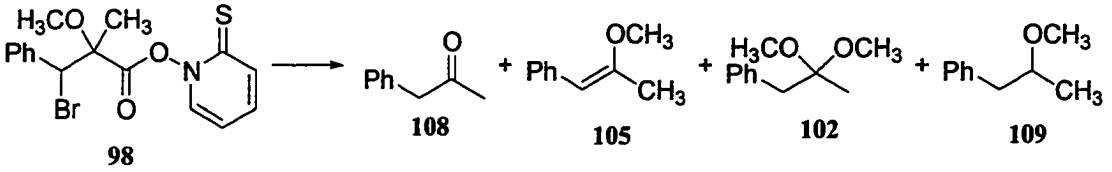

	% Yield[b]			
Composition	**108**	**105**	**102**	**109**
98	1.7 ± 0.2	20.5 ± 1.9	4.3 ± 0.7	2.4 ± 0.2
102	-[d]	-[d]	1.7 ± 0.1[c]	-[d]
98 + **102**	1.6 ± 0.1	19.2 ± 1.8	6.4 ± 0.7[c]	2.1 ± 0.3

[a] [PTOC] = 5 mM, [TBP] = 10 mM, [CHD] = 500 mM, 4:1 MeOH:AcN (by volume), [MeOH] = 19.75 M. [b] Yield based on [PTOC]. [c] [**102**] = 85 μM. [d] Not observed.

Benzyl vinyl ether **106** underwent significant decomposition upon photolysis in the presence of the radical precursors (**98** or **99**). ^{1}H NMR studies showed **106** to be stable in 4:1 methanol:acetonitrile at rt for 2 d. However, decomposition of **106** was observed when **106** was photolyzed at λ_{max} = 350 nm in the presence and absence of TBP in 4:1 methanol:acetonitrile for 20 min (Table 6). Due to this photochemical decomposition, low and variable yields of **106** were observed upon photolysis of **98** or **99** in the presence of CHD and TBP. It is possible that the yield of **106** is equal to the mass balance that is unaccounted for from the yields of **102**, **105**, and **109**, giving an upper limit of 70.7% and 57.3% for the yield of **106** from the photolysis of **98** and **99** respectively. However, high yields of **106** are unlikely as **106** is believed to be derived from allylic radical **107** (see Figure 22), which is not formed in high enough concentrations to be detected by LFP in the 4:1 methanol:acetonitrile solutions used for the product studies (see below).

Table 6. Decomposition of **106** upon photolysis with 1,4-cyclohexadiene (CHD) in the presence and absence of 2,6-di-*t*-butylpyridine (TBP).[a]

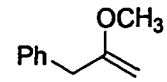

106

[TBP] (M)	% Decomp.[b]
0	35.9 ± 6.3
0.5	46.8 ± 6.0

[a] [**106**] = 1.88 mM, [CHD] = 0.5 M, 4:1 MeOH/AcN. [b] Yield based on initial concentration of [**106**].

Photolysis of **98** in the presence of added bromide **100** suggests that **109** is generated from **100** (Table 7). This was confirmed by the observation that **109** was produced in low yield upon photolysis of **100**. A very low yield of vinyl ether **105** was also generated from the photolysis of **100**. The corresponding phosphate compound **101** could not be observed by GC due to low volatility. However, analysis of photolysates by ^{1}H NMR showed that **101** was not generated upon photolysis of the phospho-PTOC (**99**).

Table 7. Product yields obtained from photolysis of bromo-PTOC **98** as a function of added **100**.[a]

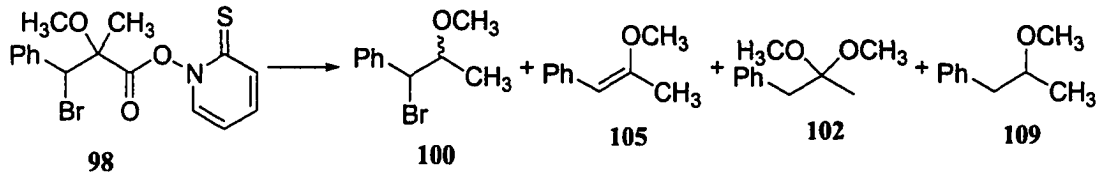

98 **100** **105** **102** **109**

	%Yield[b]			
Composition	**100**	**105**	**102**	**109**
98 + **100**	56.5 ± 5.1[c]	25.3 ± 0.8	2.54 ± 0.26	39.6 ± 1.8
100	81.3 ± 11.1[c]	0.31 ± 0.07	-[d]	6.89 ± 0.59

[a] [PTOC] = 5 mM, [TBP] = 10 mM, [CHD] = 500 mM, 4:1 MeOH:AcN (by volume), [MeOH] = 19.75 M. [b] Yield based on [PTOC]. [c] [**100**] = 5 mM. [d] Not observed.

3.4 Dependence of Product Yields on 1,4-Cyclohexadiene Concentration.

The product yields obtained from photolysis of either the bromo-PTOC (**98**) or the phospho-PTOC (**99**) are dependent upon the concentration of CHD (Table 8). All product yields decrease with decreasing CHD concentration, indicating that CHD is involved in the formation of **102**, **103**, and **109**. However, the product yields are not dependent to the same extent upon the concentration of CHD as can be seen by comparing the ratio of **105** to **102** in Table 8. The different dependencies of the formation of **102**, **105**, and **109** are most likely due to differences in rates of the reaction of the radical precursors to **102**, **105**, and **109** with other possible hydrogen atom donors such as methanol and acetonitrile or radical radical reactions. As a result, radicals which do not react readily with other hydrogen atom donors may participate in radical radical reactions, effectively reducing the product yields.

Table 8. Product distribution as a function of 1,4-cyclohexadiene (CHD) concentration.[a]

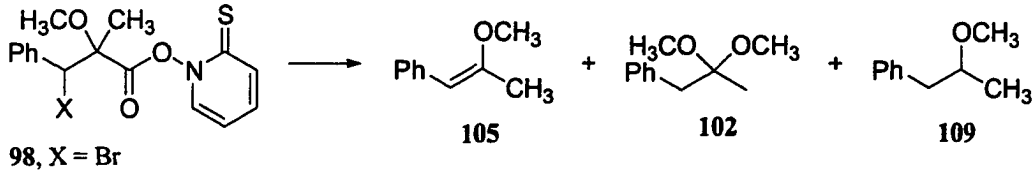

98, X = Br
99, X = $O_2P(OPh)_2$

		% Yield			
PTOC	[CHD] (M)	**105**	**102**	**109**	**105:102**
98	0.5	22.4 ± 1.2	3.7 ± 0.3	3.2 ± 0.2	6.1 ± 0.6
98	0.25	18.2 ± 0.5	1.4 ± 0.3	3.0 ± 0.1	13.0 ± 2.8
98	0.125	14.1 ± 0.7	0.8 ± 0.1	2.6 ± 0.1	17.6 ± 2.4
99	0.5	38.3 ± 2.2	4.4 ± 0.7	-[b]	8.7 ± 1.5
99	0.25	33.6 ± 1.1	2.4 ± 0.1	-[b]	14.0 ± 0.7
99	0.125	26.4 ± 1.0	1.2 ± 0.2	-[b]	22.0 ± 3.8

[a] [PTOC] = 5 mM, [TBP] = 10 mM, 4:1 MeOH:AcN (by volume), [MeOH] = 19.75 M.
[b] Not observed.

Photolysis of **98** or **99** in the presence of TBP and 3,3,6,6-tetradeuterio-1,4-cyclohexadiene (d_4-CHD) showed apparent kinetic isotope effects of 2.24 ± 0.38 and 1.77 ± 0.17 for the formation of **105** from bromo-PTOC **98** and phospho-PTOC **99** respectively (Table 9). The kinetic isotope effects were determined from the ratio of the yield of product in the presence of CHD to the yield in the presence of d_4-CHD (Eq 12).

$$K.I.E. = \frac{[product]_{CHD}}{[product]_{d_4\text{-}CHD}} \qquad (12)$$

A kinetic isotope effect was not observed for the formation of dimethylketal **102** from either radical precursor in the presence of d_4-CHD. The absence of a kinetic isotope effect on the formation of **102** was unexpected since **102** was believed to arise through formation of a radical intermediate. Therefore, the possibility of hydrogen atom transfer from the solvent to the radical intermediates formed upon photolysis of either the bromo-PTOC (**98**) or the phospho-PTOC (**99**) was investigated. Photolysis of **98** or **99** in the presence of d_4-CHD and d_4-MeOH led to increased deuterium incorporation in dimethylketal **102** relative to that observed in the absence of d_4-MeOH (Table 10). Consistent with the deuterium increase, kinetic isotope effects of 1.76 ± 0.29 and 1.91 ± 0.52 were observed for the formation of **102** in the presence of d_4-methanol from bromo-PTOC **98** and phospho-PTOC **99** respectively, indicating that methanol is functioning as a hydrogen atom donor in the formation of **102**. The addition of d_3-acetonitrile had no effect on the amount of deuterium incorporated in any of the observed products and did not contribute to any observable kinetic isotope effects.

Table 9. Product distribution in the presence of 1,4-cyclohexadiene (CHD) and 3,3,6,6-tetradeuterio-1,4-cyclohexadiene (d_4-CHD) as a function of solvent.[a]

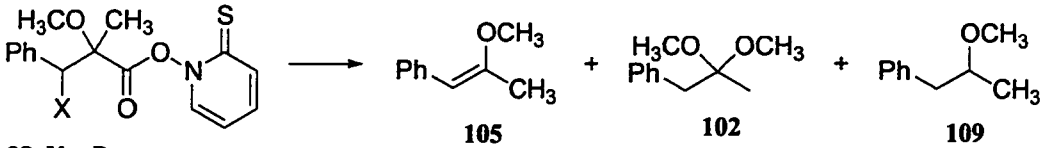

98, X = Br
99, X = $O_2P(OPh)_2$

			% Yield		
PTOC	trap	Solvent[b]	**105**	**102**	**109**
98	CHD	MeOH	22.4 ± 1.2	3.7 ± 0.3	3.2 ± 0.2
98	d_4-CHD	MeOH	10.0 ± 1.6	3.7 ± 0.5	2.5 ± 0.2
98	d_4-CHD	d_4-MeOH	11.3 ± 1.5	2.1 ± 0.2	2.9 ± 0.3
99	CHD	MeOH	38.3 ± 2.2	4.4 ± 0.7	-[c]
99	d_4-CHD	MeOH	21.6 ± 1.6	4.4 ± 0.7	-[c]
99	d_4-CHD	d_4-MeOH	22.2 ± 1.9	2.3 ± 0.5	-[c]

[a] [PTOC] = 5 mM, [TBP] = 10 mM, [CHD] = [d_4-CHD] = 500 mM, 4:1 MeOH:AcN (by volume). [b] [MeOH] = 19.75 M, [d_4-MeOH] = 19.73 M. [c] Not observed.

Table 10. The effect of solvent deuteration on deuterium incorporation in the presence of 3,3,6,6-tetradeuterio-1,4-cyclohexadiene (d_4-CHD).[a]

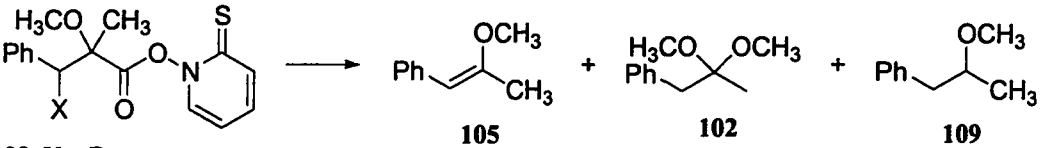

98, X = Br
99, X = $O_2P(OPh)_2$

		% ^{2}H		
PTOC	Solvent[b]	**105**	**102**	**109**
98	MeOH	3.0 ± 0.6	47.9 ± 0.8	71.0 ± 0.7
98	d_4-MeOH	2.2 ± 0.5	63.1 ± 1.5	82.1 ± 6.5
99	MeOH	2.4 ± 0.4	60.2 ± 0.4	-[c]
99	d_4-MeOH	2.0 ± 0.2	76.9 ± 3.1	-[c]

[a] [PTOC] = 5 mM, [TBP] = 10 mM, [d_4-CHD] = 500 mM, 4:1 MeOH:AcN (by volume). [b] [MeOH] = 19.75 M, [d_4-MeOH] = 19.73 M. [c] Not observed.

3.5 Laser Flash Photolysis Studies.

Laser flash photolysis studies carried out on **98** in THF gave the time resolved spectra shown in Figure 23. The spectra do not show the characteristic pattern for a benzylic radical ($\lambda_{max} \approx 325$ nm), but more closely resembles that of the 2-methyl-1-phenylallyl radical ($\lambda_{max} = 305$ nm).[57,87] As a result, the spectra were assigned to the 2-methoxy-1-phenylallyl radical (**107**) which is believed to arise through deprotonation of olefin cation radical **103** by the bromide leaving group within the solvent cage. The rate constant for formation of **107** from **96** was measured to be $(2.8 \pm 0.5) \times 10^5$ s^{-1} from first order kinetic plots of the natural log of the concentration of **107** as a function of time (Figure 23 inset).

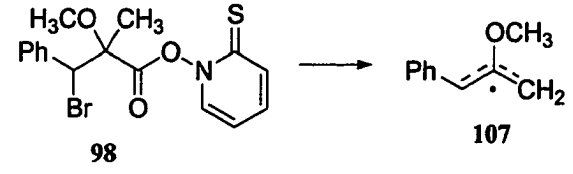

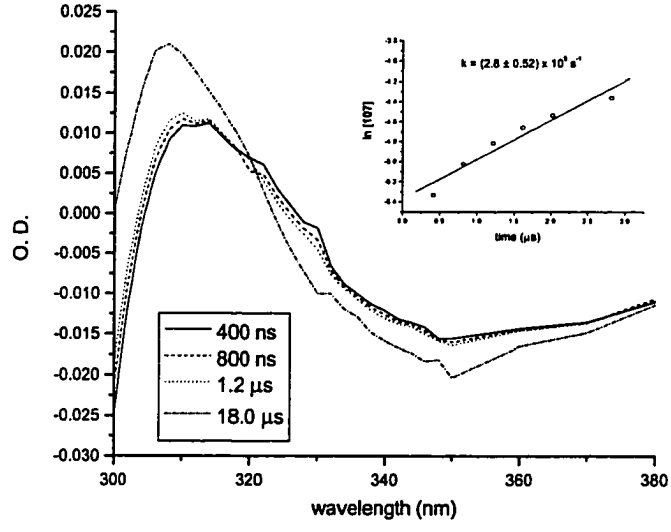

Figure 23. Time-resolved spectra from photolysis of **98** in THF. The traces are at 0.4, 0.8, 1.2, and 18.0 µs after irradiation with the signal at 50 ns subtracted to give a baseline. The inset shows a plot of the ln [**107**] versus time. The concentration of **107** was followed by monitoring the U.V. absorbance at 306 nm.

A similar spectrum to that observed from LFP studies carried out using **98** in THF was obtained from LFP studies using **99** under the same conditions (Figure 24). The presence of the λ_{max} = 308 nm indicates that photolysis of **99** in THF results in the formation of the 2-methoxy-1-phenylallyl radical (**107**) rather than the corresponding benzylic radical which is expected to be generated from phosphate migration. Deprotonation of **103** diphenylphosphate within the solvent cage is proposed to account for the formation of **107**. The rate of formation of **107** from **97** was determined in an identical manner to that described for the formation of **107** from **97**. Plots of the natural log of the concentration of **107** as a function of time obeyed first order kinetics and yielded a rate constant for the formation of **107** of (3.4 ± 0.9) x 10^6 s^{-1} (Figure 24 inset).

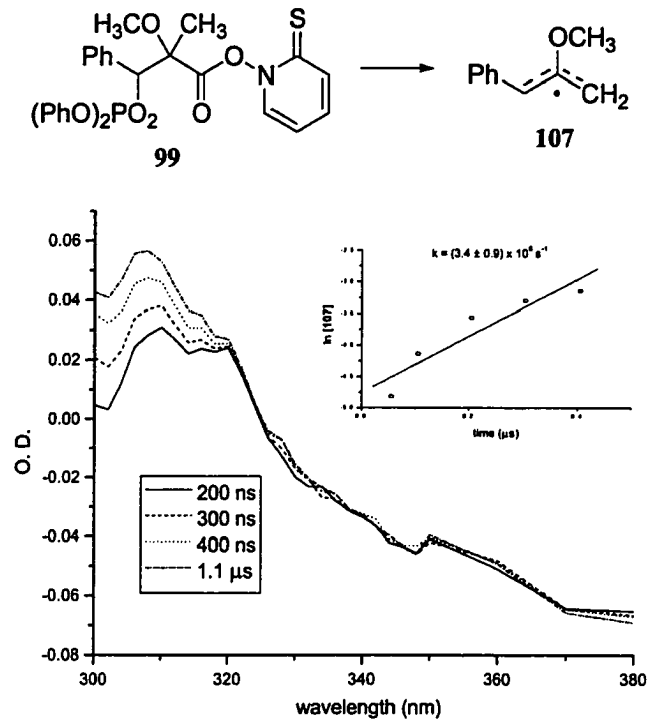

Figure 24. Time-resolved spectrum from photolysis of **99** in THF. The traces are at 0.4, 0.8, 1.2, and 18.0 µs after irradiation with the signal at 50 ns subtracted to give a baseline. The inset shows a plot of the ln[**107**] versus time. The concentration of **107** was followed by monitoring the U.V. absorbance at 306 nm.

Laser flash photolysis studies of **98** in acetonitrile gave the time resolved spectra shown in Figure 25. Due to the extremely rapid reaction of **97** in acetonitrile, time resolved spectra were not obtained for **99**. However, photolysis of **99** gave rise to spectra identical to those obtained for **98.** The spectra shown in Figure 25 are very similar to that reported for simple styrene radical cations and the spectrum observed for the *p*-methoxy-β,β-dimethylstyrene radical cation (**51**).[24,79] As a result, the spectra obtained from the independent photolysis of **98** and **99** is attributed to olefin cation radical **103**. No change in the spectrum obtained from photolysis of either radical precursor in acetonitrile solutions with up to 1.0 M methanol was observed, indicating that **103** is formed efficiently in the presence of methanol.

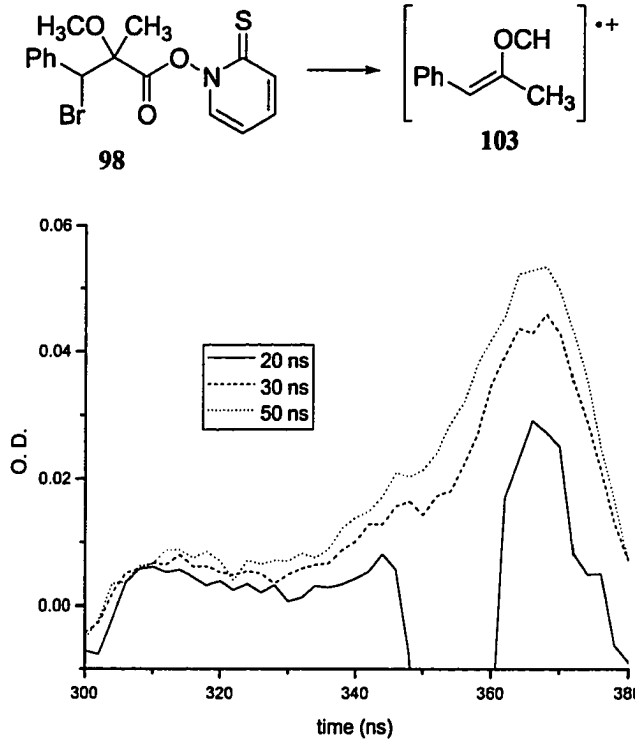

Figure 25. Time-resolved spectra from photolysis of **98** in acetonitrile. The traces are at 20, 30, and 50 ns after the photolysis; the negative signal in the trace at 20 ns results from the PM tube which has not recovered from the scattered laser light of the photolysis.

The yield of olefin cation radical **103** generated from photolysis of either the bromo-PTOC (**98**) or the phospho-PTOC (**99**) was estimated through the use of a reporter compound.[84] Generation of **103** in the presence of tris(*p*-bromophenyl)amine ((*p*-$BrC_6H_4)_3N$) in acetonitrile results in reduction of **103** and formation of the corresponding aminium cation radical (Eq 13, Figure 26). The concentration of the

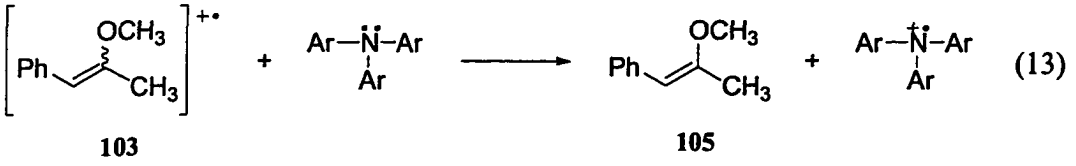

103 **105** (13)

Ar = *p*-bromo-phenyl

aminium cation radical relative to the concentration of the pyridine-2-thiyl radical byproduct produced upon initial photolysis of the PTOC ester was estimated using the molar extinction coefficient for the aminium cation radical measured by triplet chloranil oxidation of (*p*-$BrC_6H_4)_3N$. Photolysis of **98** or **99** gave relative aminium cation radical yields in the range of 65 – 85%. This is considered to be a lower limit for the quantity of **103** formed as the presence of reaction pathways other than electron transfer to **103** for (*p*-$BrC_6H_4)_3N$ are likely. For example, initial quantitation studies carried out using Ph_3-N, which has a lower oxidation potential than (*p*-$BrC_6H_4)_3N$, gave aminium cation radical yields in the 40 – 50% range. The lower yield of aminium cation radical is presumably due to reaction between **103** and Ph_3N through pathways not involving electron transfer and include nucleophilic addition of Ph_3N to the phenyl ring in **103**.[88,89]

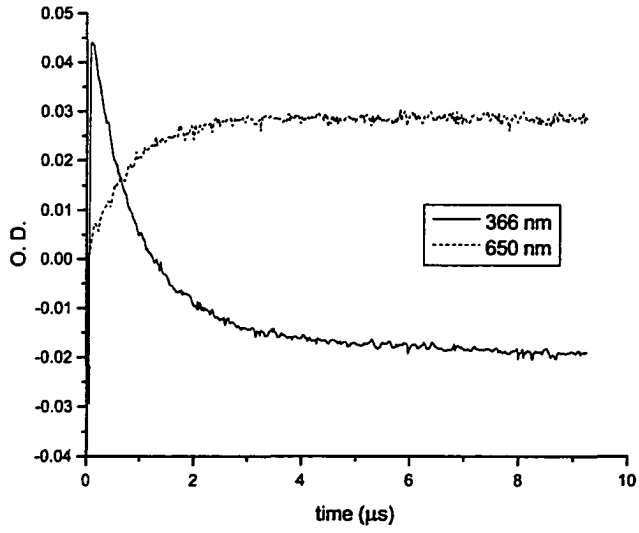

Figure 26. Plot of O. D. as a function of time for the photolysis of **99** with (p-$BrC_6H_4)_3N$ in acetonitrile. The absorbance at 366 nm is due to **103** and the absorbance at 650 nm is due to the aminium cation radical of (p-$BrC_6H_4)_3N$.

The kinetics of olefin cation radical formation from radicals **96** and **97** were followed by LFP in acetonitrile. The rate constant for loss of bromide from **96** was measured to be (8.0 ± 0.4) x 10^7 s^{-1} at 20 °C (Figure 27). The rate constant for loss of phosphate from radical **97** occurred at a rate faster than the resolution of the LFP apparatus used, suggesting a lower limit of 1 x 10^8 s^{-1} for formation of **103** at 20 °C. Since increasing the solvent polarity has been shown to increase the rate of heterolysis for radicals with leaving groups in the β-position, changing the photolysis solvent from the neat acetonitrile ($E_T(30)$ = 45.6 kcal mol^{-1}) used for in the LFP experiments to the 4:1 methanol:acetonitrile solvent system ($E_T(30)$ = 56.2 kcal mol^{-1}) used for the product studies should actually increase the rate of β-leaving group heterolysis.[24,32,40,58,78]

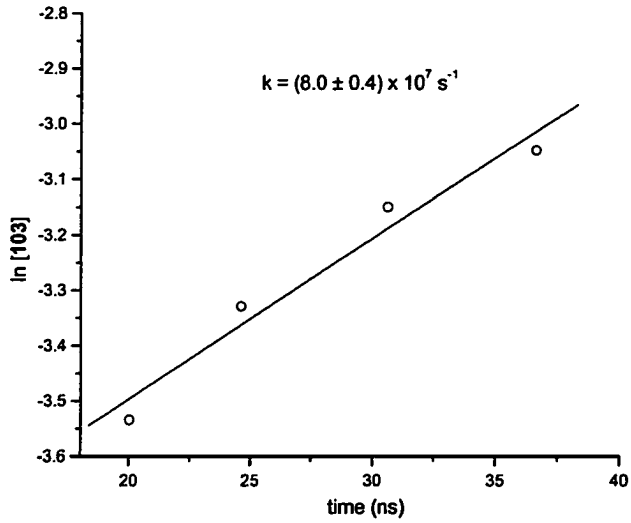

Figure 27. Plot of the ln [**103**] versus time from the photolysis of **98** in acetonitrile. The concentration of **103** was followed by monitoring the U.V. absorbance at 366 nm.

The rates of reaction of **103** with CHD and methanol were also measured by LFP. Monitoring the rate of decay of **103** in the presence of varying concentrations of 1,4-cyclohexadiene yielded an approximate rate constant of $(6.0 \pm 0.3) \times 10^5$ M^{-1} s^{-1} from a plot of the observed rate constants for reaction between **103** and CHD as a function of CHD concentration (Figure 28). The rate constant is considered an approximation as biexponential decays were observed at all concentrations of CHD studied. Generation of **103** in the presence of 1.0 M methanol showed no increase in the rate of decay of **103** on the time scale of the laser flash photolysis experiments. As a result, only an upper limit for the rate of reaction between **103** and methanol of 1×10^3 M^{-1} s^{-1} could be estimated. This rate is at least two orders of magnitude slower than that measured for the reaction of methanol with **90**, and at least an order of magnitude slower than that measured for methanol reaction with the cation radical of *p*-methoxystyrene.[15]

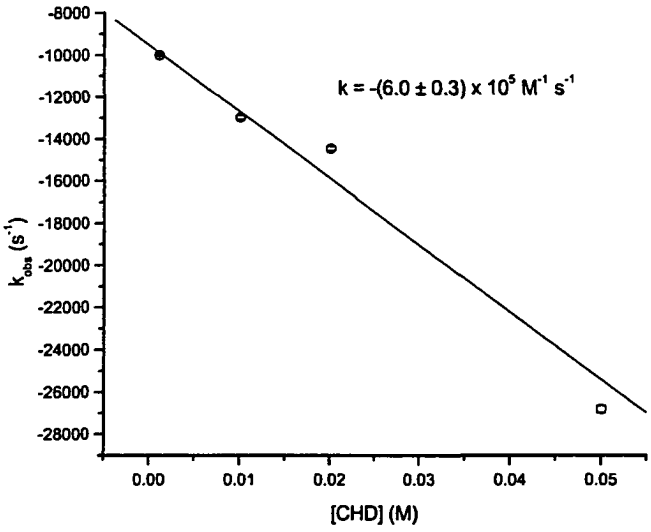

Figure 28. Plot of the pseudo-first order rate of decay of **103** generated from photolysis of **99** in acetonitrile as a function of CHD concentration.

3.6 Mechanisms of Product Formation.

3.6.1 Mechanism for the Formation of Vinyl Ether 105.

A variety of mechanisms involving several intermediates can be envisioned to explain the formation of **105** upon photolysis of **98** and **99**. The possible mechanisms are as follows: 1) β-scission of the bromide or phosphate in **96** and **97** respectively (Figure 29, pathway a); 2) hydrogen atom abstraction by **96** or **97** followed by elimination of HBr or diphenylphosphoric acid respectively (Figure 29, pathway b); 3) migration of the leaving group followed by sequential hydrogen atom abstraction and elimination as described for mechanism 2 (Figure 29, pathway c); 4) formation of allylic radical **107** by deprotonation of olefin cation radical **103** by either bromide or diphenylphosphate, followed by hydrogen atom donation to **107** (Figure 29, pathway d); 5) hydrogen atom

abstraction by **103** at either carbon or oxygen followed by deprotonation (Figure 29, pathway e).

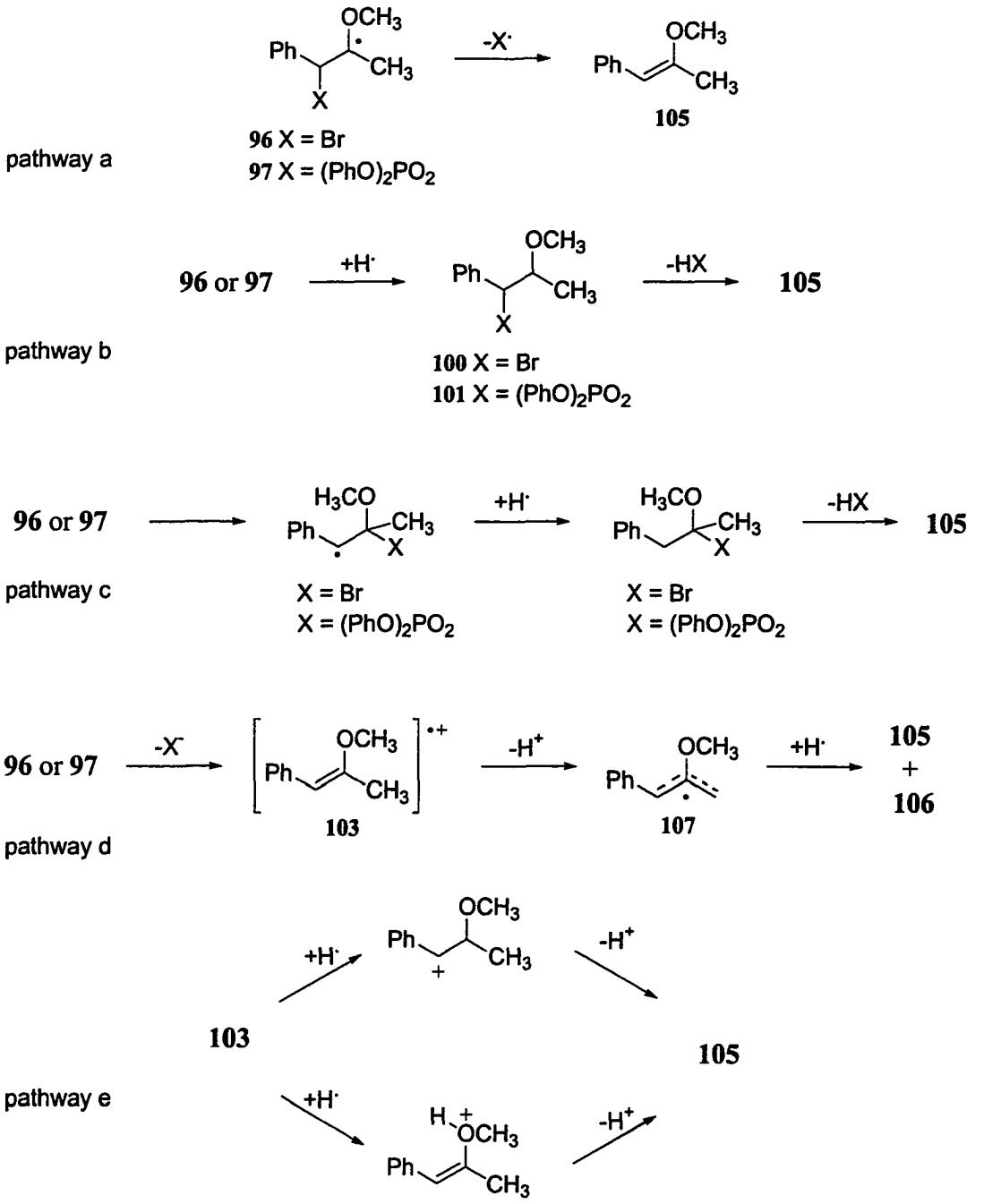

Figure 29. Possible mechanisms accounting for the formation of **105**.

Due to the high energy of oxygen centered phosphatoxy radicals, β-scission of the diphenylphosphate group in **97** was deemed unlikely (Figure 29, pathway a).[55] While β-scission of halides is a known process, the dependence of the yield of **105** on the concentration and isotopic content of CHD is inconsistent with the unimolecular nature of the β-scission reaction. Furthermore, LFP studies show that olefin cation radical **103** is formed from decay of both **96** and **97** in acetonitrile solutions. This reaction pathway is not expected to change upon increasing the solvent polarity from the acetonitrile solutions used for the LFP experiments to the 4:1 methanol:acetonitrile solutions used for the product studies based on the effect of solvent polarity on the formation of freely diffusible olefin cation radicals.[24,40] This is supported by similar ratio of **105**:**102** generated from photolysis of **98** or **99** which indicates that both compounds react through formation of a common intermediate (Table 8). Thus, on the basis of kinetic and product studies neither **96** or **97** produce vinyl ether **105** directly by homolysis of the β-leaving group.

Hydrogen atom donation to **96** or **97** followed by elimination of either HBr or diphenylphosphoric acid (Figure 29, pathway b) was also ruled out by product and LFP studies. Independently synthesized **101** (the product resulting from hydrogen atom transfer to β-phosphatoxy radical **97**) was shown by ^{1}H NMR to be stable to the reaction conditions. The corresponding bromide (**100**) was shown to react when exposed to the photolysis conditions to generate methyl ether **109** but not vinyl ether **105**. In addition, hydrogen atom transfer to radicals **96** and **97** from CHD is not expected to be kinetically competent as decay of radicals **96** and **97** was shown to occur with unimolecular rates greater than 10^7 s^{-1}, whereas CHD donates a hydrogen atom to alkyl radicals with a

bimolecular rate on the order of 10^5 M^{-1} s^{-1}.[87,90] This mechanism is also inconsistent with the ratio of **105**:**102** formed from photolysis of **98** and **99** which indicates that both systems generate **105** and **102** through a common intermediate (Table 8).

Migration of either the bromide in the case of **96**, or the diphenylphosphate in the case of **97**, followed by hydrogen atom abstraction and subsequent elimination (Figure 29, pathway c) can be ruled out as the major pathway accounting for the formation of **105** on the basis that benzylic radicals were not observed in appreciable yields by LFP studies. Also, this mechanism does not meet the requirement that **98** and **99** appear to react through formation of a common intermediate on the basis of the ratio of the yields of **105** and **102** (Table 8). Also inconsistent with this mechanism is the low incorporation of deuterium in **105** when photolyses of **98** or **99** were carried out in the presence of d_4-CHD. The kinetic isotope effect for elimination of HCl from 1-chloroethane has been measured to be 2.1.[91] As such, elimination of the proton to leave deuterium in **105** should be favored to yield ~ 66% deuterium incorporation in **105**. These observations do not allow a migration mechanism to be completely ruled out as a low level of deuterium is incorporated in **105** when **96** or **97** are reacted in the presence of d_4-CHD (Table 10). However, the fact that benzylic radicals are not observed by LFP with the systems discussed here, as well as other systems, indicate that migration is not a prominent reaction path in the high polarity solvents used.[24]

As mentioned above, both LFP experiments and the ratio of products obtained from the photolyses of **98** and **99** indicate that radicals **96** and **97** react to form **102** and **105** through a common intermediate (Table 8). Laser flash photolysis experiments carried out in acetonitrile provided spectroscopic evidence that the primary intermediate

formed is olefin cation radical **103**. As such, **105** is most likely formed through subsequent reaction of **103** in solution. This proposal is consistent with the identical ratio of **102**:**105** generated from photolysis of both **96** and **97** which indicates that both compounds are formed from a common intermediate (Table 8).

Deprotonation of cation radicals to generate the corresponding radical is a well known process.[92-95] Deprotonation of **103** generates allylic radical **107**, which upon hydrogen atom abstraction will generate vinyl ethers **105** and **106** (Figure 29, pathway d). This pathway should give rise to **105** with significantly higher levels of deuterium incorporation than are observed when **96** or **97** are generated in the presence of d_4-CHD. However, the observation of **106** in low yield and the presence of low levels of deuterium incorporation in **105** does not eliminate this reaction mechanism completely. While allylic radical **107** was not observed during LFP experiments carried out in acetonitrile, it was observed when THF was used as the solvent. Thus, the presence of **107** at concentrations below the detection limit of the LFP apparatus used, or within the solvent cage in more polar solvents, cannot be ruled out.

Laser flash photolysis experiments support trapping of olefin cation radical **103** by CHD with hydrogen atom transfer occurring either to carbon or oxygen (Figure 29, pathway e). Hydrogen atom transfer to carbon will result in the formation of a carbocation which is expected to react as an electrophile with methanol faster than deprotonation to generate **105**.[96] Nucleophilic reaction of methanol with the carbocation will form either dimethylketal **102** or vicinal ether **104**. As vicinal ether **104** is not observed and low yields of **102** are formed, hydrogen atom transfer to carbon cannot be a major pathway accounting for the formation of **105**. The low level of deuterium

incorporation observed in vinyl ether **105** when d_4-CHD is used as the hydrogen atom donor is also consistent with this reaction mechanism acting as a minor pathway for the formation of **105** on the basis of the kinetic isotope effects discussed above.

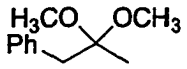

102

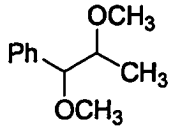

104

The mechanism most consistent with the observed data is that of hydrogen atom transfer from 1,4-cyclohexadiene to the oxygen in **103**, followed by deprotonation to generate **105**. Hydrogen atom abstraction by ether and sulfide cation radicals has been observed in the gas phase and may also occur in the reactions of fullerene olefin cation radicals in the solution phase.[61,97-102] The involvement of CHD in the formation of **105** is supported by the dependence of the yield of **105** on the concentration of CHD (Table 8). The observed kinetic isotope effect of 2.24 ± 0.38 and 1.77 ± 0.17 for the formation of **105** from **98** and **99** respectively is a combination of both primary and secondary effects. This is consistent with the primary KIE in the range of 1.2 to 1.6 for McLafferty rearrangements, reactions of ether cation radicals, and intermediates in the Loeffler-Freytag reaction.[103,104] This mechanism is also consistent with the low levels of deuterium incorporation in **105** observed upon photolysis of **98** or **99** in the presence of d_4-CHD as the isotopic label is lost upon deprotonation. In addition, similar kinetic isotope effects for the formation of **105** from either **98** or **99** (KIE_{86}/KIE_{87} = 1.27 ± 0.25) indicate that **105** arises from an intermediate common to both systems, consistent with the similar ratio of **105**:**102** produced from the photolysis of **98** or **99** under identical

conditions. This is supported by the LFP observation that both **98** and **99** generate olefin cation radical **103** upon photolysis in acetonitrile solutions.

The fact that alkane C-H bonds have been observed to be hydrogen atom donors to cation radicals in the gas phase led to the investigation of hydrogen atom donation to **103** by methanol.[61,97-102] Laser flash photolysis results provides no evidence for the donation of hydrogen atoms to **103** from methanol, and provides an upper limit to trapping of **103** by methanol of 1×10^3 M^{-1} s^{-1}. This result is supported by the fact that a kinetic isotope effect for the formation of **103** and an increase in the deuterium content in **103** were not observed upon substitution of d_4-MeOH for MeOH.

The intermediacy of **103** and the formation of **105** as the primary product from photolysis of **98** or **99** in 4:1 methanol:acetonitrile solutions may also explain the low mass balances observed. Since cycloaddition reactions between olefin cation radicals and alkenes occur at or near the diffusional limit, as the concentration of **105** increases during the 20 min photolysis cycloaddition reactions may become competitive with hydrogen atom transfer from CHD to **103**.[10,11,16] Due to the large number of products which can be envisioned to arise from the reaction motif with regard to the regiochemical and diastereomeric mixtures of these products, independent preparation and/or detection of these compounds is not feasible using the methods employed in this study. As a result, the formation of cycloaddition products cannot be ruled out and their presence may explain the low mass balances observed from photolysis of **98** and **99**.

3.6.2 Mechanism for the Formation of Dimethylketal 102.

Several mechanisms can be envisioned to account for the formation of **102** upon photolysis of **98** or **99**: 1) $S_{RN}2'$ reaction between β-substituted radicals **96** or **97** and MeOH (Figure 30, pathway a); 2) methanolysis of the product resulting from migration

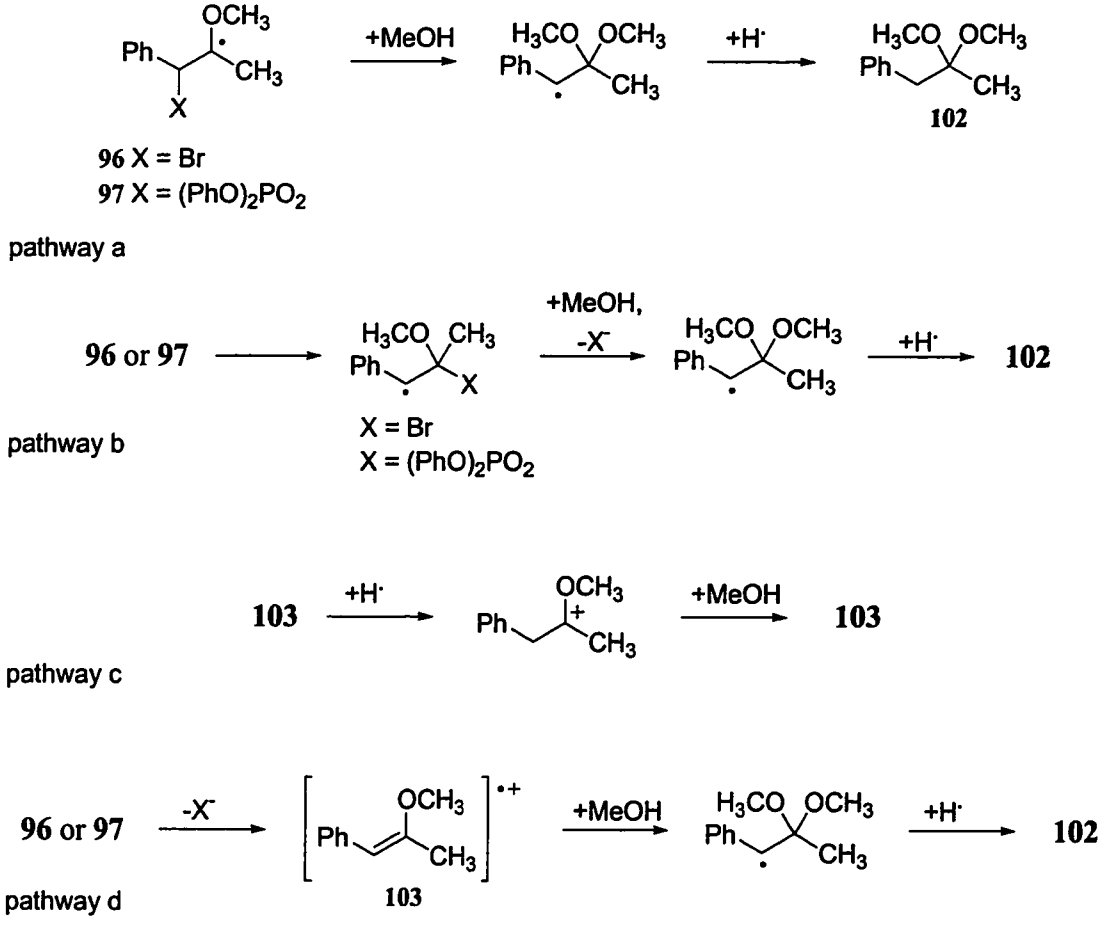

Figure 30. Possible mechanisms accounting for the formation of **102**.

of either bromide in the case of **96** or diphenylphosphate in the case of **97**, followed by hydrogen atom abstraction (Figure 30, pathway b); 3) hydrogen atom transfer to **103** at the benzylic position, followed by nucleophilic trapping of the resulting oxocarbenium

ion (Figure 30, pathway c); 4) nucleophilic trapping of olefin cation radical **103**, followed by hydrogen atom transfer to the resulting benzylic radical (Figure 30, pathway d).

Laser flash photolysis data does not allow complete elimination of the formation of **102** through either $S_{RN}2'$ substitution, or migration of the β-substituent and subsequent methanolysis, followed by hydrogen atom donation (Figure 30, pathway a). Based on the conservative estimate of < 10% formation of the benzylic radical relative to the amount of olefin cation radical produced by LFP, an upper limit of 6.5% to 8.5% yield of the benzylic radical could be generated during photolysis of these systems. The known dependence of the rate of heterolysis in these systems on the solvent polarity indicates that even lower yields of the benzylic radical in 4:1 methanol:acetonitrile solutions can be expected. However, invoking either of these mechanisms requires that **105** and **102** be generated from reactive intermediates other than olefin cation radical **103**, which is inconsistent with the identical ratio of **105**:**102** derived from both radical precursors. The common product ratio indicates that both products are derived from a common intermediate, the olefin cation radical **103** (Table 8).

The hypothesis that **102** is generated from **103** is consistent with the results of the product studies, as well as the laser flash photolysis studies. Competition between hydrogen atom transfer to oxygen leading to formation of **105**, and hydrogen atom transfer to carbon can be envisioned to account for the formation of both products through the intermediacy of **103** (Figure 30, pathway c). Hydrogen atom transfer to the benzylic carbon in **103**, followed by nucleophilic trapping of the resulting oxocarbenium ion is supported by the isotopic incorporation in **102** when d_4-CHD and d_4-MeOH are

used (Table 10). The regiochemistry of the hydrogen atom transfer can be rationalized on the basis of sterics. The slow rate of hydrogen atom transfer from CHD to benzylic radicals ($k < 10^2\ M^{-1}\ s^{-1}$) relative to the rate of hydrogen atom transfer from CHD to the oxygen in **103** ($k = (6.0 \pm 0.3) \times 10^5\ M^{-1}\ s^{-1}$) may explain the low yields of **103** observed from photolysis of **98** or **99** in 4:1 methanol:acetonitrile.[89]

Regioselective nucleophilic attack by methanol at the homobenzylic position of **103**, followed by hydrogen atom transfer to the resulting benzylic radical may contribute to the formation of **102** as well (Figure 30, pathway d). Isotopic labeling studies indicate that either CHD and/or methanol is responsible for transfer of a hydrogen atom to the resulting benzylic radical (Table 10). The unexpected role of methanol as a hydrogen atom donor is most likely a result of the slow rate of hydrogen atom abstraction by benzylic radicals from 1,4-cyclohexadiene ($k < 10^2\ M^{-1}\ s^{-1}$).[89] While the rate constant for the transfer of a hydrogen atom from methanol to a benzylic radical is not known, it is expected to be slower than that for CHD on the basis of the corresponding C-H bond strengths.[105] Unfortunately, LFP studies between **103** and methanol do not provide any insight into the pathway by which methanol reacts with **103**. The relatively slow rate of reaction between methanol and olefin cation radical **103** observed by LFP ($k < 10^3\ M^{-1}\ s^{-1}$) may be overcome by the high concentrations of methanol ([MeOH] = 19.75 M) present in the 4:1 methanol:acetonitrile solutions used for the product analyses.

Differentiation between these two mechanisms for the formation of **102** is not straightforward with the current data. Using the upper limit ($10^3\ M^{-1}\ s^{-1}$) for reaction of methanol with **103** and the measured rate constant ($6 \times 10^5\ M^{-1}\ s^{-1}$) for reaction of CHD with **103** coupled with the concentrations of reagents ([CHD] = 0.5 M and [MeOH] =

19.75 M), a ratio of **105:102** of ≥ 16 would be expected assuming nucleophilic attack by methanol on **103** followed by hydrogen atom transfer was the sole pathway accounting for the formation of **102**. A ratio of **105:102** ≥ 16 is observed upon decreasing the concentration of CHD, indicating that at low concentrations of CHD nucleophilic attack of methanol on **103** may be the only operative pathway for the formation of **102** (Table 8).

Seemingly contradictory to the regiochemistry of methanol attack on **103** is the failure of β-(phosphatoxy)alkyl radical **97** to undergo phosphate migration under conditions where phosphate migration has been observed in systems lacking the methoxy substituent. The failure of **97** to undergo migration indicates that the α-alkoxy radical is more stable than the benzylic radical. This implies that methanol trapping of olefin cation radical **103** should occur at the benzylic position, generating the more stable α-methoxy radical and ultimately resulting in the formation of vicinal ether **104**. However, the regiochemistry of nucleophilic attack is most likely governed by the kinetics of the reaction rather than the thermodynamics of the resulting product. While it is clear from the ratio of **105:102** that nucleophilic trapping of **103** by methanol followed by hydrogen atom transfer to the resulting radical is not the sole reaction pathway accounting for the formation of **102** in the presence of high concentrations of CHD (Table 8), the presence of this reaction motif cannot be completely ruled out at low CHD concentrations either. As such, **102** is most likely formed through a combination of the two proposed pathways, nucleophilic trapping of **103**, followed by hydrogen atom transfer to the resulting benzylic radical, and hydrogen atom donation to olefin cation radical **103**, followed by methanol trapping of the resulting oxocarbenium ion.

3.7 Conclusions.

Through the use of radical precursors containing distinct leaving groups in the β-position, the measurement of product ratios was employed to probe for the involvement of reactive species other than olefin cation radicals in high polarity solvents. Product studies are consistent with olefin cation radical **103** being the only reactive intermediate obtained from photolysis of bromo-PTOC **98** and phospho-PTOC **99**. This is confirmed by laser flash photolysis experiments, which indicate that olefin cation radical **103** is produced in approximately equal yields from both precursors in acetonitrile solutions.

The major pathway of decay for olefin cation radical **103** in the presence of 1,4-cyclohexadiene and 2,6-di-*t*-butylpyridine leads to the formation of vinyl ether **105**. On the basis of the dependence of the yield on the concentration of CHD and labeling studies, **105** is proposed to arise from hydrogen atom transfer from CHD to the oxygen in **103** followed by deprotonation (Scheme 31). Laser flash photolysis studies have provided a rate constant of $(6 \pm 0.3) \times 10^5$ M^{-1} s^{-1} for the reaction of CHD with olefin cation radical **103**. While this reaction motif has been observed previously in the gas phase, it has never been observed in the solution phase and may provide further insight into the reactivity of enol ether olefin cation radicals in solution.[97-102]

Dimethylketal **102** is also produced in low yields from photolysis of both radical precursors. Based on the ratio of **102**:**105** generated from both radical precursors, it is apparent that **102** and **105** arise from an intermediate common to both systems, olefin cation radical **103**. Kinetic experiments carried out using LFP have provided an upper limit of 1×10^3 M^{-1} s^{-1} for the reaction of methanol with olefin cation radical **103**. While this rate is on the order of four orders of magnitude slower than that reported for the

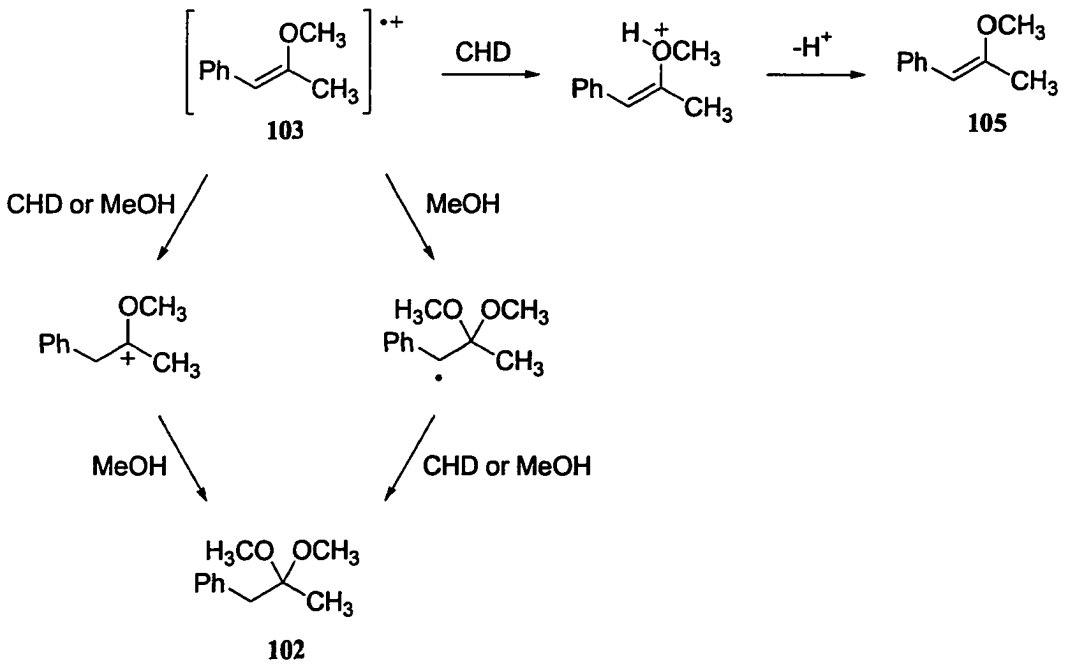

Figure 31. Mechanism for the formation of **102** and **105** from **103**.

reaction of methanol with the styrene radical cation, it is only one to two orders of magnitude slower than that reported for the reaction of methanol with **90**.[15] The slower rate of reaction most likely reflects the increased steric hindrance and increased stability of **103** relative to the styrene cation radical.

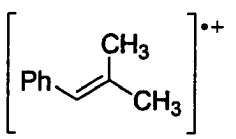

90

Product studies suggest that methanol reacts with **103** either by nucleophilic attack at the homobenzylic position of **103** to generate a benzylic radical which is

quenched by hydrogen atom transfer from CHD and/or methanol to the benzylic carbon of **103** followed by nucleophilic trapping of the resulting oxocarbenium ion by methanol (Scheme 31). Based on the ratio of rate constants for methanol and CHD reaction with **103**, it is clear that nucleophilic trapping of **103** by methanol is not the sole pathway accounting for the formation of **102**. Most likely, **102** is produced through a combination of both reaction motifs.

4 Experimental Methods.

General Methods: All reactions were performed under an argon atmosphere in oven dried glassware. All chemicals were obtained commercially and purified according to known procedures: THF was distilled from sodium benzophenone ketyl; acetonitrile was passed through anhydrous copper sulfate and then distilled from calcium hydride; methylene chloride, diisopropylethylamine, *N,N*-dimethylbenzylamine, and methanol were distilled from calcium hydride; benzaldehyde and benzylbromide were distilled from $MgSO_4$; diisopropylamine was distilled from NaOH; diethylether was distilled from sodium; CCl_4 and MeI were distilled from themselves. 2,2'-Dithiopyridine-1,1'-dioxide was prepared according to literature.[72] Bis(cyclopentadienyl)dimethyltitanium was prepared according to literature, and stored as a 0.5 M solution in THF in the dark.[106] All other reagents were used as received. Alkyl lithium reagents were titrated prior to use using 1,10-phenanthroline as the indicator and *sec*-butanol (1.0 M in benzene) as the titrant.

^1H NMR spectra were referenced to $CHCl_3$ (7.27 ppm), ^{13}C NMR spectra were referenced to $CDCl_3$ (77.23 ppm), and ^{31}P NMR spectra were referenced to H_3PO_4 (0 ppm). GC analyses were performed using a 60 m CP-SIL19CB column and He as the carrier gas with the retention times and response factors shown in Table 11. Oven conditions were as follows: Initial temperature 90 °C for 7 min, rate 5 °C/min to 150 °C, rate 20 °C/min to 190 °C for 3 min, rate 20 °C/min to 250 °C for 8 min. GC/MS analyses were performed using a 50 m DB-1 column and He as the carrier gas with the retention times and selective ion monitoring (SIM) shown in Table 12. Oven conditions were as follows: initial temperature 70 °C, rate 10 °C/min to 170 °C for 2 min.

Table 11. Response factors and retention times for analytical GC analysis of **102**, **104**, **105**, **108**, and **109**.[a]

Compound	Retention Time	Response Factor[b]
102	22.9 min	1.48
104	21.0 and 21.7 min	1.38
E-**105**	23.3 min	1.97
Z-**105**	21.2 min	1.97
108	20.8 min	1.49
109	18.3 min	1.62

[a] See text for oven conditions. [b] Determined from plots of [X]/[Decane] versus A_X/A_{Decane}.

Table 12. Retention times and SIM masses for GC/MS analysis of **102**, *Z*-**105**, and **109**.[a]

Compound	Retention Time	SIM mass
102	8.0 min	149.1, 150.1[b]
Z-**105**	7.0 min	148.1, 149.1
109	5.5 min	150.1, 151.1

[a] See text for oven conditions. [b] 152.1 and 153.1 were used when d_4-MeOH was used as solvent.

Laser Flash Photolysis Studies. Laser flash photolysis studies were carried out by Professor Martin Newcomb and John H. Horner at Wayne State University and were performed in the general manner previously reported.[58] Flowing solutions of **98** and **99** with an absorbance at 355 nm of approximately 0.4 AU were employed. The samples were irradiated with 355 nm light (third harmonic) from a Nd-YAG laser. Kinetic analyses were performed with Applied Photophysics software.

Continual photolysis of PTOCs. All samples were prepared by syringe in pyrex tubes wrapped in aluminum foil at the following concentrations in 4:1 MeOH/AcN: PTOC (5 mM), 2,6-di-*t*-butylpryidine (10 mM), 1,4-cyclohexadiene (0.5 M), and

dodecane (2.2 mM) as internal standard. The samples were degassed (freeze, pump 3 min, thaw; 3 cycles), sealed *in vacuo*, and irradiated for 20 min at λ_{max} = 350 nm in a Rayonet photoreactor (16 lamps). After irradiation, the samples were stored at 77 K prior to GC analysis.

Product stability studies. Samples were prepared by syringe in pyrex tubes wrapped in aluminum foil at the following concentrations in 4:1 MeOH/AcN: product (0.083 – 5.0 mM), PTOC (5 mM), 2,6-di-*t*-butylpyridine (10 mM), 1,4-cyclohexadiene (0.5 M), and dodecane (2.2 mM) as internal standard. The samples were then degassed, photolyzed, and stored as described above prior to GC analysis.

PTOC stability studies. NMR samples were prepared by syringe in NMR tubes wrapped in aluminum foil at the following concentrations in 4:1 d_4-MeOH/d_3-AcN: PTOC (26 mM), diisopropylethylamine (53 mM), and hexamethyldisilane (1.5 mM) as an internal standard). The samples were stored in the dark at rt for 12 h and ^{1}H NMR spectra were obtained at 0, 0.5, 2, 4, 11, and 12 h.

1-(Diphenylphosphatoxy)-2-methoxy-1-phenylpropane (101) thermal stability studies. NMR samples were prepared by syringe in NMR tubes at the following concentrations in 4:1 d_4-MeOH/d_3-AcN: **101** (26 mM), 1,4-cyclohexadiene (53 mM), 2,6-di-*t*-butylpyridine (53 mM), and hexamethyldisilane (1.5 mM) as an internal standard. The samples were then thermolyzed at 50 °C for 6 d. ^{1}H and ^{31}P NMR spectra were obtained at 1, 2, 4, 8, 20, 48, 96, and 144 h.

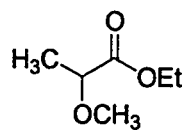

Synthesis of ethyl (*S*)-2-methoxypropanoate (112). To a solution containing NaH (2.246 g, 94.3 mmol) dissolved in THF (135 mL) at 0 °C was added ethyl-(*S*)-(-)-lactate (**111**) (10.42 g, 88.2 mmol) over a period of 1 h. To the solution was then added MeI (15.04 g, 106 mmol), the solution was warmed to rt, and stirred for 12 h. The reaction was quenched by the addition of saturated NH_4Cl (100 mL) and extracted with Et_2O (3x75 mL). The organic layers were combined, washed with brine (75 mL), and dried over anhydrous $MgSO_4$. Filtration and removal of the solvent left a yellow oil. The oil was purified by distillation (60 °C at ~20 mmHg) to provide 6.93 g (60%) of the desired product as a clear oil: ^{1}H NMR ($CDCl_3$) δ 4.28 (q, J = 7.2 Hz, 2H), 3.90 (q, J = 6.6 Hz, 1H), 3.42 (s, 3H), 1.43 (d, J = 6.6 Hz, 3H), 1.33 (t, J = 7.2 Hz, 3H). ^{13}C NMR ($CDCl_3$) δ 173.4, 76.7, 61.1, 57.9, 18.6, 14.5. IR (neat on salt plate) 2986, 1748, 1270, 1193, 1071, 1033 cm^{-1}.

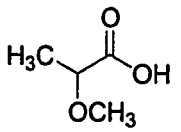

Synthesis of 2-methoxypropionic acid (113). A solution containing ethyl-(S)-2-methoxypropionate (**112**) (3.175 g, 24.0 mmol) and KOH (3.36 g, 60.0 mmol) dissolved in 95% ethanol (40 mL) was refluxed for 3 h. The ethanol was removed *in vacuo* to leave a yellow oil which was taken up in H_2O (20 mL) and extracted with EtOAc (3x15 mL). The aqueous layer was then acidified to pH 1 with 6 N HCl and extracted with EtOAc (3x15 mL). The organic layers from the second extraction were combined, washed with brine (15 mL), and dried over anhydrous $MgSO_4$. Filtration and removal of the solvent left a yellow oil which was purified by distillation (60 °C, ~1 mmHg) to give 2.26 g (92%) of the desired product: ^{1}H NMR ($CDCl_3$) δ 11.36 (bs, 1H), 3.91 (q, J = 6.9 Hz, 1H), 1.44 (d, J = 6.9 Hz, 3H), 3.42 (s, 3H).

^{13}C NMR ($CDCl_3$) δ 178.6, 76.2, 58.0, 18.3. IR (neat on salt plate) 2990, 2942, 1731, 1463, 1201, 1069, 855 cm^{-1}.

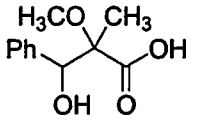

Synthesis of 3-hydroxy-2-methoxy-2-methyl-3-phenylpropionic acid (110). To a solution containing diisopropylamine (1.03 g, 10.2 mmol) dissolved in THF (33.5 mL) at -78 °C was added 1.03 M *sec*-BuLi in hexanes (9.4 mL, 9.68 mmol) and the resulting solution was stirred at -78 °C for 5 min followed by warming to rt. To the solution was added a solution containing 2-methoxypropionic acid (**113**) (0.5038 g, 4.88 mmol) dissolved in THF (4.5 mL) and the resulting solution was stirred at rt for 1 h. To the solution was then added benzaldehyde (0.511 g, 4.85 mmol), the reaction was stirred at rt for 24 h, and quenched by pouring over ice. The resulting aqueous layer was extracted with Et_2O (5x50 mL). The aqueous layer was then acidified to pH 1 with 6 N HCl and then extracted with Et_2O (3x50 mL). The organic layers from the second extraction were combined, washed with brine (50 mL), and dried over anhydrous $MgSO_4$. Filtration and removal of the solvent left a gold oil. Flash column chromatography (50 g silica gel) (EtOAc/hexanes 50:50) yielded 0.9937 g (97%) of the desired product: ^1H NMR ($CDCl_3$) δ 7.36-7.25 (m, 5H), 4.87 (s, 1H), 3.35 (s, 3H), 1.37 (s, 3H). ^{13}C NMR ($CDCl_3$) δ 175.7, 138.0, 128.5, 128.2, 127.6, 83.2, 78.5, 52.9, 16.2. IR (neat on salt plate), 3429, 3032, 2992, 2836, 1720, 1454, 1116, 701 cm^{-1}.

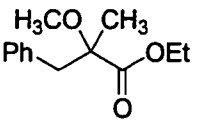

Synthesis of ethyl 2-methoxy-2-methyl-3-phenylpropionate (115). To a solution containing diisopropylamine (1.032 g, 10.2 mmol)

dissolved in THF (65 mL) at 0 °C was added 2.0 M *n*-BuLi in cyclohexane (4.90 mL, 9.80 mmol). The solution was stirred for 10 min at 0 °C and then cooled to -78 °C. To the solution was then added a solution containing ethyl (*S*)-2-methoxypropionate (**112**) (1.077 g, 8.15 mmol) dissolved in THF (10.0 mL). The solution was stirred at -78 °C for 30 min and benzylbromide (2.16 g, 12.6 mmol) was added. The solution was warmed to rt and stirred for 16 h. The reaction was quenched by the addition of saturated NH_4Cl (75 mL) and extracted with EtOAc (3x50 mL). The organic layers were combined, washed with brine (50 mL), and dried over anhydrous $MgSO_4$. Filtration and removal of the solvent left a yellow oil. Flash column chromatography (40 g silica gel) (EtOAc/hexanes:20/80) yielded 1.494 g (83%) of the desired compound as a colorless oil: ^{1}H NMR ($CDCl_3$) δ 7.31-7.22 (m, 5H), 4.22 (q, J = 6.0 Hz, 2H), 3.36 (s, 3H), 3.07 (m, 2H), 1.39 (s, 3H), 1.29 (t, J = 6.0 Hz, 3H). ^{13}C NMR ($CDCl_3$) δ 173.7, 136.2, 130.5, 128.0, 126.7, 81.0, 61.0, 52.1, 44.7, 19.9, 14.2. IR (neat on salt plate) 2983, 1733, 1455, 1190, 1104, 700 cm^{-1}.

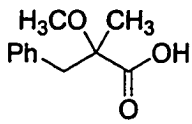

Synthesis of 2-methoxy-2-methyl-3-phenylpropionic acid (116). A solution containing ethyl 2-methoxy-2-methyl-3-phenylpropionate (**115**) (1.072 g, 4.85 mmol) and KOH (0.704 g, 12.6 mmol) dissolved in 95% EtOH (48 mL) was refluxed for 3 h. The EtOH was removed *in vacuo* and the remaining oil was dissolved in H_2O (20 mL) and extracted with EtOAc (3x15 mL). The aqueous layer was then acidified to pH 1 with 6N HCl and extracted with EtOAc (3x15 mL). The organic layers from the second extraction were combined, washed with brine (15 mL), and dried over anhydrous $MgSO_4$. Filtration and removal of the solvent left 0.906 g

(96%) of the desired acid as a clear oil: ^{1}H NMR ($CDCl_3$) δ 9.90 (bs, 1H), 7.31-7.19 (m, 5H), 3.44 (s, 3H), 3.08 (m, 2H), 1.53 (s, 3H). ^{13}C NMR ($CDCl_3$) δ 178.4, 135.7, 130.5, 128.4, 127.1, 81.1, 52.1, 43.6, 20.2. IR (neat on salt plate), 2926, 1712, 1453, 1101 cm^{-1}.

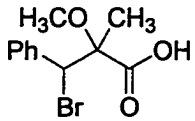

Synthesis of 3-bromo-2-methoxy-2-methyl-3-phenyl-propionic acid (117). To a sparged solution containing 2-methoxy-2-methyl-3-phenylpropionic acid (**116**) (0.090 g, 0.463 mmol) and *N*-bromosuccinimide (0.168 g, 0.942 mmol) dissolved in freshly distilled CCl_4 (4 mL) was added AIBN (0.0105 g, 0.064 mmol) and the solution was refluxed for 30 min. The cooled solution was filtered to remove succinamide, and removal of the solvent left a yellow oil. The crude oil was carried on as a 1:1 mixture of diastereomers without further purification: ^{1}H NMR (crude) ($CDCl_3$) (Diastereomer A) δ 9.22 (bs, 1H), 7.57-7.31 (m, 5H), 5.27 (s, 1H), 3.47 (s, 3H), 1.67 (s, 1H); (Diastereomer B) δ 9.22 (bs, 1H), 7.57-7.31 (m, 5H), 5.27 (s, 1H), 3.49 (s, 3H), 1.40 (s, 3H). IR (neat on salt plate) 2927, 1718, 1100, 699 cm^{-1}.

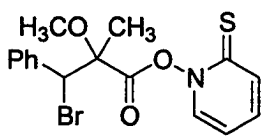

Synthesis of (1H)-2-thioxo-1-pyridyl 3-bromo-2-methoxy-2-methyl-3-phenylpropionate (98). A solution containing 3-bromo-2-methoxy-2-methyl-3-phenyl-propionic acid (**117**) (0.443 g, 1.62 mmol), PPh_3 (0.533 g, 2.03 mmol), and 2,2'-dithiopyridine-1,1'-dioxide (0.490 g, 1.94 mmol) dissolved in CH_2Cl_2 (16 mL) was stirred in the dark at rt for 1 h. The reaction was quenched by the addition of 5% Na_2CO_3 (10 mL) and extracted with CH_2Cl_2 (3x10 mL). The organic layers were combined, washed with brine (10 mL), and dried

over anhydrous $MgSO_4$. Filtration and removal of the solvent in vacuo in the dark left a yellow oil. Flash column chromatography (30 g silica gel) (EtOAc/hexanes:40/60) in the dark provided 0.256 g (41% over two steps) of the desired PTOC as a 1:1 mixture of diastereomers: ^{1}H NMR ($CDCl_3$) (Diastereomer A) δ 7.76-7.59 (m, 3H), 7.41-7.14 (m, 5H), 6.77-6.72 (m, 1H), 5.25 (s, 1H), 3.75 (s, 3H), 1.91 (s, 3H); (Diastereomer B) δ 7.76-7.59 (m, 3H), 7.41-7.14 (m, 5H), 6.59-6.56 (m, 1H), 5.31 (s, 1H), 3.71 (s, 3H), 1.64 (s, 3H). ^{13}C NMR ($CDCl_3$) δ 138.0, 137.5, 137.4, 137.3, 137.2, 136.4, 133.5, 133.0, 130.4, 130.3, 129.3, 129.0, 128.6, 128.4, 128.1, 84.2, 83.8, 59.2, 58.6, 54.8, 54.2, 20.0, 19.7. IR (neat on salt plate) 3080, 1794, 1607, 1447, 1130 cm^{-1}. HRMS (FAB) $C_{16}H_{16}BrNO_3S$ calcd. (M+H): 384.0092, found: 384.0092.

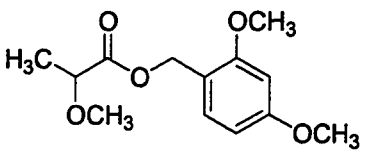

Synthesis of 2,4-dimethoxybenzyl 2-methoxypropionate (118). To a solution containing 2-methoxypropoinic acid (**113**) (0.726 g, 6.98 mmol), 2,4-dimethoxybenzyl alcohol (1.249 g, 7.43 mmol), and PyBOP (4.389 g, 8.43 mmol) dissolved in CH_2Cl_2 (50 mL) was added diisopropylethylamine (1.981 g, 15.3 mmol). The reaction was stirred at rt for 3 h and quenched by the addition of H_2O (40 mL). The resulting solution was then extracted with CH_2Cl_2 (3x30 mL). The organic layers were combined, washed with brine (50 mL), and dried over anhydrous $MgSO_4$. Filtration and removal of the solvent left a purple oil. Flash column chromatography (40 g silica gel) (EtOAc/hexanes:40/60) yielded 1.503 g (85%) of the desired ester as a clear oil: ^{1}H NMR ($CDCl_3$) δ 7.34-7.33 (m, 1H), 6.56-6.52 (m, 2H), 5.30-5.10 (m, 2H), 3.96 (q, J = 6.9 Hz, 1H), 3.90 (s, 3H), 3.46 (s, 3H), 1.47(d, J = 6.9 Hz, 3H). ^{13}C NMR ($CDCl_3$) δ

173.5, 161.6, 116.6, 104.2, 98.8, 76.6, 62.4, 57.9, 55.6, 18.7. IR (neat on salt plate), 2985, 1744, 1617, 1380, 1035 cm^{-1}.

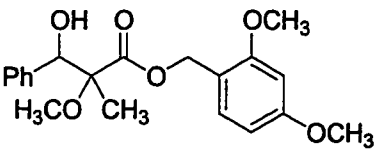

Synthesis of 2,4-dimethoxybenzyl 3-hydroxy-2-methoxy-2-methyl-3-phenylpropionate (119). To a solution containing diisopropylamine (0.298 g, 2.94 mmol) dissolved in THF (10 mL) at 0 °C was added 1.9 M *n*-BuLi in cyclohexane (1.48 mL, 2.81 mmol). The solution was stirred at 0 °C for 10 min and then cooled to -78 °C. To the solution was then added a solution containing 2,4-dimethoxybenzyl 2-methoxypropionate (**118**) (0.599 g, 2.35 mmol) dissolved in THF (11 mL). The resulting solution was stirred at -78 °C for 30 min at which point benzaldehyde (0.376 g, 3.54 mmol) was added. The reaction was stirred at -78 °C for 1.5 h and quenched by the addition of saturated NH_4Cl (20 mL). The solution was warmed to rt and extracted with EtOAc (3x20 mL). The organic layers were combined, washed with brine (20 mL), and dried over anhydrous $MgSO_4$. Filtration and removal of the solvent left a yellow oil. Flash column chromatography (25 g silica gel) (EtOAc/hexanes:20/80) yielded 0.780 g (92%) of the desired alcohol as a 2:1 mixture of diastereomers: ^1H NMR ($CDCl_3$) (Diastereomer A) δ 7.38-7.18 (m, 6H), 6.51 (m, 2H), 5.15 (m, 2H), 4.89 (d, J = 4.8 Hz, 1H), 3.85 (s, 6H), 3.34 (s, 3H), 3.27 (d, J = 4.8 Hz, 1H), 1.38 (s, 3H); (Diastereomer B) δ 7.38-7.18 (m, 6H), 6.48 (m, 2H), 5.23 (m, 2H), 5.01 (d, J = 4.6 Hz, 1H), 3.85 (s, 6H), 3.37 (s, 3H), 3.19 (d, J = 4.6 Hz, 1H), 1.26 (s, 3H). ^{13}C NMR ($CDCl_3$) δ 172.3, 161.6, 159.2, 139.1, 131.8, 128.0, 127.9, 127.8, 116.4, 104.2, 100.5, 98.8, 88.5, 83.9, 83.6, 78.5,

78.1, 66.1, 62.9, 55.6, 52.7, 52.6, 16.3, 15.5, 15.2. IR (neat on salt plate) 3508, 3062, 2992, 1731, 1615, 1590, 1377, 1209 cm^{-1}.

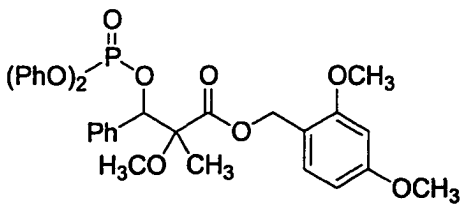

Synthesis of 2,4-dimethoxybenzyl 3-(diphenylphosphatoxy)-2-methoxy-2-methyl-3-phenylpropionate (120). To a solution containing 2,4-dimethoxybenzyl 3-hydroxy-2-methoxy-2-methyl-3-phenylpropionate (**119**) (0.376 g, 1.08 mmol) and DMAP (0.158 g, 1.29 mmol) dissolved in CH_2Cl_2 (10.8 mL) was added diphenylchlorophosphate (0.347 g, 1.29 mmol). The solution was stirred at rt for 14 h and quenched by the addition of H_2O (10 mL). The solution was then extracted with EtOAc (3x10 mL). The organic layers were combined, washed with brine (10 mL), and dried over anhydrous $MgSO_4$. Filtration and removal of the solvent left a yellow oil. Flash column chromatography (20 g silica gel) (EtOAc/hexanes:40/60) yielded 0.519 g (81%) of the desired product as a 2:1 mixture of diastereomers: ^1H NMR ($CDCl_3$) (Diastereomer A) δ 7.38-7.10 (m, 15 H), 6.97-6.93 (m, 2H), 6.47-6.44 (m, 2H), 5.82 (d, J = 9.3 Hz, 1H), 5.20-4.96 (m, 2H), 3.85 (s, 6H), 3.26 (s, 3H), 1.48 (s, 3H); (Diastereomer B) δ 7.38-7.10 (m, 15 H), 6.97-6.93 (m, 2H), 6.47-6.44 (m, 2H), 5.86 (d, J = 8.4 Hz, 1H), 5.16-4.96 (m, 2H), 3.82 (s, 6H), 3.32 (s, 3H), 1.33 (s, 3H). ^{13}C NMR ($CDCl_3$), δ 186.7, 159.2, 131.9, 130.1, 129.7, 128.6, 127.8, 126.2, 125.4, 120.2, 104.2, 100.2, 98.6, 95.0, 82.0, 62.9, 55.6, 52.4, 16.0. ^{31}P NMR ($CDCl_3$) (Diastereomer A) δ -13.12; (Diastereomer B) -12.84. IR (neat on salt plate) 3066, 2946, 1950, 1876, 1737, 1613, 1592, 1490, 1291, 1191, 1031, 956 cm^{-1}.

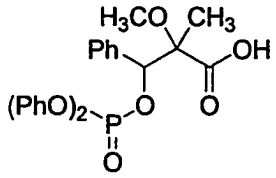

Synthesis of 3-(diphenylphosphatoxy)-2-methoxy-2-methyl-3-phenylpropionic acid (121). To a solution containing 2,4-dimethoxybenzyl 3-(diphenyl-phosphatoxy)-2-methoxy-2-methyl-3-phenylpropionate (**120**) (0.237 g, 0.399 mmol) dissolved in 10:1 AcN/H_2O (10 mL) was added CAN (0.482 g, 0.879 mmol). The reaction was stirred at rt for 1 h, quenched by the addition of H_2O (10 mL), and extracted with EtOAc (3x10 mL). The organic layers were combined, washed with brine (10 mL), and dried over anhydrous $MgSO_4$. Filtration and removal of the solvent left an orange oil. The oil was taken up in EtOAc (20 mL) and stirred with 15% $NaHSO_3$ (20 mL) for 2 h. The layers were separated, the organic layer was washed with H_2O (20 mL), brine (20 mL), and dried over anhydrous $MgSO_4$. Filtration and removal of the solvent left a light orange oil as 3:1 mixture of diastereomers which was carried on without further purification: ^1H NMR ($CDCl_3$) (Diastereomer A) δ 7.45-7.11 (m, 13 H), 7.00-9.97 (m, 2H), 5.81 (d, J = 9.0 Hz, 1H), 3.48 (s, 3H), 1.51 (s, 3H); (Diastereomer B) δ 7.45-7.11 (m, 13 H), 6.95-6.92 (m, 2H), 5.76 (d, J = 8.7 Hz, 1H), 3.35 (s, 3H), 1.37 (s, 3H). ^{31}P NMR ($CDCl_3$) (Diastereomer A) δ -12.61; (Diasteromer B) -12.44. IR (neat on salt plate) 2994, 1739, 1675, 1598, 1456, 1280, 1188, 1023, 959 cm^{-1}.

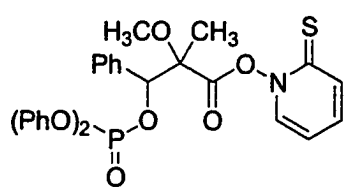

Synthesis of (1H)-2-thioxo-1-pyridyl 3-(diphenyl-phosphatoxy)-2-methoxy-2-methyl-3-phenylpropionate (99). A solution containing 3-(diphenylphosphatoxy)-2-methoxy-2-methyl-3-phenylpropionic acid (**120**) (0.264 g, 0.597 mmol), 2,2'-dithiopyridine-1,1'-dioxide (0.157 g, 0.623 mmol), and triphenylphosphine (0.193 g,

0.735 mmol) dissolved in CH_2Cl_2 (6 mL) was stirred in the dark at rt for 1 h. The reaction was quenched by the addition of 10% Na_2CO_3 (10 mL) and the solution was extracted with CH_2Cl_2 (3x10 mL). The organic layers were combined, washed with brine (10 mL), and dried over anhydrous $MgSO_4$. Filtration and removal of the solvent left a yellow oil. Flash column chromatography in the dark (12 g silica gel) (EtOAc/hexanes:80/20) gave 0.204 g (62% over two steps) of the desired product as a 3:1 mixture of diastereomers: ^{1}H NMR ($CDCl_3$) (Diastereomer A) δ 7.86-7.68 (m, 2H), 7.64-7.11 (m, 14 H), 6.95-6.92 (m, 2H), 6.55-6.47 (m, 1H), 5.85 (d, J = 9.0 Hz, 1H), 3.59 (s, 3H), 1.65 (s, 3H); (Diastereomer B) δ 7.86-7.68 (m, 2H), 7.64-7.11 (m, 14 H), 6.87-6.84 (m, 2H), 6.55-6.47 (m, 1H), 5.84 (d, J = 9.0 Hz, 1H), 3.60 (s, 3H), 1.63 (s, 3H). ^{13}C NMR ($CDCl_3$) δ 138.7, 137.0, 130.0, 129.9, 129.5, 129.2, 128.7, 128.2, 128.0, 125.9, 125.6, 120.6, 120.5, 120.1, 120.0, 83.0, 54.1, 53.6, 15.1. ^{31}P NMR ($CDCl_3$) (Diasteromer A) δ -12.79; (Diastereomer B) -11.97. IR (neat on salt plate) 3073, 1800, 1654, 1608, 1590, 1489, 1410, 1376, 1282, 1022, 960 cm^{-1}. HRMS (FAB) $C_{28}H_{26}NO_7PS$ calcd. (M+H): 552.1245, found: 552.1237.

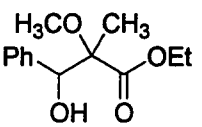

Synthesis of ethyl 3-hydroxy-2-methoxy-2-methyl-3-phenylpropionate (123). To a solution containing diisopropylamine (0.939 g, 9.28 mmol) dissolved in THF (35 mL) at 0 °C was added 1.9 M *n*-BuLi in cyclohexane (4.70 mL, 8.93 mmol). The solution was stirred at 0 °C for 10 min and then cooled to -78 °C and a solution containing ethyl 2-methoxypropionate (**112**) (0.987 g, 7.47 mmol) dissolved in THF (10 mL) was added. The solution was stirred at -78 °C for 30 min and benzaldehyde (1.19 g, 11.2 mmol) was added. After stirring for 1.5

h at -78 °C the reaction was quenched by the addition of saturated NH_4Cl (50 mL). The resulting solution was extracted with EtOAc (3x50 mL). The organic layers were combined, washed with brine (50 mL), and dried over anhydrous $MgSO_4$. Filtration and removal of the solvent left a yellow oil. Flash column chromatography (40 g silica gel) (EtOAc/hexanes:50/50) gave 1.63 g (92%) the desired compound as a 6:1 mixture of diastereomers: ^1H NMR ($CDCl_3$) (Diastereomer A) δ 7.36-7.25 (m, 5H), 4.82 (d, J = 4.5 Hz, 1H), 4.11-4.06 (m, 2H), 3.37 (d, J = 4.5 Hz, 1H), 3.29 (s, 3H), 1.34 (s, 3H), 1.17 (t, J = 6.9 Hz, 3H); (Diastereomer B) δ 7.36-7.25 (m, 5H), 4.88 (d, J = 5.7 Hz, 1H), 4.11-4.06 (m, 2H), 3.36 (s, 3H), 3.25 (d, J = 5.7 Hz, 1H), 1.34 (s, 3H), 1.40 (t, J = 3.6 Hz, 3H). ^{13}C NMR ($CDCl_3$) δ 172.7, 172.2, 139.1, 138.6, 128.0, 127.8, 127.7, 127.6, 83.6, 83.2, 78.5, 78.1, 61.3, 61.1, 52.5, 52.4, 16.4, 16.2, 15.1, 14.3, 14.2. IR (neat on salt plate) 3496, 3062, 2986, 1959, 1887, 1732, 1604, 1551, 1254, 1114, 1055, 911 cm^{-1}.

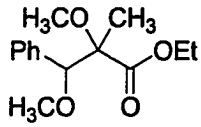

Synthesis of ethyl 2,3-dimethoxy-2-methyl-3-phenylpropionate (124). To a solution containing NaH (0.0714 g, 2.97 mmol) dissolved in THF (10 mL) at -78 °C was added a solution containing ethyl 3-hydroxy-2-methoxy-2-methyl-3-phenylpropionate (**123**) (0.465 g 1.95 mmol) dissolved in THF (9 mL). The solution was stirred at -78 °C for 20 min and MeI (0.551 g, 3.89 mmol) was then added. The solution was slowly warmed to rt, quenched by the addition of saturated NH_4Cl (15 mL), and extracted with EtOAc (3x15 mL). The organic layers were combined, washed with brine (15 mL), and dried over anhydrous $MgSO_4$. Filtration and removal of the solvent left a yellow oil. Flash column chromatography (15 g silica gel) (EtOAc/hexanes:20/80) provided 0.323 g (66%) of the desired compound as a 3:2

mixture of diastereomers: ^{1}H NMR ($CDCl_3$) (Diastereomer A) δ 7.42-7.35 (m, 5H), 4.55 (s, 1H), 4.36-4.22 (m, 2H), 3.29 (s, 3H), 3.21 (s, 3H), 1.39-1.30 (m, 3H), 1.24 (s, 3H); (Diastereomer B) δ 7.42-7.35 (m, 5H), 4.46 (s, 1H), 4.36-4.22 (m, 2H), 3.39 (s, 3H), 3.24 (s, 3H), 1.39-1.30 (m, 3H), 1.28 (s, 3H). ^{13}C NMR ($CDCl_3$) δ 173.3, 172.8, 136.7, 136.3, 129.3, 128.5, 128.3, 127.9, 127.8, 88.5, 86.5, 83.0, 61.2, 57.8, 57.6, 53.0, 52.1, 17.3, 14.6, 14.5. IR (neat on salt plate) 3062, 2984, 1958, 1886, 1737, 1493, 1371, 1254, 1172 cm^{-1}.

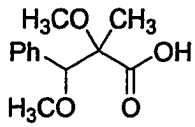

Synthesis of 2,3-dimethoxy-2-methyl-3-phenylpropionic acid (125). A solution containing ethyl 2,3-dimethoxy-2-methyl-3-phenylpropionate (**124**) (0.322 g, 1.28 mmol) and KOH (0.373 g, 6.66 mmol) dissolved in 95% EtOH (12.8 mL) was refluxed for 16 h. The reaction was cooled and the EtOH was removed *in vacuo*. The remaining residue was taken up in H_2O (10 mL) and extracted with EtOAc (3x10 mL). The aqueous layer was acidified to pH 1 with 6 N HCl and extracted with EtOAc (3x10 mL). The organic layers from the second extraction were combined, washed with brine (10 mL), and dried over anhydrous $MgSO_4$. Filtration and removal of the solvent left 0.241 g (84%) of the desired acid as an off white solid (m.p.= 109-110 °C) (1:1 mixture of diastereomers): ^{1}H NMR ($CDCl_3$) (Diastereomer A) δ 9.75 (bs, 1H), 7.43-7.36 (m, 5H), 4.50 (s, 1H), 3.35 (s, 3H), 3.28 (s, 3H), 1.41 (s, 3H); (Diastereomer B) δ 9.75 (bs, 1H), 7.43-7.36 (m, 5H), 4.37 (s, 1H), 3.46 (s, 3H), 3.29 (s, 3H), 1.33 (s, 3H). ^{13}C NMR ($CDCl_3$) δ 177.1, 175.8, 136.1, 135.6, 129.4, 128.7, 128.5, 128.3, 88.1, 87.1, 83.0, 82.7, 58.0, 57.7, 53.2, 52.7, 17.6, 15.6. IR (KBr pellet) 3083, 3001, 2942, 1717, 1491, 1290, 1144, 1057, 942 cm^{-1}.

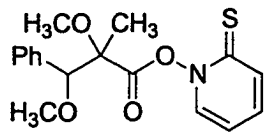

Synthesis of (1H)-2-thioxo-1-pyridyl 2,3-dimethoxy-2-methyl-3-phenylpropionate (122). A solution containing 2,3-dimethoxy-2-methyl-3-phenylpropionic acid (**124**) (0.064 g, 0.285 mmol), PPh_3 (0.097 g, 0.371 mmol), and 2,2'-dithiopyridine-1,1'-dioxide (0.090 g, 0.357 mmol) dissolved in CH_2Cl_2 (2.85 mL) was stirred at rt in the dark for 1 h. The reaction was quenched by the addition of 10% Na_2CO_3 (5 mL) and extracted with CH_2Cl_2 (3x5 mL). The organic layers were combined, washed with brine (5 mL), and dried over anhydrous $MgSO_4$. Filtration and removal of the solvent left a yellow oil. Flash column chromatography in the dark (12 g silica gel) (EtOAc/hexanes:30/70) gave 0.078 g (82%) the desired PTOC as a yellow solid (3:2 mixture of diastereomers): ^1H NMR ($CDCl_3$) (Diastereomer A) δ 7.73-7.68 (m, 1H), 7.47-7.18 (m, 7H), 6.69-6.67 (m, 1H), 4.62 (s, 1H), 3.50 (s, 3H), 3.35 (s, 3H), 1.45 (s, 3H); (Diastereomer B) δ 7.73-7.68 (m, 1H), 7.47-7.18 (m, 7H), 6.69-6.67 (m, 1H), 4.51 (s, 1H), 3.59 (s, 3H), 3.27 (s, 3H), 1.52 (s, 3H). ^{13}C NMR ($CDCl_3$), δ 138.0, 137.8, 137.4, 135.7, 129.7, 128.9, 128.8, 128.6, 128.2, 89.1, 87.2, 57.9, 57.8, 54.1, 53.7, 18.2, 15.1. IR (neat on salt plate) 3095, 2992, 19798, 1608, 1408, 1281, 1132, 1030 cm^{-1}. HRMS (FAB) $C_{17}H_{19}NO_4S$ calcd. (M+H): 334.1113, found: 334.1117.

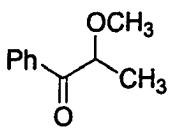

Synthesis of 2-methoxy-1-phenyl-1-propanone (128). To a solution containing diisopropylamine (0.736 g, 7.28 mmol) dissolved in THF (54 mL) at 0 °C was added 2.0 M *n*-BuLi in cyclohexane (3.56 mL, 6.98 mmol). The solution was stirred at 0 °C for 10 min and cooled to -78 °C. To the solution was then added 2-methoxyacetophenone (**127**) (0.872 g, 5.80 mmol). After stirring at -78

°C for 30 min MeI (1.81 g, 12.7 mmol) was added and the solution was allowed to warm to rt over a period of 16 h. The reaction was quenched by the addition of saturated NH_4Cl (50 mL) extracted with EtOAc (3x50 mL). The organic layers were combined, washed with brine (50 mL), and dried over anhydrous $MgSO_4$. Filtration and removal of the solvent left an orange oil. Flash column chromatography (20 g silica gel) (EtOAc/hexanes:10/90) provided 0.675 g (71%) of the desired product as a clear oil: ^1H NMR ($CDCl_3$) δ 7.87-7.85 (m, 2H), 7.40-7.25 (m, 3H), 4.47 (q, J = 6.9 Hz, 1H), 3.19 (s, 3H), 1.29 (d, J = 6.9 Hz, 3H). ^{13}C NMR ($CDCl_3$) δ 200.0, 134.6, 133.1, 128.4, 79.8, 57.0, 18.3. IR (neat on salt plate) 3062, 2984, 1694, 1127 cm^{-1}.

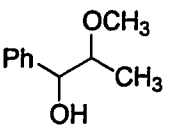

Synthesis of 2-methoxy-1-phenyl-1-propanol (126). To a solution containing 2-methoxy-1-phenyl-1-propanone (**128**) (0.134 g, 0.817 mmol) dissolved in MeOH (8.2 mL) was added $NaBH_4$ (0.0163 g, 0.431 mmol). The solution was stirred at rt for 3 h and quenched by the addition of brine (10 mL). The resulting solution was extracted with EtOAc (3x10 mL). The organic layers were combined, washed with brine (10 mL), and dried over anhydrous $MgSO_4$. Filtration and removal of the solvent left a yellow oil. Flash column chromatography (12 g silica gel) (EtOAc/hexanes: 30/70) yielded 0.116 g (85%) of the desired product as a 3:2 mixture of diastereomers: ^1H NMR ($CDCl_3$) (Diastereomer A) δ 7.42-7.29 (m, 5H), 4.91 (m, 1H), 3.55 (m, 1H), 3.42 (s, 3H), 3.20 (d, J = 3.0Hz, 1H), 1.05 (d, J = 6.3 Hz, 3H); (Diastereomer B) δ 7.42-7.29 (m, 5H), 4.44 (dd J = 5.7, 1.8 Hz, 1H), 3.60 (d, J = 1.8Hz, 1H), 3.42-3.40 (m, 1H), 3.45 (s, 3H), 1.01 (d, J = 5.7 Hz, 3H). ^{13}C NMR ($CDCl_3$) δ

140.8, 140.5, 128.2, 128.0, 127.8, 127.2, 127.1, 126.3, 81.7, 81.0, 78.2, 74.5, 56.7, 56.6, 14.8, 12.7. IR (neat on salt plate) 3490, 3064, 2993, 1154 cm^{-1}.

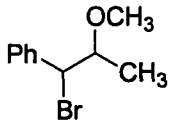

Synthesis of 1-bromo-2-methoxy-1-phenylpropane (100). A solution containing 2-methoxy-1-phenyl-1-propanol (**126**) (0.155 g, 0.930 mmol) and PBr_3 (0.100 g, 0.368 mmol) dissolved in Et_2O (9.3 mL) was stirred at 0 °C for 16 h. The reaction was quenched by the addition of H_2O (10 mL) and extracted with Et_2O (3x10 mL). The organic layers were combined, washed with brine (10 mL), and dried over anhydrous $MgSO_4$. Filtration and removal of the solvent left a yellow oil. Flash column chromatography (12 g silica gel) (EtOAc/hexanes: 10/90) yielded 0.070 g (33%) of the desired product as a 5:4 mixture of diastereomers: ^1H NMR ($CDCl_3$) (Diastereomer A) δ 7.50-7.30 (m, 5H), 4.89 (d, J = 6.9Hz, 1H), 3.76 (m, 1H), 3.72 (s, 3H), 1.12 (d, J = 6.3Hz, 3H); (Diastereomer B) δ 7.50-7.30 (m, 5H), 5.00 (d, J = 6.3Hz, 1H), 3.76 (m, 1H), 3.34 (s, 3H), 1.36 (d, J = 6.3Hz, 3H). ^{13}C NMR ($CDCl_3$) δ 139.7, 139.4, 128.8, 128.7, 128.6, 128.5, 128.4, 80.9, 80.8, 59.0, 58.4, 57.6, 57.5, 17.2, 17.1. IR (neat on salt plate) 3062, 2980, 1950, 1494, 1215, 1095 cm^{-1}. HRMS (EI) $C_{10}H_{13}BrO$ calcd.: 228.0150, found: 228.0147.

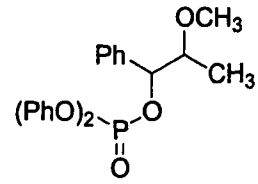

Synthesis of 1-(diphenylphosphatoxy)-2-methoxy-1-phenyl-propane (101). To a solution containing 2-methoxy-1-phenyl-1-propanol (**126**) (0.0510 g, 0.307 mmol) and DMAP (0.0601 g, 0.492 mmol) dissolved in CH_2Cl_2 (3 mL) was added diphenylchlorophosphate (0.100 g, 0.372 mmol). The solution was stirred at rt for 16 h and quenched by the addition of H_2O

(5 mL). The resulting solution was then extracted with CH_2Cl_2 (3x5 mL). The organic layers were combined, washed with brine (5 mL), and dried over anhydrous $MgSO_4$. Filtration and removal of the solvent left a yellow oil. Flash column chromatography (15 g silica gel) (EtOAc/hexanes:15/85) yielded 0.1084 g (89%) of the desired product as a 1:1 mixture of diastereomers: ^{1}H NMR ($CDCl_3$) (Diastereomer A) δ 7.39-6.94 (m, 15H), 5.58 (m, 1H), 3.71 (m, 1H), 3.35 (s, 3H), 1.27 (d, J = 6.0 Hz, 3H); (Diastereomer B) δ 7.39-6.94 (m, 15H), 5.45 (m, 1H), 3.71 (m, 1H), 3.39 (s, 3H), 0.97 (d, J = 6.0 Hz, 3H). ^{13}C NMR ($CDCl_3$) δ 150.8, 136.9, 129.9, 129.8, 129.7, 128.8, 128.6, 128.5, 128.4, 127.7, 127.4, 125.4, 125.3, 125.2, 120.6, 120.5, 120.4, 120.3, 84.8, 83.2, 83.1, 80.1, 80.0, 79.6, 79.5, 57.5, 15.3, 14.7. ^{31}P NMR ($CDCl_3$) (Diastereomer A) δ -11.6; (Diastereomer B) -11.8. IR (neat on salt plate) 3065, 2980, 1590, 1488, 1190, 1020 cm^{-1}. HRMS (FAB) $C_{22}H_{23}O_5P$ calcd.: (M+H): 399.1361, found: 399.1361.

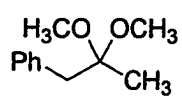

Synthesis of 2,2-dimethoxy-1-phenylpropane (102). A solution containing 1-phenyl-2-propanone (0.051 g, 0.38 mmol), *p*-toluenesulfonic acid (0.013 g, 0.68 mmol), and trimethylorthoformate (0.048 g, 0.45 mmol) in MeOH (3.7 mL) was heated to 30 °C for 2 h. The reaction was cooled to rt and sodium methoxide was added until the pH was neutral. The solution was then partitioned between Et_2O (10 mL) and H_2O (10 mL). The layers were separated, the organic layer was washed with brine (10 mL), and dried over anhydrous K_2CO_3. Removal of the solvent left a clear liquid. Flash column chromatography (4 g silica gel prewashed with hexanes/Et_3N:99/1) (100 % hexanes) yielded 0.068 g (99%) of the desired product as a clear oil: ^{1}H NMR ($CDCl_3$) δ 7.40-7.20 (m, 5H), 3.32 (s, 6H), 2.97 (s, 2H), 1.18 (s, 3H).

^{13}C NMR ($CDCl_3$) δ 137.6, 130.4, 128.2, 126.4, 102.0, 48.6, 43.0, 21.4. IR (neat on salt plate) 3028, 2988, 1496, 1125, 1050 cm^{-1}.

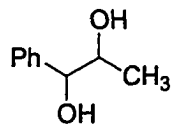

Synthesis of 1-phenyl-1,2-propandiol. To a solution containing *E,Z* β-methylstyrene (0.200 g, 1.7 mmol) and 60% *N*-methylmorpholine *N*-oxide in H_2O (2.93 mL, 17.0 mmol) dissolved in 6:1 acetone:H_2O (16 mL) was added one crystal of OsO_4. The solution was stirred at rt for 3 h and quenched by the addition of saturated $NaHSO_3$ (1 mL). The solution was stirred for an additional 20 min and then extracted with Et_2O (3x10 mL). The organic layers were combined and dried over anhydrous $MgSO_4$. Filtration and removal of the solvent left a brown oil. Flash column chromatography (20 g silica gel) (EtOAc/hexanes:40/60) yielded 0.210 g (81%) of the desired diol as a 1:1 mixture of diastereomers: ^1H NMR ($CDCl_3$) (Diastereomer A) δ 7.44-7.30 (m, 5H), 4.73 (dd, J = 4.1, 2.4 Hz, 1H), 4.07 (m, 1H), 2.44 (d, J = 3.0 Hz, 1H), 1.95 (d, J = 4.8 Hz, 1H), 1.14 (d, J = 6.9 Hz, 3H); (Diastereomer B) δ 7.44-7.30 (m, 5H), 4.42 (dd J = 7.2, 1.8 Hz, 1H) 3.91 (m, 1H), 2.70 (d, J = 3.0 Hz, 1H), 2.54 (d, J = 1.8 Hz, 1H), 1.11 (d, J = 6.6 Hz, 3H). IR (neat on salt plate) 3387, 3033, 1724, 1604, 1200, 1080 cm^{-1}.

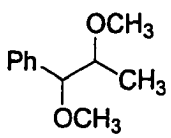

Synthesis of 1,2-dimethoxy-1-phenylpropane (104). A solution containing 1-phenyl-1,2-propandiol (0.160 g, 1.05 mmol) and NaH (0.161 g, 6.72 mmol) dissolved in THF (10.5 mL) was stirred at 0 °C for 30 min. To the solution was then added MeI (0.372 g, 2.61 mmol) and the solution was stirred at rt for 16 h. The reaction was quenched by the addition of saturated NH_4Cl (10 mL) and

extracted with EtOAc (3x10 mL). The organic layers were combined, washed with brine (10 mL), and dried over anhydrous $MgSO_4$. Filtration and removal of the solvent left a brown oil. Flash column chromatography (12 g silica gel) (EtOAc/hexanes:10/90) yielded 0.145 g (77%) of the desired product as a 1:1 mixture of diastereomers: ^{1}H NMR ($CDCl_3$) (Diastereomer A) δ 7.36-7.27 (m, 5H), 4.09 (d, J = 6.6 Hz, 1H), 3.52 (m, 1H), 3.43 (s, 3H), 3.30 (s, 3H), 0.92 (d, J = 6.6 Hz); (Diastereomer B) δ 7.36-7.27 (m, 5H), 4.20 (d, J = 4.2 Hz, 1H), 3.43 (m, 1H), 3.30 (s, 3H), 3.25 (s, 3H), 1.12 (d, J = 6.3 Hz, 3H). ^{13}C NMR ($CDCl_3$) δ 139.3, 128.4, 128.3, 128.0, 127.9, 127.7, 127.6, 87.6, 86.2, 80.8, 80.2, 57.4, 57.2, 15.8, 14.4. IR (neat on salt plate) 3189, 2938, 1612, 1248, 1116 cm^{-1}.

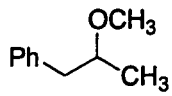

Synthesis of 2-methoxy-1-phenylpropane (109). To a solution containing NaH (0.115 g, 4.55 mmol) dissolved in THF (10 mL) at 0 °C was added a solution containing 1-phenyl-2-propanol (0.498 g, 3.65 mmol) dissolved in THF (26 mL). The solution was warmed to rt and after stirring for 30 min, MeI (0.713 g, 4.34 mmol) was added and the solution was stirred at rt for 14 h. The reaction was quenched by the addition of saturated NH_4Cl (30 mL) and extracted with Et_2O (3x30 mL). The organic layers were combined, washed with brine (30 mL), and dried over anhydrous $MgSO_4$. Filtration and removal of the solvent left 0.552 g (91%) of the desired ether as a light yellow oil: ^{1}H NMR ($CDCl_3$) δ 7.38-7.24 (m, 5H), 3.60 (sextuplet, J = 6.6 Hz, 1H), 3.40 (s, 3H), 2.99 (dd, J = 13.5, 6.3 Hz, 1H), 2.69 (dd, J = 13.2, 6.6 Hz, 1H), 1.19 (d, J = 6.3 Hz, 3H). ^{13}C NMR ($CDCl_3$)

δ 139.1, 129.5, 128.3, 126.2, 78.2, 56.5, 42.9, 19.1. IR (neat on salt plate) 3085, 2820, 1605, 1374, 1093 cm^{-1}.

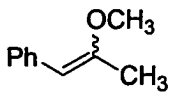

Synthesis of 2-methoxy-1-phenylpropene (105). To a solution containing 0.130 g (0.476 mmol) of 3-bromo-2-methoxy-2-methyl-3-phenylpropionic acid (**117**) dissolved in CH_2Cl_2 (4.8 mL) was added diisopropylethylamine (0.058 g, 0.574 mmol). The solution was stirred at rt for 1 min and the solvent was removed to leave a yellow oil. Flash column chromatography (8 g silica gel prewashed with hexanes/Et_3N:99/1) (100% hexanes) gave 0.070 g (98%) of the desired alkene as a 1:1 mixture of *E* and *Z* isomers: ^1H NMR ($CDCl_3$) (*E* isomer) δ 7.56-7.54 (m, 1H), 7.31-7.19 (m, 4H), 5.61 (s, 1H), 3.75 (s, 3H), 2.02 (s, 3H); (*Z* isomer) δ 7.56-7.54 (m, 1H), 7.31-7.19 (m, 4H), 5.33 (s, 1H), 3.68 (s, 3H), 2.07 (s, 3H). ^{13}C NMR ($CDCl_3$), δ 153.5, 136.8, 128.8, 128.2, 127.9, 125.3, 125.2, 106.6, 100.1, 99.6, 55.3, 54.7, 34.9, 25.5, 18.9, 18.1. IR (neat on salt plate) 3019, 2942, 1654, 1353, 1055 cm^{-1}.

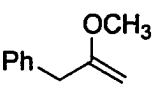

Synthesis of 2-methoxy-3-phenyl-1-propene (106). To a solution containing methyl phenylacetate (0.094 g, 0.626 mmol) dissolved in THF (3.6 mL) in the dark was added 0.5 M bis(cyclopentadienyl)dimethyl titanium in THF (2.60 mL, 1.30 mmol). The solution was refluxed in the dark for 60 h and quenched by removal of the solvent. Flash column chromatography (10 g silica gel prewashed with hexanes/Et_3N:99/1) (100% hexanes) yielded 0.038g (46%) of the desired compound as a clear oil: ^1H NMR ($CDCl_3$) δ 7.34-7.30 (m, 5H), 4.03 (d, J = 2.1 Hz, 1H), 3.95 (d, J =

2.1 Hz), 3.58 (s, 3H), 3.45 (s, 2H). ^{13}C NMR ($CDCl_3$) δ 163.3, 138.7, 129.0, 128.5, 126.5, 82.4, 55.2, 41.7. IR (neat on salt plate) 3062, 2965, 1655, 1282, 1065 cm^{-1}.

5 References.

[1] Wurster, C.; Sendtner, R. "Zur Kenntniss des Dimethylparaphenylen Diamins." *Chem. Ber.* **1879**, *12*, 1803-1807.

[2] Wurster, C. "Ueber die Durch Oxydationsmittel aus Di – und Tetraparaphenylendiamin Entstehenden Farbstoffe." *Chem. Ber.* **1879**, *12*, 2071-2072.

[3] Gomberg, M. "An Example of Trivalent Carbon" *J. Am. Chem. Soc.* **1900**, *22*, 757-771.

[4] von Baeyer, A.; Villiger, V. "Dibenzalaceton und Triphenylmathan. Ein Beitrag zur Farbtheorie." *Chem. Ber.* **1902**, *35*, 1189-1234.

[5] Weitz, E.; Schwechten, H. W. "Über den Ammonium-Charakter der Triarylamine (VII. Mitteiling über freie Ammonium Radikale." *Chem. Ber.* **1926**, *59*, 2307-2314.

[6] Michaelis, L. "Semiquinones, the Intermediate Steps of Reversible Organic Oxidation-Reduction." *Chem. Rev.* **1935**, *16*, 243-286.

[7] Weiss, J. "Simple Electron Transfer Processes in Systems of Conjugated Double Bonds." *Trans. Faraday Soc.* **1946**, *42*, 116-125.

[8] Meerwein, H.; Van Emster, K. "Über die Gleichgewichts-Isomerie Zwischen Bornylchlorid, Isobonylchlorid, und Camphen-Chlorhydrate." *Chem. Ber.* **1922**, *55*, 2500-2522.

[9] Paneth, F.; Hofeditz, W. "Über die Darstellung von Freiem Methyl." *Chem. Ber.* **1929**, *62*, 1335-1347.

[10] Schmittel, M.; Burghart, A. "Understanding Reactivity Patterns of Radical Cations." *Angew. Chem. Int. Ed. Engl.* **1997**, *36*, 2550-2589.

[11] Bauld, N. L. "Cation Radical Cycloadditions and Related Sigmatropic Reactions." *Tetrahedron.* **1989**, *45*, 5307-5363.

[12] Greenberg, M. M. "Investigating Nucleic Acid Damage Processes via Independent Generation of Reactive Intermediates." *Chem. Res. Toxicol.* **1998**, *11*, 1235-1248.

[13] Snider, B. B.; Shi, B.; Quickley, C. A. "Oxidative Cyclization of Unsaturated Ketene Dithioacetals with Ceric Ammonium Nitrate to Form Bicyclic Lactones." *Tetrahedron*, **2000**, *56*, 10127-10132.

[14] Kwon, T.; Snider, B. B. "Oxidative Cyclization of δ,ε- and ε,ζ- Unsaturated Enol Silyl Ethers." *J. Org. Chem.* **1990**, *55*, 4786-4788.

[15] Johnston, L. J.; Schepp, N. P. "Reactivities of Radical Cations: Characterization of Styrene Radical Cations and Measurements of Their Reactivity toward Nucleophiles." *J. Am. Chem. Soc.* **1993**, *115*, 6564-6571.

[16] Schepp, N. P.; Johnston, L. J. "Reactivity of Radical Cations. Absolute Kinetic Data for Cycloaddition Reactions of Styrene Radical Cations to Alkenes." *J. Am. Chem. Soc.* **1994**, *116*, 10330-10331.

[17] Bauld, N. L.; Pabon, R. "Cation Radical Catalyzed Olefin Cyclodimerization." *J. Am. Chem. Soc.* **1983**, *105*, 633-634.

[18] Bauld, N. L. "An ab Initio Theoretical Reaction Path Study of the Cation Radical Diels-Alder Reaction." *J. Am. Chem. Soc.* **1992**, *114*, 5800-5804.

[19] Dizdaroglu, M.; von Sonntag, C.; Schulte-Frohlinde, D. "Strand Breaks and Surgar Release by γ-Irradiation of DNA in Aqueous Solution." *J. Am. Chem. Soc.* **1975**, *97*, 2277-2278.

[20] Behrens, G.; Koltzenburg, G.; Schulte-Frohlinde, D. "Model Reactions for the Degradation of DNA-4' Radicals in Aqueous Solution. Fast Hydrolysis of α-Alkoxyalkyl Radicals with a Leaving Group in β-Position Followed by Radical rearrangement and Elimination Reactions." *Z. Naturforsch.* **1982**, *37 c*, 1205-1227.

[21] Peukert, S.; Giese, B. "Radical-Induced S_N1 Substitution Reactions." *Tetrahedron Lett.* **1996**, *37*, 4365-4368.

[22] Glatthar, R.; Spichty, M.; Gugger, A.; Batra, R.; Damm, W.; Mohr, M.; Zipse, H.; Giese, B. "Mechanistic Studies in the Radical Induced DNA Strand Cleavage-Formation and Reactivity of the Radical Cation Intermediate." *Tetrahedron*, **2000**, *56*, 4117-4128.

[23] Giese, B.; Dussy, A.; Meggers, E.; Petretta, M.; Schwitter, U. "Conformation, Lifetime, and Repair of 4'-DNA Radicals." *J. Am. Chem. Soc.* **1997**, *119*, 11130-11131.

[24] Whitted, P. O.; Horner, J. H.; Newcomb, M.; Huang, X.; Crich, D. "Heterolytic Cleavage of a β-Phosphatoxyalkyl Radical Resulting in Phosphate Migration or Radical Cation Formation as a Function of Solvent Polarity." *Org. Lett.* **1999**, *1*, 153-156.

[25] Newcomb, M.; Miranda, N.; Sannigrahi, M.; Huang, X.; Crich, D. "Direct Measurement of Enol Ether Radical Cation Reaction Kinetics." *J. Am. Chem. Soc.* **2001**, *123*, 6445-6446.

[26] Zipse, H. "The Methylenology Principle: How Radicals Influence the Course of Ionic Reactions." *Acc. Chem. Res.* **1999**, *32*, 571-578.

[27] Beckwith, A. L.; Crich, D.; Duggan, P.; Yao, Q. "Chemistry of β-(Acyloxy)alkyl and β-(Phosphatoxy)alkyl Radicals and Related Species: Radical and Radical Ionic Migrations and Fragmentations of Carbon-Oxygen Bonds." *Chem. Rev.* **1997**, *97*, 3273-3312.

[28] Behrens, G.; Bothe, E.; Koltzenburg, G.; Schulte-Frohlinde, D. "Formation and Structure of 1,1-Dialkoxyalkene Radical Cations in Aqueous Solution. An *in situ* Electron Spin Resonance and Pulse Conductivity Study." *J. Chem. Soc. Perkin II* **1980**, 883-889.

[29] Behrens, G.; Koltzenburg, G.; Ritter, A.; Schulte-Frohlinde, D. "Influence of Protonation or Alkylation of Phosphate Group on ESR-Spectra and on Rate of Phosphate Elimination from 2-Methoxyethyl Phosphate 2-yl Radicals." *Int. J. Radiat. Biol.* **1978**, *33*, 163-171.

[30] Behrens, G.; Bothe, E.; Koltzenburg, G.; Schulte-Frohlinde, D. "Reactions of 1,1-Dialkoxyalkene Radical Cations in Aqueous Solution with OH^-, HPO_4^{2-}, and H_2O. Electron Spin Resonance Spectroscopic, Pulse Conductometric, and Product Analytical Studies." *J. Chem. Soc. Perkin II* **1981**, 143-154.

[31] Reichardt C. "Emperical Parameters of Solvent Polarity." *Angew. Chem.* **1965**, *77*, 30-40.

[32] Reichardt, C. "Solvatochromatic Dyes as Solvent Polarity Indicators." *Chem. Rev.* **1994**, *94*, 2319-2358.

[33] Giese, B.; Burger, J.; Kang, T. W.; Kesselheim, C.; Wittmer, T. "Model Studies on the Radical Induced DNA Strand Cleavage." *J. Am. Chem. Soc.* **1992**, *114*, 7322-7324.

[34] Newcomb, M. "Competition Methods and Scales for Alkyl Radical Reaction Kinetics." *Tetrahedron* **1993**, *49*, 1151-1176.

[35] Giese, B.; Erdmann, P.; Giraud, L.; Göbel, T.; Metretta, M.; Schäfer, T. "Heterolytic C,O-Bond Cleavage of 4'-Nucleotide Radicals." *Tetrahedron Lett.* **1994**, *35*, 2683-2686.

[36] Peukert, S.; Giese, B. "Radical Induced S_N1 Substitution Reactions." *Tetrahedron Lett.* **1996**, *37*, 4365-4368.

[37] Giese, B.; Beyrich-Graf, X.; Burger, J.; Kesselheim, C.; Senn, M.; Schäfer, T. "The Mechanism of Anaerobic, Radical-Induced DNA Strand Scission." *Angew. Chem. Int. Ed. Engl.* **1993**, *32*, 1742-1743.

[38] Giese, B.; Beyrich-Graf, X.; Erdmann, P.; Petretta, M.; Schwitter, U. "The Chemistry of Single-Stranded 4'-DNA Radicals – Influence of the Radical Precursor on Anaerobic and Aerobic Strand Cleavage." *Chem. Biol.* **1995**, *2*, 367-375.

[39] Akhlaq, M. S.; Schuchmann, H.. P.; von Sonntag, C. "The Reverse of the Repair Reaction of Thiols – H-Abstraction at Carbon by Thiyl Radicals." *Int. J. Rad. Biol.* **1987**, *51*, 91-102.

[40] Cozens, F. L.; O'Niell, M.; Bogdanova, R.; Schepp, N. "Dynamics of Ionization Reactions of β-Substituted Radicals. Substituent and Solvent Effects." *J. Am. Chem. Soc.* **1997**, *119*, 10652-10659.

[41] Lowry, T. H.; Richardson, K. S. *Mechanism and Theory in Organic Chemistry*, 3rd ed.; HarperCollins Publishers: New York, NY, 1987; pp 364-367.

[42] Workentin, M. S.; Schepp, N. P.; Johnston, L. J.; Wayner, D. D. M. "Solvation Control of Chemoselectivity in Reactions of Radical Cations." *J. Am. Chem. Soc.* **1994**, *116*, 1141-1142.

[43] Lewis, F. D.; Bedell, A. M.; Dykstra, R. E.; Elbert, J. E.; Gould, I. R.; Farid, S. "Photochemical Generation, Isomerization, and Oxygenation of Stilbene Cation Radicals." *J. Am. Chem. Soc.* **1990**, *112*, 8055-8064.

[44] Newcomb, M.; Miranda, N.; Huang, X.; Crich, D. "Laser Flash Photolysis Kinetic Studies of α-Methoxy-β-phosphatoxyalkyl Radical Heterolysis Reactions: A Method for Alkoxyalkyl Radical Cation Detection." *J. Am. Chem. Soc.* **2000**, *122*, 6128-6129.

[45] Crich, D.; Ranganathan, K.; Huang, X. "Generation and Reaction of Alkene Radical Cations under Nonoxidizing Conditions: Synthesis of the Pyrrolizidine Nucleus." *Org. Lett.* **2001**, *3*, 1917-1919.

[46] Surzur, J.-M.; Teissier, P. "Radical Addition of Esters to Ethyleneic Alcohols." *C. R. Acad. Sci. Fr. Ser. C.* **1967**, *264*, 1981-1984.

[47] Tanner, D. D.; Law, F. C. "Free-Radical Acetoxy Group Migration." *J. Am. Chem. Soc.* **1969**, *91*, 7535-7537.

[48] Julia, S. A.; Lorne, R. "Reductions of Steroidal Halohydrins and Theeir Esters by Tri-*n*-Butyltin Hydride; Some Stereospecific 1.2-Migrations of Acetoxy – or Benzoxy-Groups." *Tetrahedron* **1986**, *42*, 5011-5017.

[49] Crich, D.; Yao, Q.; Filzen, G. F. "Chemistry of β-(Phosphatoxy)alkyl and β-(Acyloxy)alkyl Radicals – Migration Reactions – Scope and Stereoselectivity of β-(Phosphatoxy)alkyl rearrangement – Mechanism of β-(phosphatoxy)alkyl and β-(acetoxy)alkyl Migration." *J. Am. Chem. Soc.* **1995**, *117*, 11455-11470.

[50] Beckwith, A. L. J.; Duggan, P. L. "The Mechanism of the β-(Acyloxy)alkyl Radical Rearrangement: Substituent and Solvent Effects." *J. Am. Chem. Soc.* **1996**, *118*, 12838-12839.

[51] Barclay, L. R. C.; Griller, D.; Ingold, K. U. "Kinetic Applications of Electron Paramagnetic Resonance Spectroscopy. 38. Rearrangements of β-(Acyloxy)alkyl and β-(Benzoyloxy)alkyl Radicals." *J. Am. Chem. Soc.* **1982**, *104*, 4399-4403.

[52] Zipse, H. "[1,2]-Acyloxy Shifts in Radicals. A Computational Investigation of Substituent and Solvent Effects." *J. Am. Chem. Soc.* **1997**, *119*, 1087-1093.

[53] Crich, D.; Yao, Q. "The β-(Phosphonooxy)alkyl Radical Rearrangement." *J. Am. Chem. Soc.* **1993**, *115*, 1165-1166.

[54] Kock, A.; Lamberth, C.; Wetterich, F.; Giese, B.; "Radical Rearrangement of 2-*O*-(Diphenylphosphoryl)glycosyl Bromides – A New Synthesis for 2-Deoxydisccharides and 2-Deoxyribonucleosides." *J. Org. Chem.* **1993**, *58*, 1083-1089.

[55] Kock, A.; Giese, B. "Radical Rerrangements of 2-*O*-(Diphenyoxyphosphoryl)-glycosyl Bromides." *Helv. Chim. Acta.* **1993**, *76*, 1687-1701.

[55] Steenken, S.; Goldbergerova, L. "Photoionization of Organic Phosphates by 193 nm Laser Light in Aqueous Solution: Rapid Intramolecular H-Transfer to the Primarily Formed Phosphate Radical. A Model for Ionization-Induced Chain-Breakage in DNA?" *J. Am. Chem. Soc.* **1998**, *120*, 3928-3934.

[56] Zipse, H. "Computational Insight into the Chemistry of β-(Phosphatoxy)alkyl Radicals: [3,2]- and [1,2]-Phosphatoxy Rearrangements and a New Pathway for *syn*-Elimination of Phosphate." *J. Am. Chem. Soc.* **1997**, *119*, 2889-2893.

[57] Choi, S.-Y.; Crich, D.; Horner, J. H.; Huang, X.; Martinez, F. N.; Newcomb, M.; Wink, D. J.; Yao, Q. "Absence of Diffusively Free Radical Cation Intermediates in Reactions of β-(Phosphatoxy)alkyl Radicals." *J. Am. Chem. Soc.* **1998**, *120*, 211-212.

[58] Newcomb, M.; Horner, J. H.; Whitted, P. O.; Crich, D.; Huang, X.; Yao, Q.; Zipse, H. "β-Phosphatoxyalkyl Radical Reactions: Competing Phosphate Migration and Phosphoric Acid Elimination from a Radical Cation-Phosphate Anion Pair Formed by Heteroltic Fragmentation." *J. Am. Chem. Soc.* **1999**, *121*, 10685-10694.

[59] Zipse, H. "The $S_{RN}2$ Pathway – A Mechanistic Alternative for Radicals in Polar Media?" *Angew. Chem. Int. Ed. Engl.* **1994**, *33*, 1985-1988.

[60] Zipse, H. "Open Shell Analogs of Closed Shell Reaction Paths: The $S_{RN}2$' Case." *J. Am. Chem. Soc.* **1994**, *116*, 10773-10774.

[61] Stirk, K.M.; Kiminkinen, M.; Kenttämaa, H. I "Ion-Milecule Reactions of Distonic Radical Cations." *Chem. Rev.* **1992**, *92*, 1949-1665.

[62] Stirk, K.G.; Kenttämaa, H. I. "Imolecular Reactions of the β-Distonic Isomer of the Ethanol Radical Cation – $CH_2CH_2OH_2^+$." *J. Phys. Chem.* **1992**, *96*, 5272-5276.

[63] Sugiyama, H.; Ohmori, K.; Saito, I. "Oligonucleotides Containing a Radical Trap: The Trapping of Deoxyribose C4' Radical in Bleomycin-Mediated Reactions." *J. Am. Chem. Soc.* **1994**, *116*, 10326-10327.

[64] Wagner, P. J.; Lindstrom, M. J.; Sedon, J. H.; Ward, D. R. "Photochemistry of δ-Halo Ketones: Anchimeric Assistance in Triplet-State γ-Hydrogen Abstraction and β-Elimination of Halogen Atoms from the Resulting Diradicals." *J. Am. Chem. Soc.* **1981**, *103*, 3842-3849.

[65] Wagner, P. J.; Sedon, J. H.; Lindstrom, M. J. "Rates of Radical β-Cleavage in Photogenerated Diradicals." *J. Am. Chem. Soc.* **1978**, *100*, 2579-2580.

[66] Barton, D. H. R.; Crich, D.; Motherwell, W. B. "The Invention of New Radical Chain Reactions 8. Radical Chemistry of Thiohydroxamic Esters – A New Method for the Generation of Carbon Radicals." *Tetrahedron* **1985**, *41*, 3901-3924.

[67] Brookhart, M.; Liu, Y. M.; Goldman, E. W.; Timmers, D. A.; Williams, G. D. "Enantioselective Cyclopropane Synthesis Using the Chiral Carbene Complexes (S_{Fe})- and (R_{Fe})-$C_5H_5(CO)(PR_3)Fe{=}CHCH_3^+$ – A Mechanistic Analysis of the Carbene Transfer-Reaction." *J. Am. Chem. Soc.* **1991**, *113*, 927-939.

[68] Levene, P. A.; Marker, R. E. "Optical Rotations of Configurationally Related Methoxypropionic and β-Methoxybutyric Nitriles." *J. Biol.Chem.* **1933**, *102*, 297-302.

[69] Meier, I. K.; Schwartz, J. "Olefin Synthesis by Vanadium(V) – Induced Oxidative Decarboxylation – Deoxygenation of 3-Hydroxy Carbyxylic Acids." *J. Org. Chem.* **1990**, *55*, 5619-5624.

[70] Adam, W.; Baeza, J.; Liu, J.-C. "Stereospecific Introduction of Double Bonds *via* Thermolysis of β-Lactones." *J. Am. Chem. Soc.* **1972**, *94*, 2000-2006.

[71] Jager, J.; Graafland, T.; Schenk, H.; Kirby, A. J.; Engberts, J. B. F. N. "Intramolecular-catalyzed Sulfonamide Hydrolysis. VII. The Thorp-Ingold Effect in the Intramolecular Carboxyl-Catalyzed Hydrolysis of Sulfonamides." *J. Am. Chem. Soc.* **1984**, *106*, 139-143.

[72] Barton, D. H. R.; Samadi, M. "The Invention of Radical Reactions. Part XXV. A Convenient Method for the Synthesis of the Acyl Derivatives of *N*-Hydroxyperidine-2-thione." *Tetrahedron* **1992**, *48*, 7083-7090.

[73] Steenken, S.; McClelland, R. A. "Lifetimes of α-Dialkoxy Carbocations Produced via Radical Cations Generated by Electron Transfer and Photoionization in Aqueous Solution." *J. Am. Chem. Soc.* **1989**, *111*, 4967-4973.

[74] Bassetti, M.; Flores, B. "Metalation of Alkynes. Part 2. Behavior of Alkynes with Mercury (II) Acetate in Methanol: a Systematic Reinvestigation." *J. Chem. Soc. Perkin Trans. 2* **1988**, 227-233.

[75] Kriz, G. S.; Lampman, G. M.; Pavia, D. L. "*Introduction to Spectroscopy*, 2nd ed.; Saunders College: New York, 1996; pp 473.

[76] Gaudry, M.; Marquet, A. "Étude des Stabilités Relatives de Quelques Éthers d'Énols Isoméres." *Bull. Soc. Fchim. Fr.* **1969**, 4178-4182.

[77] Csuck, R.; Glänzer, B. I. "Methylenation of Aldonolactones." *Tetrahedron* **1991**, *47*, 1655-1664.

[78] Langhals, H. "Polarity of Binary Liquid Mixtures." *Angew. Chem. Int. Ed. Engl.* **1982**, *21*, 724-733.

[79] Schepp, N. P.; Johnston, L. J. "Reativity of Radical Cations. Effect of Radical Cation and Alkene Structure on the Absolute Rate Constants of Radical Cation Mediated Cycloaddition Reactions." *J. Am. Chem. Soc.* **1996**, *118*, 2872-2881.

[80] Fukuzumi, S.; Fujita, M.; Otera, J.; Fujita, Y. "Electron-Transfer Oxidation of Ketene Silyl Acetals and other Organosilanes – The Mechanistic Insight into Lewis Acid Mediated Electron-Transfer." *J. Am. Chem. Soc.* **1992**, *114*, 10271-10278.

[81] Liu, W.-Z.; Bordwell, F. G. "Gas-Phase and Solution-Phase Homolytic Bond Dissociation Energies of H-N^+ Bonds in the Conjugate Acids of Nitrogen Bases." *J. Org. Chem.* **1996**, *61*, 4778-4783.

[82] Nelson, S. F.; Hintz, P. J. "Electrochemical Oxidation of Tertiary Amines. The Effect of Structure upon Reversibility." *J. Am. Chem. Soc.* **1972**, *94*, 7114-7117.

[83] *CRC Handbook Series in Organic Electrochemistry*; Meites, L.; Zuman, P., Eds.; CRC: Cleveland, OH, 1974; Vol. 1.

[84] Stoub, D. G.; Goodman, J. L. "Diarylcarbene Cation Radicals: Generation and Chemical Reactivity in Solution." *J. Am. Chem. Soc.* **1997**, *119*, 11110-11111.

[85] Asmus, K.-D.; Bonifacic, M. in *S-Centered Radicals*; Alfassi, Z. B., Ed.; John Wiley & Sons: New York, 1999.

[86] Shono, T.; Ikeda, A.; Hayashi, J.; Hakozaki, S. "Electroorganic Chemistry. 19. Anodic-Oxidation of Nonconjugated Dienes." *J. Am. Chem. Soc.* **1975**, *97*, 4261-4264.

[87] Chatgilialoglu, C. In *Handbook of Organic Photochemistry*; Scaiano, J. C., Ed.; CRC: Boca Raton, FL, 1989; Vol. 2, pp 3-11.

[88] Arnold, D. R.; McManus, K. A. "Radical Ions in Photochemistry. Photochemical Nucleophile-Olefin Combination, Aromatic Substitution (photo-NOCAS) reaction: Methanol, β-Myrcene, and 1,4-Dicyanobenzene. Intramolecular Cyclization of an Ene-Diene Radical Cation." *Can. J. Chem.* **1998**, *76*, 1238-1248.

[89] Arnold, D. R.; McManus, K. A.; Chan, M. S. "Radical Ions in Photochemistry. 42. Photochemical Nucleophile-Olefin Combination, Aromatic Substitution (photo-NOCAS) Reaction. The Scope and Limitations of the Reaction with Cyanide Anion as the Nucleophile." *Can. J. Chem.* **1997**, *75*, 1055-1075.

[90] Hawari, J. A.; Engel, P. S.; Griller, D. "Rate Constants for the Reactions of Alkyl Radicals with 1,4-Cyclohexadiene." *Int. J. Chem. Kinet.* **1985**, *17*, 1215-1219.

[91] Clark, W. G.; Setser, D. W.; Dees, K. "Nonequilibrium Kinetic Isotope Effects and other aspects of Models for Hydrogen Chloride and Deuterium Chloride Elimination from Chloroethane-d_0, -d_3, and -d_5." *J. Am. Chem. Soc.* **1971**, *93*, 5328-5335.

[92] Baciocchi, E.; Bietti, M.; Lanzalunga, O. "Mechanistic Aspects of –Bond-Cleavage Reactions of Aromatic Radical Cations." *Acc. Chem. Res.* **2000**, *33*, 243-251.

[93] Baciocchi, E. "Side-Chain Reactivity of Aromatic Radical Cations." *Acta Chem. Scand.* **1990**, *44*, 645-652.

[94] Bordwell, F. G.; Cheng, J.-P. "Radical-Cation Acidities in Solution and in the Gas Phase." *J. Am. Chem. Soc.* **1989**, *111*, 1792-1795.

[95] Bauld, N. L. *Radicals, Ion Radicals, and Triplets*; Wiley-VCH: New York, 1997; pp 152-157.

[96] Thibblin, A. "Borderline Between E_1 and E_2 Mechanisms – Bimolecular Base-Promoted Elimination via Ion-Pairs Competing with Concerted E_2 Elimination." *J. Am. Chem. Soc.* **1989**, *111*, 5412-5416.

[97] Biermann, H. W.; Morton, T. H. "Reversible Tautomerization of Radical Cations. Photoionization of 2-Methoxyethanol and 3-Methoxy-1-propanol." *J. Am. Chem. Soc.* **1983**, *105*, 5925-5930.

[98] Morton, T. H.; Beauchamp, J. L. "Chain-Length Effects upon the Interaction of Functional Groups. The Low Energy Impact Mass Spectra of α,ω-Dialkoxyalkanes

Examined by Ion Cyclotron Resonance Spectrospy." *J. Am. Chem. Soc.* **1975**, *97*, 2355-2362.

[99] Berruyerpenaud, F.; Bouchoux, G.; Tortajada, J. "Dissociation of Positively-Charged Aliphatic Epoxides. 3. $[C_4H_8O]^+$ Epoxides and α,β-Unsaturated Ethers." *J. Rapid Commun. Mass Spectrom.* **1992**, *6*, 37-45.

[100] Chyall, L. J.; Byrd, M. H.; Kenttämaa, H. I. "Reactions of the Charged Radical $(CH_3)_2S^+$-CH_2• with Cyclic Alkenes." *J. Am. Chem. Soc.* **1994**, *116*, 10767-10772.

[101] Siedschlag, C.; Luftmann, H.; Wolff, C. Mattay, J. "[60]Fullerene Radical Cation: Reactions and Mechanism." *Tetrahedron* **1999**, *55*, 7805-7818.

[102] Dunsch, L.; Ziegs, F.; Siedschlag, C.; Mattay, J. "ESR Spectroscopy of the C-60 Cation Produced by Photolinduced Electron Transfer." *Chem. Eur. J.* **2000**, *6*, 3547-3550.

[103] Green, M. M. "A Stereochemical Bridge Between Mass Spectrometry and Free Radical Chemistry." *Tetrahedron* **1980**, *36*, 2687-2699.

[104] Morton, T. H. "Gas Phase Analogues of Solvolysis Reactions." *Tetrahedron* **1982**, *38*, 3195-3243.

[105] *Handbook of Chemistry and Physics*, 75th ed.; Lide, D. R., Ed.; CRC: Boca Raton, FL, 1994; pp 9-64.

[106] *Encyclopedia of Reagents for Organic Synthesis*; Paquette, L. A., Ed.; John Wiley and Sons: New York, 1995; Vol. 1, pp 470-473.

Part 2.

The Mechanism of Copper Phenanthroline Induced DNA Strand Scission.

1 Introduction.

A wide variety of chemical species have been shown to damage single stranded and duplex DNA.[1-4] The most well studied of these damaging agents are the products resulting from γ-radiolysis of H_2O, which include hydrogen atoms, solvated electrons, and hydroxyl radicals.[1] Of theses species, the most damaging to DNA is the hydroxyl radical which reacts primarily through addition to the nucleobase.[1,2,4-6] While hydroxyl radical addition to purines does not lead to direct strand scission, the resulting modification of the nucleobases affect the integrity of the genetic information contained within the DNA. For example, the two major base modifications produced by the

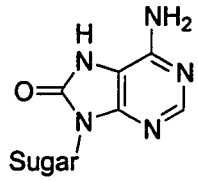

8-oxo·dA

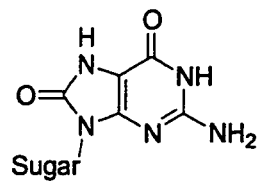

8-oxo·dG

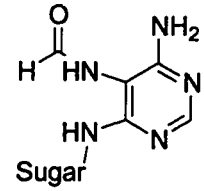

Fapy·dA

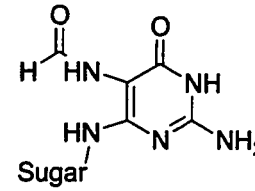

Fapy·dG

Sugar =

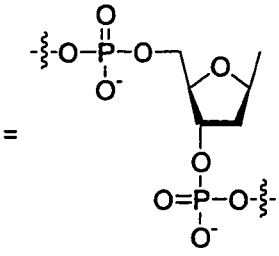

addition of hydroxyl radicals to the C8 position of purines are the 8-oxopurines and formamidopyrimidines, both of which have been shown to lead to base misincorporation opposite the lesion by DNA polymerase enzymes.[7-9]

Hydrogen atom abstraction from the sugar moiety by hydroxyl radicals directly or by peroxyl radicals generated from O_2 trapping of nucleobase radicals has been shown to occur primarily at the C1'-, C4'-, and C5'-positions.[2,10-12] While products attributable to hydrogen atom abstraction from the C2'- and C3'-positions have been observed from the γ-radiolysis of DNA in aqueous solutions, this reaction manifold is less efficient than reaction at other positions of the sugar moiety.[1-3,13] The reason for the reduced reactivity of the C2'-position has been attributed to the fact that the C-H bonds at the C2'-position are stronger than the C-H bonds at the other position of the sugar moiety.[14] The reduced reactivity of the C3'-hydrogen has been hypothesized on the basis of computational experiments to be a result of the pucker of the 2-deoxyfuranose ring, although experimental evidence for this has not been obtained.[15] Formation of direct strand breaks, cleavage of the phosphate backbone without additional exogenous reagents, has been observed upon generation of both the C4'- and C5'-radicals under aerobic conditions.[1,3,16] However, generation of the C1'-radical in the presence of O_2 has been shown to result in loss of the nucleobase in conjunction with the formation of the 2-deoxyribonolactone abasic site (**1**).[1,3,4,17,18]

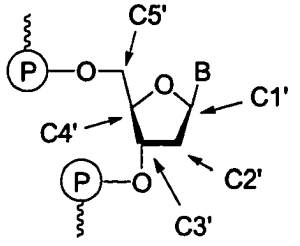

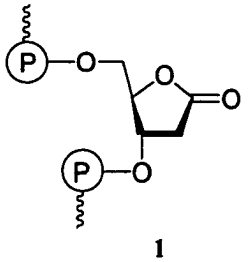

1

In addition to DNA damage mediated by ionizing radiation, a wide range of chemical species, both natural and synthetic in origin, have been discovered which are capable of effecting cleavage of the phosphate backbone through reaction at the sugar moiety.[3,4] Damage to the 2-deoxyfuranose ring can arise from direct interaction between the damaging agent and the sugar moiety or through the production of freely diffusible reactive intermediates such as hydroxyl radicals. The majority of the complexes which damage DNA through reaction at the sugar moiety have been proposed to do so through hydrogen atom abstraction.[1-4] However, several metal-oxo complexes have been proposed to react with the sugar moiety by hydride transfer from the sugar moiety to the reactive metal-oxo complex.[19,20]

With the exception of the photoactivated rhodium complexes, which are proposed to react by hydrogen atom abstraction from the C3'-position of the sugar, most DNA damaging agents which produce direct strand breaks involve reaction at either the C4'-or C5'-positions.[21-23] These hydrogen atoms are readily accessible to molecules bound in the minor groove of the DNA duplex. A variety of natural and synthetic complexes have been shown to effect direct DNA strand scission through reaction at the C4'- and/or the C5'-positions from the minor groove including Fe(II)·bleomycin (**2**), neocarzinostatin (**3**), copper aminoglycosides such as **4**, the cationic manganese porphyrin Mn-TMPyP (**5**), and bis(1,10-phenanthroline)copper ($Cu(OP)_2$) (**6**) (Figure 1).[3,24-26]

As the C1'-position is located deep in the minor groove, it is not a primary target for DNA damaged induced by **2-4**.[3,4] However, several compounds damage the sugar moiety through reaction at the C1'-position including hydroxyl radicals, **3**, **5**, and a series of oxo-ruthenium complexes. $Cu(OP)_2$ (**6**) is an exception in that it reacts primarily at the

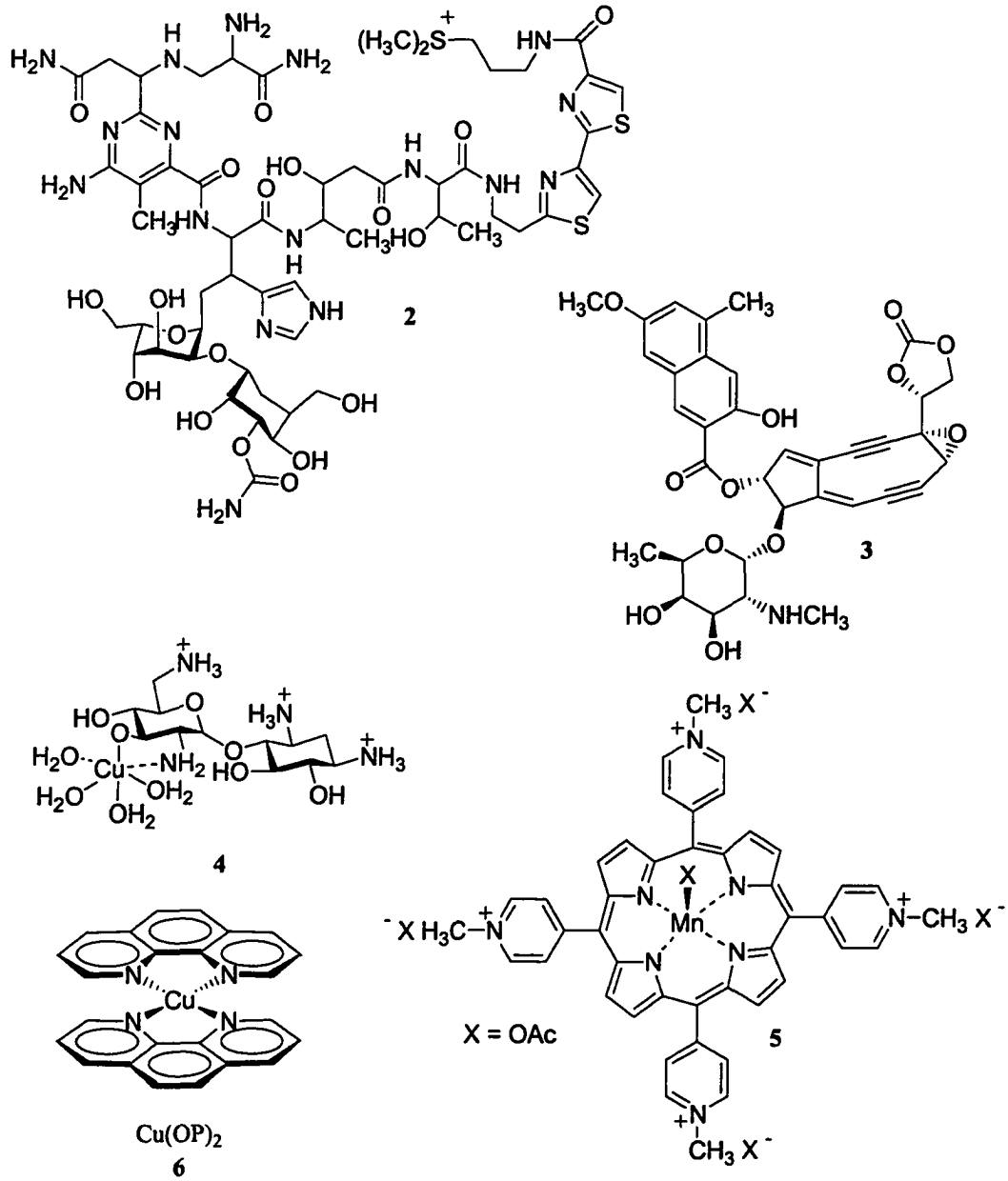

Figure 1. Chemical agents which damage DNA by reaction at the sugar moiety.

C1'-position.[26] Both hydroxyl radicals and neocarzinostatin have been shown to react at the C1'-position through hydrogen atom abstraction, while the oxo-ruthenium complexes have been proposed to react through hydride transfer from the C1'-position to the oxo functionality.[1,19,20,27] The exact nature of the reaction for $Cu(OP)_2$ is not known, but the

majority of the evidence to date supports abstraction of the C1'- and C4'-hydrogen atoms as the events leading to DNA damage induced by $Cu(OP)_2$.[26]

Generation of the C1'-radical or cation by hydrogen atom abstraction or hydride transfer respectively results in the formation of **1**.[17-20] This lesion is stable under physiological conditions and does not give rise to direct strand breaks. Hwang developed a series of reactions that are used to detect the presence of **1** through the formation of adducts of cleavage products which exhibit different migrational aptitudes when analyzed by denaturing polyacrylamide gel electrophoresis (PAGE), effectively generating a "fingerprint" for **1**.[28] In addition, this lesion can be revealed by treatment with base to induce the β,δ-elimination to generate 5-methylenefuranone (**7**) and is commonly referred to as an alkali labile lesion (Eq 1). Recently, the 2-deoxyribonolactone lesion

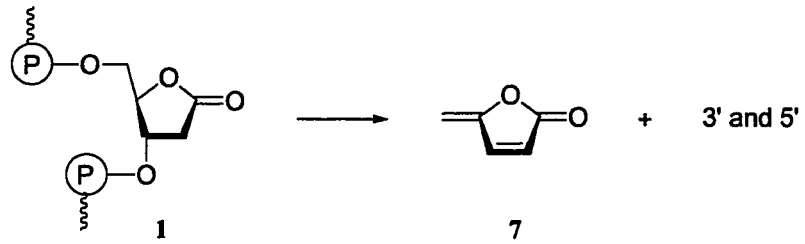

1 **7** (1)

has been shown to be capable of covalently cross-linking to DNA repair and polymerase enzymes, indicating that its formation in DNA may be more lethal than originally thought.[29,30]

Formation of direct strand breaks from reaction of $Cu(OP)_2$ with duplex DNA has been observed, and several mechanisms have been put forward to account for cleavage of the phosphate backbone.[31-34] These proposals include direct strand scission arising

through reaction at both the C1'-and C4'-positions with either position postulated to be the primary site of reaction leading to direct strand breaks. In order to help resolve this mechanistic controversy, the focus of this research project has been to test whether $Cu(OP)_2$ induces elimination of the 2-deoxyribonolactone (**1**) generated from hydrogen atom abstraction from the C1'-position of the sugar moiety.

2 Background

Since the report that $Cu(OP)_2$ was capable of inducing direct DNA strand scission, the mechanism of action has been the subject of considerable study. While the exact nature of the reactive copper species is unknown, it was generally accepted that $Cu(OP)_2$ reacts by hydrogen atom transfer primarily from the C1'- and to a lesser extent from the C4'-position of the sugar moiety to the reactive copper species.[26,35,36] Treatment of DNA with $Cu(OP)_2$ in the presence of a reductant, typically either ascorbate or thiols, and in the presence of an oxidant, either O_2 or H_2O_2 gives rise to direct strand breaks and alkali labile lesions. Direct strand scission arising from generation of the C4'-radical has significant precedent arising from the large body of mechanistic work surrounding the Fe(II)·bleomycin mediated cleavage of DNA.[3,4] However, it has also been proposed that $Cu(OP)_2$ produces strand scission through reaction predominantly at the C1'-position, which represents a novel pathway for the formation of direct strand breaks.[3,4,31-33] The focus of this research has been to determine whether or not direct strand scission induced by $Cu(OP)_2$ occurs through a copper induced elimination of **1** that is believed to be produced as a result of C1'-hydrogen atom abstraction.

2.1 Discovery of the Nuclease Activity of $Cu(OP)_2$.

The nuclease activity of $Cu(OP)_2$ was first reported by Sigman and co-workers in 1979 while investigating the 1,10-phenanthroline (OP) inhibition of *E. coli* DNA polymerase I.[37] This polymerase inhibition was originally attributed to the sequestering of the zinc ions in solution by 1,10-phenanthroline, which were believed to be a cofactor for DNA polymerase I. However, the observation that the inhibition required thiol and

copper(II) coupled with the fact that increased inhibition was observed upon preincubation of the DNA in the presence of Cu(II), OP and 3-mercaptopropionic acid (MPA) indicated that a reaction was occurring between the copper and the DNA.[26,35-37] Since 3'-phosphatemonoester termini were known to be effective inhibitors of *E. coli* DNA polymerase I, it was hypothesized that the $Cu(OP)_2$ complex was damaging the DNA in a manner which produced 3'-phosphatemonoester termini.[36,38]

It should also be noted that copper in the presence of one equivalent of 1,10-phenanthroline (Cu(OP)) (**8**) has also been shown to damage DNA.[26,35,39] While the rate of cleavage of duplex DNA with Cu(OP) is slower than that observed from reaction of $Cu(OP)_2$, both complexes produce identical products in similar ratios, indicating that Cu(OP) and $Cu(OP)_2$ react through similar if not identical mechanisms.[35] The reason for the reduced reactivity of Cu(OP) compared to $Cu(OP)_2$ is not clear at this time.

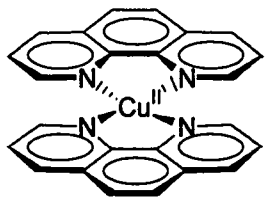

$Cu(OP)_2$
6

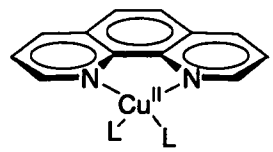

Cu(OP)
8

Cleavage inhibition by catalase, showed that H_2O_2 is required in order for $Cu(OP)_2$ to exhibit nuclease activity.[40] It has since been observed that under aerobic conditions H_2O_2 is generated from reaction of Cu(II), OP, thiol and O_2 (Eq 2 and 3).[40] It has also been shown that $Cu(II)(OP)_2$ does not damage DNA in the absence of a reductant, indicating that $Cu(I)(OP)_2$ must be formed during the DNA cleavage reaction.

$$(OP)_2Cu^{2+} + RSH \rightarrow (OP)_2Cu^{+} + \tfrac{1}{2}RSSR + H^{+} \quad (2)$$

$$2(OP)_2Cu^{+} + O_2 + 2H^{+} \rightarrow 2(OP)_2Cu^{2+} + H_2O_2 \quad (3)$$

Thiols are not the only class of reductants which can be used to reduce Cu(II) to Cu(I) in this reaction system. This is demonstrated by the fact that superoxide, and ascorbate have also been used to generate the reactive copper species responsible for damage of duplex DNA.[26,40-42]

Footprinting studies have shown that minor groove binding molecules inhibit DNA damage induced by $Cu(OP)_2$, indicating that $Cu(OP)_2$ reacts from the minor groove in duplex DNA.[36,43] This hypothesis is consistent with the products resulting from treatment of duplex DNA with **6**, which have been shown to be both 3'- and 5'-phosphates, free nucleobases, and minor amounts of 3'-phosphoglycolate (**9**) (Eq 4).[43]

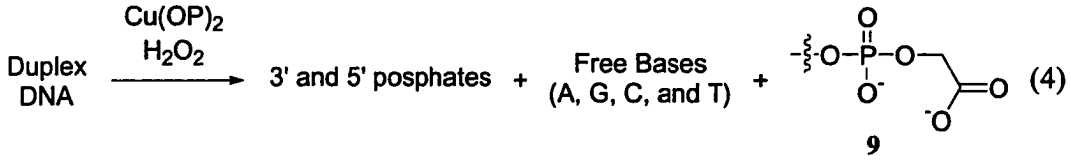

(4)

9

Studies on the Fe(II)·bleomycin mediated damage of DNA have established that 3'-phosphoglycolate (**9**) is diagnostic of C4'-hydrogen atom abstraction from (Figure 2).[3,16,23] Based on the fact that **9** is formed in less than 30% yield from reaction of $Cu(OP)_2$ with duplex DNA, it was concluded that C4'-chemistry was not the major pathway accounting for the observed direct strand scission.[36]

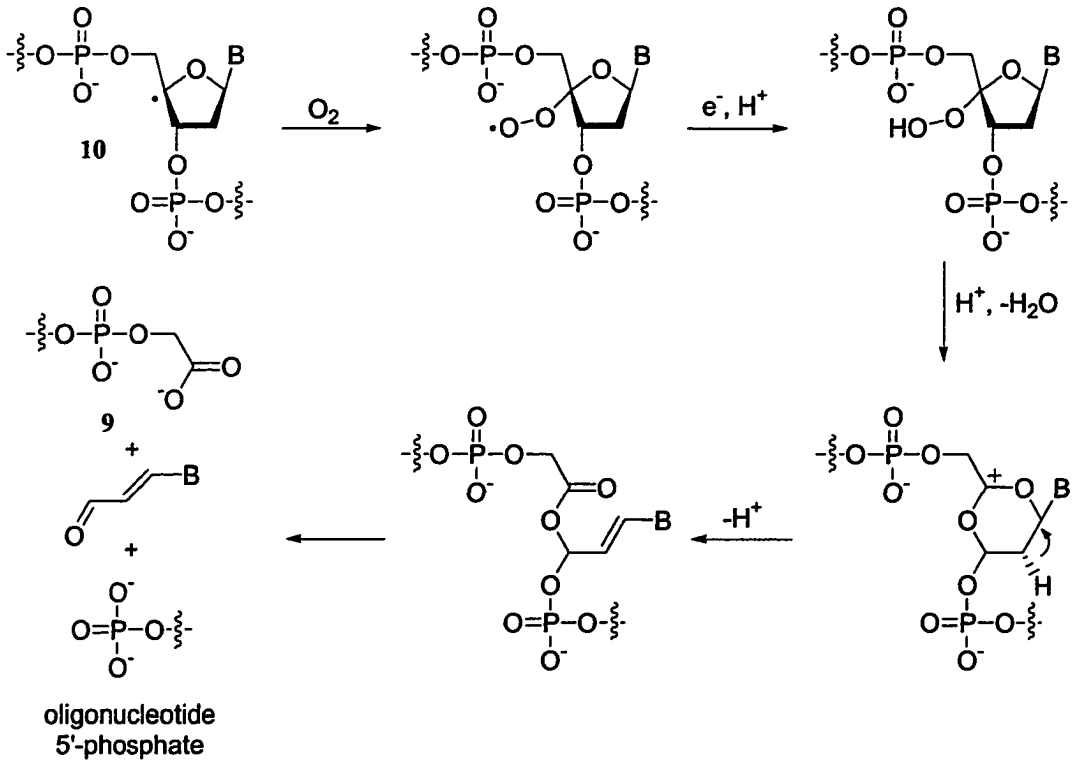

Figure 2. Proposed mechanism for the formation of **9** from the C4'-radical.[23]

It has recently been shown that hydrogen atom abstraction from the C4'-position is also capable of generating both 3'- and 5'-phosphate termini by Giese and co-workers.[44-47] Hydrogen atom abstraction from the C4'-position generates **10**, which has been shown to undergo heterolytic cleavage of the 3'-phosphate to generate a 5'-phosphate terminus and the corresponding olefin cation radical (**11**) under anaerobic conditions (Figure 3). Subsequent trapping of **11** by H_2O followed by heterolysis of the 5'-phosphate accounts for the observed 3'-phosphate terminus. Under aerobic conditions the C4' radical is trapped by oxygen 500 times faster than the rate of heterolytic scission of the 3'-phosphate.[48] In the presence of hydrogen atom donors such as thiols, the resulting peroxyl radical (**12**) is trapped to generate the corresponding hydroperoxide (**13**) which decomposes to generate 3'-phosphoglycolate (**9**) through the pathway shown in

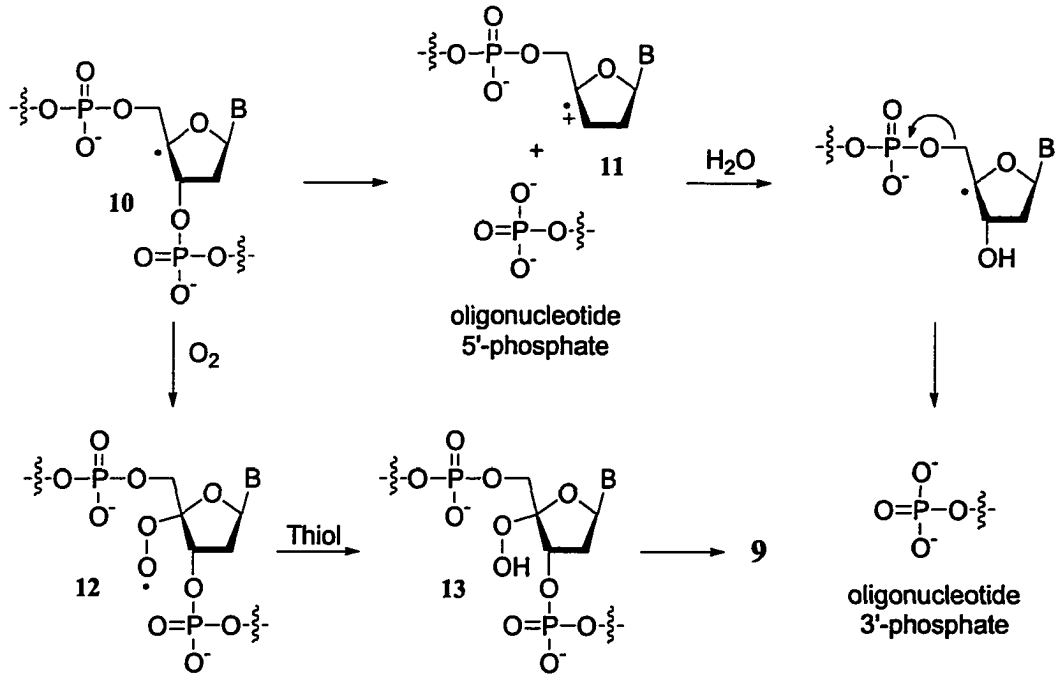

Figure 3. Products resulting from formation of olefin cation radical **11**.[46]

Figure 2.[48] Since $Cu(OP)_2$ cleavage reactions are carried out under aerobic conditions and commonly in the presence of thiols, formation of 3'- and 5'-phosphate termini through heterolytic cleavage of the 3'-phosphate in **10** can be ruled out.

Insight into the nature of the chemical intermediate responsible for the formation of the majority of 3'- and 5'-phosphates was gained from the observation that quenching the $Cu(OP)_2$ reaction with DNA by freezing showed the formation of a product which migrated more slowly than the corresponding 3'-phosphate upon denaturing PAGE analysis. This slower moving product was readily converted to the 3'-phosphate upon treatment with 1.0 M piperdine at 90 °C, which led to the proposal that the alkali labile lesion was butenolide **14** (Figure 4).[43] The butenolide was proposed to arise from β-elimination of the 3'-phosphate from the 2-deoxyribonolactone (**1**), although no direct evidence for the formation of **14** has been obtained to date.

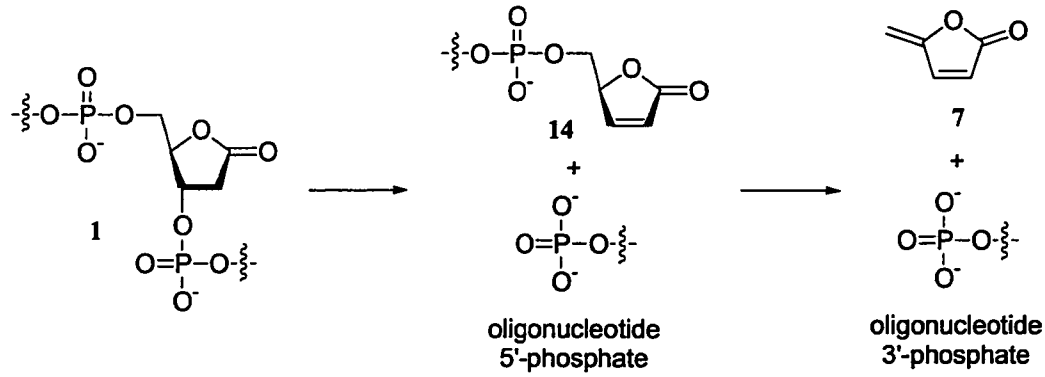

Figure 4. Proposed pathway for formation of **7** and **14** upon treatment of duplex DNA with $Cu(OP)_2$.[43]

Formation of the 2-deoxyribonolatone (**1**) has been observed from generation of the C1'-radical and the C2'-radical. The mechanism of formation of **1** from the C1'-radical under aerobic conditions has recently been elucidated (Figure 5).[17,18,28,49,50] Aerobic photolysis of oligonucleotides containing C1'-*t*-butyl ketone (**15**) at λ_{max} = 350

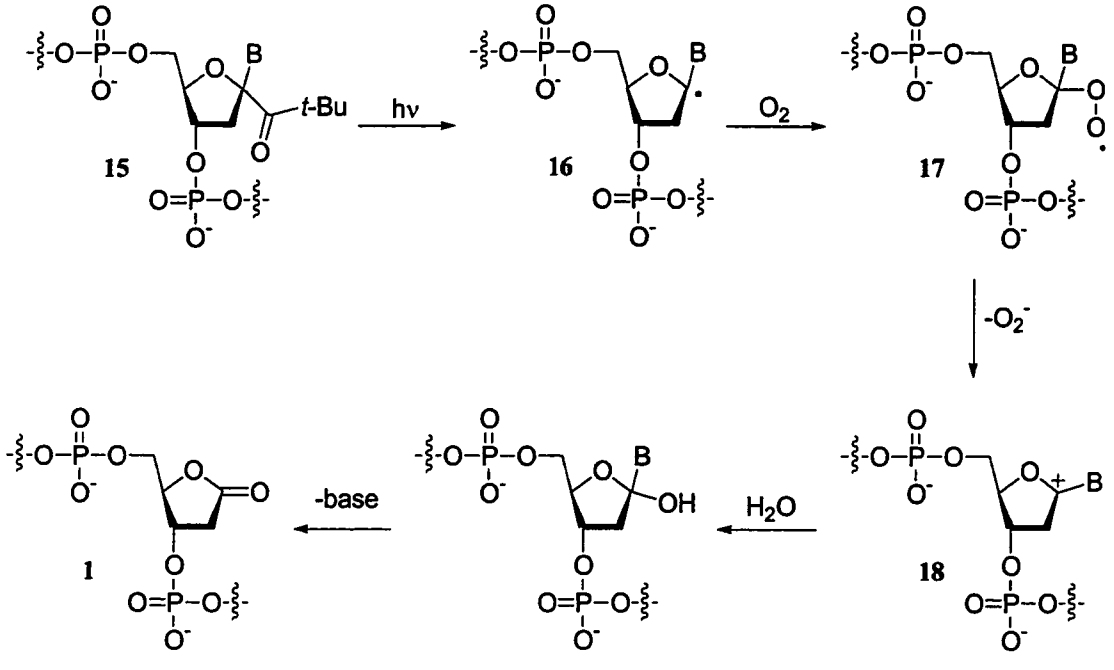

Figure 5. Mechanism for the formation of **1** from **16**.[17]

nm generates the C1'-radical.[28,50] Under aerobic conditions, the C1'-radical reacts with oxygen to form the corresponding C1'-peroxyl radical (**17**). Subsequent loss of superoxide generates the C1'-cation (**18**), which upon trapping with H_2O and hydrolysis forms **1**.

Generation of the C2'-radical under aerobic conditions has been shown to result in the formation of **1** (Figure 6).[51] Photolysis of the C2'-iodide is followed by oxidation of

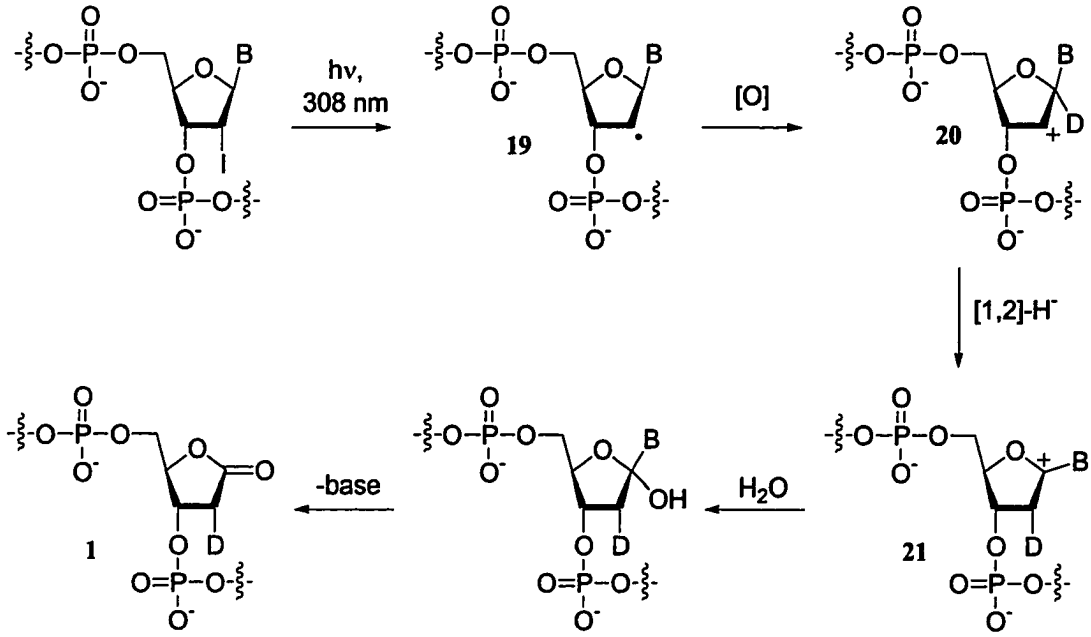

Figure 6. Proposed pathway for the formation of **1** from the formation of the C2'-radical.[51]

the resulting radical (**19**) to the corresponding cation (**20**). The 1,2-hydride migration to generate the C1'-oxocarbenium ion **21** has been shown to occur stereospecifically with the hydride remaining on the α-face of the sugar.[51] Reaction of **21** with H_2O followed by hydrolysis forms **1**. This reaction may be a unique situation as a result of the radical pair

formed from the initial photolysis. The alkyl radical iodine pair may facilitate the subsequent oxidation of **19** to form the corresponding cation (**20**).

In an attempt to rule out the formation of 5-methylenefuranone (**7**) through hydrogen atom abstraction at the C2'-position by $Cu(OP)_2$, Sigman and co-workers studied the reactivity of C1'-deuterated DNA.[32] Analysis of the resulting 5-methylenefuranone (**7**) by GC/MS showed no deuterium incorporation in **7**, leading to the conclusion that $Cu(OP)_2$ does not react through hydrogen atom abstraction from the C2'-position. However, the absence of deuterium in **7** does not completely rule out this mechanism since *syn*-elimination of the 3'-phosphate and stereoselective hydride migration will result in loss of the isotopic label. While this possibility was not considered in the analysis presented by Sigman and co-workers, it is not unreasonable. Evidence has been obtained for the Endonuclease III and V induced syn elimination of the 3'-phosphate in abasic sites.[52]

2.2 Utility of $Cu(OP)_2$ as a Structural Probe.

2.2.1 Utility as a Footprinting Agent.

Since $Cu(OP)_2$ damages DNA from the minor groove, and shows moderate sequence specificity, it has been employed as a minor groove footprinting agent.[26,35,53] As a result of the groove specificity of $Cu(OP)_2$, molecules which interact with DNA in the major groove only do not give a footprint. This makes $Cu(OP)_2$ a useful probe for distinguising between molecules that bind in the major and minor grooves of DNA. However, the modest preference of $Cu(OP)_2$ for reaction at nucleotides flanked by thymidine limits its usefulness in this manner.[35,54]

While $Cu(OP)_2$ provides the advantage of easily distinguishing between major and minor groove binding molecules, the endonuclease DNase I and Fe·EDTA are also commonly used footprinting agents.[55-58] Footprinting by DNase I is somewhat limited by the fact that it exhibits a marked sequence specificity for cleavage on the 5'-side of pyrimidine containing nucleotides, as well as the fact that DNase I is a large molecule and tends to give exaggerated footprints. Fe·EDTA has been shown to function as a footprinting agent by the production of freely diffusible hydroxyl radicals through Fenton chemistry (Eq 5).[58-60] As a result, Fe·EDTA footprinting does not generate oversized

$$H_2O_2 + Fe^{2+} \rightarrow Fe^{3+} + HO^- + HO^{\cdot} \qquad (5)$$

footprints and is capable of footprinting molecules which interact with DNA in both the major and minor grooves, making Fe·EDTA footprinting a common method for the study of the region of interaction of DNA binding molecules.[60]

2.2.2 Utility of $Cu(OP)_2$ as a DNA and RNA Structure Probe.

Since $Cu(OP)_2$ reacts with duplex DNA from the minor groove, it does not damage single stranded DNA.[26,35,36] The explanation of the inability of $Cu(OP)_2$ to react with single stranded DNA has been proposed to result from the absence of a minor goove, which is required for DNA binding.[36] The interaction between $Cu(OP)_2$ and duplex DNA within the minor groove, has been proposed to be sensitive to changes in its shape. This is reflected by an 83–86% reduction in the rate of $Cu(OP)_2$ cleavage of A-DNA compared to the reactivity of B-DNA.[61] Duplex DNA in the Z-form is not

cleaved.[40,61,62] Since the minor groove is significantly more shallow in A and Z form DNA, it has been proposed that $Cu(OP)_2$ does not bind to the biopolymer efficiently, resulting in the observed reduction in the efficiency of strand scission.[26,63]

As a result of the preference of $Cu(OP)_2$ for cleavage of B-DNA over A form, Z form, and single stranded DNA, it has been used as a probe of the secondary structures of DNA.[62,64] For example, the formation of hairpins in single stranded DNA have been detected by $Cu(OP)_2$, since the single stranded portion of the hairpin loop is not cleaved while the duplex regions are damaged.[62,64] This not only indicates the formation of a hairpin, but also allows for determination of the position of the hairpin within the oligonucleotide.

This damaging agent has also been employed for the detection of single strand bulges and loops in RNA.[65-67] However, the results obtained with RNA substrates are opposite of those obtained with DNA substrates, with preferential cleavage of single stranded RNA over duplex RNA. The reason for the change in reactivity of duplex DNA and duplex RNA with $Cu(OP)_2$ likely has to do with the preference for the formation of an A-type structure in duplex RNA.[26,63]

Two other DNA structural motifs have been shown to be efficiently cleaved by $Cu(OP)_2$. Holiday junctions (**22**), which are cross strand exchanges and occur primarily during cell meiosis, are efficient substrates for DNA damage induced by $Cu(OP)_2$.[68,69] Transcriptionally active open complexes formed during gene transcription have also been shown to be cleaved by $Cu(OP)_2$ in a highly efficient manner (Figure 7).[70] No difference between the reactivity of prokaryotic and eukaryotic transcriptionally active open complexes has been observed leading to the use of $Cu(OP)_2$ as a probe for the

determination of the start position for a variety of genes *in vivo*.[70-74] Interestingly, reaction of $Cu(OP)_2$ with these structural motifs involves cleavage of single stranded sections of DNA. This has been rationalized through the hypothesis that the presence of the enzymatic machinery required for the formation of both Holiday junctions and open complexes is capable of inducing enough secondary structure within the single stranded region of DNA to allow $Cu(OP)_2$ to bind and cleave the DNA.[26,36,70]

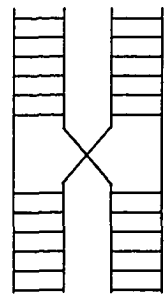

22

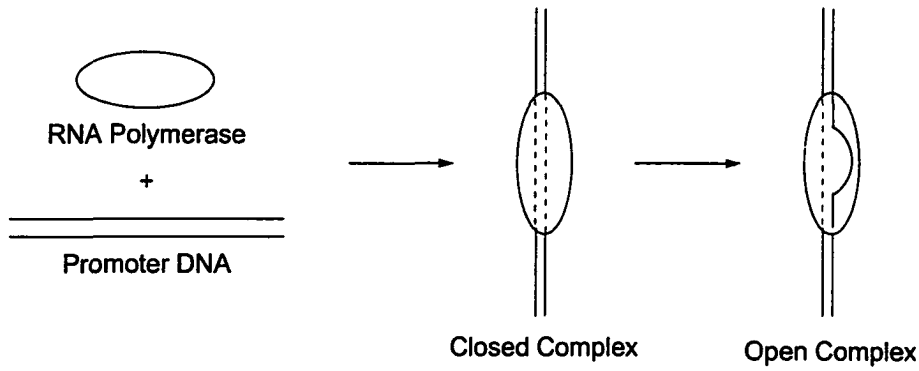

Figure 7. Formation of a transcriptionally active open complex.

2.3 The Use of $Cu(OP)_2$ as a Site Specific Cleaving Agent.

The ability to convert DNA binding proteins into site specific cleaving agents provides access to cleaving agents which have DNA recognition regions three to four

times longer than those of naturally occurring restriction enzymes.[75-78] Duplex DNA cleaving compounds with longer DNA recognition regions provide the ability to cleave DNA in a more specific manner than is currently possible through the use of naturally occurring restriction enzymes. The first example of conversion of $Cu(OP)_2$ to a site specific cleavage compound was reported by Sigman and co-workers in 1987.[75] This process was carried out by chemically modifying the *E. coli L*-tryptophan (trp) repressor protein with 2-iminothiolane hydrochloride, followed by conjugation with 5-iodoacetamido-1,10-phenanthroline (**23**) (Figure 8). Since that time, several other proteins including cAMP-binding protein and the bacterio-phage λ Cro protein have been converted into site specific nucleases through this method.[76-78]

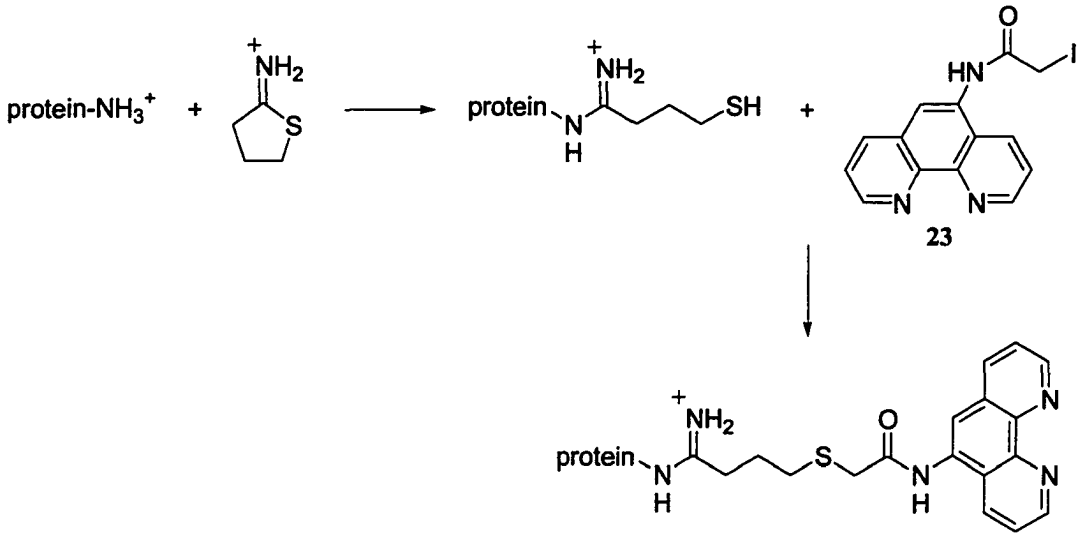

Figure 8. Pathway for conversion of DNA binding proteins into site specific cleaving agents.[75]

While this method allows for easy conversion of any DNA binding protein containing a suitably positioned nucleophilic amino acid into a site specific cleagave agent, this method suffers from several limitations. The 2-iminothiolane hydrochloride will react with all accessible nucleophiles such as asparagine, glutamine, lysine, arginine, and cysteine residues present in the DNA binding protein. This can result in a protein which has been modified at multiple sites and is capable of cleaving DNA at several locations. DNA cleavage activity will only be observed by the modified protein if the modification(s) occur in locations which allow delivery of the copper phenanthroline complex to the minor groove of the DNA. Destabilization of the protein DNA complex can also occur if modification occurs in a region which interacts with the DNA duplex during protein binding. As a result, the cleavage efficiency of the modified protein can be compromised due to reduced binding affinity.

In an elegant study demonstrating that these problems could be overcome through the use of site directed mutagenesis, Sigman and co-workers created a genetically mutated *E. coli* trp repressor protein (E49C) through the substitution of glutamic acid-49 for a cysteine residue.[78] This genetic modification provides the ability to incorporate a single 1,10-phenanthroline ligand into the protein through direct conjugation of **23** and the cysteine residue in E49C to generate E49C-OP. Glutamic acid-49 was chosen as the site of genetic modification from analysis of the co-crystal structure of the *E. coli* trp repressor with one of its operators, which showed that E49 was located near the homodimer dyad axis and pointing toward the minor groove of the DNA duplex (Figure 9).[79] From the crystal structure, it is also apparent that E49 is not near the region of the

Figure 9. Crystal structure of the *E. coli* Trp Repressor DNA complex. The tryptophan co-factor is shown in blue and glutamic acid-49 is shown in green.[78]

protein which is responsible for DNA recognition. Thus, it was expected that modification of this residue would not affect the DNA binding ability of the trp repressor.

The DNA cleavage ability of the 1,10-phenanthroline conjugated E49C (E49C-OP) was used to address the questions regarding the *E.coli* trp repressor binding orientation. The validity of the crystal structure with respect to binding in dilute solution was challenged on the basis of the proposal that the *E. coli* trp repressor binds to DNA in a manner centered at a pseudodyad axis rather than the dyad axis as shown in Figure 8.[80] Since the incorporation of the phenanthroline moiety is near the dyad axis in E49C, the

fact that E49C-OP cleaves the *trp R* operator at a site in accord with the original crystal structure was taken to indicate that the crystal structure was correct and that the *E. coli* trp repressor binds in a manner centered about the dyad axis.

However, because these studies involved the use of a mutant protein, and no crystal structure of the E49C protein has been obtained, changes in the tertiary structure as a result of the glutamic acid-49 mutation have not been ruled out. The mutation may cause a shift in either the binding orientation or sequence specificity. Because the protein has been hypothesized to bind to DNA through recognition of subtle differences in sequence geometry rather than through recognition of the DNA sequence directly, subtle changes in the protein structure as a result of single site mutagenesis could be expected to alter either the sequence specificity or binding orientation.

The effectiveness of of DNA binding proteins converted into site specific cleaving agents using this method is compromised by the stoichiometry of the copper phenanthroline complex employed. In all of the cases discussed above, the copper phenanthroline stoichiometry is 1:1. While the 1:1 complex has been shown to react with duplex DNA to form direct strand breaks, the cleavage efficiency could be expected to be greatly improved through the development of conjugates which allow the formation of a 2:1 phenanthroline to copper complex.

A series of complexes containing both 1:1 and 2:1 phenanthroline to copper stoichiometries conjugated to an analogue of the minor groove DNA binding molecule distamycin prepared by Meunier and co-workers damage duplex DNA (Figure 10).[81-83] The linkage of the phenanthroline moiety in the compounds containing two phenanthroline ligands has been carried out using a serinol bridge through either the 3'

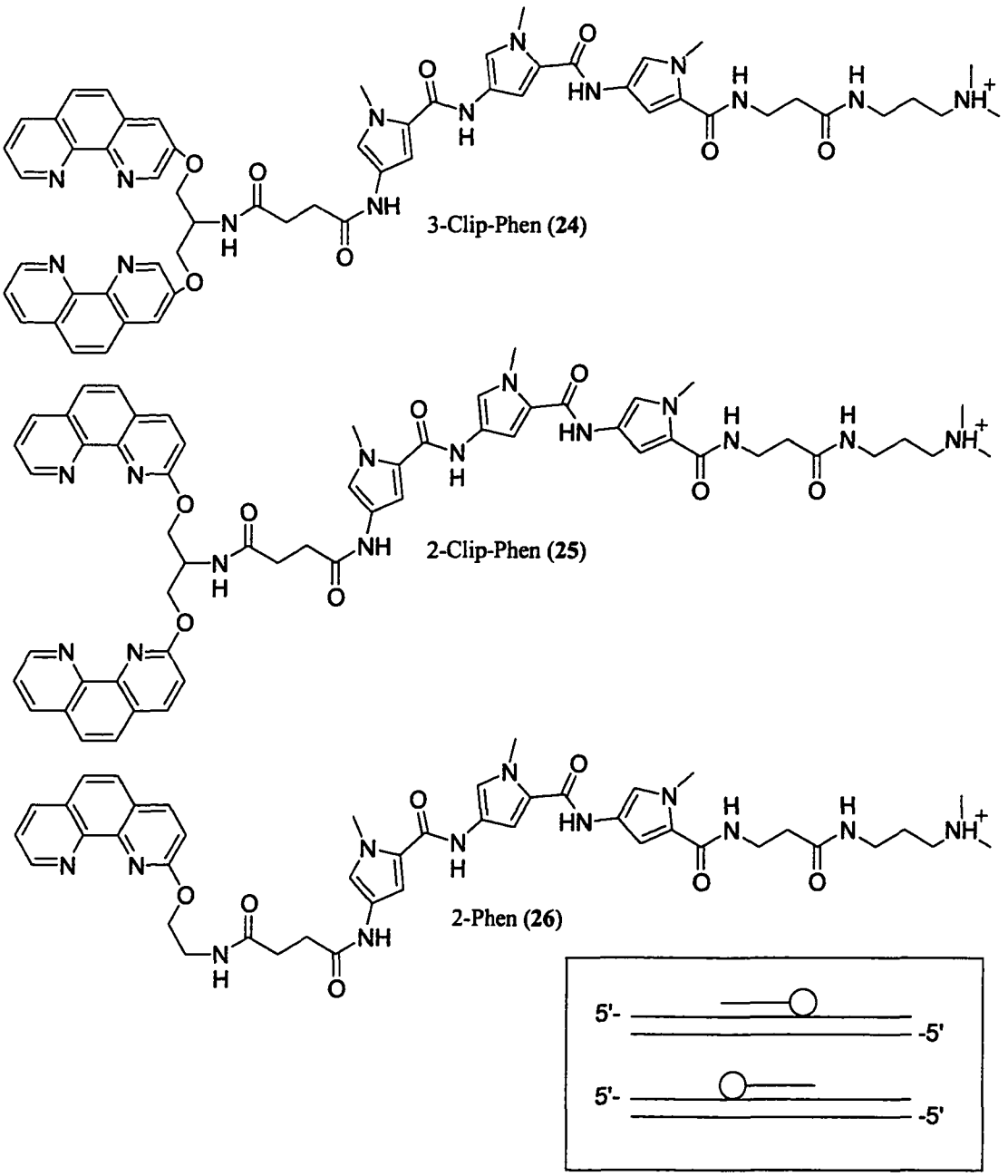

Figure 10. Structures of **24-26**. Inset shows the two binding orientations of **24-26.**

(3-Clip-Phen) (**24**), or 2' (2-Clip-Phen (**25**), 2-phen) (**26**) positions of the phenanthroline ligand.[82-85] The use of a distamycin analogue allows targeting of the 1,10-phenanthroline copper complex through the recognition of the distamycin moiety for five contiguous A·T

base pairs. The distamycin conjugate can bind in two orientations within the minor groove (Figure 10). The exact site of reaction with DNA is determined from a combination of the following factors: 1) The distance from the phenanthroline moiety to the DNA binding portion of the molecule; 2) The binding preference of the 1,10-phenanthroline moiety within the minor groove; 3) The orientation of the distamycin conjugate within its binding region.

Comparison of the quantity of cleavage generated from **24-26** at a given time shows that the 3-Clip-Phen complex (**24**) is more efficient at damaging duplex DNA than the 2-Clip-Phen complex (**25**) or the 2-Phen complex (**26**). This suggests that the position of the serinol bridge is important in determining the cleavage efficiency of the $Cu(OP)_2$ moiety.[82] This effect may be due alteration of the orientation of the phenanthroline ligands around the copper in the complexes containing 1,10-phenanthroline ligands substituted at the 2-position. Reduced cleavage efficiency resulting from substitution of the 2-position of the 1,10-phenanthroline ligands is consistent with the observation that 2,9-dimethylphenanthroline complexes of copper (**27**) are incapable of damaging duplex DNA.[35]

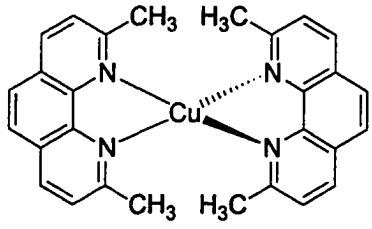

27

Analysis of the products resulting from treatment of duplex DNA with **24** after heating showed the presence of **7** (> 50%), 3'-phosphoglycolate (**9**) (~ 15%), and furfural (**28**) (~ 15%). The presence of **7** and **9** are indicative of C1'- and C4'-hydrogen atom

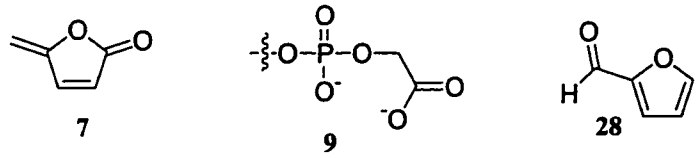

7 **9** **28**

abstraction, while **28** is indicative of the formation of C5'-radicals. Hydrogen atom abstraction from the C5'-position generates direct strand breaks in the presence of oxygen (Figure 11).[16] Reaction of the C5'-radical (**29**) with oxygen, followed by hydrogen atom abstraction generates the C5'-peroxide **30**, which has been proposed to solvolyze to

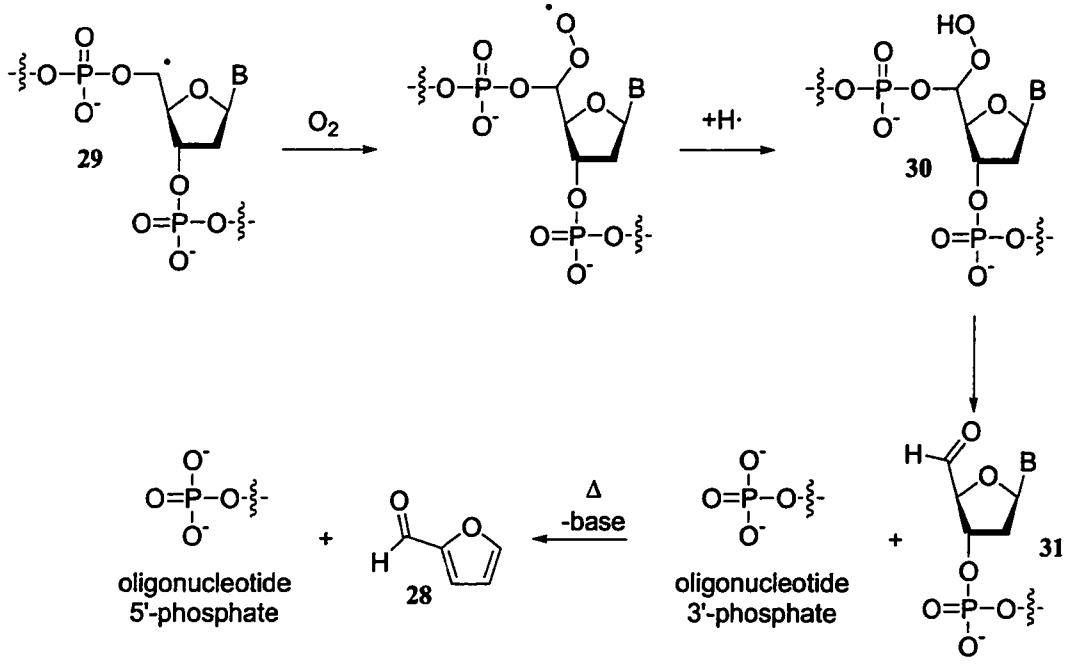

Figure 11. Mechanism for the formation of **28** from the C5'-radical.[16]

generate **31** and the corresponding C3'-phosphate. Observation of C5'- reactivity for **24** was proposed to be a result of reduced binding affinity of the 1,10-phenanthroline moiety in **24** within the minor groove compared to that of $Cu(OP)_2$ in the presence of $MgCl_2$ (25 mM).[83]

The mono phenanthroline analogue (**26**) is the least efficient cleaving agent of the three compounds. This is consistent with the decreased efficiency of Cu(OP) compared to $Cu(OP)_2$.[39] All three compounds are capable of damaging DNA in the micromolar concentration range, high concentrations of duplex DNA, on the order of 1.0 μM, are required in order to observe efficient strand scission. This is the result of a relatively weak binding affinity for the distamycin conjugate, as compared to the nanomolar concentration ranges required for cleavage for both duplex DNA and the modified proteins described above.[78,81]

While **24-26** provide the ability to site specifically cleave DNA, they suffer from a major limitation with regard to sequence specificity. The distamycin analogue used in **24-26** binds to only five successive A·T base pairs. Extension of the sequence specificity can be achieved through the use of the hairpin polyamides, although the ability of these compounds to recognize DNA sequences is limited when compared to naturally occurring restriction enzymes and the site specific cleavage agents prepared from DNA binding proteins.[86-88] These compounds have the potential to serve as mechanistic probes for the $Cu(OP)_2$ induced cleavage of DNA by providing the ability to site specifically deliver the $Cu(OP)_2$ or Cu(OP) moieties. This ability coupled with site specific incorporation of potential intermediates in the pathway leading to direct strand scission may provide useful insight into the mechanism of the $Cu(OP)_2$ reaction with DNA.

2.4 Proposed Mechanisms to Account for the Formation of Direct Strand Breaks Induced by $Cu(OP)_2$ and Cu(OP).

Three mechanisms have been put forward to explain the formation of direct strand scission and the observed products generated upon treatment of duplex DNA with $Cu(OP)_2$ or Cu(OP) in the presence of a reductant and oxygen or hydrogen peroxide.[31-35] These mechanisms are: 1) Solvolysis of the 3'-phosphate present in a 1',2'-dehydronucleotide generated from C1'-hydrogen atom abstraction (Figure 12, pathway a);[31] 2) A copper induced β-elimination of **1** formed from C1'-hydrogen atom abstraction

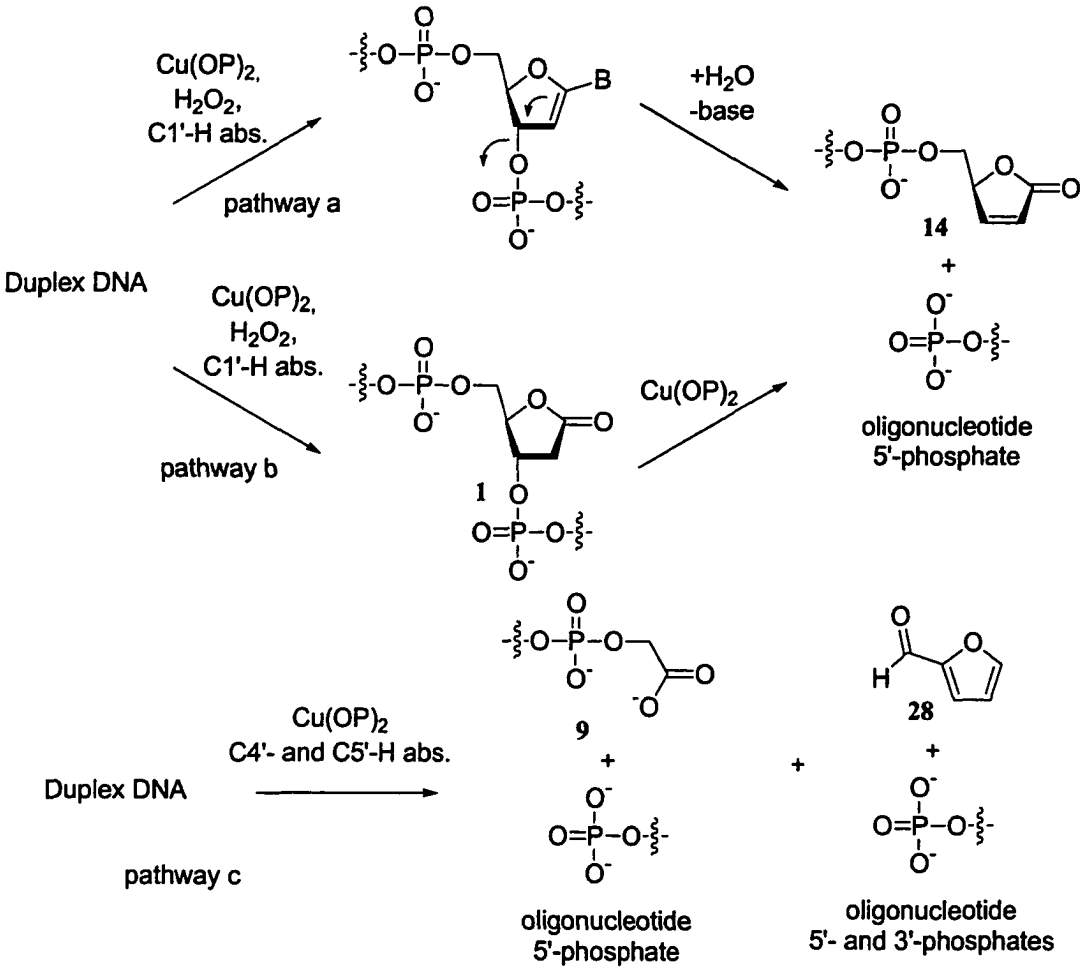

Figure 12. Proposed pathways for the formation of direct strand breaks produced by $Cu(OP)_2$.

(Figure 12, pathway b);[33] 3) Direct strand scission resulting from hydrogen atom abstraction from the C4'- and C5'-positions only (Figure 12, pathway c).[34]

As mentioned previously, analysis of DNA treated with $Cu(OP)_2$ showed the formation of low yields of 3'-phosphoglycolate (**9**) (< 30%), indicative of C4'-oxidation. The yield of 3'-phosphoglycolate **9** was observed to vary as a function of DNA sequence, although no qualitative sequence specificity leading to the formation of **9** has been clearly identified.[36] A slower migrating product was also observed by denaturing PAGE and was attributed to butenolide **14** based upon its conversion to a 3'-phosphate terminus upon treatment with hot piperdine and even more mild conditions.[43]

Additional evidence for the formation of the butenolide termini was obtained from analysis of DNA treated with $Cu(OP)_2$ in the presence of H_2O_2 by HPLC, which showed the formation of 5-methylenefuranone (**7**), the expected degradation product from butenolide **14**.[89] Generation of the $Cu(I)(OP)_2$ and H_2O_2 required for DNA strand damage was carried out using $Cu(II)(OP)_2$ in the presence of superoxide produced from γ-radiolysis of aqueous solutions containing tris(hydroxymethyl)aminomethane (Tris).[90] Hydrogen peroxide was proposed to be generated by the dismutation of superoxide mediated by $Cu(OP)_2$.[41,90]

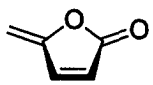

7

Quantitation of the 3'- and 5'-phosphate termini produced from reaction of duplex DNA with $Cu(OP)_2$ was carried out through measurement of the amount of inorganic

phosphate produced from alkaline phosphatase treatment. Inorganic phosphate and **7** were observed in a 2:1 ratio, which is consistent with one equivalent of **7** produced for each direct strand break resulting in 3'- and 5'-phosphate termini. However, the quantitation of the amount of **7** produced upon $Cu(OP)_2$ treatment of duplex DNA is somewhat suspect it was based on an HPLC peak with a maximum absorbance of 0.002 A.U.[89] While Sigman and co-workers propose that the ratio of **7** produced to the amount of phosphate generated is an upper limit due to the possibility of incomplete phosphate hydrolysis, this ratio may also be incorrect as a result of the inability to observe **7** at a high enough concentration to allow accurate quantitation.

Experiments carried out between $Cu(OP)_2$ and duplex DNA in the presence of either $H_2{}^{18}O_2$ or $H_2{}^{18}O$ showed that the carbonyl oxygen in **7** is derived from H_2O rather than from the copper species generated from the reaction with H_2O_2 or O_2.[31] The observation that the carbonyl oxygen in **7** is derived from H_2O can also be accounted for with a mechanism involving the formation of **1** from the C1'-radical (Figure 5). In fact, early mechanistic proposals put forward by Sigman and co-workers invoked the intermediacy of **1**.[26,35,36] Since **1** is stable in the absence of alkali or heat (not required for $Cu(OP)_2$ induced direct strand scission), Sigman and co-workers proposed the formation of butenolide **14**, and subsequently **7**, through a pathway which does not generate **1** as an intermediate (Figure 13). This marks a significant departure from the previously proposed mechanisms which involved the intermediacy of **1**.[26,35,36] Hydrogen atom abstraction from the C1'-position of the sugar moiety by the active $Cu(OP)_2$ species is followed by oxidation of the resulting radical (**16**) to the oxocarbenium ion (**18**). Subsequent loss of a C2'-proton results in the formation of 1',2'-dehydronucleotide **32**.

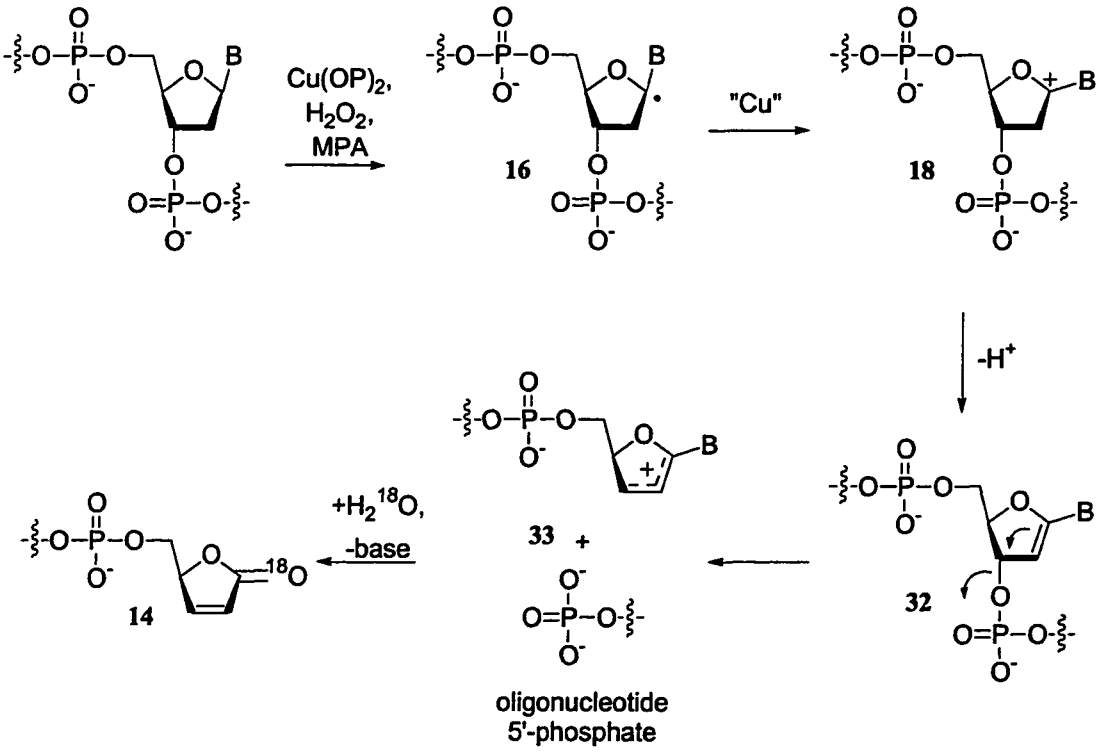

Figure 13. Mechanism proposed by Sigman and co-workers for the formation of **14**.[31]

Solvolysis of the allylic phosphate in **32** generates the corresponding allylic cation (**33**) and cleaves the phosphate backbone. Trapping of **33** with H_2O, followed by hydrolysis forms butenolide **9** without invoking the intermediacy of **1**.

In order for the proposed mechanism to be correct, the C1',C2'-dehydronucleotide **32** must undergo solvolysis on the order of minutes, the time scale for the $Cu(OP)_2$ cleavage reaction.[33] 1',2'-Dehydronucleoside analogues have been shown to hydrolyze in aqueous solutions when subjected to elevated temperatures or mildly acidic conditions, consistent with their similarity to ketene acetals.[91-94] To assess the stability of **32** under conditions relevent to $Cu(OP)_2$ cleavage reactions, Greenberg and Chen prepared the C1',C2'-dehydronucleotide **34**.[33] Stability studies were carried out at rt for 48 h in pH =

7.4 HEPES buffer both in the presence and absence of $Cu(II)(OP)_2$. The dehydronucleotide model (**34**) did not solvolyze under these conditions (Figure 14).

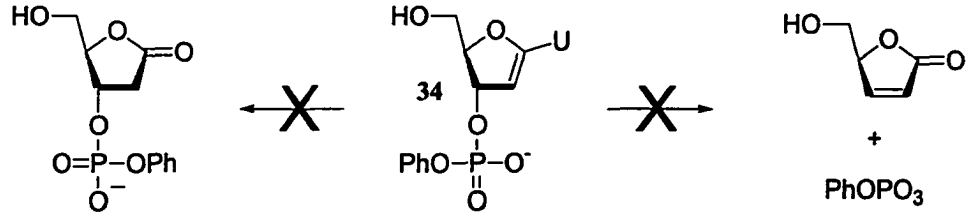

Figure 14. Pathways for the decomposition of **34**.[33]

In order to provide an alternative mechanism which is consistent with the $H_2{}^{18}O$ labeling studies, it was proposed that $Cu(OP)_2$ was capable of inducing a β-elimination of the 3'-phosphate from the 2-deoxyribonolactone (**1**) (Eq 6).[31,33] Exposure of **35** to

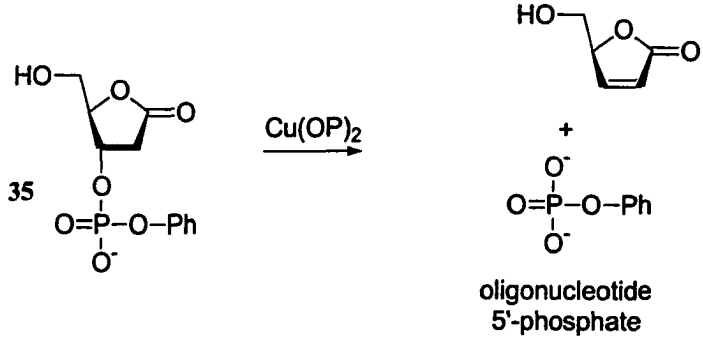

(6)

$Cu(OP)_2$ in the presence of HEPES buffer at pH = 7.4 at rt resulted in clean formation of phenyl phosphate. The decomposition of **35** was quantitatively accounted for by phenyl phosphate formation. Measurement of the rate of decay of **35** gave a value of 1.50×10^{-3} M^{-1} s^{-1} yielding a half life of approximately 1.5 years at the 10 μM concentration ranges typically used for $Cu(OP)_2$ cleavage experiments. Since significantly faster rates of

cleavage have been observed for the reaction of $Cu(OP)_2$ with duplex DNA, the relevance of the slow rate measured in this experiment was rationalized by proposing that the effective molarity of the $Cu(OP)_2$ is significantly higher when it is bound in the minor groove of B-DNA. This hypothesis is supported by the observation that the effective molarity of noncovalent complexes can be as high as 10^4-10^6.[95] Extrapolation of the observed rate constant to 10 M $Cu(OP)_2$ gives a half life for **35** of 46 s, indicating that if the results observed in the model system can be extrapolated to duplex DNA, the $Cu(OP)_2$ catalyzed elimination reaction is kinetically viable.

The use of the phenyl phosphate diester in **35** rather than an alkyl phosphate diester, which is present in DNA, is expected to have little effect on the rate of cleavage as both alkyl and aryl phosphate monoesters have similar pK_a values (pK_{a1} ~ 1.6 and pK_{a2} ~ 6.6).[96] The mechanism of the elimination reaction is somewhat uncertain as the sugar product produced upon formation of phenyl phosphate was not identified. However, the likelihood that the formation of phenyl phosphate occurs through copper catalyzed hydrolysis of the phosphate diester is minimal since the Cu(II)(bpy) (bpy = 2,2'-bipyridine) catalyzed hydrolysis of ethyl *p*-nitrophenyl phosphate (**36**) results in the formation of *p*-nitrophenol rather than ethanol (Eq 7).[97] This indicates that if the

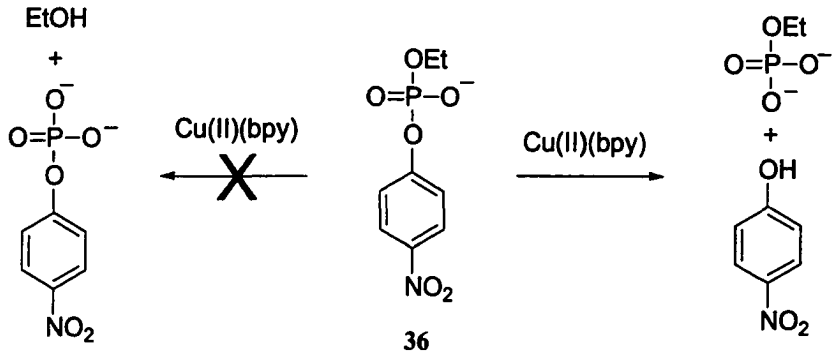

(7)

$Cu(OP)_2$ was degrading **35** by phosphate diester hydrolysis, phenol rather than phenylphosphate would have been observed.

In order to gain further insight into the mechanism of direct strand break formation from the reaction of $Cu(OP)_2$ with duplex DNA, Sugiyama and Oyoshi analyzed the products resulting from this reaction using HPLC-MS.[34] Treatment of duplex hexamer **37a** with $Cu(OP)_2$ in the presence of MPA was carried out in Tris buffer

5'-d(CGT ACG)
3'-d(GCA TGC)
37a

(pH = 7.5) at 0 °C. Because of the short length of **37a**, the melting temperature (T_M) (20.5 °C at 4.15 μM duplex concentration) was measured in order to ensure that the observed $Cu(OP)_2$ reaction was carried out using duplex DNA. HPLC-MS analysis of crude reaction mixtures showed the products resulting from direct strand scission to be oligonucleotides containing 3'-phosphoglycolate and 3'-phosphate termini in a ratio of 1.5:1. Measurement of the quantity of direct strand scission through enzymatic digestion of $Cu(OP)_2$ treated **37a** gave a yield of approximately 13.5%. Oligonucleotides containing the C4'-abasic site **38** accounted for 6.9% of the observed DNA damage, and intact oligonucleotides containing 2-deoxyribonolactone (**1**) (**37b-d**) were observed as the major DNA damage products (34.0%).

5'-d(CGT 1CG) **37b** 5'-d(CGT A1G) **37c** 5'-d(C1T ACG) **37d**

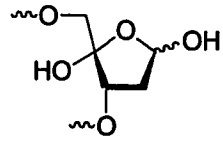

38

Since **37b-d** were stable under these reaction conditions, the 3'-phosphate generated was attributed to hydrogen atom abstraction from the C5'-position of the sugar. This conclusion was confirmed through reduction of the resulting aldehyde (**31**) with sodium borohydride. From these data, the reactive copper species responsible for the degradation of the duplex DNA was proposed to be incapable of inducing an α,β-elimination in **1** to generate butenolide **14**. This led to the conclusion that while the majority of the $Cu(OP)_2$ reaction with duplex DNA generates **1** from hydrogen atom abstraction at the C1'-position, reaction at the C4'- and C5'-positions are the only pathways which lead to the formation of direct strand breaks.

The remaining 49% of the DNA damage was proposed to be a result of damage to the nucleobases in **37a** in a manner which does not produce direct strand breaks, although no direct evidence for damaged nucleobases was obtained using GC-MS or HPLC-MS. Damage to the nucleobases in duplex DNA by $Cu(OP)_2$ has been quantitated by Dizdaroglu and co-workers, and it was concluded that base damage occurs 5.4-7.7 times more readily than damage at the sugar moiety.[98] However, the 2-thiobarbituric acid assay used to determine the amount of sugar damage only allows for quantitation of the products produced from C4'-chemistry and not from C1'-chemistry.[3] As the ratio of C1'- to C4'- chemistry for the reaction of $Cu(OP)_2$ with duplex DNA is greater than 2:1, the ratio of base damage to sugar damage may be much closer to 1:1, supporting the hypothesis put forward by Sugiyama and co-workers.

A potential problem exists with the extension of the results of this study to longer, more relevant pieces of duplex DNA. The thermal stability of **37b-d** can be expected to be significantly lower than that of **37a**. For example, incorporation of the tetrahydrofuran

analogue of the abasic site (**39**) into duplex DNA has been shown to reduce the T_M of the duplex by 10-20 °C depending on the length and local sequence context of the oligonucleotide.[99-101] Generation of **1** in the hexamer used may result in melting of the duplex under the experimental conditions used. Since $Cu(OP)_2$ has been shown not to act effectively on single stranded DNA as a result of the inability of $Cu(OP)_2$ to bind to the DNA,[35,36] a copper induced β-elimination of **1** potentially would not be observed under the experimental conditions.

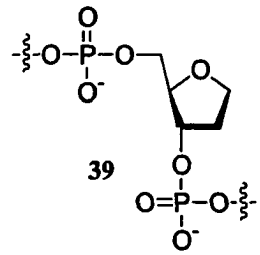

39

If the mechanism proposed by Sugiyama and Oyoshi is applicable to longer strands of duplex DNA, a significant increase in the quantity of strand scission would be observed upon treatment of $Cu(OP)_2$ damaged DNA with alkali as both the 2'-deoxyribonolacone (**1**) and the C4' abasic site (**38**) are alkali labile. From the yields of the material attributed to direct strand scission and the yields of **1** and **38** reported, an alkali enhancement of approximately four can be estimated based upon the ratio of products present from $Cu(OP)_2$ treated **37a**.[34] This is inconsistent with the qualitative enhancements observed from alkali treatment of longer fragments of duplex DNA after reaction with $Cu(OP)_2$ and its derivatives with distamycin analogues, which are no larger than two.[43,83] This indicates that the mechanism proposed by Sugiyama and Oyoshi for

the formation of direct strand breaks upon treatment of duplex DNA with $Cu(OP)_2$ does not account for all of the possible pathways leading to direct strand scission, possibly as a result of duplex melting as described previously.

2.5 The Reactivity of $Cu(OP)_2$, Cu(OP), and Similar Analogues.

As mentioned above, the exact nature of the copper species which damages the sugar moiety in duplex DNA is unknown. DNA damage has been proposed to arise as a result of the generation of freely diffusible hydroxyl radicals, which are generated in a manner similar to the Fenton reaction. In this mechanism, $Cu(I)(OP)_2$ generated from reduction of $Cu(II)(OP)_2$ reacts with hydrogen peroxide to generate hydroxide and a hydroxyl radical (eq 8).[102-105] This hypothesis is inconsistent with the observation that

$$Cu(I) + H_2O_2 \rightarrow Cu(II) + HO^- + HO^{\cdot} \qquad (8)$$

generation of hydroxyl radicals by γ-radiolysis of aqueous duplex DNA solutions produces equal amounts of DNA sugar damage at both the C4'- and C1'-positions rather than the greater than 2:1 ratio of C1'- to C4'-damage observed from $Cu(OP)_2$ treated duplex DNA.[36] Furthermore, in several spin trapping experiments, adducts are observed by electron spin resonance spectroscopy from the reaction of $Cu(OP)_2$ with MPA that are inconsistent with the intermediacy of freely diffusible hydroxyl radicals.[106-108]

Detection of the intermediate responsible for degradation of duplex DNA is further hampered by the partial fluctionality of the 1,10-phenanthroline ligands as a function of copper oxidation state and employed reductant. The association constants for

the generation of Cu(II)(OP) and Cu(II)$(OP)_2$ have been measured spectroscopically. The K_a for the formation of Cu(II)(OP) from free 1,10-phenanthroline and Cu(II) is 1.0×10^9 M^{-1} and 5.0×10^6 M^{-1} for the formation of Cu(II)$(OP)_2$ from free 1,10-phenanthroline and Cu(II)(OP) in aqueous solution (eqs 9 and 10).[109] Reduction of Cu(II) to Cu(I)

$$Cu(II) + OP \rightarrow Cu(II)(OP) \quad K_a = 10^9\ M^{-1} \tag{9}$$

$$Cu(II)(OP) + OP \rightarrow Cu(II)(OP)_2 \quad K_a = 10^{6.7}\ M^{-1} \tag{10}$$

effectively increases the association constants of Cu(I) for 1,10-phenanthroline to 6.3×10^{15} M^{-1} for the association of the first 1,10-phenanthroline ligand but decreases the association of the second 1,10-phenanthroline ligand to 1×10^6 M^{-1} in aqueous solution (eqs 11 and 12).[110] These results indicate that in order for 99% of the copper(II) present

$$Cu(I) + OP \rightarrow Cu(I)(OP) \quad K_a = 10^{15.8}\ M^{-1} \tag{11}$$

$$Cu(I)(OP) + OP \rightarrow Cu(I)(OP)_2 \quad K_a = 10^6\ M^{-1} \tag{12}$$

to exist as Cu(II)$(OP)_2$ at equilibrium in a 10 μM solution of Cu(II)(OP), 1,10-phenanthroline must be present in two fold excess. However, the same ratio of reagents will only yield 60% of Cu(I)$(OP)_2$ at equilibrium upon reduction of Cu(II) to Cu(I).

While these thermodynamic results imply that the Cu(I)$(OP)_2$ complex can dissociate, the kinetics of the dissociation process will determine the ratio of Cu(I)$(OP)_2$ to Cu(I)(OP) present in solution when Cu(I)$(OP)_2$ is generated by reduction of

$Cu(II)(OP)_2$. Unfortunately, the rate of dissociation of 1,10-phenanthroline from $Cu(I)(OP)_2$ has not been measured, but is expected to be slow with respect to the subseqent reaction with H_2O_2 which is required for degredation of duplex DNA. This prediction is based on the observation that $Cu(I)(OP)_2$ has been detected by U.V. spectroscopy when generated by reduction of $Cu(II)(OP)_2$ with ascorbate.[39,110]

However, $Cu(I)(OP)_2$ has not been observed spectroscopically when it is generated from $Cu(II)(OP)_2$ using the most commonly used reductant for $Cu(OP)_2$ mediated damage of DNA, MPA.[39] The failure to observe $Cu(I)(OP)_2$ in the presence of MPA has been attributed to the displacement of one of the 1,10-phenanthroline ligands by the reductant.[39] The observation of different chemical shifts of the protons in the 1,10-phenanthroline ligands when $Cu(II)(OP)_2$ is reduced with either ascrobate or MPA supports this conclusion. Whether or not the substitution of one of the 1,10-phenanthroline ligands occurs prior to or after reduction of the copper center has not been addressed. Based on the association constants for the second 1,10-phenanthroline ligand for Cu(II)(OP) and Cu(I)(OP), it can be expected that the reduction of the copper center occurs prior to the ligand exchange.

Irrespective of the structure of the copper species responsible for the initial C1' hydrogen atom abstraction, if direct strand scission arises from a copper induced β-elimination of the 3'-phosphate in **1**, a copper species generated during the DNA cleavage reaction must be able to induce the elimination. This elimination reaction can be envisioned to occur through several pathways: 1) Through hydroxide bound to $Cu(OP)_2$ acting as a general base catalyst with H_2O (Figure 15, pathway a); 2) Reaction of $Cu(OP)_2$ with **1** through Lewis acid catalyzed enolate formation (Figure 15, pathway b);

3) A combination of the previous two mechanisms with the HO-Cu(OP)$_2$ acting as both a Lewis acid and a general base (Figure 15, pathway c).

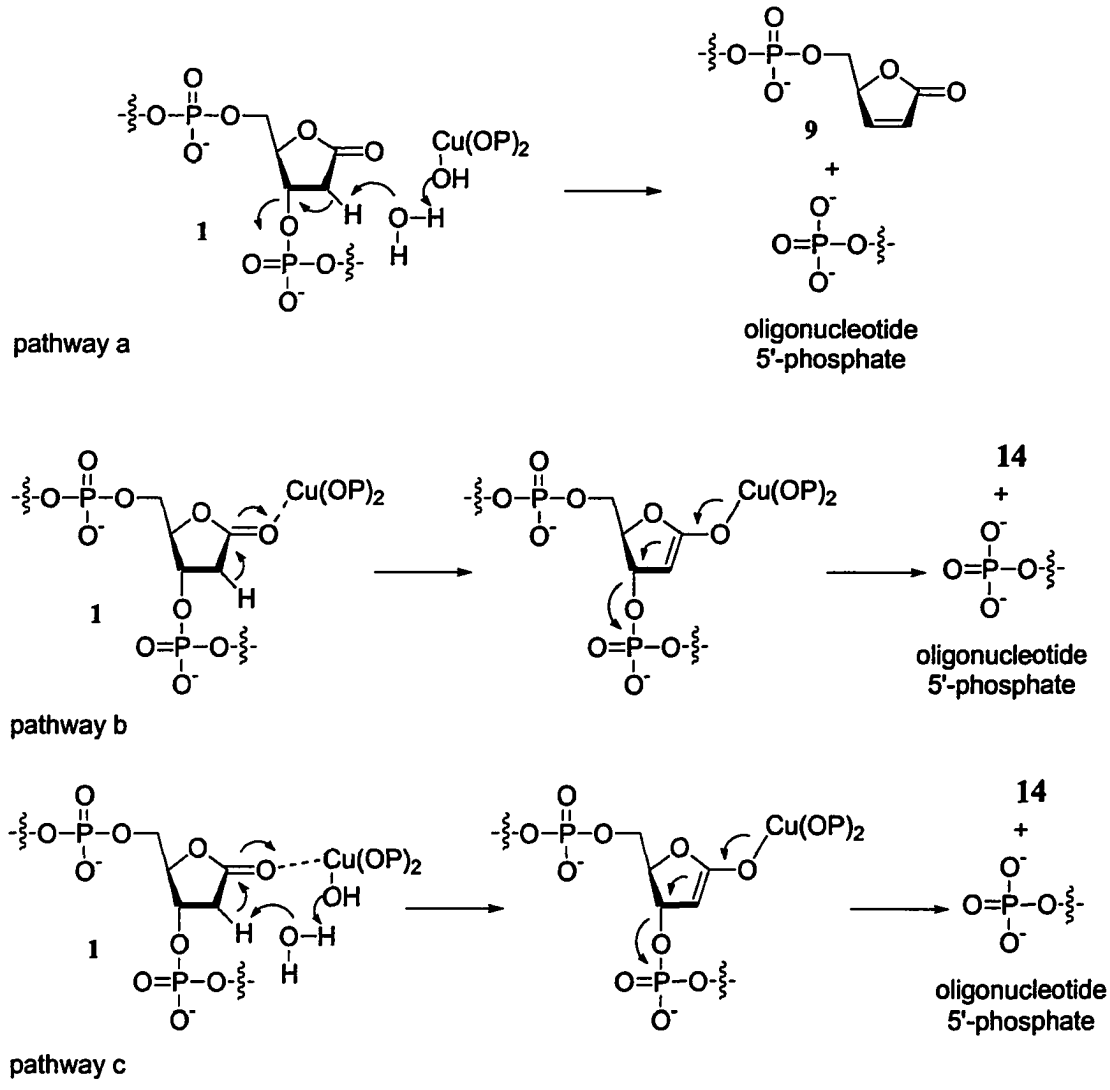

Figure 15. Possible pathways for the Cu induced β-elimination of **1**.

A variety of copper based ribonuclease mimics have been prepared which catalyze either the trans-esterification or phosphate hydrolysis of RNA through mechanisms similar to those described for the copper induced elimination of **1**.[111-114]

While the structures of these compounds vary widely and commonly include both bimetallic and monometallic complexes, several ligands which are electronically similar to 1,10-phenanthroline have been employed in the mononuclear copper containing ribonuclease mimics, including 2,2'-bipyridines (bpy) and 2,2',2"-terpyridines (tpy).[115,116]

The differences in electronic effects between 2,2',2"-terpyridine, 2,2'-bipyridine, and 1,10-phenanthroline ligands is best demonstrated by examining the pK_a of the corresponding H_2O bound copper(II) complexes. The pK_a values for the 2,2',2"-terpyridine aquo complex (**40**), 2,2'-bipyridine bis(aquo) complex (**41**) and 2,9-dimethyl-1,10-phenanthroline bis(aquo) complex (**42**) have been measured to be 8.2, 7.8, and 7.0 respectively.[117] This indicates that of the three ligands, the 1,10-phenanthroline analogue leads to the most Lewis acidic copper complex. However, the small differences in the observed pK_a values for the copper bound H_2O indicates that the three ligands are electronically similar.

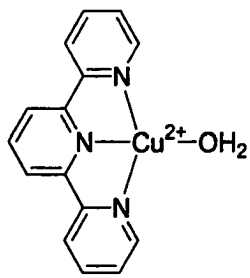

40

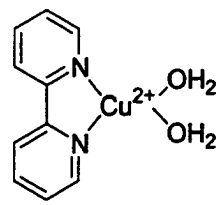

41

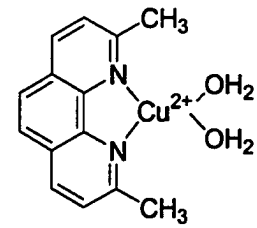

42

pK_a	8.2	7.8	7.0

Consistent with the Lewis acidic nature of these compounds, **40-42** have been proposed to catalyze the hydrolysis of ribonucleotide dimer **43** through Lewis acid activation of the phosphate diester (Figure 16).[117] Also consistent with the Lewis

acidities of these compounds is the observation that the rates of ribonucleotide dimer hydrolysis parallels the pK_a of the bound H_2O. Thus, **42** is most efficient at catalyzing the hydrolysis of **43** at pH = 7.0 while **40** is the least efficient.

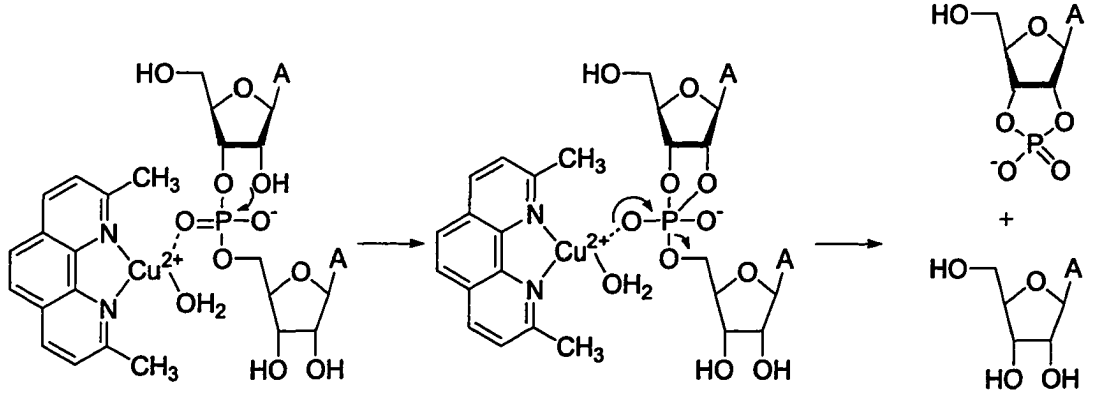

42 **43**

Figure 16. Proposed mechanism for the Lewis acid catalyzed transesterification of **43** catalyzed by **42.**[117]

Measurement of the rate of phosphate diester hydrolysis at pH above the pK_a of the aquo ligand shows that the rate of catalysis by 1,10-phenanthroline analogue **42** is more than 10^3 times faster than of **40**. To explain this observation, it was proposed that **42** was capable of increasing the electrophilicity of the phosphorous by chelating to both free oxygens in the phosphate diester to form **44**. An alternative explanation that was not

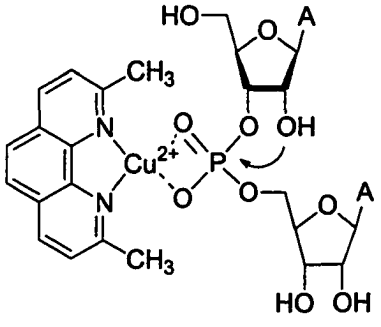

44

considered is the possibility that all three compounds are capable of functioning as a general base, and that **42** functions as a more efficient general base as a result of the fact that a greater portion exists as a copper bound hydroxide at pH = 7.0 (Figure 17).

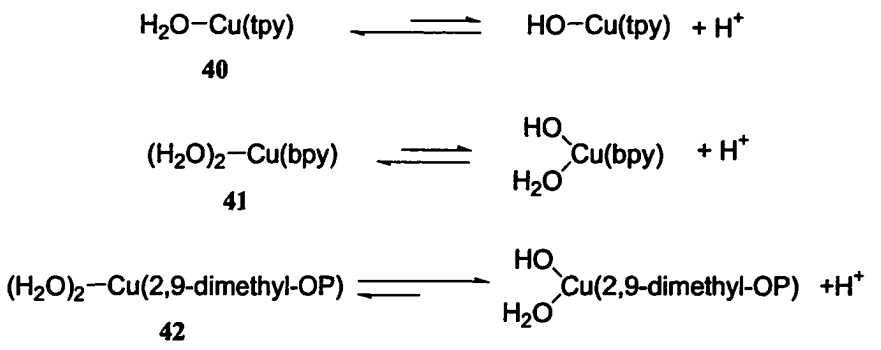

Figure 17. Partitioning of copper bound hydroxide in **40-42** at pH = 7.0.

Evidence for copper bound hydroxide reactivity in conjunction with copper centered Lewis acid activation is consistent with the observation that Cu(II)(bpy) hydrolyzes the lithium salt of ethyl *p*-nitrophenylphosphate (**36**) more rapidly at a pH of 7.85 than at pH 6.0.[97] A 6.3 x 10^3 fold rate increase at pH 7.85 upon addition of the copper catalyst over the hydrolysis rate in the absence of the catalyst was observed. The dependence of the rate of hydrolysis on the concentration of Cu(I)(2,2'-bipyridine)(OH) and not on the concentration of Cu(II)(bpy) shows that the copper bound hydroxide is required for phosphate hydrolysis. Based on these data, phosphate hydrolysis was proposed to occur through coordination of the copper species to oxygen, followed by nucleophilic attack of the copper bound hydroxide at the resulting electrophilic phosphorous (Figure 18). However, based on these results the possibility of the copper

bound hydroxide acting as a general base during H_2O attack on the electrophilic phosphorous cannot be ruled out (Figure 15, pathway a).

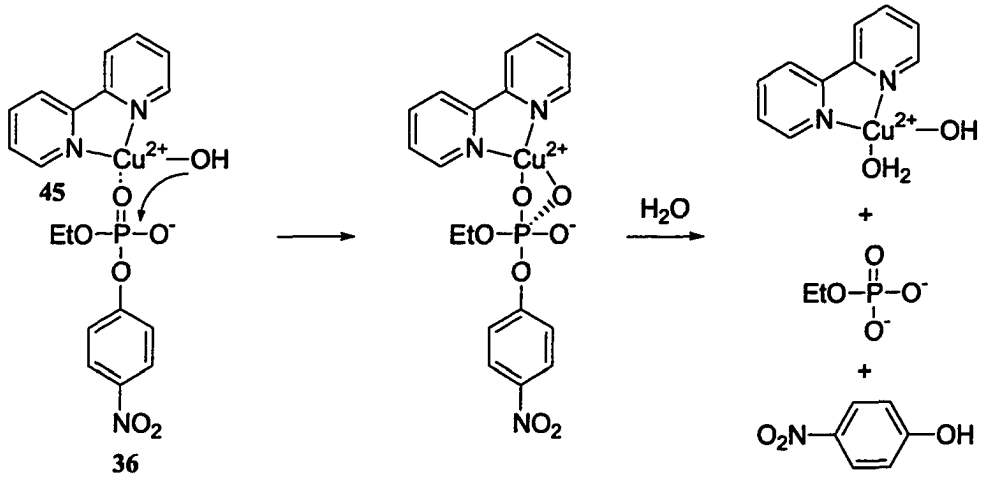

Figure 18. Proposed mechanism for the hydrolysis of **36** by **45** at pH = 7.85.[97]

Evidence for general base catalysis by copper bound hydroxide species has been obtained from catalysis of a phosphodiester transeterification in a model compound (**46**) by Cu(II)(tpy) (**40**).[118] The pH profile for the reactivity of **40** shows a maximum rate of catalysis at pH 9.0, which is consistent with the involvement of a copper bound hydroxide (**47**) in the transesterification reaction. The reduced rate of reactivity of **40** at pH lower than 9.0 was proposed to be a result of protonation of the copper bound hydroxide, effectively converting **47** into the corresponding copper(II)aquo species (**40**). This conclusion is consistent with the pK_a of 8.2 measured for this copper(II)aquo species.[117] From these data, it was proposed that the copper bound hydroxide is responsible for removal of the proton of the pendant alcohol through general base catalysis in conjunction with Lewis acidic activation of the phosphate diester (Figure 19).

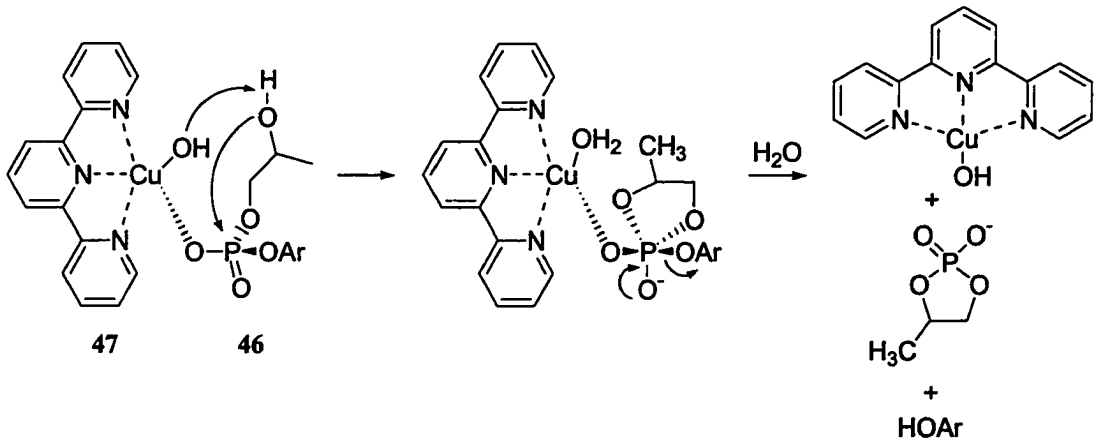

Figure 19. Proposed mechanism for the transesterification of **46** catalyzed by **47** at pH = 9.0.[118]

2.6 Statement of Research Objectives.

From the information presented above, several proposals have been put forth with regard to the mechanism of direct strand scission of duplex DNA induced by $Cu(II)(OP)_2$ and Cu(II)(OP) in the presence of a reductant under aerobic conditions:

1) The majority of the $Cu(OP)_2$ reaction with duplex DNA occurs at the C1'-position of the sugar moiety and has been proposed to lead to direct strand scission.[26,35,36]

2) Direct strand scission of duplex DNA mediated by $Cu(OP)_2$ also occurs to a limited extent through hydrogen atom abstraction from the C4' position of the sugar moiety.[26,35,36]

3) Analysis of $Cu(OP)_2$ treated hexameric duplex DNA by HPLC-MS indicates that the 2-deoxyribonolactone (**1**) is stable in the presence of $Cu(OP)_2$ and that direct strand scission arises from hydrogen atom abstraction at the C4'- and C5'-positions of the sugar moiety.[34]

3) Studies carried out on a mononucleotide model compound indicate that Cu(II)$(OP)_2$ is capable of catalyzing the β-elimination of the 3'-phosphate from the 2-deoxyribonolactone (**1**).[33]

4) Based on the reactivity exhibited by 1,10-phenanthroline, 2,2'-bipyridine, and 2,2',2"-terpyridine systems with regard to the hydrolysis and transesterification of phosphate diesters, it is possible that $Cu(OP)_2$ aquo complexes are capable of catalyzing the β-elimination of the 3'-phosphate through Lewis acid and/or general base catalysis.

The mechanistic studies described above present a contradictory picture with respect to the mechanism of direct strand scission of duplex DNA induced by $Cu(OP)_2$. Model studies indicate that Cu(II)$(OP)_2$ is capable of catalyzing the β-elimination of the 3'-phosphate.[33] Studies carried out using oligonucleotides six bases in length indicate that the 2-deoxyribonolactone (**1**) is stable in the presence of the $Cu(OP)_2$ species responsible for degradation of duplex DNA.[34] However, as mentioned above the oligonucleotide studies may be in error as the stability of the hexamer used containing the 2-deoxyribonolactone was not addressed.

The goal of this research is to address the following questions through the use of site specific incorporation of the 2'-deoxyribonolatone into oligonucleotides and the use of compounds which allow site specific delivery of $Cu(OP)_2$ and Cu(OP) to duplex DNA:

1) Will the incorporation of the 2-deoxyribonolactone (**1**) lesion into oligonucleotides six bases in length destabilize the oligonucleotide to the point that melting occurs under the DNA cleavage conditions employed?

2) Can evidence be obtained for direct strand scission arising from C1'-hydrogen atom abstraction by measurement of the enhancement in strand cleavage upon alkali treatment of duplex DNA damaged with $Cu(OP)_2$?

3) Can evidence be obtained for the copper induced β-elimination of the 3'-phosphate group by site specifically incorporating the 2-deoxyribonolactone (**1**) into oligonucleotides and site specifically delivering $Cu(OP)_2$ or Cu(OP) to the site of 2-deoxyribonolactone incorporation (Figure 20)?

4) By taking advantage of the ability to site specifically deliver $Cu(OP)_2$ or Cu(OP) to the site of 2-deoxyribonolactone can conclusions be drawn with respect to the difference in rates of reaction of $Cu(OP)_2$ or Cu(OP) with duplex DNA?

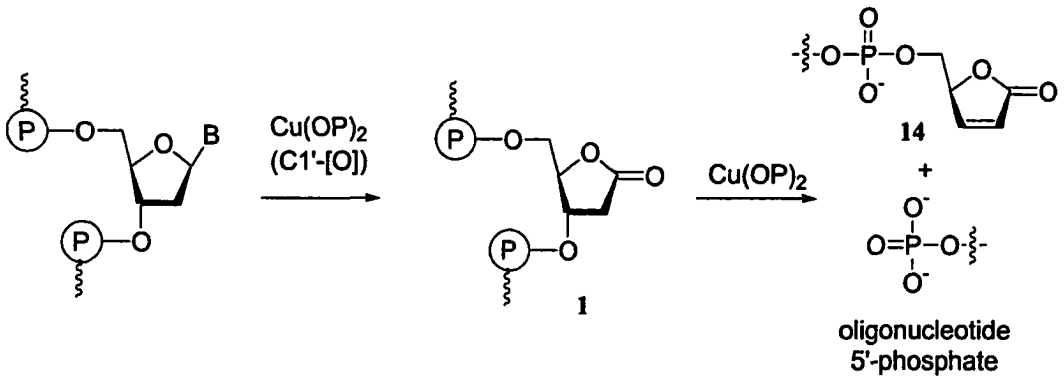

Figure 20. Hypothesized pathway for the formation of direct strand breaks from $Cu(OP)_2$ reaction with duplex DNA.

3 Results and Discussion.

3.1 Stability of Oligonucleotides Containing the 2-Deoxyribonolactone Lesion.

In order to determine whether or not the results of Sugiyama and Oyoshi are relevant with respect to the ability of copper to catalyze the β-elimination of the 3'-phosphate in the 2-deoxyribonolactone lesion (**1**) in duplex DNA, melting studies were undertaken to determine if complexation of **37b-d** with the respective complement

5'-d(CGT 1CG) **37b** 5'-d(CGT A1G) **37c** 5'-d(C1T ACG) **37d**

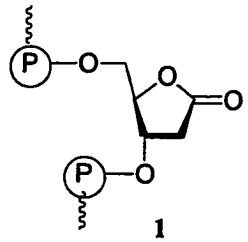

1

dehybridize under the experimental conditions.[34] Synthesis of a duplex containing **37b** is impractical due to the fact that **37a** is palindromic. Synthetic incorporation of 2-deoxyribonolatone (**1**) in this sequence would result in the measurement of the T_M of a duplex containing two 2-deoxyribonolactone lesions. In order to avoid this possibility and to allow for meaningful comparison of the T_M data obtained between **37b-d**, a non-palindromic oligonucleotide which showed similar thermal stability to **37a** was required.

In the search for an oligonucleotide which exhibits similar duplex stability to **37a**, the effects of salt and oligonucleotide concentration need to be considered. Oligonucleotide duplex stability has been shown to be a function of both salt concentration, as well as the concentration of the duplex.[119] Increasing duplex stability is observed with increasing salt concentration and/or increasing duplex concentration. In

order to select a hexamer of relevant sequence, the T_M values for several oligonucleotides including **37a** were calculated empirically from thermodynamic parameters using eq 13

$$\frac{1}{T_M} = \frac{(n-1)R}{\Delta H^O}\ln(C_T) + \frac{\Delta S^O - (n-1)R\ln(2) + R\ln(n)}{\Delta H^O} \quad (13)$$

$$\frac{1}{T_M} = \frac{(n-1)}{\Delta H^O}\ln(C_T) + \frac{\Delta S^O - (n-1)(R)\ln(2n)}{\Delta H^O} \quad (14)$$

for palindromic sequences and eq 14 for non-palindromic sequences (n = 2 for the melting of duplex DNA and C_T is the concentration of the duplex).[119] The thermodynamic parameters, $\Delta S°$ and $\Delta H°$, were calculated using nearest-neighbor parameters for duplex DNA in 1.0 M NaCl.[120-123] Comparison of the calculated T_M values for duplexes **37a** and **48-52** at the duplex concentration used for the $Cu(OP)_2$ experiments carried out by Sugiyama and co-workers (4.15 μM) shows a predicted T_M for **48** which is very similar to **37a**.

Table 1. Calculated T_M values for oligonucleotides **37a** and **48-52**.[a]

Oligonucleotide	T_M (°C)[b]
5'-d(CGT ACG) (**37a**) 3'-d(GCA TGC)	25.4
5'-d(GCT ACG) (**48**) 3'-d(CGA TGC)	25.9
5'-d(GCA ACG) (**49**) 3'-d(CGT TGC)	23.2
5'-d(CGA AGC) (**50**) 3'-d(GCT TCG)	21.2
5'-d(GCT TCG) (**51**) 3'-d(CGA AGC	20.5
5'-d(CAG TCG) (**52**) 3'-d(GTC AGC)	18.4

[a] [duplex DNA] = 4.15 μM; 1.0 M NaCl. [b] Calculated from ref. 120-123.

Syntheses of both strands of duplex **48** were carried out using standard phosphoramidite chemistry and the T_M values of **37a** and **48** were measured by U.V. spectroscopy using buffer and concentration conditions identical to the $Cu(OP)_2$ experiments (4.15 μM duplex concentration in 50 mM Tris at pH = 7.5) in 1.0 M NaCl (Table 2).[34] The absorbance at 260 nm was monitored as a function of increasing temperature from 2.5 °C to 45 °C (0.5 °C/min). The absorbance (A) vs. temperature (T) data was fit to eq 15 where a, b, c, and d were varied until the best fit of the data was

$$A = \frac{a}{1+e^{b-c(T)}} + d \qquad (15)$$

obtained.[119] The T_M value was then determined from maximum of its first derivative, which was calculated using Origin 6.1. Surprisingly, the measured T_M value for **48** was lower than the calculated value by 7.0 °C, while the measured T_M for **37a** was lower by only 2.5 °C. While the exact reason for the significantly lower measured T_M value is uncertain, it is clear that **48** is not a good analogue for **37a**.

Table 2. Measured T_M values for oligonucleotides **37a** and **48**.[a]

Oligonucleotide	T_M (°C)[b]	ΔT_M (°C)[c]
5'-d(CGT ACG) (**37a**) 3'-d(GCA TGC)	23.4 ± 1.3	-2.5
5'-d(GCT ACG) (**48**) 3'-d(CGA TGC)	18.9 ± 2.12	-7.0

[a] [duplex DNA] = 4.15 μM; 1.0 M NaCl; 50 mM Tris, pH = 7.5. [b] T_M values were determined by U.V. absorbance at 260 nm as a function of temp. [c] $\Delta T_M = T_M(obs.) - T_M(calc.)$.

Determination of the T_M value for **49** using the same conditions described for **37a** and **48** gave a value much closer to the that of **37a** (Table 3). Upon decreasing the salt concentration to 100 mM, both oligonucleotides showed T_M values that were identical within experimental error. Measurement of the T_M values using the conditions of the $Cu(OP)_2$ experiments (50 mM Tris, pH = 7.5; 0.0 M NaCl) reported by Sugiyama and Oyoshi showed a higher T_M for **49** than **37a**.

Table 3. Effect of NaCl concentration on the T_M for **37a** and **49**.[a]

5'-d(CGT ACG) 3'-d(GCA TGC) **(37a)**	5'-d(GCA ACG) 3'-d(CGT TGC) **(49)**

Oligonucleotide	[NaCl] (M)	T_M (°C)[b]
37a	1.0	23.4 ± 1.3
37a	0.1	16.9 ± 1.1
37a	0.0	13.2 ± 0.7
49	1.0	21.1 ± 0.7
49	0.1	17.4 ± 1.1
49	0.0	15.9 ± 1.3

[a] [Duplex DNA] = 4.15 μM; 50 mM Tris, pH = 7.5. [b] T_M values were determined by U.V. absorbance at 260 nm as a function of temp.

Site specific generation of **1** was carried out using the method of Greenberg and co-workers using C1'-*t*-butyl ketone **15**.[28,49,50] The site of incorporation of **15** and ultimate generation of **1** in oligonucleotide duplex **49** was governed by the fact that incorporation of **1** in the center of the oligonucleotide should provide the best opportunity to observe duplex formation in the presence of the 2-deoxyribonolactone lesion. Furthermore, location of **1** near the center of duplex **49** provides the ability to maintain the same flanking sequence present in **37b**. Generation of **1** opposite a deoxyadenosine

residue is predicted to show the smallest decrease in the T_M value from results obtained using the abasic site analogue **39**.[101] Assuming **1** has the expected destabilizing effect on

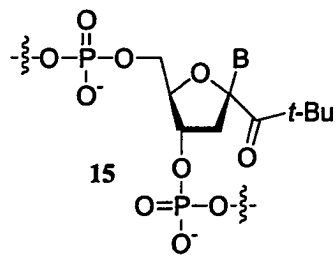

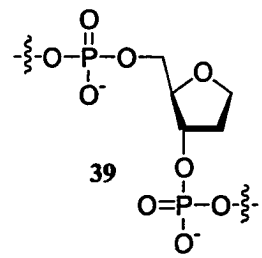

5'-(CGT **X**GC)

53a, X = **15**
53b, X = **1**

short oligonucleotides, location of **1** near either the 3'- or 5'-end of the duplex was expected to cause duplex melting through a "zipper" type effect where the end containing **1** begins to melt and the rest of the duplex effectively unzips.[99-101] In addition, replacement of a stronger G·C base pair with **1** was expected to have a greater destabilizing effect than replacement of an A·T base pair.[120-122] Thus, oligonucleotide **53a** was prepared through the use of automated oligonucleotide synthesis employing standard phosphoramidite chemistry and the C1' *t*-butyl ketone phosphoramidite, which was prepared according to previously published methods.[50,124]

Aerobic photolysis of **53a** at λ_{max} = 350 nm in aqueous solutions for 1.5 h was sufficient to convert approximately 95% of **53a** to **53b**, as measured by HPLC. Purification of the oligonucleotide containing **1** was carried out using preparative HPLC and the purity of **53b** was confirmed by analytical HPLC analysis, as well as electrospray mass spectroscopy. Quantitation of **53b** using the standard method of U.V. spectroscopy at 260 nm was not a trivial matter as calculation of the molar extinction coefficient (ε_{260}) was not straight forward. Typically, for oligonucleotides less than 30 base pairs in

length, the molar extinction coefficient is approximated using the nearest-neighbor method.[125] Because **1** was not expected to have an effect on the absorbance of the neighboring bases, it was hypothesized that ε could be approximated by summing the calculated ε value for the DNA fragments on either side of **1**. To confirm this hypothesis, oligonucleotides **54-56** were prepared using the tetrahydrofuran analogue of the abasic site (**39**) and their molar extinction coefficients were determined from solutions of known molarity resulting from DNA of known mass. Due to complications with purifying **54** by PAGE an accurate value for its ε_{260} could not be determined. Comparison of the measured values of ε to those calculated by taking the sum of the fragments on either side of **39** for **55** and **56** confirmed the validity of this method for calculation of ε for **53b** (Table 4).

Table 4. Calculated and measured values of ε for oligonucleotides **54-56**.[a]

Oligonucleotide	Fragments[b]	Calc. ε [c] (M^{-1} cm^{-1})	Meas. ε [d] (M^{-1} cm^{-1})
5'-d(CGT **39**GC) **(54)**	5'-d(CGT) 5'-d(GC)	28,000	–[e]
5'-d(AGT GCA **39**TA GCT) **(55)**	5'-d(AGT GCA) 5'-d(TA GCT)	87,100	85,400
5'-d(AGT GCA **39**AA GCT) **(56)**	5'-d(AGT GCA) 5'-d(AA GCT)	91,100	88,300

[a] ε at 260 nm. [b] DNA fragments used in calculation. [c] Calculated as a sum of the DNA fragments on either side of **39** according to ref 125. [d] Measured at 260 nm using DNA solutions of known molarity. [d] Not measured.

Melting studies using oligonucleotide **53b** (ε_{260} = 28,000 M^{-1} cm^{-1}) and its complement were carried out under conditions identical to those described above. Monitoring the U.V. absorbance as a function of temperature in the presence of 1.0 M

NaCl did not show an absorbance increase as a function of increasing temperature typical of duplex melting (Figure 21).[119] This result indicates that either **53b** and its complement do not form a stable duplex, or that the 2-deoxyribonolactone decomposes under the experimental conditions.

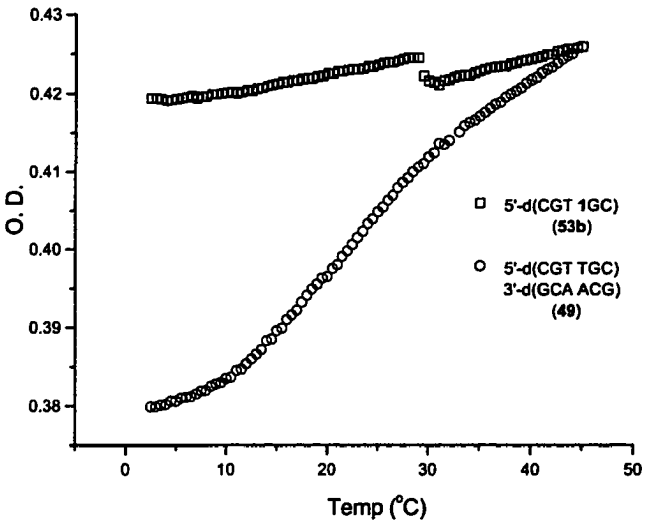

Figure 21. Plot of absorbance vs. time for the melting of **49** and **53b** and its complement at 4.15 μM duplex concentration in the presence of Tris buffer (50 mM) at pH = 7.5 with 1.0 M NaCl.

In order to rule out the latter possibility, the melt samples were analyzed by HPLC at the completion of the experiment and did not show any signs of decomposition of **53b**. As a result, it was concluded that **53b** is in-capable of forming a stable duplex under high salt conditions, which favor duplex formation. Based on the similar melting temperatures for oligonucleotides **37a** and **49**, it is reasonable to assume that a similar loss of duplex stability will occur upon generation of **37b-d**. As a result, **37b-d** will be expected to melt under the $Cu(OP)_2$ reaction conditions used by Sugiyama and Oyoshi, leading to formation of single stranded DNA containing **1**.[34] Cleavage of **1** would not be

observed since $Cu(OP)_2$ is not expected to bind single stranded DNA.[26,35,36] While the conclusions drawn by Sugiyama and co-workers with respect to $Cu(OP)_2$ inducing direct strand scission as a result of C4'-hydrogen atom abstraction are accurate, the study does not address the question of the ability of $Cu(OP)_2$ to induce the β-elimination of the 3'-phosphate of the 2-deoxyribonolactone (1).

3.2 Quantitation of the Alkali Labile Lesions Produced upon Treatment of Duplex DNA with $Cu(OP)_2$ and H_2O_2.

Evidence against the proposal that direct strand breaks (cleavage of the phosphate backbone in the absence of exogenous agents) generated from the action of $Cu(OP)_2$ and H_2O_2 on duplex DNA occur only through reaction at the C4'- and C5'-positions has been obtained by measuring the ratio of the quantity of direct strand breaks and alkali labile lesions to direct strand breaks (base enhancement) at a given time. In order to avoid complications arising from potential melting of the duplex upon the formation of alkali labile lesions, a 50-mer (**57**) was utilized as the $Cu(OP)_2$ target. Treatment of **57** with

5'-^{32}P-d(AGT CGC CGA ATG TAC TAG AGA ACT AGT GCA TTA GCT TAT TTT TTT GTT AT)
3'-d(TCA GCG GCT TAC ATG ATC TCT TGA TCA CGT AAT CGA ATA AAA AAA CAA TA)

(57)

$Cu(OP)_2$ and MPA was carried out to low conversion in order to approximate "single hit" conditions. Eliminating multiple strand breaks or alkali labile lesions in each duplex simplifies data analysis. The amount of duplex degradation was controlled by varying the reaction time and the concentration of $Cu(OP)_2$.

Reactions of **57** with $Cu(OP)_2$ and MPA in Tris buffer (pH = 7.0) for 15 min at 37 °C were quenched by either freezing in dry ice or by treatment with 0.1 M NaOH at 55 °C for 20 min. The latter conditions were shown to provide complete cleavage of the alkali labile lesions present, as treatments for longer periods of time showed no change in the base enhancement. Sodium hydroxide was chosen as the alkali source because of the ability to quench the alkali treatment with HCl rather than by removal of the solvent as in the case of the more common 1.0 M piperidine treatment. This avoids complications resulting from incomplete resuspension of the DNA. Analysis by PAGE showed a 1.5 fold increase in the amount of DNA strand damage upon treating with NaOH (Table 5). In order to gain insight as to whether or not the pH has an effect on the fraction of direct strand breaks generated from the reaction of $Cu(OP)_2$ with duplex DNA, the base enhancement was measured in Tris buffer at pH = 7.5 and 8.0. In order to rule out the possibility that direct strand scission was arising from reactivity of the primary amine present in Tris buffer rather than from the $Cu(OP)_2$ species generated upon reaction, the base enhancement was also measured in potassium phosphate buffer at pH = 7.0 and 8.0.

Table 5. The base enhancement in strand cleavage upon reaction of $Cu(OP)_2$ treated **57** with 0.1 M NaOH at 55 °C.[a]

Buffer	pH	Base Enhancement[b]
Tris	7.0	1.49 ± 0.16
Tris	7.5	1.52 ± 0.18[c]
Tris	8.0	1.47 ± 0.12
Potassium Phosphate	7.0	1.78 ± 0.09
Potassium Phosphate	8.0	1.75 ± 0.08

[a] 15 min at 37 °C; [Buffer] = 50 mM; [$MgCl_2$] = 10 mM; [**57**] = 58.3 nM; [$Cu(OP)_2$] = 0.96 μM; [MPA] = 4.8 mM. [b] (Direct strand scission + alkali labile lesions)/(direct strand scission). [c] [$MgCl_2$] = 0.0 M.

There is no change in the base enhancement upon increasing the solution pH from 7.0 to 8.0. However, a slight increase in this ratio was observed upon changing the buffer from Tris to potassium phosphate. The small change may indicate that the Tris buffer is involved in the formation of direct strand breaks to a limited extent. Comparison of the base enhancement measured using **57** to that derived from the yields given by Sugiyama and Oyoshi (~ 4) supports the hypothesis that direct strand scission in $Cu(OP)_2$ treated duplex DNA does not arise solely from hydrogen atom abstraction from the C4'- and C5'-positions.[34] Direct comparison between the two experiments can be made using the data obtained from the reaction of $Cu(OP)_2$ with **57** in 50 mM Tris at pH = 7.5 in the absence of $MgCl_2$ with the only significant difference being the length of the duplex DNA. The amount of alkali labile lesions generated upon treatment of **57** with $Cu(OP)_2$ is 6 times lower than the amount generated from treatment of **37a** with $Cu(OP)_2$. This leads to the conclusion that one or more of the processes leading to the formation of direct strand breaks are less efficient in **37a**. One possible explanation for this is the instability of hexameric oligonucleotides containing **1**.

3.3 Kinetics of the $Cu(OP)_2$ and Cu(OP) Induced β-Elimination of the 2-Deoxyribonolactone (1).

To provide further evidence for a copper induced β-elimination of **1**, the kinetics of the reaction between **1** and $Cu(OP)_2$ analogues were measured. Kinetic measurements between oligonucleotides containing **1** and $Cu(OP)_2$ directly are impractical as the reaction must be carried out to low conversion to avoid the formation of multiple strand breaks in a single oligonucleotide. This difficulty can be overcome through site specific delivery of the $Cu(OP)_2$ moiety to the 2-deoxyribonolactone (**1**) using **24-26** and E49C-

OP. The rate of formation and decay of alkali labile lesions, as well as the rate of formation of direct strand breaks can also be measured using these compounds. It was hypothesized that analysis of the resulting data through the use of the kinetic model shown in Figure 22 would provide insight into the ability of $Cu(OP)_2$ to induce a β-elimination in **1**, forming direct strand breaks as a result of C1'-hydrogen atom abstraction.

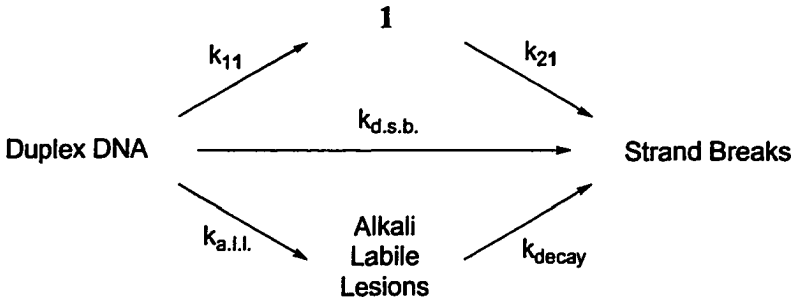

k_{11} = rate of formation of **1**
k_{21} = rate of cleavage of **1** to yield strand breaks
$k_{d.s.b.}$ = rate of formation of direct strand breaks

$k_{a.l.l.} = \sum_{i=2}^{n} k_{1i} + k_{11}$ k_{1i} = processes which form alkali labile lesions other than **1**

$k_{decay} = \sum_{i=2}^{n} k_{2i} + k_{21}$ k_{2i} = decay of alkali labile lesions other than **1** to give strand breaks

$k_{ox} = k_{a.l.l.} + k_{d.s.b.}$

Figure 22. Kinetic model for the analysis of the rates of DNA damage induced by $Cu(OP)_2$.

The kinetic model shown in Figure 22 is based on the kinetics for two sequential first-order reactions. The rate of formation of **1** is represented by k_{11} and its decay to give strand breaks is represented by k_{21}. The rate of formation of direct strand breaks (cleavage of the phosphate backbone without added exogenous reagents) is represented

by $k_{d.s.b.}$. The rate of formation of alkali labile lesions ($k_{a.l.l.}$) (lesions which give strand breaks after treatment with alkali) is the sum of k_{11} and the rates for the formation of all other alkali labile lesions. The rate of decay of alkali labile lesions to give direct strand breaks (k_{decay}) is the sum of k_{21} and the rate of decay of all other alkali labile lesions. The overall rate of DNA damage (k_{ox}) is the sum of $k_{a.l.l.}$ and $k_{d.s.b.}$.

3.3.1 Kinetics of the 3-Clip-Phen (24) Reaction with the 2-Deoxyribonolactone (1).

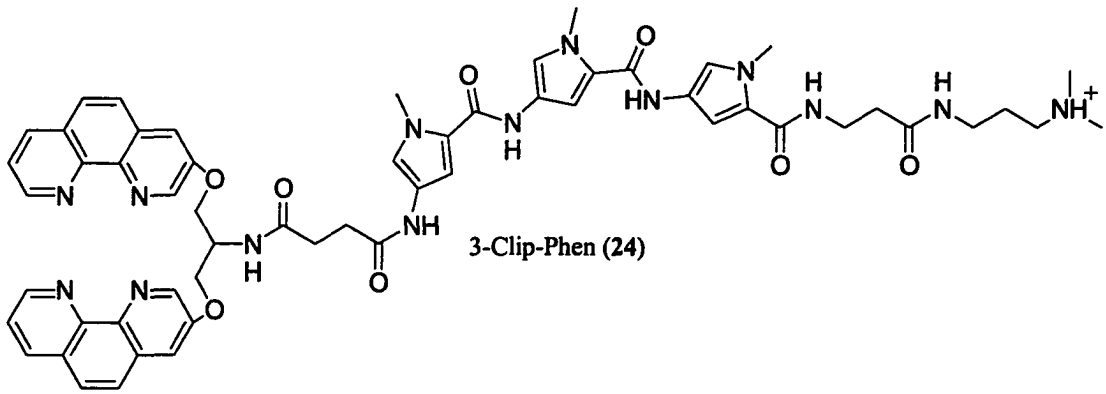

3-Clip-Phen (24)

The knowledge of the primary site of reaction of **24** with duplex DNA was required in order to prepare an oligonucleotide containing **1** at the appropriate location. Duplex **58** was chosen as the DNA substrate for **24** based on the sequence previously reported to be a target for **24**.[82,83] Reaction of **58** with **24** in the presence of $CuCl_2$ and

5'-^{32}P-d(GTA GTT TAT CAC A_{13}GT TAA ATT GCT AAC_{27} GCA GTC AG)
3'-d(CAT CAA ATA GTG T CA ATT TAA CGA TTG CGT CAG TC)

58

MPA as the reductant showed two regions of cleavage, with the primary site of cleavage located at A_{13} (numbering from the 5' end of the labeled oligonucleotide) (Figure 23). The two sites of cleavage arise as a result of distinct orientations of **24** within the A·T tract binding region. The $Cu(OP)_2$ moiety can be pointed toward or away from the 5' end of the radiolabeled strand as shown in Figure 10. Interestingly, 3'-phosphoglycolate (**9**) was not observed at either of the two cleavage sites. This is contradictory to previously reported results.[83] The absence of 3'-phosphoglycolate in these experiments may be the result of the different $MgCl_2$ concentrations used in these experiments and those reported by Meunier and co-workers. This is supported by the fact that the reactivity of $Cu(OP)_2$ is sensitive to the structure of the minor groove and salt concentration has an effect on the structure of duplex DNA.[126]

Measurement of the base enhancement at A_{13} and C_{27} after reaction of **58** with **24** was carried out in a similar manner to that described for the reaction of $Cu(OP)_2$ with **57**. After 30 min reactions at 37 °C (Tris buffer, pH = 7.0) values of 1.72 ± 0.29 and 1.60 ± 0.26 were measured for A_{13} and C_{27} respectively. The overall base enhancement (A_{13} and C_{27}) for the reaction of **24** with **58** using the same conditions is 1.66 ± 0.06. This value is within experimental error of the value obtained for the treatment of **57** with $Cu(OP)_2$ in Tris buffer. This indicates that **24** and $Cu(OP)_2$ produce similar ratios of direct strand breaks to alkali labile lesions in two comparable substrates. Furthermore, these ratios of alkali labile lesions to direct strand breaks are significantly lower than that determined by Sugiyama and Oyoshi using a hexanucleotide duplex (**37a**).[34]

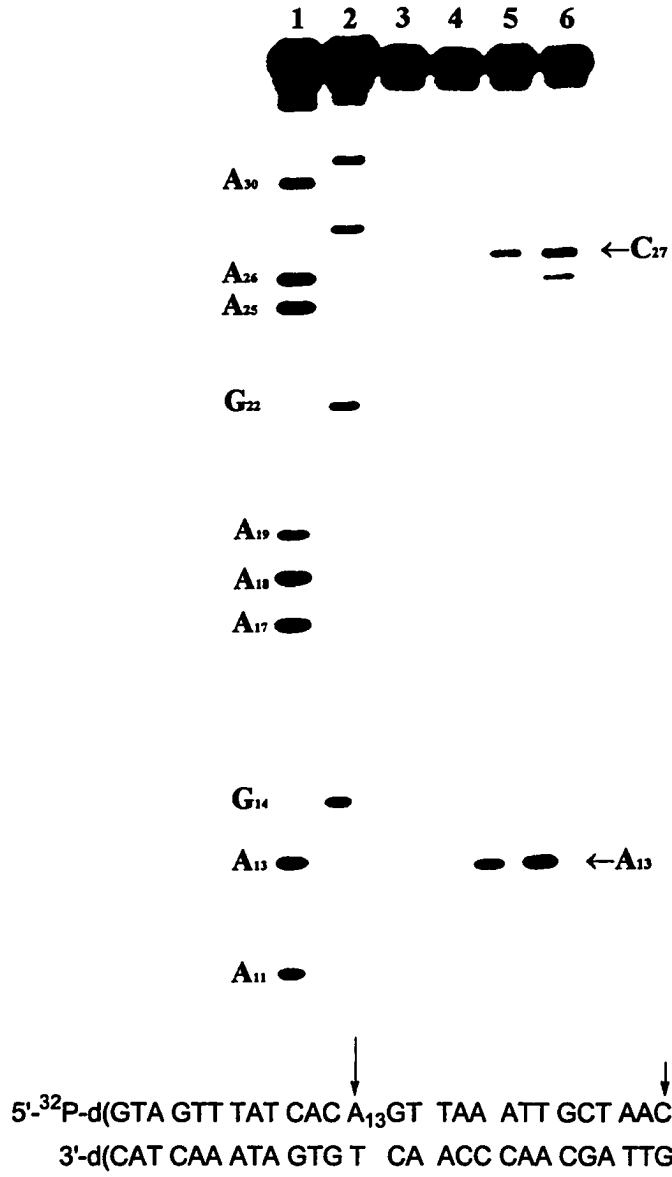

Sites of reaction of **24** with **58**

Figure 23. Autoradiogram of **58** treated with **24**. Lane 1, dA selective sequencing reaction. Lane 2, dG selective sequencing reaction. Lanes 3 and 4 contain **58**: lane 3, no further treatment; lane 4, NaOH (0.1 M), 20 min, 37 °C. Lanes 5 and 6 contain **58** treated with **24** ([**24**] = 10.0 μM, [$CuCl_2$] = 10.0 μM, [**58**] = 1.0 μM, [MPA] = 2.0 mM in 10 mM Tris, pH = 7.0) for 30 min at 37 °C: lane 5, no further treatment; lane 6, NaOH (0.1 M), 20 min, 37 °C. The height of the arrows is a qualitative indication of the strength of cleavage.

Generation of an oligonucleotide containing 1 at A_{13}.

With the knowledge of the major site of cleavage for the reaction of **24** with **58**, **59a** was prepared with A_{13} being substituted for **15**. The yields of 2-deoxyribonolactone

5'-^{32}P-d(GTA GTT TAT CAC **X**GT TAA ATT GCT AAC GCA GTC AG)
3'-d(CAT CAA ATA GTG TCA ATT TAA CGA TTG CGT CAG TC)

59a, X = 15
59b, X = 1

(**1**) generated from aqueous photolysis of **59a** showed inefficient photochemical conversion of **59a** to **59b** compared to the photochemical conversion of **53a**. Photolysis of **59a** for 1.5 h led to the formation of only 19.5% of the 2-deoxyribonolactone, compared to the photolysis of **53a** which produced > 95% of **53b** under identical photolysis conditions. The inefficiency of the photochemical conversion of **15** in **59a** was attributed to quenching of the excited state of the ketone by the adjacent dG residue. Deoxyguanosine is the most efficient of the four nucleobases at quenching triplet excited states.[127,128] While longer photolysis times led to the formation of **59b** in greater yields, potential complications were anticipated due to the possibility of increasing amounts of oxidative damage at G_{14}.

This hypothesis was supported by experiments carried out to provide evidence for oxidative damage of the base at G_{14}. While oxidation of dG does not always lead to the formation of alkali labile lesions, oxidatively damaged dG and dA bases can be converted to alkali labile lesions upon treatment with Na_2IrCl_6.[129,130] Because **15** is between the 5'-^{32}P label and G_{14} in **59a**, alkali induced cleavage of G_{14} treated with Na_2IrCl_6 would be invisible when **1** is also present. To avoid this complication,

5'-d(GTA GTT TAT CAC $\mathbf{X}G_{14}$T TAA ATT GCT AAC GCA GTC AG)-^{32}P-dd(A)
3'-d(CAT CAA ATA GTG TC A ATT TAA CGA TTG CGT CAG TC)

60a, X = 15
60b, X = 1

oligonucleotide **60a** was prepared with the radiolabel at the 3'-terminus using α-^{32}P-dideoxy-ATP. Photochemical conversion of **60a** to **60b**, followed by treatment with Na_2IrCl_6 and alkali showed significant damage to G_{14} (numbering from the 5'-terminus) (~ 25%) (Figure 24).

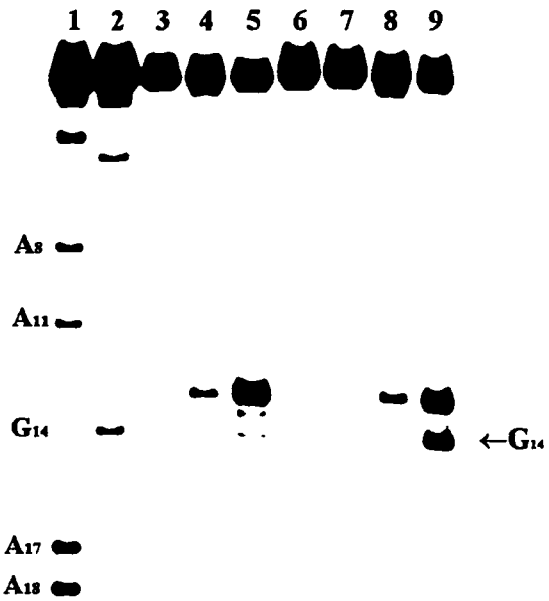

Figure 24. Autoradiogram of **60b**. Lane 1, dA selective sequencing reaction. Lane 2, dG selective sequencing reaction. Lane 3, **60a**. Lanes 4 and 5 contain **60b**: lane 4, no further treatment; lane 5, NaOH (0.1 M), 20 min, 37 °C. Lanes 6 and 7 contain **60a** treated with Na_2IrCl_6 (0.1 M), 20 min, rt: lane 6, no further treatment; lane 7, piperidine (1.0 M), 20 min, 90 °C. Lanes 8 and 9 contain **60b** treated with Na_2IrCl_6 (0.1 M), 20 min, rt: lane 8, no further treatment; lane 9, piperidine (1.0 M), 20 min, 90 °C.

Fortunately, photolysis of single stranded DNA containing **15** (**61a**) showed a marked increase in the efficiency of formation of **61b**, with photolysis for 1.5 h at λ_{max} =

5'-^{32}P-d(GTA GTT TAT CAC **X**GT TAA ATT GCT AAC GCA GTC AG)

61a, X = 15
61b, X = 1

350 nm being sufficient to yield 80-90% of **61b**. The reason for the increased efficiency of the formation of **61b** from photolysis in single stranded DNA as compared to photolysis of **59a** is most likely due to the increased flexibility of the DNA chain. This allows the DNA to adopt a conformation which disfavors quenching of the excited state of the *t*-butyl ketone (**15**) by G_{14}. Hybridization of **61b** to its complement to generate **59b** was carried out by heating at 55 °C for 5 min, followed by slow cooling to rt and subsequent removal of the MOPS buffer (pH = 7.0) through the use of ion exchange resin. Analysis of the material by non-denaturing PAGE showed that **61b** was completely hybridized. Analysis of the hybridized material by denaturing PAGE showed that less than 5% of the 2-deoxyribonolactone (**1**) present was cleaved.

The reaction of **59b** with **24** in the presence of $CuCl_2$ and MPA was followed by the removal of aliquots of the reaction at constant time intervals. The aliquots were analyzed by denaturing PAGE and the amount of cleaved oligonucleotide was quantified using ImageQuant 5.1 software. The quantity of 2-deoxyribonolactone (**1**) present at a given time was determined by subtraction of the amount of cleavage from the amount of **1** present at the beginning of the experiment. The initial amount of **1** was determined by treatment of **59b** with 0.1 M NaOH at 37 °C for 20 min, followed by quantitation of the amount of cleavage. Plots of the natural log of the fraction of intact **59b** as a function of time for over four half lives provided a first-order rate for the decay of **1** (k_{21}) in the presence of **24**, $CuCl_2$, and MPA of (5.63 ± 0.69) x 10^{-4} s^{-1} at 37 °C ($t_{1/2}$ = 20.5 min)

(Figure 25). Interestingly, no cleavage of 1 in **59b** as function of time was observed in the absence of MPA.

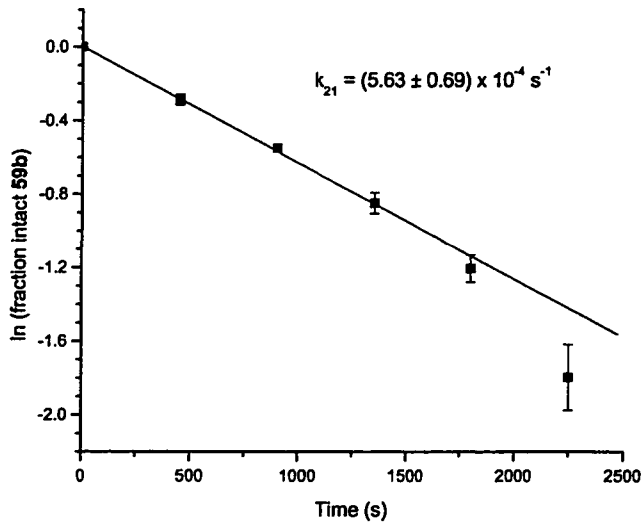

Figure 25. Plot of the ln (fraction intact **59b**) versus time at 37 °C in the presence of **24**, $CuCl_2$, and MPA ([**59b**] = 1.0 μM, [**24**] = 10.0 μM, [$CuCl_2$] = 10.0 μM, [MPA] = 2.0 mM in 10.0 mM Tris, pH = 7.0).

To rule out the possibility that cleavage of **59b** was due to reaction of **24** with duplex **59b** without bound copper, control experiments were carried out between **59b** and **24** in the absence of copper. No cleavage of **59b** was observed under these conditions for 2.5 h. Plots of the natural log of the fraction of intact **59b** in the absence of **24** as a function of time also showed good linearity and behaved in a first-order manner for 2.5 h, yielding a rate of decay (k_{21}) of (5.40 ± 0.84) x 10^{-6} s^{-1} ($t_{1/2}$ = 35.7 h) at 37 °C (Figure 26). The fact that the first-order rate of decay of **59b** in the absence of **24** is over two orders of magnitude slower than that observed in the presence of **24** under the same conditions and that no decay of **59b** is observed in the presence of **24** without copper indicates that **24** in the presence of copper significantly enhances the rate of

decay of **59b**. The error associated with the decay of **59b** in the absence of **24** is a result of the fact that small changes in the concentration of intact **59b** are being measured. This coupled with the error associated with the quantification method (± 5%) is responsible for the observed error.

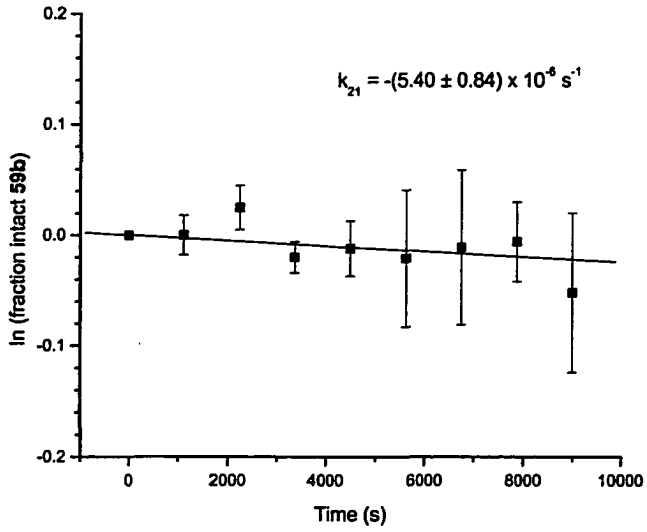

Figure 26. Plot of the ln (fraction intact **59b**) versus time at 37 °C in the presence of $CuCl_2$ and MPA ([**59b**] = 1.0 μM, [$CuCl_2$] = 10.0 μM, [MPA] = 2.0 mM in 10.0 mM Tris, pH = 7.0).

As mentioned above, Tris buffer contains a primary amine. It is reasonable to expect that the buffer could be involved in the degradation of **1**. When **24** is bound to **59b**, the 2-deoxyribonolactone may be shielded from the Tris buffer, preventing the decomposition of **59b**. This may explain why **59b** shows a faster rate of decomposition in the absence of **24** than in the presence of **24** without copper.

In order to determine whether or not the rate of copper induced cleavage of **59b** is faster than the rate of copper induced DNA damage (k_{OX}, Figure 22), **58** was reacted with **24** in the presence of $CuCl_2$ and MPA. The rates of formation of alkali labile lesions and direct strand breaks (k_{OX}) at A_{13} and C_{27} were determined from the fraction

of intact DNA after treatment with alkali (0.1 M NaOH at 37 °C for 20 min) as a function of time. Because **24** cleaves duplex DNA at more than one site, the fraction of cleavage at position "X" ($Base_{Xt}$) is determined by the ratio of cleavage at "X" to the total of intact and cleaved DNA ($DNA_{tot.}$) (Eq 16, Figure 22). At time = 0, the value for $Base_{X0}$ is 0, and DNA_{tot} is defined as 1. Since DNA_{tot} does not change during the course of the

$$Base_{Xt} = \frac{Cleavage_X}{DNA_{Tot}} \tag{16}$$

$$\ln\left[\frac{Base_{X0} + DNA_{Tot} - Base_{Xt}}{DNA_{Tot}}\right] = -kt \tag{17}$$

$$\text{If } Base_{X0} = 0, \text{ and } DNA_{Tot} = 1$$

$$\ln[1 - Base_{Xt}] = -kt \tag{18}$$

experiment, substitution of these values into the integrated first order rate law (Eq 17) yields equation 18.[131] Plots of the natural log of one minus the fraction of cleavage at A_{13} or C_{27} (ln 1 - $Base_{Xt}$) as a function of time showed good linearity and provided first-order rates for the formation of direct strand breaks and alkali labile lesions (k_{OX}) of $(2.44 \pm 0.49) \times 10^{-5}$ s^{-1} ($t_{1/2}$ = 7.9 h) for A_{13} and $(1.35 \pm 0.61) \times 10^{-6}$ s^{-1} ($t_{1/2}$ = 142.6 h) for C_{27} at 37 °C (Figure 27). The sum of these rate constants gives an overall value of k_{OX} for the reaction of **24** with **58** of $(2.58 \pm 0.49) \times 10^{-5}$ s^{-1} ($t_{1/2}$ = 7.4 h)

Quantitation of the mol fraction of alkali labile lesions present at a given time can be determined from the difference in the mol fraction of cleavage before and after treatment with alkali at a given time (0.1 M NaOH at 37 °C for 20 min). Fitting of the mol fraction of alkali labile lesions ([*L*]) as a function of time to eq 19 which describes

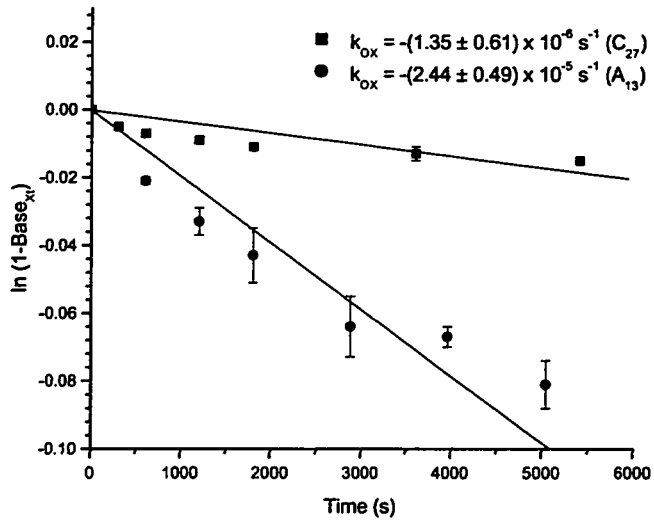

Figure 27. Plot of the ln (1 - $Base_{X_t}$) versus time at 37 °C at A_{13} and C_{27} in the presence of **24**, $CuCl_2$ and MPA ([**58**] = 1.0 μM, [**24**] = 10.0 μM, [$CuCl_2$] = 10.0 μM, [MPA] = 2.0 mM in 10.0 mM Tris, pH = 7.0).

the kinetics for two sequential first-order reactions yields $k_{a.l.l.}$ and k_{decay}.[131] For the reaction of **24** with **58** using MPA as the reductant, this process gives rates of formation ($k_{a.l.l.}$) and decay (k_{decay}) of alkali labile lesions at A_{13} of (1. 5 ± 0.5) x 10^{-5} s^{-1} ($t_{1/2}$ = 12.8 h) and -(4.7 ± 0.9) x 10^{-4} s^{-1} ($t_{1/2}$ = 24.5 min) respectively (Figure 28). Identical rates (within experimental error) of (1.0 ± 0.4) x 10^{-5} s^{-1} and -(9.8 ± 4.6) x 10^{-4} s^{-1} are obtained for the formation ($k_{a.l.l.}$) and decay (k_{decay}) of alkali labile lesion using ascorbate as the reductant (Figure 28 inset). The large error associated with the quantity of alkali labile lesions is a result of generation of small numbers (mol fraction of alkali labile lesions) from the difference of two large numbers (quantity of intact DNA before and after alkali treatment).

$$[L] = \frac{k_{a.l.l.}}{k_{decay} - k_{a.l.l.}} (e^{-k_{a.l.l.}t} - e^{-k_{decay}t}) \qquad (19)$$

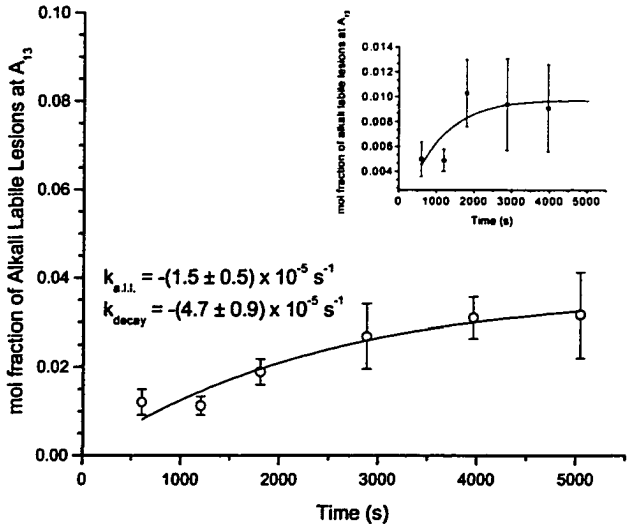

Figure 28. Plot of the mol fraction of alkalki labile lesions in **58** at A_{13} versus time at 37 °C in the presence of **24**, $CuCl_2$ and MPA ([**58**] = 1.0 μM, [**24**] = 10.0 μM, [$CuCl_2$] = 10.0 μM, [MPA] = 2.0 mM in 10.0 mM Tris, pH = 7.0); k_1' = rate of formation of alkali labile lesions and k_2' = rate of alkali labile lesion decay. The inset shows a similar plot using ascorbate (2.0 mM) as the reductant.

The rate of decay of **59b** (k_{21}) and alkali labile lesions (k_{decay}) at the same site in the oligonucleotide in the presence of **24**, $CuCl_2$, and MPA are within experimental error of each other ($k_{21}/k_{decay} = 0.83 \pm 0.22$). The fact that identical rates are observed for the cleavage of **1** in **59b** and the decay of alkali labile lesions generated at the same site from reaction of **24** with **58** provides strong evidence for the conclusion that the rate of decay of alkali labile lesions is due to copper induced cleavage of **1** ($k_{decay} = k_{21}$). As a result, the rate of formation of alkali labile lesions ($k_{a.l.l.}$) at A_{13} is effectively the overall rate of formation of **1** (k_{11}) ($k_{11} = k_{a.l.l.}$) at A_{13} upon reaction of **58** with **24** in the presence of $CuCl_2$ and MPA.

On the basis of the fact that the measured rate of copper induced cleavage of **1** (k_{21}) is 31 times faster than the rate of its formation, the independently measured rate of

formation of direct strand breaks and alkali labile lesions (k_{OX}) at A_{13} also serves as a measurement of the rate of formation of **1** (k_{11}) at A_{13} since $k_{21} = k_{decay}$. These results clearly lead to the conclusion that the majority of the direct strand breaks produced from the interaction of **24** with duplex DNA in the presence of copper and MPA are a result of C1'-oxidation to generate the 2-deoxyribonolactone (**1**) and its subsequent cleavage induced by a $Cu(OP)_2$ moiety.

As mentioned previously, product analysis of the reaction of **24** with duplex DNA revealed products consistent with ~ 15% reaction at the C5'-position and ~ 15% reaction at the C4'-position, generating direct strand breaks.[83] The possibility of hydrogen atom abstraction from the C5'-position cannot be ruled out on the basis of the result presented here as the error in the measured rate of formation of alkali labile lesions and direct strand breaks is greater than 15%. As mentioned above, the absence of **9** in the reaction of **24** with **58** is possibly a result of the absence of $MgCl_2$ in the reaction solutions.[126]

3.3.2 Kinetics of the 2-Clip-Phen (25) and 2-Phen (26) Reactions with Duplex 58.

To provide further examples for a faster rate of elimination of alkali labile lesions (k_{decay}) than the rate of their formation ($k_{a.l.l.}$) in these systems, **58** was treated with 2-Clip-Phen (**25**) and 2-Phen (**26**). The kinetics for the formation of damaged DNA (k_{OX}), and the formation ($k_{a.l.l.}$) and decay (k_{decay}) of alkali labile lesions were measured. Several differences between the reactivity of **24-26**, including the efficiency of cleavage and the primary sites of DNA damage have been reported.[82,83] The differences in the sites of DNA cleavage between **24-26** are most likely due to different local structure

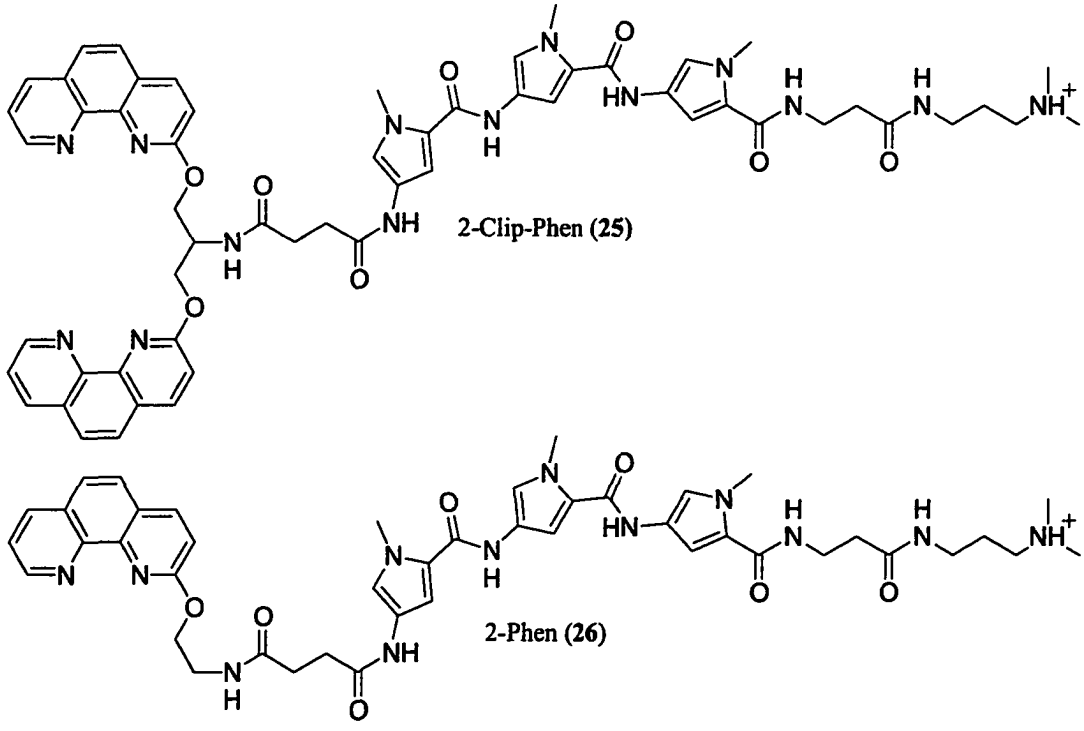

2-Clip-Phen (25)

2-Phen (26)

preferences for the different 1,10-phenanthroline conjugates since all the conjugates can be expected to bind within the seven base pair A·T stretch in **58**.

Treatment of **58** with **25** in the presence of $CuCl_2$ and ascorbate showed only one major and one minor region of cleavage after denaturing PAGE analysis (Figure 29). The major site of cleavage occurs at A_{17} and the minor cleavage band is present at T_{16}. The faster moving of the two products at T_{16} is believed to be 3'-phosphoglycolate (**9**) and the slower migrating product the corresponding 3'-phosphate. Measurement of the base enhancement at T_{16}, A_{17}, and C_{23} after reaction of **58** with **25** for 30 min at 37 °C in Tris buffer (pH = 7.0) gave values of 1.78 ± 0.06, 2.38 ± 0.19, and 2.21 ± 0.31 respectively. The overall base enhancement for the reaction of **25** with **58** under the same conditions is 2.12 ± 0.25. This is slightly higher than that measured for the reaction of **24** with **58** (1.66 ± 0.06).

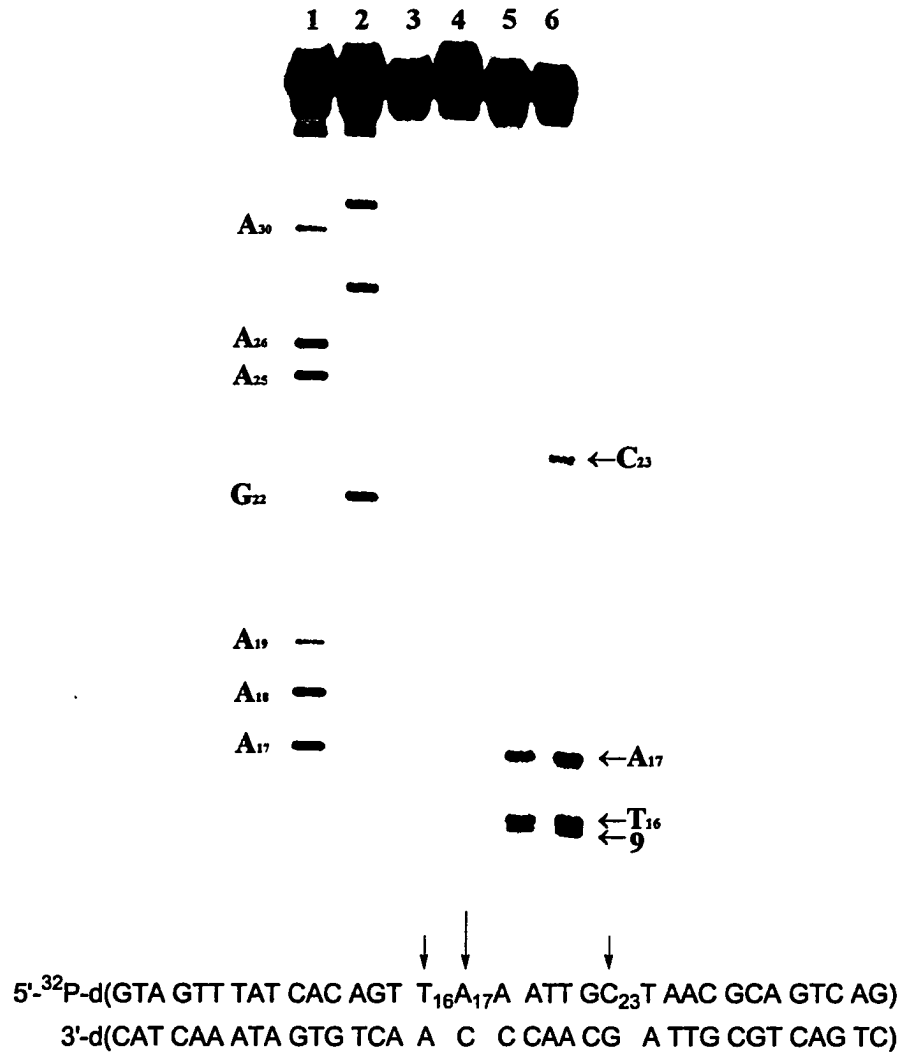

Figure 29. Autoradiogram of **25** treated **58**. Lane 1, dA selective sequencing reaction. Lane 2, dG selective sequencing reaction. Lanes 3 and 4 contain **58**: lane 3, no further treatment; lane 4, NaOH (0.1 M), 20 min, 37 °C. Lanes 5 and 6 contain **58** treated with **25** ([**25**] = 20.0 μM, [$CuCl_2$] = 20.0 μM [**58**] = 1.0 μM, [ascorbate] =200 μM in 10 mM Tris, pH = 7.0), 30 min, 37 °C: lane 5, no further treatment; lane 6, NaOH (0.1 M), 20 min, 37 °C. The height of the arrows is a qualitative indication of the strength of cleavage.

The rate of reaction of **25** in the presence of copper and ascorbate to form damaged DNA (k_{OX}) was measured at each cleavage site. Plots of the natural log one minus the fraction of cleavage at T_{16}, A_{17}, or C_{23} (ln 1- $Base_{Xt}$) as a function of time

provided first-order rates for the formation of direct strand breaks and alkali labile lesions (k_{OX}) of (8.29 ± 2.21) x 10^{-7} s^{-1} ($t_{1/2}$ = 232 h), (2.99 ± 0.37) x 10^{-6} s^{-1} ($t_{1/2}$ = 64.4 h), and (1.48 ± 0.16) x 10^{-6} s^{-1} ($t_{1/2}$ = 130 h) for T_{16}, A_{17}, and C_{23} respectively (Figure 30). The sum of these rate constants gives a value of k_3' for the overall reaction of **25** with **58** of (5.30 ± 0.46) x 10^{-6} s^{-1} ($t_{1/2}$ = 36.3 h).

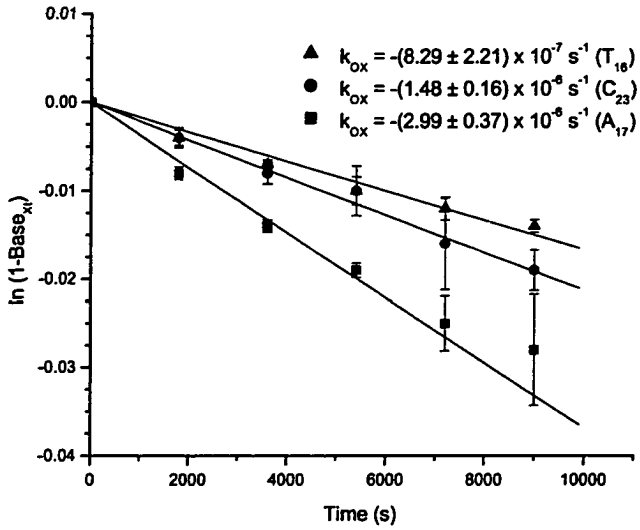

Figure 30. Plot of the ln (1 - $Base_{Xt}$) versus time at 37 °C at T_{16}, C_{23}, and A_{17} in the presence of **25**, $CuCl_2$ and ascorbate ([**58**] = 1.0 μM, [**25**] = 20.0 μM, [$CuCl_2$] = 20.0 μM, [ascorbate] = 200 μM in 10.0 mM Tris, pH = 7.0).

The rates of formation ($k_{a.l.l.}$) and decay (k_{decay}) of alkali labile lesions were determined in a similar manner to that described for the reaction of **24** with **58**. Fitting the quantity of alkali labile lesions as a function of time at A_{17} to eq 19 gave a value of (2.74 ± 0.64) x 10^{-6} s^{-1} ($t_{1/2}$ = 70.2 h) for the rate of formation of alkali labile lesions ($k_{a.l.l.}$) and a value of (2.20 ± 0.20) x 10^{-4} s^{-1} ($t_{1/2}$ = 52.5 min) for their decay (k_{decay}) at 37 °C (Figure 31). The rates of reaction of **25** with **58** ($k_{a.l.l.}$ and k_{decay}) are slower than those measured for the reaction of **24** with **58**. This is consistent with the observations of

Meunier and co-workers in which **24** was shown to react with duplex DNA more efficiently than either **25** or **26**.[82]

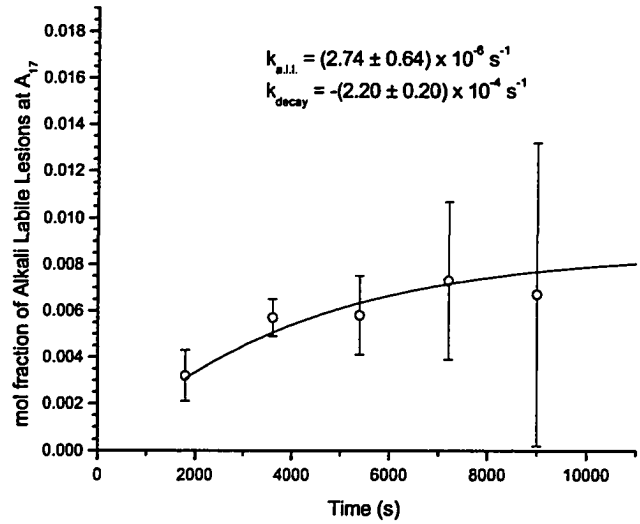

Figure 31. Plot of the mol fraction of alkali labile lesions at A_{17} as a function of time in **58** at 37 °C in the presence of **25**, $CuCl_2$ and ascorbate ([**58**] = 1.0 μM, [**25**] = 20.0 μM, [$CuCl_2$] = 20.0 μM, [ascorbate] = 200 μM in 10.0 mM Tris, pH = 7.0); k_1' is the rate of formation of alkali labile lesions and k_2' is the rate of alkali labile lesion decay.

The rate of formation of 3'-phosphoglycolate (**9**) at T_{16} was also measured from plots of the natural log of the fraction of **9** at T_{16}. The kinetic plots gave a rate for the formation of **9** (k_9) of (1.75 ± 0.45) x 10^{-7} s^{-1} ($t_{1/2}$ = 1100 h) (Figure 32). The rate of formation of **9** at T_{16} is more than four fold slower than the rate of formation of the corresponding phosphate ((8.29 ± 2.21) x 10^{-7} s^{-1}). This is consistent with the observation that $Cu(OP)_2$ produces < 30% of **9** upon reaction with duplex DNA.[36] Quantitation of the base enhancement for the formation of **9** gave a value of 0.65 ± 0.02, indicating that the amount of **9** present decreases upon treatment with 0.1 M NaOH for

30 min at 37 °C. This is consistent with the results reported by Meunier and co-workers for the quantity of **9** present after reaction of **24** with duplex DNA.[83]

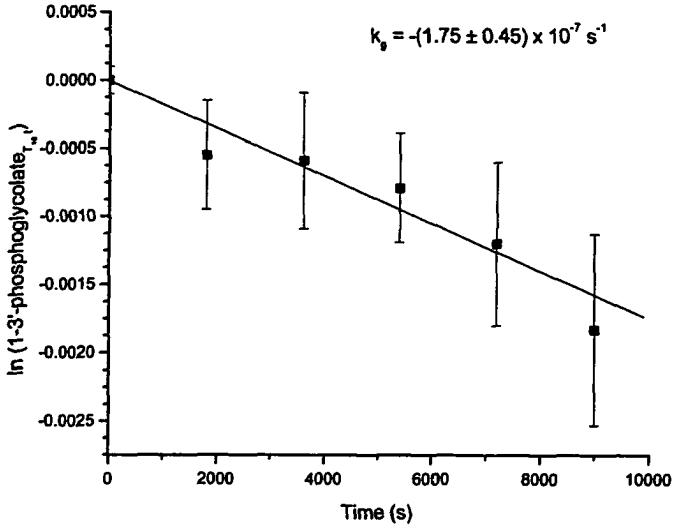

Figure 32. Plot of the ln (1 – 3'-phosphoglycolate) versus time at 37 °C at T_{16} in the presence of **25**, $CuCl_2$ and ascorbate ([**58**] = 1.0 μM, [**25**] = 20.0 μM, [$CuCl_2$] = 20.0 μM, [ascorbate] = 200 μM in 10.0 mM Tris, pH = 7.0).

Reaction of **58** with **26** in the presence of $CuCl_2$ and ascorbate showed the major cleavage site to be at T_{24} although significant cleavage also occurs at A_{25} (Figure 33). As mentioned above, the variation in the region of cleavage is likely due to different binding orientations of the distamycin conjugates within the A·T tract in **58** (Figure 10). Measurement of the overall base enhancement after treatment of **58** with **26** in Tris buffer (pH = 7.0) at 37 °C for 30 min gave a value of 1.98 ± 0.21. The base enhancement at T_{24} and A_{25} were 2.19 ± 0.19 and 1.77 ± 0.05 respectively.

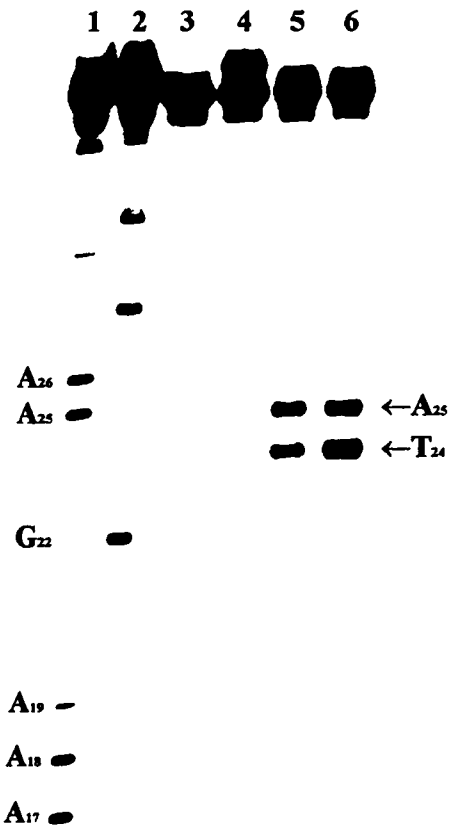

5'-^{32}P-d(GTA GTT TAT CAC AGT TAA ATT GCT$_{24}$ A$_{25}$AC GCA GTC AG)

3'-d(CAT CAA ATA GTG TCA ACC CAA CGA T TG CGT CAG TC)

Sites of reaction of **26** with **58**

Figure 33. Autoradiogram of **26** treated **58**. Lane 1, dA selective sequencing reaction. Lane 2, dG selective sequencing reaction. Lanes 3 and 4 contain **58**: lane 3, no further treatment; lane 4, NaOH (0.1 M), 20 min, 37 °C. Lanes 5 and 6 contain **58** treated with **26** ([**26**] = 20.0 μM, [$CuCl_2$] = 20.0 μM [**58**] = 1.0 μM, [ascorbate] = 200 μM in 10 mM Tris, pH = 7.0), 30 min, 37 °C: lane 5, no further treatment; lane 6, NaOH (0.1 M), 20 min, 37 °C.

The rate of reaction of **26** in the presence of copper and ascorbate to form direct strand breaks and alkali labile lesions (k_{OX}) was measured for each site of cleavage. Plots of the natural log one minus the fraction of cleavage at T_{24}, or A_{25} (ln 1 - $Base_{Xt}$) as a function of time provided first-order rates for the formation of oxidatively damaged

DNA (k_{OX}) of (8.33 ± 0.73) x 10^{-6} s^{-1} ($t_{1/2}$ = 23.1 h) and (3.78 ± 0.24) x 10^{-6} s^{-1} ($t_{1/2}$ = 50.9 h) for T_{24} and A_{25} respectively (Figure 34). The sum of these rate constants gives a value of k_{OX} for the overall reaction of **26** with **58** of (1.21 ± 0.08) x 10^{-5} s^{-1} ($t_{1/2}$ = 15.9 h). The reason for the more efficient rate of DNA damage (k_{OX}) for **26** than **25** is unclear, but may have to do with the position of the bridge substitution in **25** (see below).

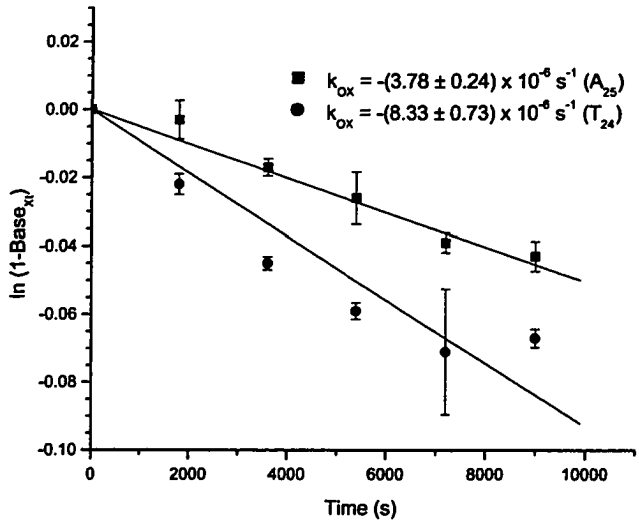

Figure 34. Plot of the ln (1 - $Base_{Xt}$) versus time at 37 °C at T_{24} and A_{25} in the presence of **26**, $CuCl_2$ and ascorbate ([**58**] = 1.0 μM, [**26**] = 20.0 μM, [$CuCl_2$] = 20.0 μM, [ascorbate] = 200 μM in 10.0 mM Tris, pH = 7.0).

The rates of formation ($k_{a.l.l.}$) and decay (k_{decay}) of alkali labile lesions were determined in a similar manner to that described for the reaction of **24** with **58**. Fitting the quantity of alkali labile lesions as a function of time at T_{24} to eq 19 gave a value of (7.43 ± 0.44) x 10^{-6} s^{-1} ($t_{1/2}$ = 25.9 h) for the rate of formation of alkali labile lesions ($k_{a.l.l.}$) and a value of (1.70 ± 0.20) x 10^{-4} s^{-1} ($t_{1/2}$ = 1.1 h) for the rate of decay of alkali labile lesions (k_{decay}) at 37 °C (Figure 35). The rate of decay of alkali labile lesions (k_{decay}) at T_{24} is slower than the values for k_{decay} measured for the reaction of **24** and **25**

with duplex DNA at A_{13} and A_{17} respectively. However, **26** shows a faster rate of formation of alkali labile lesions ($k_{a.l.l.}$) than **25**. This is consistent with the larger base enhancement observed for **26** at T_{24} than for **24** or **25** at A_{13}.

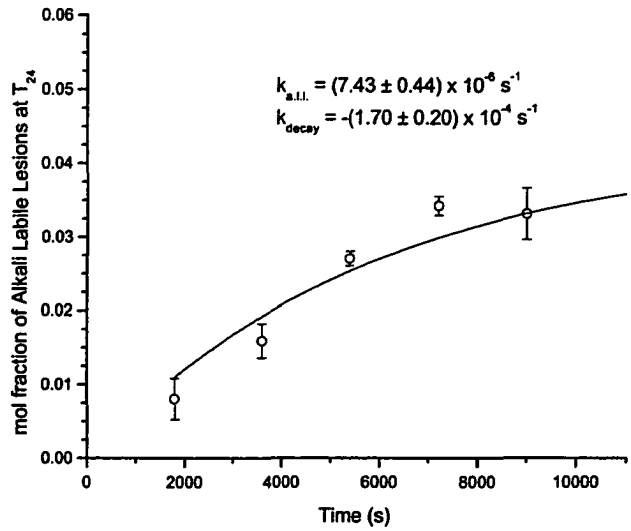

Figure 35. Plot of the mol fraction of alkali labile lesions in **58** at T_{24} versus time at 37 °C in the presence of **26**, $CuCl_2$ and ascorbate ([**58**] = 1.0 μM, [**26**] = 20.0 μM, [$CuCl_2$] = 20.0 μM, [ascorbate] = 200 μM in 10.0 mM Tris, pH = 7.0); k_1 is the rate of formation of alkali labile lesions and k_2 is the rate of alkali labile lesion decay.

Comparison of the rate constants for the formation ($k_{a.l.l.}$) and decay of alkali labile lesions (k_{decay}) for the reaction of **25** and **26** with **58** shows a faster rate for the decay of alkali labile lesions for both compounds. The measured rates for the overall formation of alkali labile lesions and direct strand breaks (k_{OX}) are within experimental error of the rates of formation of alkali labile lesions, indicating that the biexponential fits of the quantity of alkali labile lesions as a function of time are accurate for **25** and **26**. While the rates of decomposition of the 2-deoxyribonolactone (**1**) were not measured directly with these compounds, they are expected to react in a similar maner to **24**. Thus,

the rate of decay of alkali labile lesions for **25** and **26** are believed to be the result of a copper induced elimination of the 3'-phosphate in **1** ($k_{decay} = k_{21}$).

3.3.3 Kinetics of the E49C-OP Induced β-Elimination of the 2-Deoxyribonolactone.

Kinetic studies were also carried out for the reaction between the modified Trp repressor protein (E49C-OP) prepared by Sigman and co-workers and duplex DNA with and without **1** at the primary cleavage site.[78] Conjugation of E49C with **23** was carried out using **23** (Eq 20) which was prepared according to literature methods.[53] Prior to

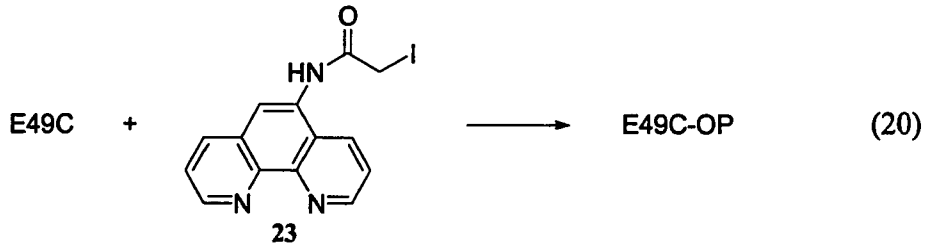

(20)

conjugation, E49C was reduced with excess dithiothreitol (DTT), which was then removed by dialysis. Purification of the conjugated material was carried out using an Amicon Microcon filter to remove the excess **23** in order to avoid complications as a result of non-specific cleavage of duplex DNA.

In order to facilitate the incorporation of **1** at the position of major cleavage induced by E49C-OP, the oligonucleotide to which E49C-OP would bind and cut was kept as small as possible. A 50-base pair section of the *aro H* operator (**57**) to which E49C-OP has been shown to bind and cleave, was used.[78,132] To confirm that E49C-OP binds **57**, footprinting studies were carried out using methidiumpropyl-EDTA·Fe(II)

5'-^{32}P-d(AGT CGC CGA ATG TAC TAG $AG_{20}A$ A_{22}CT AGT GCA TTA GCT TAT TTT TTT GTT AT)
3'-d(TCA GCG GCT TAC ATG ATC TC T T GA TCA CGT AAT CGA ATA AAA AAA CAA TA)
|----------Protein Binding Region----------|

(57)

(Fe·MPE). This generated a footprint of the E49C-OP·DNA complex identical to that previously reported (Figure 36).[57,75,86,133,134]

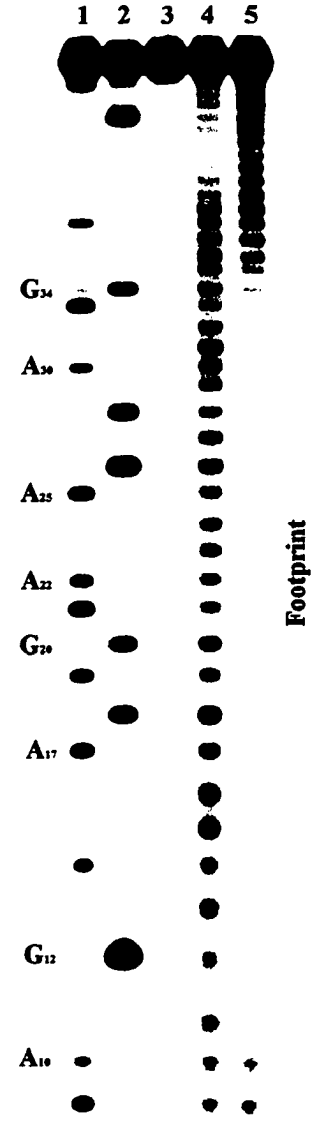

Figure 36. Autoradiogram of Fe·MPE treated E49C-OP·**57** complex. Lane 1, dA selective sequencing reaction. Lane 2, dG selective sequencing reaction. Lane 3, **57**. Lanes 4 and 5 contain Fe·MPE treated DNA ([Fe·MPE] = 1.0 mM, [DTT] = 4.0 mM, [**57**] = 70 nM in 20 mM KH_2PO_4, pH =7.0): lane 4, **57**; lane 5, E49C-OP·**57** complex ([E49C-OP] = 1.3 mM, [Trp] = 10 mM).

With the knowledge that E49C-OP binds **57**, the major site of DNA cleavage was determined in order to define the site for the incorporation of 2-deoxyribonolactone precursor **15**. Cleavage was initiated by the addition of MPA to the E49C-OP·**57** complex in the presence of $CuSO_4$. Incubation of the reaction solution at 37 °C for 30 min was sufficient to enable observation of cleavage products at A_{22}, A_{21}, G_{20}, and A_{19} with the major site of cleavage occurring at A_{22} (Figure 37). Quantitation of the overall

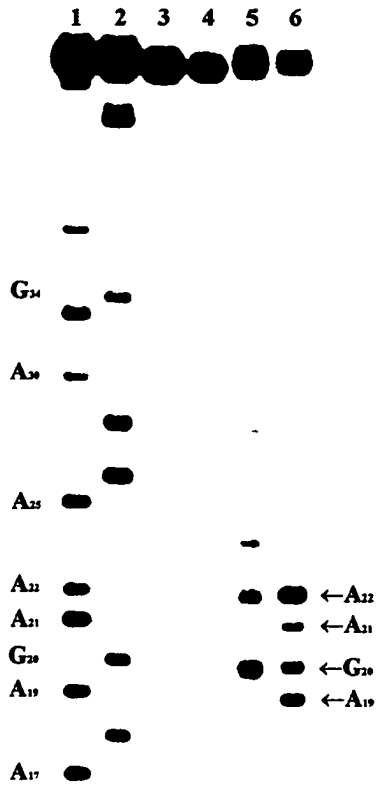

Figure 37. Autoradiogram of **57** treated with E49C-OP. Lane 1, dA selective sequencing reaction. Lane 2, dG selective sequencing reaction. Lanes 3 and 4 contain **57**: lane 3, no further treatment; lane 4, NaOH (0.1 M), 20 min, 37 °C. Lanes 5 and 6 contain **57** treated with E49C-OP ([**57**] = 70.0 nM, [E49C-OP] = 2.5 μM, [$CuSO_4$] = 5.8 μM, [trp] = 10.0 mM, [MPA] = 5.8 mM in 20.0 mM KH_2PO_4, pH = 7.0): lane 5, no further treatment; lane 6, NaOH (0.1 M), 20 min, 37 °C.

base enhancement after reaction for 30 min at 37 °C in 20 mM potassium phosphate at pH = 7.0 gave a value of 3.61 ± 0.41. Measurement of the base enhancement for the individual sites of cleavage gave values of 3.34 ± 0.41, 4.17 ± 0.15, 1.38 ± 0.02, and 5.57 ± 0.01 at A_{22}, A_{21}, G_{20}, and A_{19} respectively. These enhancements are significanly greater than those observed for $Cu(OP)_2$ and distamycin conjugates **24-26**.

Evidence for the formation of **1** from the reaction of E49C-OP with **57** in the presence of $CuSO_4$, trp, and MPA was obtained using the method developed by Greenberg and co-workers.[28] Incubation with varying concentrations and ratios of piperidine, N,N'-dimethylethylenediamine (DMEDA), and 2-mercaptoethanol (BME) yields a series of adducts which that are seperable by denaturing PAGE. The most diagnostic of these adducts are **62** and **63** which form from reaction of BME with butenolide **14** (Eq 21). The butenolide (**14**) is generated from the reaction of the

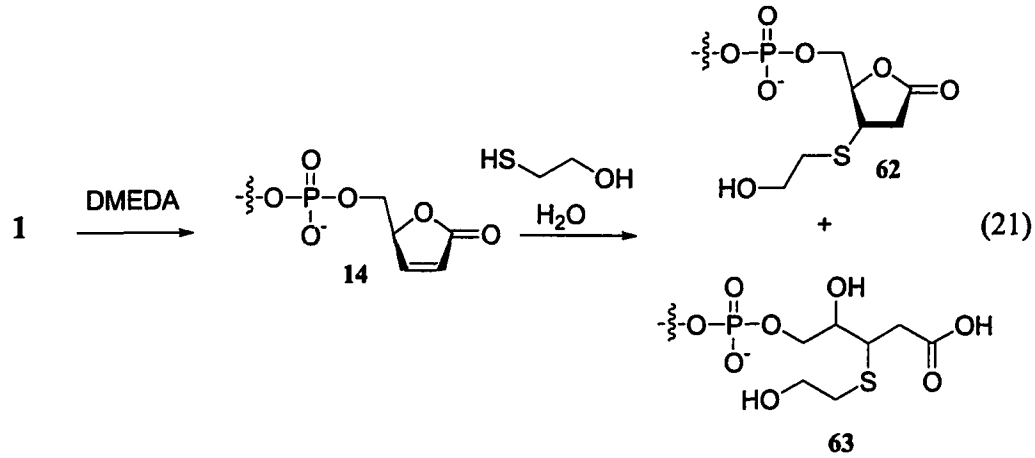

(21)

DMEDA present in the reaction solution with **1**. Comparison of the adducts observed at A_{22} upon treatment of E49C-OP damaged duplex **57** with those previously reported

confirmed the formation of **1** in E49C-OP treated DNA (Figure 38).[28] The weak intensities of several of the adducts is a result of the formation of low yields of **1** at a given time. The absence of 3'-phosphoglycolate (**9**) at the sites of cleavage indicates that little if any direct strand scission is due to reaction at the C4'-position.

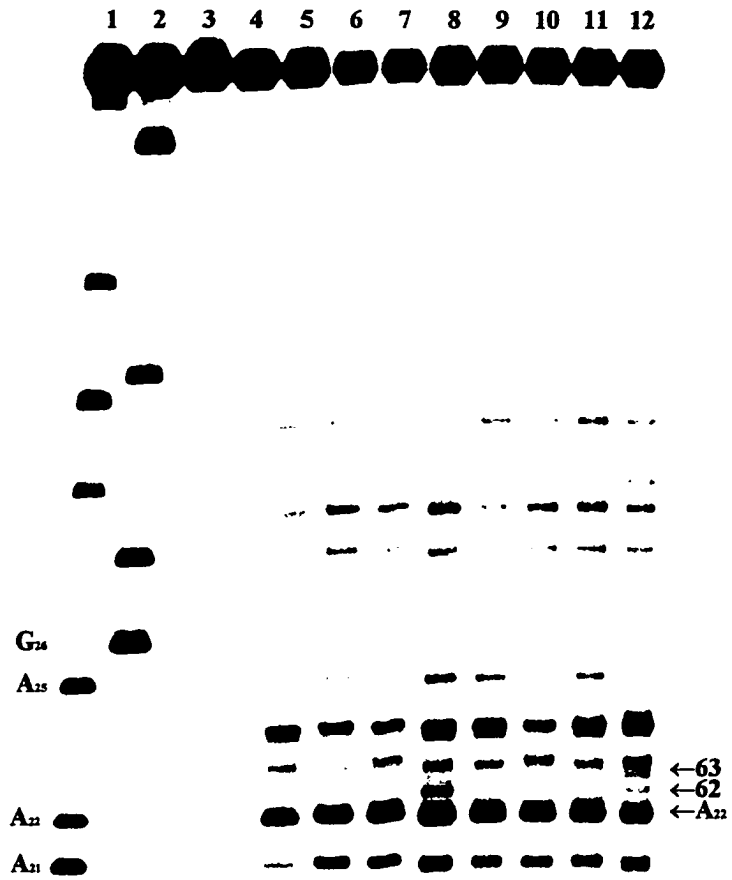

Figure 38. Autoradiogram of **57** treated with E49C-OP. Lane 1, dA selective sequencing reaction. Lane 2, dG selective sequencing reaction. Lanes 3 and 4 contain **59**: lane 3, no further treatment; lane 4, piperidine (0.1 M), 90 °C, 20 min. Lanes 5 – 12 contain **57** treated with E49C-OP ([**57**] = 70.0 nM, [E49C-OP] = 2.5 μM, [$CuSO_4$] = 5.8 μM, [trp] = 10.0 mM, [MPA] = 5.8 mM in 20.0 mM KH_2PO_4, pH = 7.0): lane 5, no further treatment; lane 6, piperidine (100 mM), 20 min, 90 °C; lane 7, piperidine (0.1 M), 20 min, 37 °C; lane 8, piperidine (0.1 M), BME (50.0 mM), 20 min, 37 °C; lane 9 DMEDA (5.0 mM), 20 min, 37 °C; lane 10, DMEDA (5.0 mM), BME (5.0 mM), 20 min, 37 °C; lane 11, DMEDA (0.1 M), 20 min, 37 °C; lane 12, DMEDA (0.1 M), BME (50.0 mM), 20 min, 37 °C.

Measurement of the rate of formation of alkali labile lesions and direct strand breaks (k_{OX}) was carried out in the same manner described for **24-26**. Reaction of **57** with E49C-OP, $CuSO_4$, trp, and MPA were carried out at 37 °C and the amount of total strand scission following alkali treatment at A_{22}, A_{21}, G_{20}, and A_{19} was measured as a function of time. Plots of the natural log one minus the fraction of cleavage at A_{22}, A_{21}, G_{20}, or A_{19} (ln 1- $Base_{Xt}$) as a function of time showed good linearity and provided first-order rates for the formation of direct strand breaks and alkali labile lesions (k_{OX}) of $(2.20 \pm 0.51) \times 10^{-5}$ s^{-1} ($t_{1/2}$ = 8.75 h), $(4.10 \pm 0.24) \times 10^{-6}$ s^{-1} ($t_{1/2}$ = 47.0 h), $(9.16 \pm 4.05) \times 10^{-6}$ s^{-1} ($t_{1/2}$ = 21.0 h), and $(8.38 \pm 0.72) \times 10^{-6}$ s^{-1} ($t_{1/2}$ = 23.0 h) for A_{22}, A_{21}, G_{20}, and A_{19} respectively (Figure 39). The sum of these rate constants gives a value of k_{OX} for the overall reaction of E49C-OP with **57** of $(4.36 \pm 0.65) \times 10^{-5}$ s^{-1} ($t_{1/2}$ = 4.4 h).

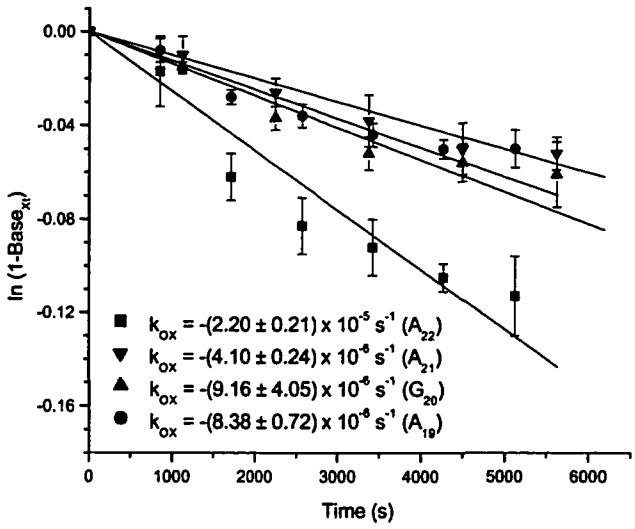

Figure 39. Plot of the ln (1 - $Base_{Xt}$) versus time at 37 °C at A_{22}, A_{21}, G_{20}, and A_{19} in the presence of E49C-OP, $CuSO_4$, trp, and MPA ([**57**] = 70.0 nM, [E49C-OP] = 2.5 μM, [$CuSO_4$] = 5.0 μM, [MPA] = 5.8 mM in 20.0 mM KH_2PO_4, pH = 7.0).

With the knowledge of the major site of cleavage, duplex **64a** was prepared where A_{22} was substituted by the C1' *t*-butyl ketone **15**. Photolytic conversion of **64a** to generate **64b** was carried out using duplex DNA in order to avoid potential thermal

5'-^{32}P-d(AGT CGC CGA ATG TAC TAG AGA **X**CT AGT GCA TTA GCT TAT TTT TTT GTT AT)
3'-d(TCA GCG GCT TAC ATG ATC TCT TGA TCA CGT AAT CGA ATA AAA AAA CAA TA)

64a, X = **15**
64b, X = **1**

decomposition of **1** as a result of hybridizing the long oligonucleotide at the required elevated temperatures. Photolysis of **64a** was carried out in 10 mM aqueous sodium phosphate buffer (pH = 7.0) for 1.5 h at λ_{max} = 350 nm, followed by removal of the buffer through the use of G-25 sephedex. These conditions were sufficient to convert approximately 50% of the **15** present to the 2-deoxyribonolactone (**1**).

With **1** present at the primary site of reaction of E49C-OP, its decay was followed in potassium phosphate buffer (pH = 7.0) by quantifying the amount of intact **64b** as a function of time. The decay of **64b** in the presence of E49C-OP, $CuSO_4$, and MPA obeyed first-order kinetics for 2.5 h. Plots of the natural log of the fraction of intact **64b** as a function of time yielded a rate for the first-order decay of **1** of $(8.60 \pm 0.06) \times 10^{-5}$ s^{-1} ($t_{1/2}$ = 2.2 h) at 37 °C (Figure 40). This rate is the summation of all of the processes leading to decomposition of 2-deoxyribonolactione (**1**) including contributions from the buffer and any basic amino acid residues present in the protein capable of inducing the β-elimination of the 3'-phosphate in **1**.

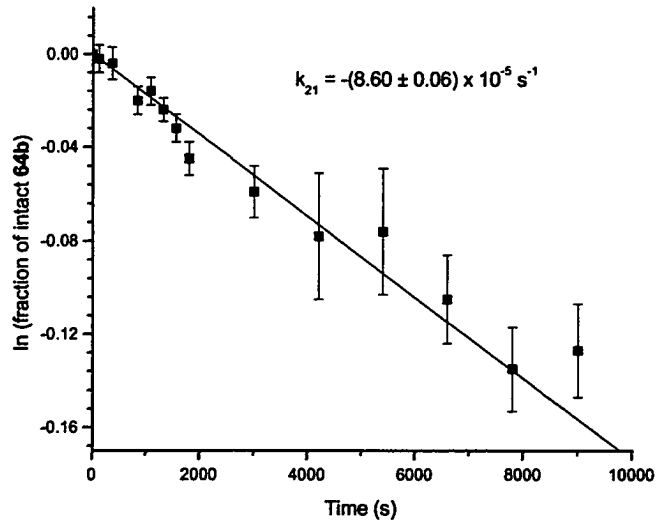

Figure 40. Plot of the ln (fraction intact **64b**) versus time at 37 °C in the presence of E49C-OP, $CuSO_4$, trp, and MPA ([**64b**] = 50.0 nM, [E49C-OP] = 2.5 μM, [$CuSO_4$] = 5.0 μM, [MPA] = 5.8 mM in 20.0 mM KH_2PO_4, pH = 7.0), 37 °C.

In order to determine the rate of decay of **1** in **64b** due to the presence of the basic argine (8 residues) and lysine (4 residues) amino acids present in the protein, kinetics were measured using the unmodified protein, E49C. The unconjugated E49C protein was used in order to include the contribution from free $CuSO_4$ and MPA. The decay of **64b** obeyed first-order kinetics for 2.5 h and a rate of (3.05 ± 0.37) x 10^{-5} s^{-1} ($t_{1/2}$ = 6.3 h) at 37 °C was determined from plots of the natural log of the fraction of intact **64b** as a function of time (Figure 41).

Kinetics for the decay of **64b** in the absence of E49C-OP were also measured in order to determine the contribution of buffer. The rate of decay of **64b** in the presence of KH_2PO_4 buffer at pH = 7.0, $CuSO_4$, trp, and MPA obeyed first-order kinetics for 2.5 h. Plots of the natural log of the fraction of intact **64b** as a function of time gave a rate of (5.18 ± 0.26) x 10^{-5} s^{-1} ($t_{1/2}$ = 3.7 h) at 37 °C (Figure 42). This rate is an order of magnitude faster than the background reaction carried out in Tris buffer and may result

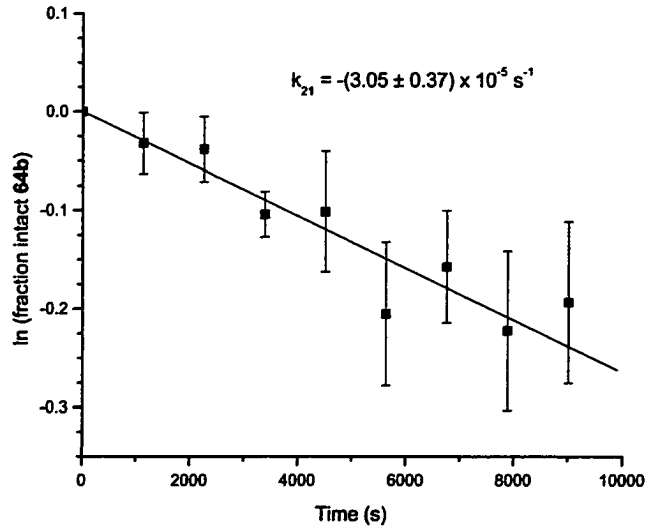

Figure 41. Plot of the ln (fraction intact **64b**) as a function of time at 37 °C in the presence of E49C, $CuSO_4$, trp, and MPA ([**64b**] = 50.0 nM, [E49C] = 2.5 μM, [$CuSO_4$] = 5.0 μM, [MPA] = 5.8 mM in 20.0 mM KH_2PO_4, pH = 7.0), 37 °C.

from the higher concentration of the phosphate buffer (20 mM) than the Tris (10 mM). The explanation for the faster rate of decay in the absence of E49C is most likely a result of protein binding. Assuming the phosphate buffer is responsible for the observed decay, bound protein may be capable of shielding the 2-deoxyribonolactone lesion from the buffer, effectively reducing the amount of exposure of **1** to the buffer and as a result, reducing the rate of decomposition of **1** present in **64b**.

By subtracting the rate of decomposition of **64b** in the presence of E49C from the measured rate in the presence of E49C-OP, an estimate for the rate of cleavage of **1** in the presence of E49C-OP, $CuSO_4$, trp, and MPA is (5.55 ± 0.37) x 10^{-5} s^{-1} ($t_{1/2}$ = 3.5 h) at 37 °C. This rate represents an upper limit for the induced cleavage of **1** by E49C-OP since the rate of cleavage in the presence of E49C was used in its calculation. Because the rate of decomposition of **64b** in the absence of the 1,10-phenanthroline moiety is

slower than the rate in the absence of added protein, the actual rate of cleavage induced by E49C-OP in the presence of copper, trp, and MPA may be slower. However, the decomposition rate should be no slower than (3.42 ± 0.27) x 10^{-5} s^{-1} ($t_{1/2}$ = 5.6 h), which is the rate of decomposition of **1** after subtracting the rate of decomposition of **64b** in the absence of added protein.

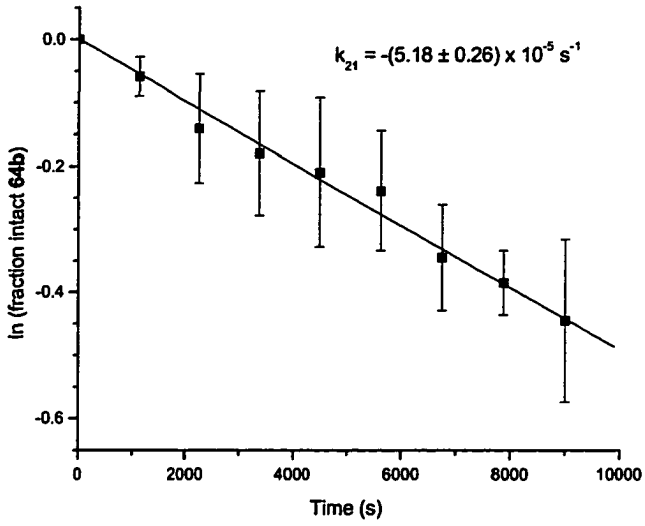

Figure 42. Plot of the ln (fraction intact **64b**) as a function of time at 37 °C in the presence of $CuSO_4$, trp, and MPA ([**64b**] = 50.0 nM, [E49C] = 2.5 μM, [$CuSO_4$] = 5.0 μM, [MPA] = 5.8 mM in 20.0 mM KH_2PO_4, pH = 7.0).

Comparison of the rate of formation of alkali labile lesions and direct strand breaks (k_{OX}) to the estimated rate of cleavage of **1** (k_{21}) at the same site (A_{22}) induced by E49C-OP shows that the rate of cleavage of **1** is only 2.5 faster. This is consistent with the relatively large base enhancement measured at A_{22} of 3.34 ± 0.41 compared to the other systems described above. Interestingly, the overall rate of DNA oxidation (k_{OX}) is most rapid of the four site specific cleaving agents studied while the rate of copper

induced cleavage of **1** (k_{21}) is the slowest. This is consistent with the larger base enhancment for the reaction of E49C-OP with duplex **57**.

3.4 The Mechanism of Cleavage of the 2-deoxyribonolactone (1) Induced by Copper 1,10-Phenanthroline and its Conjugates.

The four site specific cleaving agents examined damage DNA through the formation and subsequent cleavage of alkali labile lesions. For each compound, the rate of alkali labile lesion formation ($k_{a.l.l.}$) is less than that of their decay (k_{decay}) (Table 6).

Table 6. Rates for the formation ($k_{a.l.l.}$) and decay (k_{decay}) of alkali lablile lesions and decay of **1** (k_{21}) as a result of the reaction of duplex DNA with **24-26** and E49C-OP.[a]

Comp.[b]	Meth.[c]	$k_{a.l.l.}$ or k_{11} (s^{-1})[d]	k_{21} or k_{decay} (s^{-1})[e]
24 (A_{13})	1	$(1.87 \pm 0.55) \times 10^{-5}$	$(5.63 \pm 0.69) \times 10^{-4}$
	2	$(1.75 \pm 0.43) \times 10^{-5}$	$(4.70 \pm 0.90) \times 10^{-4}$
25 (A_{17})	1	$(2.99 \pm 0.37) \times 10^{-6}$	-[e]
	2	$(2.74 \pm 0.64) \times 10^{-6}$	$(2.20 \pm 0.20) \times 10^{-4}$
26 (T_{24})	1	$(8.33 \pm 0.73) \times 10^{-6}$	-[e]
	2	$(7.43 \pm 0.44) \times 10^{-6}$	$(1.70 \pm 0.20) \times 10^{-4}$
E49C-OP (A_{22})	1	$(2.20 \pm 0.51) \times 10^{-5}$	$(5.55 \pm 0.37) \times 10^{-5}$
	2	-[f]	-[f]

[a] Kinetic measurement carried out using the appropriate duplex DNA as described in the text. [b] Sites specific cleaving agent and primary site of cleavage for each compound. [c] Method 1 = direct kinetic measurement; method 2 = kinetic measurement by fitting the quantity of alkali labile lesions as a function of time to eq 19. [d] Rate of formation of formation of alkali labile lesions and direct strand breaks (k_{OX}) in the case of method 1 and the rate of alkali labile lesions ($k_{a.l.l.}$) in the case of method 2. [e] Rate of decay of **1** (k_{21}) in the case of method 1 and rate of decay of alkali labile lesions (k_{decay}) in the case of method 2. [f] Not measured.

The rate constant for the cleavage of **1** (k_{21}) by **24** is within experimental error of the value of k_{decay} measured at the same DNA position ($k_{21} = k_{decay}$). This implies that the major alkali labile lesion generated from the reaction of **24** with duplex DNA is the 2-

deoxyribonolactone (**1**). Since compounds **25**, **26**, and E49C-OP are expected to react with duplex DNA in a similar manner, it is concluded that these compounds also generate **1**. This is supported by the fact that 3'-phosphoglycolate (**9**), resulting from hydrogen atom abstraction from the C4'-position, is not observed at the primary site of cleavage for these compounds. Only compound **25** generated small quantities of **9** at a secondary reaction site (T_{16}). Comparison of the rate of formation of **9** ($(1.75 \pm 0.45) \times 10^{-7}$ s^{-1}) to the rate of formation of alkali labile lesions at this site ($(8.29 \pm 2.21) \times 10^{-7}$) shows **9** forms over four times more slowly. These data lead to the conclusion that compounds **24-26** and E49C-OP produce direct strand breaks through formation and cleavage of **1**.

The half life of **1** in the presence of **24** with copper and MPA is 20.5 min. This is comparable to the rate of formation of direct strand breaks induced by $Cu(OP)_2$.[26] The half life of **1** in the presence of **25** or **26** is 51 and 68 min respectively, indicating that substitution at the 2-position of the 1,10-phenanthroline ligand has a significant effect on the rate of cleavage of **1**. In the absence of copper, no change in the quantity of intact **1** was observed, indicating that the 1,10-phenanthroline ligands do not induce cleavage. Dividing the rate of reaction of **24** with **1** by the bimolecular rate constant for the reaction of $Cu(OP)_2$ with the phenyl phosphate analogue of **1** (**35**) gives an effective molarity of approximately 0.38.[33,135] This effective molarity is 1.9×10^4 higher than the actual concentration of **1** used in the kinetic experiments described herein. This leads to the conclusion that a significant rate enhancement is achieved upon binding $Cu(OP)_2$ in the minor groove of duplex DNA.

Useful kinetic information was also obtained by measuring rates of DNA oxidation (k_{OX}) by copper phenanthroline conjugates. The quantity of alkali labile lesions present at a given time was determined by subtraction of the amount of direct strand scission from the amount of strand scission observed after treatment with alkali (0.1 M NaOH at 37 °C for 20 min). Significant error is associated with this calculation as a small number is generated from the difference of two large numbers. Consequently, the rate constants measured through fitting of the quantity of alkali labile lesions as a function of time to eq 19 show significant error (>15%). While it is possible that the rate constants determined from this data may be inaccurate as a result of this error, identical rate constants ($k_{a.l.l.}$ and k_{OX}) are measured through independent methods. This indicates that mechanistic conclusions can be drawn from the rate constants calculated using eq 19.

Evidence for the formation of **1** from comparison of the rate of decay of **1** induced by E49C-OP (k_{21}) to the rate of decay of alkali labile lesions (k_{decay}) wass not possible for E49C-OP. Since the reaction between E49C-OP and duplex **57** did not go to completion low concentrations of alkali labile lesions were generated. As a result, k_{decay} could not be measured. However, evidence for the formation of **1** from the reaction of E49C-OP with duplex DNA has been obtained through the use of the "fingerprint" reaction developed by Hwang (Figure 39).[28] Comparison of the rate constants for the formation of oxidatively damaged DNA (k_{OX}) and decay of **1** (k_{21}) shows that the 2-deoxyribonolactone (**1**) decays faster than it is formed (Table 6). Cleavage of **1** by unconjugated protein (E49C) is less efficient ($(3.05 \pm 0.37) \times 10^{-5}$ s^{-1}), indicating that the copper complex plays an important role in this process.

Direct comparison of the rate of decay of **1** (k_{21}) for the four compounds studied is not possible as these rates were measured at different positions in different oligonucleotides. Comparison of the overall rates of formation of damaged DNA (k_{OX}) shows that E49C-OP is the most efficient of the four compounds at damaging duplex DNA (Table 7). Consistent with the qualitative observations reported by Meunier and co-workers, **24** is the most efficient of the three distamycin conjugates at damaging duplex DNA (k_{OX}).[83]

Table 7. Overall and individual rates of DNA damage (k_{OX}) for **24-26** and E49C-OP.[a]

Compound	Site[b]	k_{OX} (s^{-1})[c]
24	A_{13}	$(1.87 \pm 0.55) \times 10^{-5}$
	C_{27}	$(1.35 \pm 0.61) \times 10^{-6}$
	Overall	$(2.00 \pm 0.55) \times 10^{-5}$
25	T_{16}	$(8.29 \pm 2.21) \times 10^{-7}$
	A_{17}	$(2.99 \pm 0.37) \times 10^{-6}$
	C_{23}	$(1.48 \pm 0.16) \times 10^{-6}$
	Overall	$(5.30 \pm 0.46) \times 10^{-6}$
26	T_{24}	$(8.33 \pm 0.73) \times 10^{-6}$
	A_{25}	$(3.78 \pm 0.24) \times 10^{-6}$
	Overall	$(1.21 \pm 0.08) \times 10^{-5}$
E49C-OP	A_{19}	$(8.38 \pm 0.72) \times 10^{-6}$
	G_{20}	$(9.16 \pm 4.05) \times 10^{-6}$
	A_{21}	$(4.10 \pm 0.24) \times 10^{-6}$
	A_{22}	$(2.20 \pm 0.51) \times 10^{-5}$
	Overall	$(4.36 \pm 0.65) \times 10^{-5}$

[a] Kinetic measurement carried out using the appropriate duplex DNA as described in the text. [b] Numbered from the 5'-end of the appropriate oligonucleotide. [c] Rate of formation of alkali labile lesions and direct strand breaks (k_3').

The mono-phenanthroline conjugate **26** is a more efficient DNA cleaving agent than the bis-phenanthroline conjugate **25**. This is inconsistent with the observation that $Cu(OP)_2$ damages duplex DNA more efficently than Cu(OP), but this can be explained by drawing parallels between the reactivity and structure of **25** to that of Cu(II)(2,9-

dimethyl-1,10-phenanthroline)$_2$ (**42**).[36] The failure of **42** to react with duplex DNA has been proposed to be a result of the inability of **42** to undergo the redox chemistry required for generation of the reactive copper species.[26,35,36] Complex **42** binds duplex DNA and inhibits other minor groove binding molecules.[26,35,36] The inability of **42** to undergo the redox chemistry required for damage of duplex DNA is likely a result of the increased tetrahedral nature of **42** relative to Cu(OP)$_2$. The increased tetrahedral structure of **42** is due to steric interactions resulting from substitution at the 2- and 9-positions of the 1,10-phenanthroline ring.[36] Formation of the reactive intermediate is prohibited on the basis of sterics rather than the result of an electronic inhibition. Since the 1,10-phenanthroline bridge in **25** is connected at the 2-position of the 1,10-phenthroline moiety, it is possible that the reduced rate of reaction of **25** relative to that of **24** is a result the inability of the copper complex of **25** to easily adopt the conformation required for DNA damage. As a result, **25** is less efficient than **24** or the mono-OP conjugate **26** at the formation of alkali labile lesions and direct strand breaks (k_{ox}).

Comparison of the base enhancement for the four site specific cleavage agents studied to $k_{decay}/k_{a.l.l.}$ shows the expected trend (Table 8). A smaller ratio of the rate of decay of alkali labile lesions to their rate of formation ($k_{decay}/k_{a.l.l.}$) results in a greater enhancement in the quantity of strand scission observed after treatment with alkali. The reason for the enhancement of 1.78 ± 0.06 for **25** is unclear when the ratio of rate constants for the formation and decay of **1** is on the order of 70, but may be a result of difficulty in quantitating small amounts of **1**. Similar base enhancements are observed for the reaction of Cu(OP)$_2$ and the distamycin conjugates with duplex DNA. This leads

to the conclusion that the ratio of rate constants for the decay of alkali labile lesions (k_{decay}) and their formation ($k_{a.l.l.}$) for the reaction of $Cu(OP)_2$ with duplex DNA should be at least 35. Since the primary lesion formed from the reaction of **24** with duplex DNA is believed to be **1**, the similar base enhancement for **23** and $Cu(OP)_2$ indicates that this complex induces direct strand scission primarily through the formation and decay of **1**.

Table 8. The enhancement in strand cleavage upon reaction of $Cu(OP)_2$, **24-26** and E49C-OP with duplex DNA and the ratio of the rates of formation and decay of **1** by **24-26** and E49C-OP.[a]

Compound	Base	Buffer[b]	$k_{decay}/k_{a.l.l.}$[c]	Base Enhancement[d]
24	A_{13}	10.0 mM Tris	36.9 ± 10.85	1.72 ± 0.29
	C_{27}		-[e]	1.60 ± 0.26
	All		-[e]	1.66 ± 0.06
25	T_{16}	10.0 mM Tris	-[e]	2.38 ± 0.19
	A_{17}		73.56 ± 11.30	1.78 ± 0.06
	C_{23}		-[e]	2.21 ± 0.31
	All		-[e]	2.12 ± 0.25
26	T_{24}	10.0 mM Tris	22.88 ± 2.96	2.19 ± 0.19
	A_{25}		-[e]	1.77 ± 0.05
	All		-[e]	1.98 ± 0.21
E49C-OP	A_{19}	20.0 mM KH_2PO_4	-[e]	5.57 ± 0.01
	G_{20}		-[e]	1.38 ± 0.02
	A_{21}		-[e]	4.17 ± 0.15
	A_{22}		2.52 ± 0.61	3.34 ± 0.41
	All		-[e]	3.63 ± 0.41
$Cu(OP)_2$	All	50.0 mM Tris	-[e]	1.49 ± 0.16
$Cu(OP)_2$	All	50.0 mM KH_2PO_4	-[e]	1.78 ± 0.09

[a] Measurements were carried out using the appropriate duplex DNA as described in the text. [b] pH = 7.0. [c] k_2 is the rate of decay of **1** and k_1 is the rate of formation of **1**. [d] Ratio of the quantity of total strand scission after treatment with NaOH (0.1M) for 20 min at 37 °C to the quantity of direct strand scission after 30 min reactions. [e] Not measured.

Several mechanisms can be envisioned to account for the observed cleavage of **1** in the presence of the site specific cleaving agents studied: 1) Cleavage of the 3'-

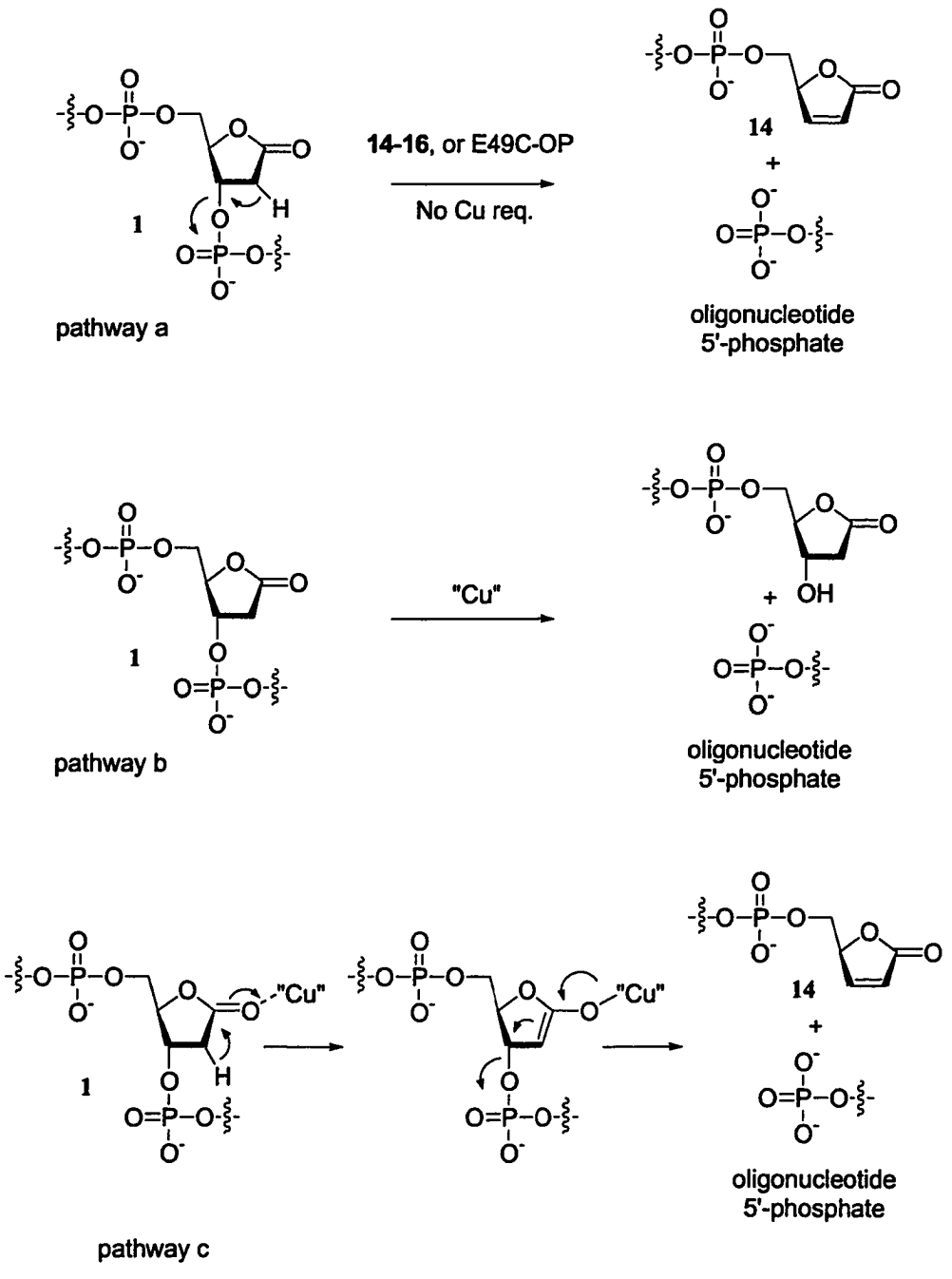

Figure 43. Possible mechanisms for the cleavage of **1** in the presence of **24-26** and E49C-OP.

phosphate through a base induced β-elimination with the distamycin conjugates or E49C-OP functioning as the base (no copper requirement) (Figure 43, pathway a); 2)

Copper catalyzed phosphate diester hydrolysis of the 3'-phosphate in **1** (Figure 43, pathway b); 3) Copper induced enolate formation of **1** with copper functioning as a Lewis acid and/or general base (Figure 43, pathway c).

Cleavage of **1** with **24-26** acting as a base through a pathway not involving copper to induce elimination of the 3'-phosphate via enolate formation can be ruled out. No change in the concentration of intact **59b** was observed in the presence of **24** without copper. Since **24-26** only vary by the number and linkage position of the 1,10-phenanthroline moieties, **25** and **26** are also not expected to be responsible for inducing elimination in the absence of copper.

Elimination induced by basic protein residues in E49C-OP can be ruled out as the sole pathway leading to cleavage of **1**. The rate of cleavage of **64b** in the presence of unconjugated protein (E49C) has been measured to be $(3.05 \pm 0.37) \times 10^{-5}$ s^{-1} at 37 °C, while the rate of cleavage of **1** in the presence of E49C-OP with copper and MPA is $(8.60 \pm 0.06) \times 10^{-5}$ s^{-1}. The enhanced rate of cleavage of **1** in the presence of E49C-OP (2.5 fold) is not due to the presence of the 1,10-phenanthroline moiety since copper is required for cleavage.

In order to conclusively determine the mechanism by which $Cu(OP)_2$, or a $Cu(OP)_2$ derived species induces cleavage of **1**, the nature of the reactive copper complex must be known. As stated above, the reactive copper species has not been identified. However, on the basis of proposals that the active species is either a copper oxo compound or a copper bound hydroxyl radical, it is reasonable to assume that the copper complex resulting from hydrogen atom abstraction of the C1'-position of the sugar moiety will either be a copper bound hydroxide, or a copper bound aquo complex

(Figure 44).[26,35,36] Since the pK_a of the Cu(II)(OP) aquo complex is 7.0, the Cu(OP) aquo complex is expected to exist as a copper bound hydroxide in the pH 7.0 solutions that are used to damage duplex DNA with $Cu(OP)_2$ and in the kinetic studies described herein.[117]

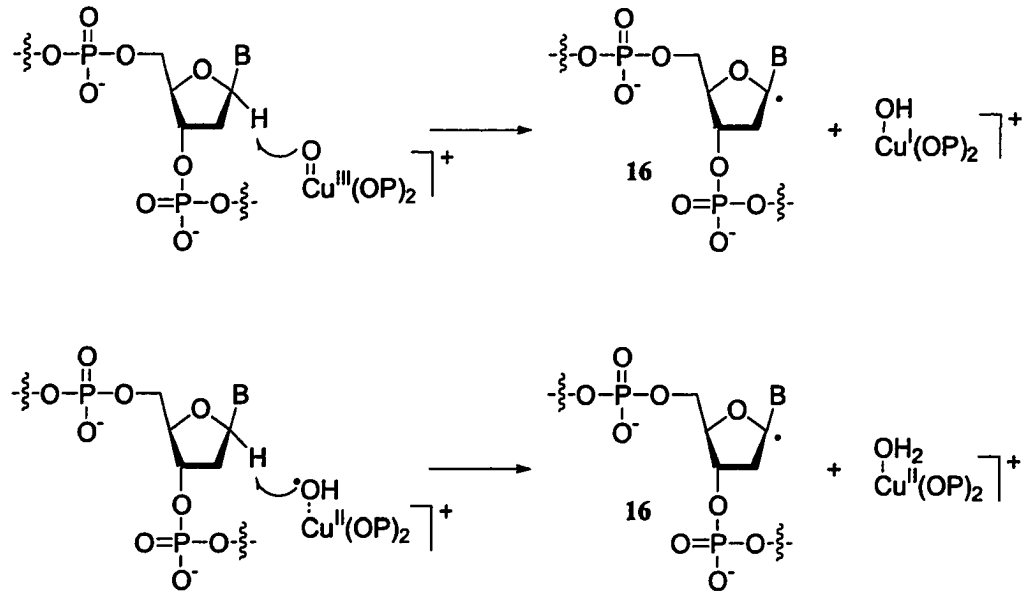

Figure 44. Possible pathways for the formation of $(OP)_2$Cu-OH.

The observation that no cleavage of **59b** in the presence of **24** with copper was detected in the absence of MPA indicates that a copper(I) complex is necessary for cleavage. It is possible that the reductant is required to generate a copper species which undergoes further reaction with the sugar moiety by hydrogen atom abstraction to generate the copper complex responsible for the cleavage of **1**. However, this is considered unlikely as **1** does not contain a C1'-hydrogen atom and abstraction of a

hydrogen atom from the C4'-position will result in the formation of 3'-phosphoglycolate (**9**) which is not observed.

Cleavage of **1** through a copper bound hydroxide catalyzed phosphate diester hydrolysis can be ruled out on the basis of kinetics. Based on the most efficient rate of phosphate diester hydrolysis observed for the reaction $(H_2O)_2Cu(bpy)$ (**41**) with ethyl *p*-nitrophenyl phosphate (**36**) of 1.1 x 10^{-2} M^{-1} s^{-1}, at the 10.0-20.0 μM concentrations used for the kinetic measurements described herein, an upper limit of for the rate of phosphate hydrolysis is 2.2 x 10^{-7} s^{-1}.[97] This number is considered an upper limit for hydrolysis of the 3'-phosphate in **1**. The estimated rate constant is for the hydrolysis of ethyl *p*-nitrophenyl phosphate (**36**), rather than for hydrolysis of a dialkyl phosphate diester, which is expected to be a slower process. This rate is over three orders of magnitude slower than the measured rates of cleavage of **1** in the presence of **24-26** with copper and reductant, indicating that the copper catalyzed phosphate hydrolysis is not kinetically competent with respect to the observed rate of cleavage of **1**. In addition, there is no clear reason why the 3'-phosphate in **1** should be more susceptible to hydrolysis than the phosphate at any other position in the oligonucleotide. If cleavage of **1** were occurring through phosphate hydrolysis, duplex DNA cleavage would be expected to occur in the absence of damage to the sugar moiety, indicating that there would not be a buildup of alkali labile lesions (base enhancement = 1.0). Since this phenomenon is not observed from the reaction of $Cu(OP)_2$ with duplex DNA, it is clear that cleavage of **1** does not occur through phosphate hydrolysis.

A mechanism consistent with the known reactivity of copper complexes containing similar ligands to 1,10-phenanthroline is that of a copper induced enolate

formation in **1**. The formation of the enolate can be envisioned to occur through Lewis acid catalyzed enolate formation or deprotonation of an α-proton in **1** by a copper bound hydroxide (general base). A combination of the two mechanisms with the copper functioning as a Lewis acid in conjunction with deprotonation of **1** by a copper bound hydroxide is favored on the basis of the pK_a arguments presented below.

Based upon the estimated Lewis acidity of Cu(II)(OP) and the pK_a values for α-protons of esters, copper induced enolate formation in **1** solely through Lewis acid activation is unlikely. While α-proton pK_a values for five-membered lactones have not been measured, estimation of the pK_a of the C2'-protons in **1** from the acidity of α-protons in esters gives a value of 24.[136] Estimation of the Lewis acidity of $Cu(I)(OP)_2$ or $Cu(II)(OP)_2$ from the effect on the pK_a of H_2O bound to Cu(II)(OP) leads to the conclusion that $Cu(OP)_2$ is capable of decreasing the pK_a of a bound molecule by approximately seven pK_a units.[133] The pK_a of Cu(II)(bpy) bound H_2O is 7.8, compared to 7.0 for H_2O bound to Cu(II)(OP) indicating the presence of the additional aryl ring in 1,10-phenanthroline increases the Lewis acidity of the copper slightly. However, addition of the second 1,10-phenanthroline ligand to form $Cu(II)(OP)_2$ is expected decrease the Lewis acidity of the copper ion as a result of the corresponding increase in electron density at the metal center. The exact effect of the interaction of $Cu(OP)_2$ as Lewis acid with the carbonyl of **1** on the pK_a of the C2'-protons is unknown. Decreasing the pK_a of the C2'-protons in **1** by 7 units (derived from the effect of copper on bound H_2O) gives an estimated minimium pK_a of 17. This sugests that cleavage of $Cu(OP)_2$ 2-deoxyribonolactone complex will not be catalyzed by H_2O at pH = 7.0.

Further support for this conclusion can be obtained from estimation of the maximum rate constant for this process (k_{21}). This reaction can be written as shown in

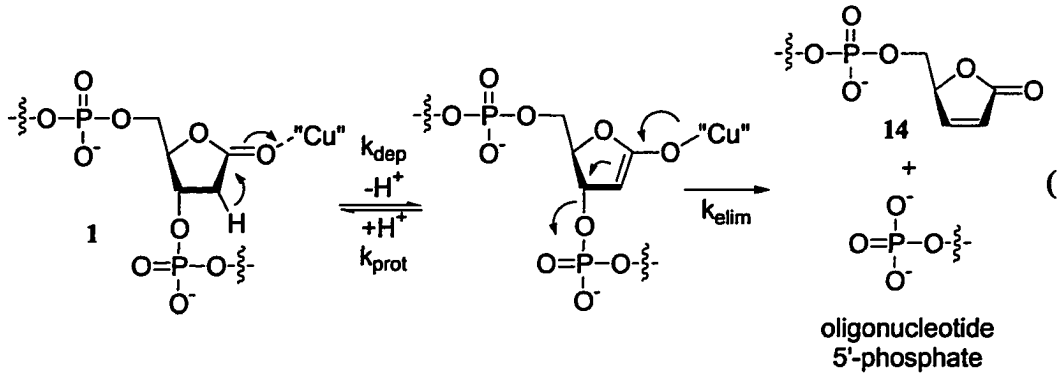

(22)

eq 22 with the deprotonation of **1** expressed as an equilibrium as between **1** and the corresponding enolate followed by elimination to form **14**. The elimination reaction can be assumed to be faster than deprotonation on the basis of the unfavorable thermodynamics associated with the formation of the enolate of **1** ($K_a = 10^{-17}$). As a result, the rate of the elimination reaction is determined by the rate of the deprotonation reaction. A minimum value for the free energy of activation ($\Delta G^{\neq}$) at 37 °C can be

$$\Delta G^{\neq} = -RT \ln(K) \qquad (23)$$

estimated using eq 23 (where K is the acidity constant for the C2'-proton, $K_a = 10^{-17}$) by assuming that the deprotonation reaction is a barrierless process. This gives a minimum value for $\Delta G^{\neq}$ of 24.11 kcal/mol . A maximum rate for the deprotonation reaction at 37 °C can then be calculated using eq 24 (k is the Boltzmann constant and h is the Planck

$$k_{21} = \frac{kT}{h} e^{-\frac{\Delta G^{\neq}}{RT}} \quad (24)$$

constant) and yields a value of 6.44 x 10^{-5} s^{-1}. This rate is an order of magnitude slower than that measured for the elimination of **1** in the presence of **24,** indicating that the copper induced elimination of **1** is not due solely to Lewis acid activation of **1** by the copper complex.

An argument based on pK_a values can also be used to rule out the $Cu(OP)_2$ induced cleavage of **1** solely through deprotonation of the C2'-position by a copper bound hydroxide. Based on the pK_a of H_2O bound to Cu(II)(OP) and the mechanism proposed for the reaction of Cu(tpy) (**40**) with **6** (Figure 19), it is reasonable to assume that the proposed deprotonation will be effected by a copper bound hydroxide for reactions carried out at pH = 7.0.[118] Based on the pK_a of the C2'-protons in **1** of approximately 24, the $Cu(OP)_2$ bound hydroxide deprotonation will be slow at 37 °C. However, if the copper bound hydroxide is capable of reacting in a manner more closely related to free hydroxide, the pK_a difference between the C2'-protons in **1** and hydroxide may be closer to 10 pK_a units. Calculation of the minimum free energy of activation ($\Delta G^{\neq}$) and the corresponding maximum rate constant for k_{21} as described above using eq 23 and 24 gives values of 14.18 kcal/mol for $\Delta G^{\neq}$ and 6.45 x 10^2 s^{-1} for k_{21}. Since the calculated maximum value for k_{21} is greater than the actual rate constant for k_{21}, the copper induced elimination of **1** occurs through a pathway with $24.11 < \Delta G^{\neq} > 14.18$ kcal/mol.

Through a combination of the Lewis acidity of $Cu(OP)_2$ and the proposed basicity of the copper bound hydroxide, the pK_a difference between the C2'-protons in **1** and the copper bound hydroxide could be lowered to as little as three pK_a units. This is based on the assumption that the copper bound hydroxide reacts in a manner more closely associated with free hydroxide ($pK_a = 14.0$). This proposal is supported by studies which indicate that **40** functions as both a Lewis acid and general base in the transesterification of **36** (Figure 19).[118] The basicity of the copper bound hydroxide could be significantly higher than that estimated from the pK_a of copper aquo complexes, as the mechanism proposed for the transesterification of **46** involves deprotonation of an alkyl alcohol, which has a pK_a in the range of 17-20.[136] The pK_a of the hydroxyl in **46** at the time of deprotonation will vary as a function of the degree of bond formation between the 2'-oxygen and the phosphate diester. The pH dependence on the rate of the transesterification reaction indicates that the basicity of the copper bound hydroxide is important in determining the rate of reaction. This leads to the conclusion that a significant degree of deprotonation is present in the transition state. As a result, it seems likely that the cleavage of **1** in the presence of $Cu(OP)_2$ is a result of Lewis acid activation of the carbonyl to reduce the pK_a of the C2'-protons in conjunction with general base catalysis of a copper bound hydroxide to form the corresponding enolate which undergoes β-elimination of the 3'-phosphate.

3.5 Conclusions.

The destabilization of duplex DNA upon incorporation of **1** shows that hexameric oligonucleotides do not provide appropriate substrates for the study of the $Cu(OP)_2$

induced damage of duplex DNA with regard to cleavage of the phosphate backbone through reaction at the C1'-position.[34] Extrapolation of the base enhancement predicted from product yields for the reaction of $Cu(OP)_2$ with hexameric DNA to longer oligonucleotides overestimates the amount of alkali labile lesions at a given time. Together, these observations indicate that hexameric DNA is not a substrate which gives results applicable to the mechanism of reaction of $Cu(OP)_2$ with longer strands of duplex DNA.

Direct evidence for the formation of strand breaks as a result of $Cu(OP)_2$ induced cleavage of **1** has been obtained through measurement of the kinetics of this process. Comparison of the rate of cleavage of **1** (k_{21}) to the overall rate of DNA oxidation (k_{OX}) for the four compounds studied shows that **1** is cleaved faster than it is formed. These measurements were carried out using site specific incorporation of the 2-deoxyribonolactone (**1**) in conjunction with site specific delivery of Cu(OP) and $Cu(OP)_2$ moieties. The site specific delivery of Cu(OP) and $Cu(OP)_2$ has been carried out by conjugation to DNA binding molecules.

The rate for cleavage of **1** by **24** (k_{21}) with copper and reductant was determined to be $(5.63 \pm 0.69) \times 10^{-4}$ s^{-1} ($t_{1/2}$ = 20.5 min). Measurement of the overall rate of DNA oxidation (k_{OX}) at the same site gives a value of $(2.00 \pm 0.55) \times 10^{-5}$ s^{-1}. Independent measurement of the rate of formation ($k_{a.l.l.}$) and decay (k_{decay}) of alkali labile lesions in this system through fitting to eq 19 gave an identical rate for the decay of alkali labile lesions and the rate of cleavage of **1**. The overall rate of DNA oxidation (k_{OX}) and formation of alkali labile lesions ($k_{a.l.l.}$) are within experimental error. From this it is

concluded that the majority of the alkali labile lesions formed are **1** and that C1'-oxidation is the major DNA damage pathway induced by **24**.

Similar observations were obtained for the reaction of **25** and **26** with duplex DNA yielding rates for the decay of alkali labile lesions (k_{decay}) of (2.20 ± 0.20) x 10^{-4} s^{-1} and (1.70 ± 0.20) x 10^{-4} s^{-1} respectively. These rate constants are at least an order of magnitude faster than the overall rate of DNA oxidation (k_{OX}) of (5.30 ± 0.46) x 10^{-6} s^{-1} and (1.21 ± 0.08) x 10^{-5} s^{-1} for **25** and **26** respectively, indicating that formation of **1** in the presence of **25** or **26** will leads to direct strand scission. Qualitatively similar relative rates were observed for the reaction of E49C-OP with duplex DNA with the rate for cleavage of **1** (k_{21}) being only two fold faster than the overall rate of DNA oxidation (k_{OX}).

Comparison of the base enhancement for reactions of **23-25**, E49C-OP, and $Cu(OP)_2$ with duplex DNA indicates that the ratio of rates of formation (k_{11}) and decay (k_{21}) of **1** are similar. As a result, it is concluded that the primary mechanism for the formation of direct strand breaks in duplex DNA induced by $Cu(OP)_2$ is C1'-hydrogen atom abstraction, which results in the formation of **1**. Subsequent cleavage of **1** to form direct strand breaks occurs by a copper induced elimination of the 3'-phosphate (Figure 45). From analysis of the reactivity of copper compounds similar to Cu(OP) and $Cu(OP)_2$, the copper induced cleavage of **1** is proposed to occur through Lewis acid activation of the carbonyl in **1** coupled with the action of a copper bound hydroxide as a general base to form the enolate of **1** which undergoes cleavage of the 3'-phosphate.

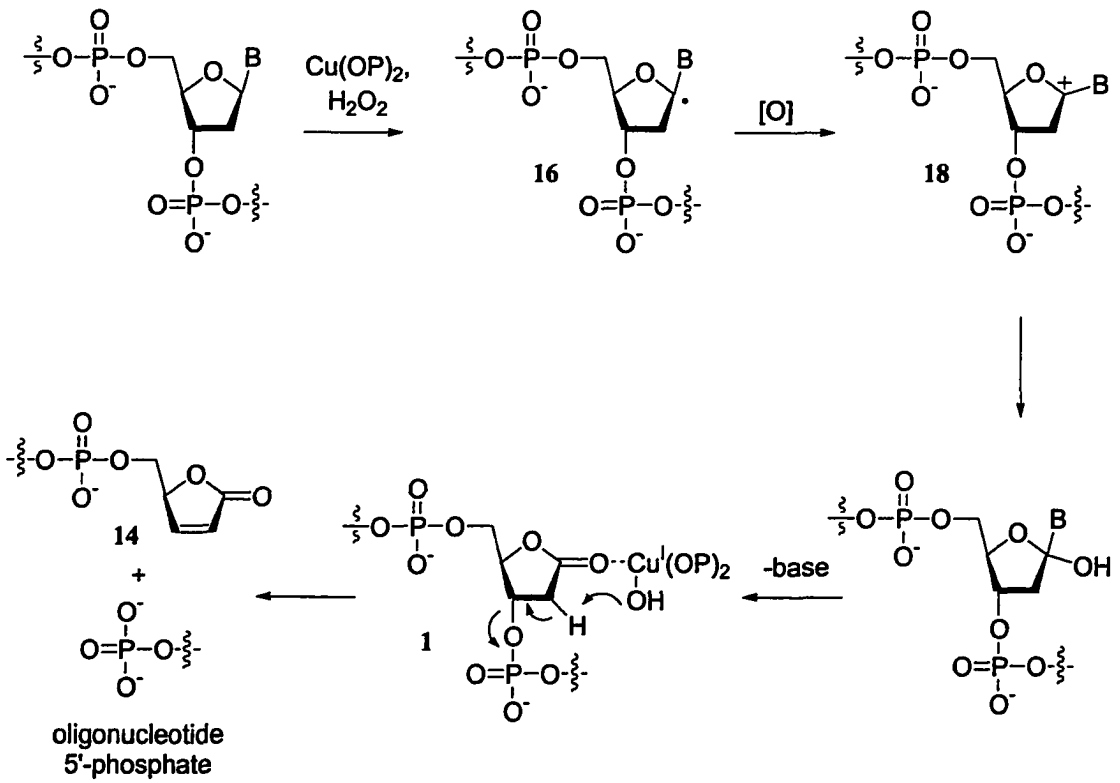

Figure 45. Proposed mechanism for the formation of direct strand breaks as a result of C1'-hydrogen atom abstraction by $Cu(OP)_2$ in the presence of reductant.

4 Experimental Methods.

General Methods. Quantification of radiolabeled oligonucleotides was carried out using a Molecular Dynamics Storm 820 phosphorimager equipped with ImageQuant version 5.1. Linear and biexponential regresion analysis of concentration vs. time data was carried out using Origin 6.1. Oligonucleotide synthesis was carried out on an Applied Biosystems Incorporated 394 DNA/RNA synthesizer using standard protocols with 5-ethylthio-1H-tetrazole as the activator. Benzoyl-protected deoxyadenosine, benzoyl-protected deoxycytidine, *iso*-butyryl-protected deoxyguanosine, and thymidine β-cyanoethyl phosphoramidites and all other synthesis reagents were obtained from Glenn Research. Oligonucleotides were deprotected for 16 h in conc. aqueous NH_4OH at 55 °C. T4 polynucleotide kinase was obtained from New England Biolabs. γ-^{32}P-dATP and α-^{32}P-dideoxyATP were obtained from Amersham. C18 Sep-Pak Plus catridges were obtained from Waters. Microdialysis cartridges (MWCO = 2000 daltons) were obtained from Bio-Tech International. Distymacin conjugates **24-26** were obtained from Professor Bernard Meunier and Dr. Marguerite Pitié. The modified trp repressor protein E49C was obtained from Professor David Sigman and Dr. Chi-hong Betty Chen.

DNA manipulations, including enzymatic labeling, were carried out using standard procedures.[138] Exchange of ammonium for sodium counter ions in oligonucleotides was carried out by precipitation from sodium phosphate. Electrospray mass spectrometry samples were prepared by precipitation from NH_4OAc (pH = 5.2, 0.52 M, for 10 min). Oligonucleotides were sequenced using reactions specific for deoxyguanosine and deoxyadenosine.[138,139] Preparative oligonucleotide seperation for **53b** were carried out using HPLC. Preparative oligonucleotide separations for all other

oligonucleotides ≤ 35 bases in length were carried out on 20% polyacrylamide denaturing gels (5% cross-link, 45% urea (by weight)). Preparative oligonucleotide separations for oligonucleotides 50 bases in length were carried out on 15% polyacrylamide denaturing gels (5% cross-link, 45% urea (by weight)).

Synthesis of oligonucleotides containing **15** were carried out using phenoxyacetyl-protected deoxyadenosine, acetate-protected deoxycytidine, *p*-isopropylphenoxyacetyl-protected deoxyguanosine, and thymidine β-cyanoethyl phosphoramidites and standard ABI coupling times. Deprotection of oligonucleotides containing **15** concentrated NH_4OH at 55 °C for 2 h. Preparation of **23** was carried out according to literature procedure.[53]

General Procedure for Hybridization of Oligonucleotides. 5'-^{32}P or 3'-^{32}P labeled oligonucleotides (700.0 nM, 50 pmols), the corresponding complementary oligonucleotide (1.05 μM, 75 nmols), and NaCl (100 mM) dissolved in H_2O (70.0 μL) were heated at 90 °C for 5 min followed by cooling to rt over a period of 2 h.

Preparation of 53b. Oligonucleotide **53a** (20 – 40 pmols) was incubated with ammonium acetate (pH = 5.6, 1.25 M) at rt for 10 min, followed by desalting using C18 Sep-Pak Plus catridges. The oligonucleotide (10.0 μM) was then taken up in H_2O and photolyzed in Pyrex vessels at λ_{max} = 350 nm for 1.5 hr. The photolyzed material was transferred to an eppendorf tube, the photolysis vessel was rinsed with H_2O (2 x 200 μL), combined with the photolysate, and evaporated to dryness. The DNA was resuspended in H_2O (25 μM) and purified by HPLC on a Microsorb MV C18 column (4.6 x 250 mm)

(solvent A: 50 mM ammonium formate (pH = 6.2), solvent B: 50% acetonitrile in 50 mM ammonium formation (pH = 6.2). Oligonucleotide **42** and was detected at 254 nm with a retention time of 37.1 min using the following gradient: 90% solvent A, 10% solvent B at t_0 for 10 min, linearly to 85% solvent A, 15% solvent B at 30 min, linearly to 40% solvent A, 60% solvent B at 45 min at a flow of 1.0 mL/min. The desired peak was collected in a 25 mL round bottomed flask and the acetonitrile was removed *in vacuo* (on a rotoevaporator) to leave the lactone containing oligonucleotide in a solution of H_2O (note: Do not evaporate to dryness). The resulting solution was desalted using C18 Sep-Pak Plus catridges. The oligonucleotide was then resuspended in 200 μL of H_2O and quantified by UV at 260 nm. The identity of **53b** was confirmed by electrospray mass spectroscopy (calcd: 1673.1, found: 1673.0).

General procedure for T_M Determination. Samples (400 μL) for thermal denaturing studies contained a 1:1 molar ratio of complementary oligonucleotides and were prepared at the following concentrations in H_2O: total DNA concentration (8.3 μM), Tris buffer (50 mM, pH = 7.5), NaCl (0, 100 mM, or 1.0 M). The melting studies were carried out in 1 cm path length quartz cells using a Beckman DU 640 spectrophotometer equipped with a thermoprogrammer and a dry nitrogen source to prevent condensation on the cell windows at low temperatures. The samples were equilibrated at 45 °C for 10 min and then cooled at 0.5 °C/min to 2.0 °C. The samples were held at 2.0 °C for 1 h and then warmed to 45 °C at 0.5 °C/min. The resulting temperature vs. O. D. was then imported into Origin ver. 6.1 and fit to eq 15. The first derivative of eq 15 was solved for the maximium to yield the melting temperature.[119]

General Procedure for the Reaction of 57 with $Cu(OP)_2$. To a solution containing **57** (58.3 nM, 0.583 pmol), and $MgCl_2$ (0 or 10 mM) in Tris or potassium phosphate buffer (50 mM, pH = 7.0, 7.5, or 8.0) in H_2O (10.0 μL) was added a solution containing 50.0 μM phenanthroline/11.5 μM $CuSO_4$ (1.0 μL, 50 pmol phenanthroline, 11.5 pmol $CuSO_4$) and 58 mM 3-mercaptoproprionic acid (1.0 μL, 58 nmols). The resulting solution was incubated at 37 °C for 15 min and the reaction volume was transferred to a new eppendorf tube. The reaction vial was rinsed with H_2O (12.0 μL) and combined with the reaction volume. Half the solution was stored at –78 °C and the other half was treated with NaOH (13.0 μL, 0.1 M) at 37 °C for 20 min and then adjusted to pH = 7.0 with 1.0 M HCl.

Treatment of 60b with Na_2IrCl_6. A solution containing **60b** (35.7 pM, 2.68 fmol) and sodium phosphate (10.0 mM, pH = 7.0) in H_2O (75.0 μL) was photolyzed in a pyrex vessel in a Rayonet Photoreactor with 16 lamps at λ_{max} = 350 nm for 4.5 h. The photolysis mixture was transferred to an eppendorf tube, followed by two H_2O washes (50.0 μL and 25.0 μL). This solution (45.0 μL) was added to a solution containing Na_2IrCl_6 (1.0 mM, 5.0 nmol) in H_2O (5.0 μL) and incubated at rt for 1 h. The reaction volume was then split in half and to each was added H_2O (30 μL), 1.3 mM calf thymus DNA (10.0 μL, 13.0 nmol) and 3.0 M NaOAc at pH = 5.2 (10.0 μL) and the solution was precipitated from EtOH (300 μL). One volume was stored at –20 °C and the other was treated with piperidine (1.0 M, 100 μL) at 90 °C for 20 min followed by removal of the solvent *in vacuo*. The resulting DNA was then lyophilized with H_2O (2x50 μL).

Preparation of 59b. A solution containing **59a** (333 nM, 15.0 fmol), NaCl (100 mM), MOPS (10.0 mM, pH = 7.0) in H_2O (45.0 μM) was photolyzed in a Pyrex vessel in a Rayonet Photoreactor with 16 lamps at λ_{max} = 350 nm for 1.5 h. The photolysate was added to a solution containing the appropriate complement (4.5 μM, 22.5 fmol) in H_2O (5.0 μL). The solution was then heated at 55 °C for 10 min followed by slow cooling to rt over a period of 2 h. The solution was then desalted using G-25 sephadex (H_2O).

Measurement of Reaction Kinetics Between 24 and 59b. A solution containing $CuCl_2$ (1.0 mM, 2.0 nmol) and **24** (1.0 mM, 2.0 nmol) in H_2O (2.0 μL) was incubated at rt for 1 h, followed by dilution with H_2O (23.0 μL). This solution (3.0 μL) was added to a solution containing **59b** (2.0 μM, 12.0 pmol), NaCl (66.7 mM), and Tris buffer (20.0 mM, pH = 7.0) in H_2O (6.0 μL) and incubated at rt for 5 min. This solution (9.0 μL) was added to a solution containing MPA (8.0 mM, 24.0 nmol) in H_2O (3.0 μM) and the resulting solution was incubated at 37 °C for 120 min with aliquots (1.0 μL) taken at 10, 20, 30, 48, 66, 84, 102, and 120 min and stored at –78 °C. Prior to denaturing PAGE analysis, samples were resuspended in formamide loading buffer (95% formamide, 20 mM EDTA) and stored at 0 °C.

Measurement of Reaction Kinetics Between 24 and 59b without $CuCl_2$. A solution containing **24** (1.0 mM, 2.0 nmol) in H_2O (2.0 μL) was incubated at rt for 1 h, followed by dilution with H_2O (23.0 μL). This solution (3.0 μL) was added to a solution containing **59b** (2.0 μM, 12.0 pmol), NaCl (100 mM), and Tris buffer (20.0 mM, pH =

7.0) in H_2O (6.0 μL) and incubated at rt for 5 min. This solution (9.0 μL) was added to a solution containing MPA (8.0 mM, 24.0 nmol) in H_2O (3.0 μM) and the resulting solution was incubated at 37 °C for 120 min with aliquots (1.0 μL) taken at 10, 20, 30, 48, 66, 84, 102, and 120 min and stored at –78 °C. Prior to denaturing PAGE analysis, samples were resuspended in formamide loading buffer (95% formamide, 20 mM EDTA) and stored at 0 °C.

Measurement of Reaction Kinetics Between 59b and Tris Buffer, pH = 7.0. A solution containing **59b** (1.33 μM, 7.98 pmol), $CuCl_2$ (13.3 μM, 120 pmol) NaCl (66.7 mM), and Tris buffer (13.3 mM, pH = 7.0) in H_2O (9.0 μL) and incubated at rt for 5 min. This solution (9.0 μL) was added to a solution containing MPA (8.0 mM, 24.0 nmol) in H_2O (3.0 μL) and the resulting solution was incubated at 37 °C for 120 min with aliquots (1.0 μL) taken at 10, 20, 30, 48, 66, 84, 102, and 120 min and stored at –78 °C. Prior to denaturing PAGE analysis, samples were resuspended in formamide loading buffer (95% formamide, 20 mM EDTA) and stored at 0 °C.

Measurement of Reaction Kinetics Between 24 and 58. A solution containing $CuCl_2$ (1.0 mM, 2.0 nmol) and **24** (1.0 mM, 2.0 nmol) in H_2O (2.0 μL) was incubated at rt for 1 h, followed by dilution with H_2O (23.0 μL). This solution (6.0 μL) was added to a solution containing **58** (1.33 μM, 15.9 pmol), NaCl (66.7 mM), and Tris buffer (13.3 mM, pH = 7.0) in H_2O (12.0 μL) and incubated at rt for 5 min. This solution was added to a solution containing MPA (8.0 mM, 48.0 nmol) in H_2O (6.0 μM) and the resulting solution was incubated at 37 °C for 120 min with aliquots (2 x 1.0 μL) taken at 10, 20,

30, 48, 66, 84, 102, and 120 min and stored at –78 °C. Half of the aliquots at each time point were incubated with NaOH (0.1 M, 5.0 μL) at 37 °C for 20 min and then adjusted to pH = 7.0 with 1.0 M HCl. Prior to denaturing PAGE analysis, samples were resuspended in formamide loading buffer (95% formamide, 20 mM EDTA) and stored at 0 °C.

Measurement of Reaction Kinetics Between 25 and 58. A solution containing $CuCl_2$ (1.0 mM, 4.0 nmol) and **25** (1.0 mM, 4.0 nmol) in H_2O (4.0 μL) was incubated at rt for 1 h, followed by dilution with H_2O (46.0 μL). This solution (6.0 μL) was added to a solution containing **58** (1.33 μM, 15.9 pmol), NaCl (0.1 M), and Tris buffer (13.3 mM, pH = 7.0) in H_2O (12.0 μL) and incubated at rt for 5 min. This solution was added to a solution containing MPA or ascorbate (800 μM, 4.8 nmol) in H_2O (6.0 μM) and the resulting solution was incubated at 37 °C for 4 h with aliquots (2 x 1.0 μL) taken every 30 min and stored at –78 °C. Half of the aliquots for each time point were incubated with NaOH (0.1 M, 5.0 μL) at 37 °C for 20 min and then adjusted to pH = 7.0 with 1.0 M HCl. Prior to denaturing PAGE analysis, samples were resuspended in formamide loading buffer (95% formamide, 20 mM EDTA) and stored at 0 °C.

Measurement of Reaction Kinetics Between 26 and 58. A solution containing $CuCl_2$ (1.0 mM, 4.0 nmol) and **26** (1.0 mM, 4.0 nmol) in H_2O (4.0 μL) was incubated at rt for 1 h, followed by dilution with H_2O (46.0 μL). This solution (6.0 μL) was added to a solution containing **58** (1.33 μM, 15.9 pmol), NaCl (66.7 mM), and Tris buffer (13.3 mM, pH = 7.0) in H_2O (12.0 μL) and incubated at rt for 5 min. This solution was added to a solution containing MPA or ascorbate (800 μM, 4.8 nmol) in H_2O (6.0 μM) and the

resulting solution was incubated at 37 °C for 4 h with aliquots (2 x 1.0 μL) taken every 30 min and stored at –78 °C. Half of the aliquots for each time point were incubated with NaOH (0.1 M, 5.0 μL) at 37 °C for 20 min and then adjusted to pH = 7.0 with 1.0 M HCl. Prior to denaturing PAGE analysis, samples were resuspended in formamide loading buffer (95% formamide, 20 mM EDTA) and stored at 0 °C.

Preparation of E49C-OP from E49C. A solution containing E49C (76.7 μM, 3.83 nmol) and fresh DTT (1.3 mM, 65.0 nmol) in TRP buffer (50.0 μL (100 mM Tris, pH = 7.5, 200 mM KCl, 1.0 mM DTT, 6.0 mM $MgCl_2$) was incubated at 4 °C for 2 h. The solution was then dialyzed with autoclaved TRP buffer (1.0 L) at 4 °C for 12 h. Fresh buffer was added after 2 h. The solution was then transferred to an eppendorf tube followed by a H_2O wash (1 x 50 μL) and a solution containing 28.0 mM **23** (2.08 μL, 58.2 nmol) in DMF was added. The resulting solution was incubated at 4 °C for 12 h and purified using an Amicon YM-10 Microcon centrifugal filter device with 9/1 H_2O/DMF pretreated in the following manner: The filter device was incubated at rt for 12 h with fat free powdered milk (500 μL, 10% wt./vol), rinsed with H_2O (3 x 500 μL), and spun at 12,000 rpm for 30 min at 4 °C to leave 20 – 30 μL in the filter device (deadstop) with H_2O (500 μL). The protein was dried *in vacuo* and resuspended in TRP buffer (50.0 μL) and the concentration was determined with the Bradford assay using BSA as the standard.[140]

Footprinting of E49C-OP with Fe·MPE. A solution containing *L*-tryptophan (12.5 mM, 100 nmol), **57** (122.5 nM, 0.98 pmol), and E49C-OP (6.25 μM, 50 pmol) dissolved in TN buffer (8.0 μL, 12.5 mM Tris, pH = 8.0; 62.5 mM NaCl) was incubated at rt for 5 min. To this solution was added a solution containing 100 μM MPE/200 μM $Fe(NH_4)_2SO_4$ (1.0 μL, 0.10 nmols MPE, 0.20 nmols $Fe(NH_4)_2SO_4$) and the resulting mixture was incubated at rt for 30 min. To the solution was then added 40 mM dithiothreitol (1.0 μL, 40.0 nmol). The solution was then incubated at 37 °C for 15 min and quenched by freezing at –78 °C. The solvent was then removed in vacuo and the remaining residue was resuspended in formamide loading buffer (10.0 μL) and analyzed by denaturing PAGE.

Preparation of 64b. A solution containing **64a** (238 μM, 3.57 nmol), NaCl (100 mM), and sodium phosphate (10 mM) in H_2O (15.0 μL) was photolyzed in a pyrex vessel in a Rayonet Photoreactor with 16 lamps at λ_{max} = 350 nm for 1.5 h. The photolysate was then desalted using G-25 sephadex (H_2O) and stored at –20 °C.

Measurement of Reaction Kinetics Between E49C-OP and 64b. A solution containing E49C-OP (6.25 μM, 31.2 pmol), $CuSO_4$ (14.5 μM, 72.5 pmol), and TRP buffer (2.25 μL (100 mM Tris, pH = 7.5, 200 mM KCl, 1.0 mM DTT, 6.0 mM $MgCl_2$) in H_2O (2.75 μL) was incubated at rt for 10 min. The resulting solution (4.0 μL) was added to a solution containing **64b** (140.0 nM, 0.70 pmol), *L*-tryptophan (20 mM, 0.10 μmol), and potassium phosphate (40.0 mM, pH = 7.0) in H_2O (5.0 μL) and incubated at rt for 5 min. The resulting solution (9.0 μL) was added to a solution containing MPA (58.0 mM,

58.0 nmol) in H_2O (1.0 μL) and incubated at 37 °C for 2.5 h with aliquots (1 x 1.0 μL) taken at 18.75 min intervals and stored at –78 °C. Prior to denaturing PAGE analysis, samples were resuspended in formamide loading buffer (95% formamide, 20 mM EDTA) and stored at 0 °C.

Measurement of Reaction Kinetics Between E49C and 64b. A solution containing E49C (6.25 μM, 31.2 pmol), $CuSO_4$ (14.5 μM, 72.5 pmol), and TRP buffer (2.25 μL) in H_2O (2.75 μL) was incubated at rt for 10 min. The resulting solution (4.0 μL) was added to a solution containing **64b** (140.0 nM, 0.70 pmol), *L*-tryptophan (20 mM, 0.10 μmol), and potassium phosphate (40.0 mM, pH = 7.0) in H_2O (5.0 μL) and incubated at rt for 5 min. The resulting solution (9.0 μL) was added to a solution containing MPA (58.0 mM) in H_2O (1.0 μL) and incubated at 37 °C for 2.5 h with aliquots (1 x 1.0 μL) taken at 18.75 min intervals and stored at –78 °C. Prior to denaturing PAGE analysis, samples were resuspended in formamide loading buffer (95% formamide, 20 mM EDTA) and stored at 0 °C.

Measurement of Reaction Kinetics of 64b in Potassium Phosphate Buffer, pH = 7.0. A solution containing **64b** (140.0 nM, 0.70 pmol), *L*-tryptophan (11.1 mM, 0.10 μmol), $CuSO_4$ (6.44 μM, 58.0 pmol), TRP Buffer (1.80 μL) and potassium phosphate (40.0 mM, pH = 7.0) in H_2O (7.2 μL) and incubated at rt for 5 min. The resulting solution (9.0 μL) was added to a solution containing MPA (58.0 mM, 58.0 nmol) in H_2O (1.0 μL) and incubated at 37 °C for 2.5 h with aliquots (1 x 1.0 μL) taken at 18.75 min intervals and

stored at –78 °C. Prior to denaturing PAGE analysis, samples were resuspended in formamide loading buffer (95% formamide, 20 mM EDTA) and stored at 0 °C.

Measurement of Reaction Kinetics Between E49C-OP and 57. A solution containing E49C-OP (6.25 μM, 62.4 pmol), $CuSO_4$ (14.5 μM, 145.0 pmol), and TRP buffer (2.25 μL) in H_2O (10.0 μL) was incubated at rt for 10 min. The resulting solution (8.0 μL) was added to a solution containing **57** (140.0 nM, 1.40 pmol), *L*-tryptophan (20 mM, 0.20 μmol), and potassium phosphate (40.0 mM, pH = 7.0) in H_2O (10.0 μL) and incubated at rt for 5 min. The resulting solution (18.0 μL) was added to a solution containing MPA (58.0 mM, 116.0 nmol) in H_2O (2.0 μL) and incubated at 37 °C for 2.5 h with aliquots (2 x 1.0 μL) taken at 18.75 min intervals and stored at –78 °C. Half of the aliquots for each time point were incubated with NaOH (0.1 M, 5.0 μL) at 37 °C for 20 min and then adjusted to pH = 7.0 with 1.0 M HCl. Prior to denaturing PAGE analysis, samples were resuspended in formamide loading buffer (95% formamide, 20 mM EDTA) and stored at 0 °C.

5 References.

[1] von Sonntag, C. *The Chemical Basis of Radiation Biology*; Taylor & Francis: London, 1987.

[2] Burrows, C.; Muller, J. G. "Oxidative Nucleobase Modifications Leading to Strand Scission." *Chem. Rev.* **1998**, *98*, 1109-1151.

[3] Pogozelski, W. K.; Tullius, T. D. "Oxidative Strand Scission of Nucleic Acids: Routes Initiated by Hydrogen Abstraction from the Sugar Moiety." *Chem. Rev.* **1998**, *98*, 1089-1107.

[4] Greenberg, M. M. "Investigating Nucleic Acid Damage Processes via Independent Generation of Reactive Intermediates." *Chem. Res. Toxicol.* **1998**, *11*, 1235-1248.

[5] Kuwabara, M. "Chemical Processes Induced by ·OH Attack on Nucleic-Acids" *Radiat. Phys. Chem.* **1991**, *37*, 691-704.

[6] Steenken, S. "Purine-Bases, Nucleosides, and Nucleotides – Aqueous-Solution Redox Chemistry and Transformation Reactions of Their Radical Cations and E- and OH Adducts." *Chem. Rev.* **1989**, *89*, 503-520.

[7] Pouget, J.-P.; Douki, T.; Richard, M.-J.; Cadet, J. "DNA Damage Induced in Cells by γ and UVA Radiation As Measured by HPLC/GC-MS and HPLC-EC and Comet Assay." *Chem Res. Toxicol.* **2000**, *13*, 541-549.

[8] Shibutani, S.; Takeshita, M.; Grollman, A. P. "Insertion of Specific Bases During DNA Synthesis Past the Oxidation-Damaged Base 8-oxodG." *Nature* **1991**, *349*, 431-434.

[9] Delaney, M. O.; Wiederholt, C. J.; Greenberg, M. M. "Fapy·dA Induces Nucleotide Misincorporation Translesionally by a DNA Polymerase." *Angew. Chem. Int. Ed.* **2002**, *41*, 771-773.

[10] Karam, L. R.; Dizdaroglu, M.; Simic, M. G. "Intramolecular H atom Abstraction from the Sugar Moiety by Thymine Radicals in Oligo- and Polydeoxynucleotides." *Radiat. Res.* **1988**, *116*, 210-216.

[11] Barvian, M. R.; Greenberg, M. M. "Independent Generation of 5,6-Dihydrothymid-5-yl and Investigation of its Ability to Effect Nucleic Acid Strand Scission via Hydrogen Atom Abstraction." *J. Org. Chem.* **1995**, *60*, 1916-1917.

[12] Greenberg, M. M.; Barvian, M. R.; Cook, G. P.; Goodman, B. K.; Matray, T. J.; Tronche, C.; Venkatesan, H. "DNA Damage Induced via 5,6-dihydrothymid-5-yl in Single-Stranded Oligonucleotides." *J. Am. Chem. Soc.* **1997**, *119*, 1828-1839.

[13] Breen, A. P.; Murphy, J. A. "Reactions of Oxyl Radicals with DNA." *Free Rad. Biol. Med.* **1995**, *18*, 1033-1077.

[14] Miaskiewicz, K.; Osman, R. "Theoretical Study on the Deoxyribose Radicals formed by Hydrogen Abstraction." *J. Am. Chem. Soc.* **1994**, *116*, 232-238.

[15] Colson, A. O.; Sevilla, M. D. "Elucidation of Primary Radiation-Damage in DNA Through Application of Ab-Initio Molecular-Orbital Theory." *Int. J. Radiat. Biol.* **1995**, *67*, 627-645.

[16] Frank, B. L.; Worth, L., Jr.; Christner, D. F.; Kozarich, J. W.; Stubbe, J.; Kappen, L. S.; Goldberg, I. H. "Isotope Effects on the Sequence-Specific Cleavage of DNA by Neocarzinostatin – Kinetic Partitioning Between 4'-Hydrogen and 5'-Hydrogen Abstraction at Unique Thymidine Sites." *J. Am. Chem. Soc.* **1991**, *113*, 2271-2275.

[17] Tallman, K. A.; Tronche, C.; Yoo, D. J.; Greenberg, M. M. "Release of Superoxide from Nucleoside Peroxyl Radicals, a Double-Edged Sword?" *J. Am. Chem. Soc.* **1998**, *120*, 4903-4909.

[18] Chatgilialoglu, C.; Ferreri, C.; Bazzanini, R.; Guerra, M.; Choi, S.-Y.; Emanuel, C.; Horner, J. H.; Newcomb, M. "Models of DNA C1' Radicals. Structural, Spectral, and Chemical Properties of the Thyminylmethyl Radical and the 2'-Deoxyuridin-1'-yl Radical." *J. Am. Chem. Soc.* **2000**, *122*, 9525-9533.

[19] Neyhart, G. A.; Cheng, C.-C.; Thorp, H. H. "Kinetics and Mechanism of the Oxidation of Sugars and Nucleotites by Oxoruthenium(IV): Model Studies for Predicting Cleavage Patterns in Polymeric DNA and RNA." *J. Am. Chem. Soc.* **1995**, *117*, 1463-1471.

[20] Cheng, C.-C.; Goll, J. G.; Neyhart, G. A.; Welch, T. W.; Singh, P.; Thorp, H. H. "Relative Rates and Potentials of Competing Redox Processes during DNA Cleavage: Oxidation Mechanisms and Sequence-Specific Catalysis of the Self-Inactivation of Oxometal Oxidants by DNA." *J. Am. Chem. Soc.* **1995**, *117*, 2970-2980.

[21] Sitlani, A.; Long, E. C.; Pyle, A. M.; Barton, J. K. "DNA Photocleavage by Phenanthrenequinone Diimine Complexes of Rhodium(III) – Shape-Selective Recognition and Reaction." *J. Am. Chem. Soc.* **1992**, *114*, 2302-2312.

[22] Worth, L., Jr.; Frank, B. L.; Christner, D. F.; Absalon, M. J.; Stubbe, J.; Kozarich, J. W. "Isotope Effects on the Cleavage of DNA by Bleomycin – Mechanism and Modulation." *Biochemistry* **1993**, *32*, 2601-2609.

[23] McGall, G. H.; Rabow, L. E.; Ashley, G. W.; Wu, S. H.; Kozarich, J. W.; Stubbe, J. "New Insight into the Mechanism of Base Propenal Formation during Bleomycin-Mediated DNA Degradation." *J. Am. Chem. Soc.* **1992**, *114*, 4958-4967.

[24] Sreedhara, A.; Cowan, J. A. "Efficient Catalytic Cleavage of DNA Mediated by Metalloaminoglycosides." *J. Chem. Soc., Chem. Commun.* **1998**, 1737-1738.

[25] Patwardhan, A.; Cowan, J. A. "Highly Specific Oxidative Damage of Double-Strand DNA by Copper Aminoglycosides." *J. Chem. Soc., Chem. Commun.* **2001**, 1490-1491.

[26] Sigman, D. S.; Landgraf, R.; Perrin, D. M.; Pearson, L. "Nucleic Acid Chemistry of the Cuprous Complexes of 1,10-Phenanthroline and Derivatives." *Met. Ions Biol. Syst.* **1996**, *33*, 485-513.

[27] Kappen, L. S.; Goldberg, I. H.; Wu. S. H.; Stubbe, J. A.; Worth, L.; Kozarich, J. W. "Isotope Effects on the Sequence-Specific Cleavage of dC in d(AGC) Sequences by Neocarzinostatin – Elucidation of Chemistry of Minor Lesions." *J. Am. Chem. Soc.* **1990**, *112*, 2797-2798.

[28] Hwang, J.-T.; Tallman, K. A.; Greenberg, M. M. "The Reactivity of the 2'-Deoxyribonolactone lesion in Single-Stranded DNA and its Implication in Reaction Mechanisms of DNA Damage and Repair." *Nucleic Acids Res.* **1999**, *27*, 3805-3810.

[29] Hashimoto, M.; Greenberg, M. M.; Kow, Y. W.; Hwang, J.-T.; Cunningham, R. P. "The 2-Deoxyribonolactone Lesion Produced in DNA by Neocarzinostatin and Other Damaging Agents Forms Cross-links with the Base-Excision Repair Enzyme Endonuclease III." *J. Am. Chem. Soc.* **2001**, *123*, 3161-3162.

[30] DeMott, M. S.; Beyret, E.; Wong, D.; Bales, B. C.; Hwang, J.-T.; Greenberg, M. M.; Demple, B. "Covalent Trapping of Human DNA Polymerase β by the Oxidative DNA Lesion 2-Deoxyribonolactone." *J. Biol. Chem.* **2002**, *277*, 7637-7640.

[31] Meijler, M. M.; Zelenko, O.; Sigman, D. S. "Chemical Mechanism of DNA Scission by (1,10-Phenanthroline)copper. Carbonyl Oxygen of 5-Methylenefuranone is Derived from Water." *J. Am. Chem. Soc.* **1997**, *119*, 1135-1136.

[32] Zelenko, O.; Gallagher, J.; Sigman, D. "Scission of DNA with Bis(1,10-phenanthroline)copper without Intramolecular Hydrogen Migration" *Angew. Chem. Int. Ed. Engl.* **1997**, *36*, 2776-2778.

[33] Chen, T.; Greenberg, M. M. "Model Studies Indicate That Copper Phenanthroline Induces Direct Strand Breaks via β-Elimination of the 2'-Deoxyribonolactone Intermediate Observed in Enediyne Mediated DNA Damage." *J. Am. Chem. Soc.* **1998**, *120*, 3815-3816.

[34] Oyoshi, T.; Sugiyama, H. "Mechanism of DNA Strand Scission Induced by (1,10-Phenanthroline)copper Complex: Major Direct DNA Cleavage Is Not through 1',2'-Dehydronucleotide Intermediate nor β-Elimination of Forming Ribonolactone." *J. Am. Chem. Soc.* **2000**, *122*, 6313-6314.

[35] Sigman, D. S.; Mazumder, A.; Perrin, D. M. "Chemical Nucleases." *Chem. Rev.* **1993**, *93*, 2295-2316.

[36] Sigman, D. S. "Nuclease Activity of 1,10-Phenanthroline-Copper Ion." *Acc. Chem. Res.* **1986**, *19*, 180-186.

[37] Sigman, D. S.; Graham, D. R.; D'Aurora, V.; Stern, A. M. "Oxygen-dependent Cleavage of DNA by the 1,10-Phenanthroline·Cuprous Complex." *J. Biol. Chem.* **1979**, *254*, 12269-12272.

[38] D'Aurora V.; Stern, A. M.; Sigman, D. S. "Inhibition of *Escherichia-coli* DNA-Polymerase-I by 1,10-Phenanthroline." *Biochem. Biophys. Res. Commun.* **1977**, *78*, 170-176.

[39] Veal, J. M.; Merchant, K.; Rill, R. L. "The Influence of Reducing Agent and 1,10-Phenanthroline Concentration on DNA Cleavage by Phenanthroline + Copper." *Nucleic Acids Res.* **1991**, *19*, 3383-3388.

[40] Marshall, L. E.; Graham, D. R.; Reich, K. A.; Sigman, D. S. "Cleavage of Deoxyribonucleic Acid by the 1,10-Phenanthroline-Cuprous Complex. Hydrogen Peroxide Requirement and Primary and Secondary Structure Specificity." *Biochemistry* **1981**, *20*, 244-250.

[41] Graham, D. R.; Marshall, L. E.; Reich, K. A.; Sigman, D. S. "Cleavage of DNA by Coordination Complexes. Superoxide Formation in the Oxidation of 1,10-Phenanthroline-Cuprous Complexes by Oxygen-Relevance to DNA-Cleavage Reaction." *J. Am. Chem. Soc.* **1980**, *102*, 5419-5421.

[42] Valentine, J. S.; Curtis, A. B. "A Convenient Preparation of Solutions of Superoxide Anion and the Reaction of Superoxide Anion with a Copper(II) Complex." *J. Am. Chem. Soc.* **1975**, *97*, 224-226.

[43] Kuwabara, M.; Yoon, C.; Goyne, T.; Thederahn, T.; Sigman, D. S. "Nuclease Activity of 1,10-Phenanthroline Copper-Ion-Reaction with CGCGAATTCGCG and its Complexes with Netripsin and Eco RI." *Biochemistry* **1986**, *25*, 7401-7408.

[44] Giese, B.; Dussy, A.; Meggers, E.; Petretta, M.; Schwitter, U. "Conformation, Lifetime, and Repair of 4'-DNA Radicals." *J. Am. Chem. Soc.* **1997**, *119*, 11130-11131.

[45] Beckwith, A. L.; Crich, D.; Duggan, P.; Yao, Q. "Chemistry of β-(Acyloxy)alkyl and β-(Phosphatoxy)alkyl Radicals and Related Species: Radical and Radical Ionic Migrations and Fragmentations of Carbon-Oxygen Bonds." *Chem. Rev.* **1997**, *97*, 3273-3312.

[46] Giese, B. "Long-Distance Charge Transport in DNA: The Hopping Mechanism." *Acc. Chem. Res.* **2000**, *33*, 631-636.

[47] Meggers, E.; Dussy, A.; Thomas, Schäfer, T.; Giese, B. "Electron Transfer in DNA from Guanine and 8-Oxoguanine to a Radical Cation of the Carbohydrate Backbone." *Chem. Eur. J.* **2000**, *6*, 485-492.

[48] Dussy, A.; Meggers, E.; Giese, B. "Spontaneous Cleavage of 4'-DNA Radicals under Aerobic Conditions: Apparent Discrepancy between Trapping Rates and Cleavage Products." *J. Am. Chem. Soc.* **1998**, *120*, 7399-7403.

[49] Goodman, B. K.; Greenberg, M. M. "Independent Generation and Reactivity of 2'-Deoxyrid-1'-yl." *J. Org. Chem.* **1996**, *61*, 2-3.

[50] Tronche, C.; Goodman, B. K.; Greenberg, M. M. "DNA Damage Induced via Independent Generation of the Radical Resulting from Formal Hydrogen Atom Abstraction from the C1'-Position of a Nucleotide." *Chem. Biol.* **1998**, *5*, 263-271.

[51] Sugiyama, H.; Fujimoto, K.; Saito, I. "Stereospecific 1,2-Hydride Shift in Ribonolactone Formation in the Photoreaction of 2'-Iododeoxyuridine." *J. Am. Chem. Soc.* **1995**, *117*, 2945-2946.

[52] Lhomme, J.; Constant, J.-F.; Demeunynck, M. "Abasic DNA Structure, Reactivity, and Recognition." *Biopolymers* **1999**, *52*, 65-83.

[53] Sigman, D. S.; Kuwabara, M. D.; Chen, C.-h. B.; Bruice, T. W. "Nuclease Activity of 1,10-Phenanthroline-Copper in Study of Protein-DNA Interactions." *Methods Enzymol.* **1991**, *208*, 414-433.

[54] Veal, J. M.; Rill, R. L. "Sequence Specificity of DNA Cleavage by bis(1,10-Phenantroline)Copper(I)." *Biochemistry* **1988**, *27*, 1822-1827.

[55] Hennighausen, L.; Lubon, H. "Interactions of Proteins with DNA *In Vitro*." *Methods Enzymol.* **1987**, *152*, 721-735.

[56] Jackson, P. D.; Felsenfeld, G. "*In Vivo* Footprinting of Specific Protein – DNA Interactions." *Methods Enzymol.* **1987**, *152*, 735-755.

[57] Hertzberg, R. P.; Dervan, P. B. "Cleavage of Double Helical DNA by (Methidiumpropyl-EDTA)Iron(II)." *J. Am. Chem. Soc.* **1982**, *104*, 313-315.

[58] Pogozelski, W. K.; McNeese, T. J.; Tullius, T. D. "What Species is Responsible for Strand Scission in the Reaction of $[Fe(II)EDTA]^{2-}$ and H_2O_2 with DNA." *J. Am. Chem. Soc.* **1995**, *117*, 6428-6433.

[59] Walling, C. "Fenton's Reagent Revisited." *Acc. Chem. Res.* **1975**, *8*, 125-131.

[60] Trauger, J. W.; Dervan, P. B. "Footprinting Methods for Analysis of Pyrrole-Imidazole Polyamide/DNA Complexes." *Methods Enzymol.* **2001**, *340*, 450-466.

[61] Pope, L. E.; Sigman, D. S.; "Secondary Structure Specificity of the Nuclease Activity of the 1,10-Phenanthroline-Copper Complex." *Proc. Natl. Aca. Sci. U.S.A.* **1984**, *176*, 3-7.

[62] Drew, H. R. "Structural Specificities of Five Commonly Used DNA Nucleases." *J. Mol. Biol.* **1984**, *176*, 535-557.

[63] Blackburn, G. M.; Gait, M. J. *Nucleic Acids in Chemistry and Biology*, 2nd Ed.; Oxford University Press: New York, 1996; pp 28-39.

[64] Sigman, D. S.; Spassky, A.; Rimsky, S.; Buc, H. "Conformational Analysis of Lac Promoters Using the Nuclease Activity of 1,10-Phenanthroline-Copper Ion." *Biopolymers* **1985**, *24*, 183-197.

[65] Murakawa, G. J.; Chen, C.-h. B.; Kuwabara, M. D.; Nierlich, D., Sigman, D. S. "Scission of RNA by the Chemical Nuclease of 1,10-Phenanthroline-Copper Ion – Preference for Single-Stranded Loops." *Nucl. Acids Res.* **1989**, *17*, 5361-5375.

[66] Mazumder, A.; Chen, C.-h. B.; Gaynor, R. B.; Sigman, D. S. "1,10-Phenanthroline-Copper, a Footprinting Reagent for Single-Stranded Regions of RNAs" *Biochem. Biophys.Res.Commun.* **1992**, *187*, 1503-1509.

[67] Pearson, L.; Chen, C.-h. B.; Gaynor, R. B.; Sigman, D. S. "Footprinting RNA – Protein Complexes Following Gel Retardation Assays – Application to the R-L7-Procoat – RNA and TAT – TAR Interactions." *Nucl. Acids Res.* **1994**, *22*, 2255-2263.

[68] Alberts, B.; Bray, D.; Lewis, J.; Raff, M.; Roberts, K.; Watson, J. D. *Molecular Biology of The Cell*, 3rd ed.; Garland Publishing: New York, 1994; p 268.

[69] Guo, Q.; Lu, M.; Seeman, N. C.; Kallenbach, N. R. "Drug-Binding by Branched DNA-Molecules – Analysis by Chemical Footprinting of Intercalation into an Immobile Junction." *Biochemistry* **1990**, *29*, 570-578.

[70] Spassky, A.; Sigman, D. S. "Nuclease Activity of 1,10-Phenanthroline Copper-Ion – Conformational-Analysis and Footprinting of the lac Operon." *Biochemistry* **1985**, *24*, 8050-8056.

[71] Spassky, A. "Passage of RNA-Polymerase From Open Complex to Elongation Mode at the *Escherichia-coli* lacUV5 Promoter – Nucleolytic Hypersensitivy as a Probe for Complex Conformational-Changes." *Biochemistry* **1992**, *31*, 10502-10509.

[72] Frantz, B.; O'Halloran, T. V. "DNA Distortion Accompanies Transcriptional Activation by the Metal-Responsive Gene-Regulatory Protein MERR." *Biochemistry* **1990**, *29*, 4747-4751.

[73] Buratowski, S.; Sopta, M.; Greenblatt, J.; Sharp, P. A. "RNA Polymerase-II-Associated Proteins are Required for a DNA Conformation Change in the Transciption Initiation Complex." *Proc. Natl. Acad. Sci. U.S.A.* **1991**, *88*, 7509-7513.

[74] Kuwabara, M. D.; Sigman, D. S. "Footprinting DNA Protein Complexes *In Situ* Following Gel Retardation Assays Using 1,10-Phenanthroline-Copper Ion – *Escherichia-coli* RNA Polymerase-Lac Promoter Complexes." *Biochemistry* **1987**, *26*, 7234-7238.

[75] Chen, C.-h. B.; Sigman, D. S. "Chemical Conversion of a DNA-Binding Protein into a Site-Specific Nuclease." *Science* **1987**, *237*, 1197-1201.

[76] Ebright, R. H.; Ebright, Y.W.; Pendergrast, P. S.; Gunasekera, A. "Conversion of a Helix-Turn-Helix Motif Sequence-Specific DNA-Binding Protein Into a Site-Specific DNA Cleavage Agent." *Proc. Natl. Acad. Sci. U.S.A.* **1990**, *87*, 2882-2886.

[77] Bruice, T. W.; Wise, J. G.; Sigman, D. S. "Engineering of a Semisynthetic Endonuclease Based on the λ-phage Cro Protein and Nuclease Activity of 1,10-Phenanthroline-Copper." *Biochemistry*, **1990**, *29*, 2185-2186.

[78] Sutton, C. L.; Mazumder, A.; Chen, C.-h. B.; Sigman, D. S. "Transforming the *Escherichia coli* Trp Repressor into a Site-Specific Nuclease." *Biochemistry* **1993**, *32*, 4225-4230.

[79] Otwinowski, Z.; Schevitz, R. W.; Zhang, R.-G.; Lawson, C. L.; Joachimiak, A.; Marmorstein, R. Q.; Luisi, B. F.; Sigler, P. B. "Crystal Structure of *Trp* Repressor/Operator Complex at Atomic Resolution." *Nature* **1988**, *335*, 321-329.

[80] Staacke, D.; Walter, B.; Kisters-Woike, B.; Wilcken-Bergmann, B. V.; Muller-Hill, B. "How Trp Repressor Binds to its Operator." *EMBO* **1990**, *9*, 1963-1967.

[81] Bailly, C.; Chaires, C. B. "Sequence Specific DNA Minor Groove Binders. Design and Synthesis of Netropsin and Distamycin Analogues." *Bioconjugate Chem.* **1998**, *9*, 513-538.

[82] Pitié, M.; Van Horn, J. D.; Brion, D.; Burrows, C. J.; Meunier, B. "Targeting the DNA Cleavage Activity of Copper Phenanthroline and Clip-Phen to A·T Tracts via Linkage to a Poly-*N*-methylpyrrole." *Bioconjugate Chem.* **2000**, *11*, 892-900.

[83] Pitié, M.; Burrows, C. J.; Meunier, B. "Mechanisms of DNA Cleavage by Copper Complexes of 3-Clip-Phen and of its Conjugate with a Distamycin Analogue." *Nucleic Acids Res.* **2000**, *24*, 4856-4864.

[84] Pitié, M.; Donnadiew, B.; Meunier, B. "Preparation of the New bis(Phenanthroline)ligand "Clip-Phen" and Evalution of the Nuclease Activity of the Corresponding Copper Complex." *Inorg. Chem.* **1998**, *37*, 3486-3489.

[85] Pitié, M.; Sudres, B.; Meunier, B. "Dramatic Increase of the DNA Cleavage Activity of Cu(Clip-Phen) by fixing the Bridging Linker on the C^3 Position of the Phenanthroline Units." *J. Chem. Soc. Chem. Commun* **1998**, 2597-2598.

[86] Dervan, P. B "Design of Sequence-Specific DNA-Binding Molecules." *Science* **1986**, *232*, 464-471.

[87] Dervan, P. B. "Molecular Recognition of DNA by Small Molecules." *Bioorg. Med. Chem.* **2001**, *9*, 2215-2235.

[88] Sluka, J. P.; Horvath, S. J.; Bruist, M. F.; Simon, M. I.; Dervan, P. B. "Synthesis of a Sequence-Specific DNA-Cleaving Peptide." *Science* **1987**, *238*, 1129-1132.

[89] Goyne, T. E.; Sigman, D. S. "Nuclease Activity of 1,10-Phenanthroline-Copper Ion. Chemistry of Deoxyribose Oxidation." *J. Am. Chem. Soc.* **1987**, *109*, 2846-2848.

[90] Goldstein, S.; Czapski, G. "Mechanisms of the Dismutation of Superoxide Catalyzed by the Copper(II) Phenanthroline Complex and of the Oxidation of the Copper(I) Phenanthroline Complex by Oxygen in Aqueous Solution." *J. Am. Chem. Soc.* **1983**, *105*, 7276-7280.

[91] Haraguchi, K.; Tanaka, H.; Maeda, H.; Itoh, Y.; Saito, S.; Miyasaka, T. "Selenoxide Elimination for the Synthesis of Unsaturated-Sugar Uracil Nucleosides." *J. Org. Chem.* **1991**, *56*, 5401-5408.

[92] Robins, M. J.; Trip, E. M. "Nucleic Acid Related Compounds. 1-(2-Deoxy-D-Erythro-Pent-1-enofuranosyl)uracil. Synthesis of the First 1',2'-Unsaturated Pyrimidine Nucleoside, a Furanoid N,O-Ketene Acetal." *Tetrahedron Lett.* **1974**, 3369-3372.

[93] Kresge, A. J.; Leibovitch, M. "Kinetics and Mechanism of the Acid-Catalyzed Hydrolysis of 1,1-dimethoxyethane (Ketene Dimethyl Acetal) and Trimethoxyethene in Aqueous Solution." *J. Am. Chem. Soc.* **1992**, *114*, 3099-3102.

[94] Okuyama, T.; Kawao, S.; Fueno, T. "Mechanism of Acid-Catalyzed Hydrolysis of Phenylketene O,O- and O,S-acetals." *J. Org. Chem.* **1982**, *46*, 4372-4375.

[95] Hollfelder, F.; Kirby, A. J.; Tawfik, D. S. "Efficient Catalysis of Proton Transfer by Synzymes." *J. Am. Chem. Soc.* **1997**, *119*, 9578-9579.

[96] Blackburn, G. M.; Gait, M. J. *Nucleic Acids in Chemistry and Biology*, 2nd Ed.; Oxford University Press: New York, 1996; p 101.

[97] Morrow, J. R.; Trogler, W. C. "Hydrolysis of Phosphate Diesters with Copper(II) Catalysts." *Inorg. Chem.* **1988**, *27*, 337-3394.

[98] Dizdaroglu, M.; Aruoma, O. I.; Halliwell, B. "Modification of Bases in DNA by Copper Ion-1,10-Phenanthroline Complexes." *Biochemistry* **1990**, *29*, 8447-8451.

[99] Pompizi, I.; Häberli, A.; Leumann, C. J. "Oligodeoxynucleotides Containing Conformationally Constrained Abasic Sites: A UV and Fluorescence Spectroscopic Investigation on Duplex Stability and Structure." *Nucleic Acids Res.* **2000**, *28*, 2702-2708.

[100] Kværnø, L.; Kumar, R.; Kahl, B. M.; Olsen, C. E.; Wengel, J. "Synthesis of Abasic Locked Nucleic Acid and Two *seco*-LNA Derivatives and Evaluation of Their Hybridization Properties Compared with Their More Flexible DNA Counterparts." *J. Org.Chem.* **2000**, *65*, 5167-5176.

[101] Gelfand, C. A.; Plum, G. E.; Grollman, A. P.; Johnson, F.; Breslauer, K. J. "Thermodynamic Consequences of an Abasic Lesion in Duplex DNA Are Strongly Dependent on Base Sequence." *Biochemistry* **1998**, *37*, 7321-7327.

[102] Gilbert, B. C.; Silvester, S.; Walton, P. H.; Whitwood, A. C. "DNA damage *via* Intercalation of Copper Complexes and Activation by Ascorbate and Peroxides: Direct EPR Evidence for Hydroxyl Radical Formation and Reaction." *J. Chem. Soc. Perkin Trans. II* **1999**, 1891-1895.

[103] Ozawa, T.; Hanaki, A. "The First ESR Spin-trapping Evidence for the Formation of Hydroxyl Radical from the Reaction of Copper(II) Complex with Hydrogen Peroxide in Aqueous Solution." *J. Chem. Soc. Chem. Commun.* **1991**, 330-332.

[104] Goldstein, S.; Czapski, G. "Mechanisms of the Reactions of Some Copper Complexes in the Presence of DNA with $O_2^{\cdot-}$, H_2O_2, and Molecular Oxygen." *J. Am. Chem. Soc.* **1986**, *108*, 2244-2250.

[105] Goldstein, S.; Czapski, G. "Kinetics of Oxidation of Cuprous Complexes of Substituted Phenanthroline and 2,2'-Bipyridyl by Molecular Oxygen and by Hydrogen Peroxide in Aquesous Solution." *J. Am. Chem. Soc.* **1985**, *24*, 1087-1092.

[106] Yamamoto, K.; Kawanishi, S. "Hydroxyl Free Radical is not the Main Active Species in Site-specific DNA Damage Induced by Copper(II) Ion and Hydrogen Peroxide." *J. Biol. Chem.* **1989**, *264*, 15435-15440.

[107] Johnson, G. R. A.; Nazhat, N. B. "Kinetics and Mechanism of the Reaction of the Bis(1,10-phenanthroline)copper(I) Ion with Hydrogen Peroxide in Aqueous Solution." *J. Am. Chem. Soc.* **1987**, *109*, 1990-1994.

[108] Johnson, G. R. A.; Nazhat, N. B.; Saadalla-Nazhat, R. A. "Reaction of the Aquocopper(I) Ion with Hydrogen Peroxide: Evidence against Hydroxyl Free Radical Formation." *J. Chem. Soc. Chem. Commun.* **1985**, 407-408.

[109] Holyer, R. H.; Hubbard, C. D.; Kettle, S. F. A.; Wilkins, R. G. "The Kinetics of Replacement Reactions of Complexes of the Transition Metals with 1,10-Phenanthroline and 2,2'-Bipyridine." *Inorg. Chem.* **1965**, *4*, 929-935.

[110] Veal, J. M.; Rill, R. L. "Noncovalent DNA Binding of Bis(1,10-phenanthroline)copper(I) and Related Compounds." *Biochemistry* **1991**, *30*, 1132-1140.

[111] Trawick, B. N.; Daniher, A. T.; Bashkin, J. K. "Inorganic Mimics of Ribonucleases and Ribozymes: From Random Cleavage to Sequence-Specific Chemistry to Catalytic Antisense Drugs." *Chem. Rev.* **1998**, *98*, 939-960.

[112] Gajda, T.; Krämer, R.; Jancsó, A. "Structure, Equilibrium, and Ribonuclease Activity of Copper(II) and Zinc(II) Complexes Formed with a Dinucleating Bis-Imidazole Ligand." *Eur. J. Inorg. Chem.* **2000**, 1635-1644.

[113] Jenkins, L. A.; Bashkin, J. K.; Pennock, J. D.; Florián, J.; Warshel, A. "Catalytic Hydrolysis of Adenosine 2',3'-Cyclic Monophosphate by Cu^{II} Terpyridine." *Inorg. Chem.* **1999**, *38*, 3215-3222.

[114] Wall, M.; Linkletter, B.; Williams, D.; Lebuis, A.-M.; Hynes, R. C.; Chin, J. "Rapid Hydrolysis of 2',3'-cAMP with a Cu(II) Complex: Effect of Intramolecular Hydrogen Bonding on the Basicity and Reactivity of a Metal-Bound Hydroxide." *J. Am. Chem. Soc.* **1999**, *121*, 4710-4711.

[115] Collman, J. P.; Hegedus, L. S.; Norton, J. R.; Finke, R. G. *Principles and Applications of Organotransition Metal Chemistry*; University Science: Mill Valley, CA, 1987; p 64.

[116] Douglas, B.; McDaniel, D.; Alexander, J. *Concepts and Models of Inorganic Chemistry*; Wiley & Sons: New York, 1994; pp 393-398.

[117] Linkletter, B.; Chin, J. "Rapid Hydrolysis of RNA with a Cu^{II} Complex." *Angew. Chem. Int. Ed. Engl.* **1995**, *34*, 472-474.

[118] Liu, S.; Hamilton, A. D. "Catalysis of Phosphodiester Transesterification by Cu(II)-terpyridine Complexes with Peripherial Pendent Base Groups: Implications for the Mechanism." *Tetrahedron Lett.* **1997**, *38*, 1107-1110.

[119] Breslauer, K. J. "Extracting Thermodynamic Data from Equilibrium Melting Curves for Oligonucleotide Order-Disorder Transitions." *Methods Enzymol.* **1995**, *259*, 221-242.

[120] Allawi, H. T.; SantaLucia, J. Jr. "Thermodynamics and NMR of Internal G•T Mismatches in DNA." *Biochemistry* **1997**, *36*, 10581-10594.

[121] SantaLucia, J. Jr. "A Unified View of Polymer, Dumbbell, and Oligonucleotide DNA Nearest-Neighbor Thermodynamic." *Proc. Natl. Acad. Sci. U.S.A.* **1998**, *95*, 1460-1465.

[122] Peyret, N.; Seneviratne, A.; Allawi, H. T.; SantaLucia, J. Jr. "Nearest Neighbor Thermodynamics and NMR of DNA Sequences with Internal A·T, C·C, G·G, and T·T Mismatches." *Biochemistry* **1999**, *38*, 3468-3477.

[123] Santalucia, J. Jr. HyTher – Module 1. http://ozone.chem.wayne.edu/Hyther/hytherm1main.html (accessed May 2002).

[124] Caruthers, M. H.; Barone, A. D.; Beaucage, S. L.; Dodds, D. R.; Fisher, E. F.; McBride, L. J.; Matteucci, M.; Stabinsky, Z.; Tang, J. Y. "Chemical Synthesis of Deoxyoligonucleotides by the Phosphoramidite Method." *Methods Enzymol.* **1987**, *154*, 287-313.

[125] Burer, P. N. In *Handbook of Biochemistry and Molecular Biology*, 3rd ed.; Fasman, G. D. Ed.; CRC Press: Cleveland, OH, 1975; vol 2, p 589.

[126] Blackburn, G. M.; Gait, M. J. *Nucleic Acids in Chemistry and Biology*, 2nd Ed.; Oxford University Press: New York, 1996; pp 333-336.

[127] Gut, I. G.; Wood, P. D.; Redmond, R. W. "Interaction of Triplet Photosensitizers with Nucleotides and DNA in Aqueous Solution at Room Temperature." *J. Am. Chem. Soc.* **1996**, *118*, 2366-2373.

[128] Wood, P. D.; Redmond, R. W. "Triplet State Interactions between Nucleic Acid Bases in Solution at Room Temperature: Intermolecular Energy and Electron Transfer." *J. Am. Chem. Soc.* **1996**, *118*, 4256-4263.

[129] Hickerson, R. P.; Chepanoske, C. L.; Williams, S. D.; David, S. S.; Burrows, C. J. "Mechanism-Based DNA-Protein Cross-Linking of MutY via Oxidation of 8-Oxoguanosine." *J. Am. Chem. Soc.* **1999**, *121*, 9901-9902.

[130] Muller, J. G.; Duarte, V.; Hickerson, R. P.; Burrows, C. J. "Gel Electrophoretic Detection of 7,8-Dihydro-8-oxoguanine and 7,8-Dihydro-8-oxoadenine via Oxidation by Ir(IV)." *Nucleic Acids Res.* **1998**, *26*, 2247-2249.

[131] Weston, R. E. Jr.; Schwarz, H. A. *Chemical Kinetics*; Prentice-Hall: New York, 1972; pp 17-20.

[132] Gunsalus, R. P.; Yanofsky, C. "Nucleotide Sequence and Expression of the *Escherichia coli trpR*, the Structural Gene for the *trp* Aporepressor." *Proc. Natl. Acad. Sci. U.S.A.* **1980**, *77*, 7117-7121.

[133] van Dyke, M. W.; Dervan, P. B. "Methidiumpropyl-EDTA·Fe(II) and DNAse (I) Foortprinting Report Different Small Molecule-Binding Site Sizes on DNA." *Nucleic Acids Res.* **1983**, *11*, 5555-5567.

[134] Hertzberg, R. P.; Dervan, P. B. "Cleavage of DNA with Methidiumpropyl-EDTA·Iron(II) – Reaction Conditions and Product Analyses." *Biochemistry* **1984**, *23*, 3934-3945.

[135] Dugas, H. *Bioorganic Chemistry*, 2nd ed.; Springer-Verlag: New York, 1989; p 190.

[136] Lowry, T. H.; Richardson, K. S. *Mechanism and Theory in Organic Chemistry*, 3rd ed.; HarperCollins Publishers: New York, NY, 1987; pp 297-298.

[137] Lowry, T. H.; Richardson, K. S. *Mechanism and Theory in Organic Chemistry*, 3rd ed.; HarperCollins Publishers: New York, NY, 1987; p 253.

[138] Sambrook, J.; Fritsch, E. F.; Maniatis, T. *Molecular Cloning: A Laboratory Manual*, 2nd ed.; Cold Spring Harbor Laboratory Press: New York, 1989.

[139] Iverson, B. L.; Dervan, P. B. "Adenine Specific DNA Chemical Sequencing Reaction." *Nucleic Acids Res.* **1987**, *15*, 7823-7830.

[140] Bradford, M. "A Rapid and Sensitive Method for the Quantitation of Microgram Quantities of Protein Utilizing the Principle of Protein-Dye Binding." *Anal. Biochem.* **1976**, *72*, 248-254.

Appendix A:

Response Factor Plots

Response factor plots

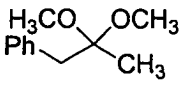

102

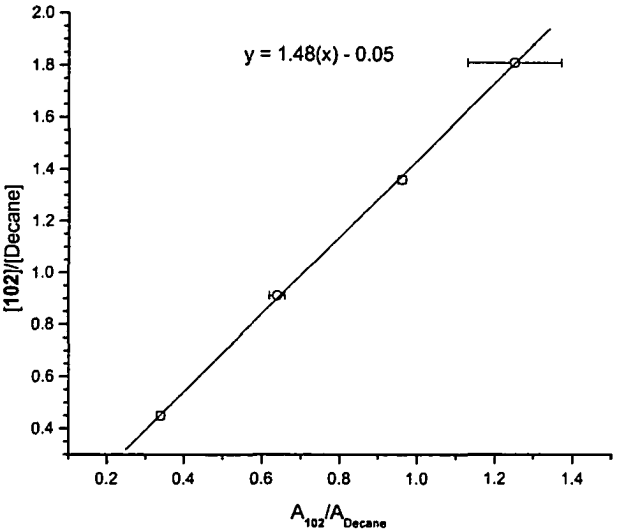

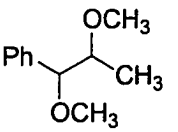

104

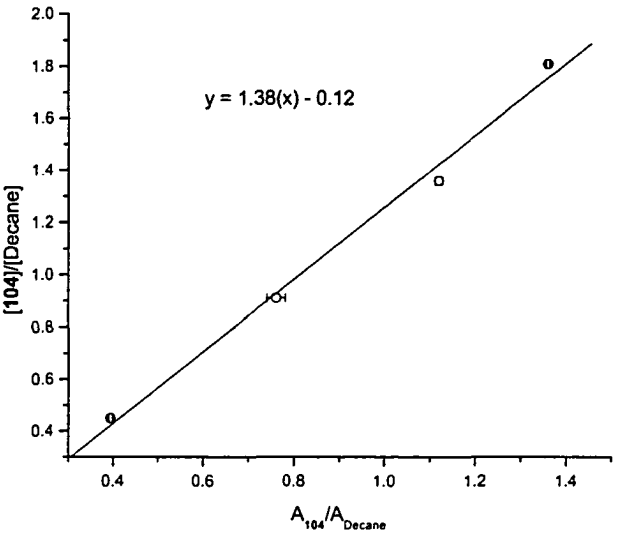

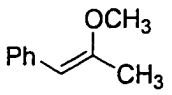

105

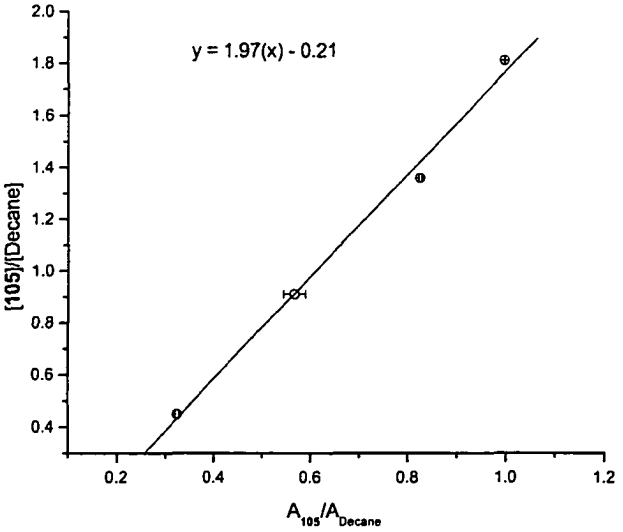

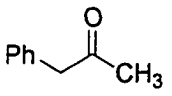

108

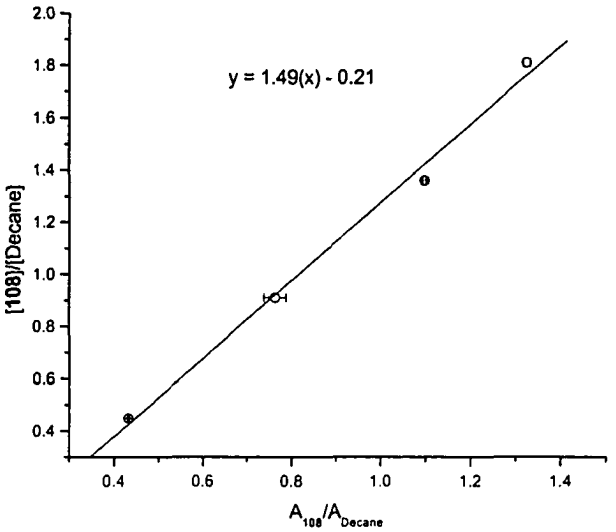

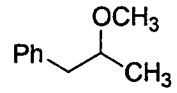

109

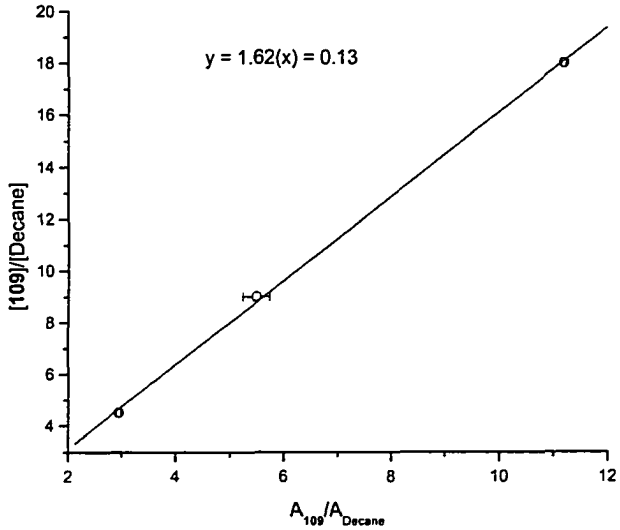

Appendix B:

NMR, IR, and MS Spectra

bcb2189

Solvent: CDCl3
Ambient temperature
File: bcb2189
INOVA-500 "greenberg"

PULSE SEQUENCE
Pulse 30.0 degrees
Acq. time 2.667 sec
Width 6000.0 Hz
16 repetitions
OBSERVE H1, 300.1559448 MHz
DATA PROCESSING
Sq. sine bell 2.667 sec
Shifted by -2.667 sec
FT size 32768
Total time 1 minute

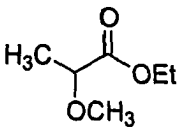

112

13C OBSERVE

BcB2199c13

Pulse Sequence: s2pul

Solvent: CDCl3
Ambient temperature
INOVA-300 "elfin"

PULSE SEQUENCE
Relax. delay 1.000 sec
Pulse 45.0 degrees
Acq. time 0.800 sec
Width 20000.0 Hz
866 repetitions
OBSERVE C13, 75.4645944 MHz
DECOUPLE H1, 300.1190283 MHz
Power 33 dB
continuously on
WALTZ-16 modulated
DATA PROCESSING
Line broadening 1.5 Hz
FT size 32768
Total time 502456 hr, 42 min, 40 sec

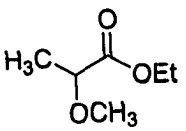

112

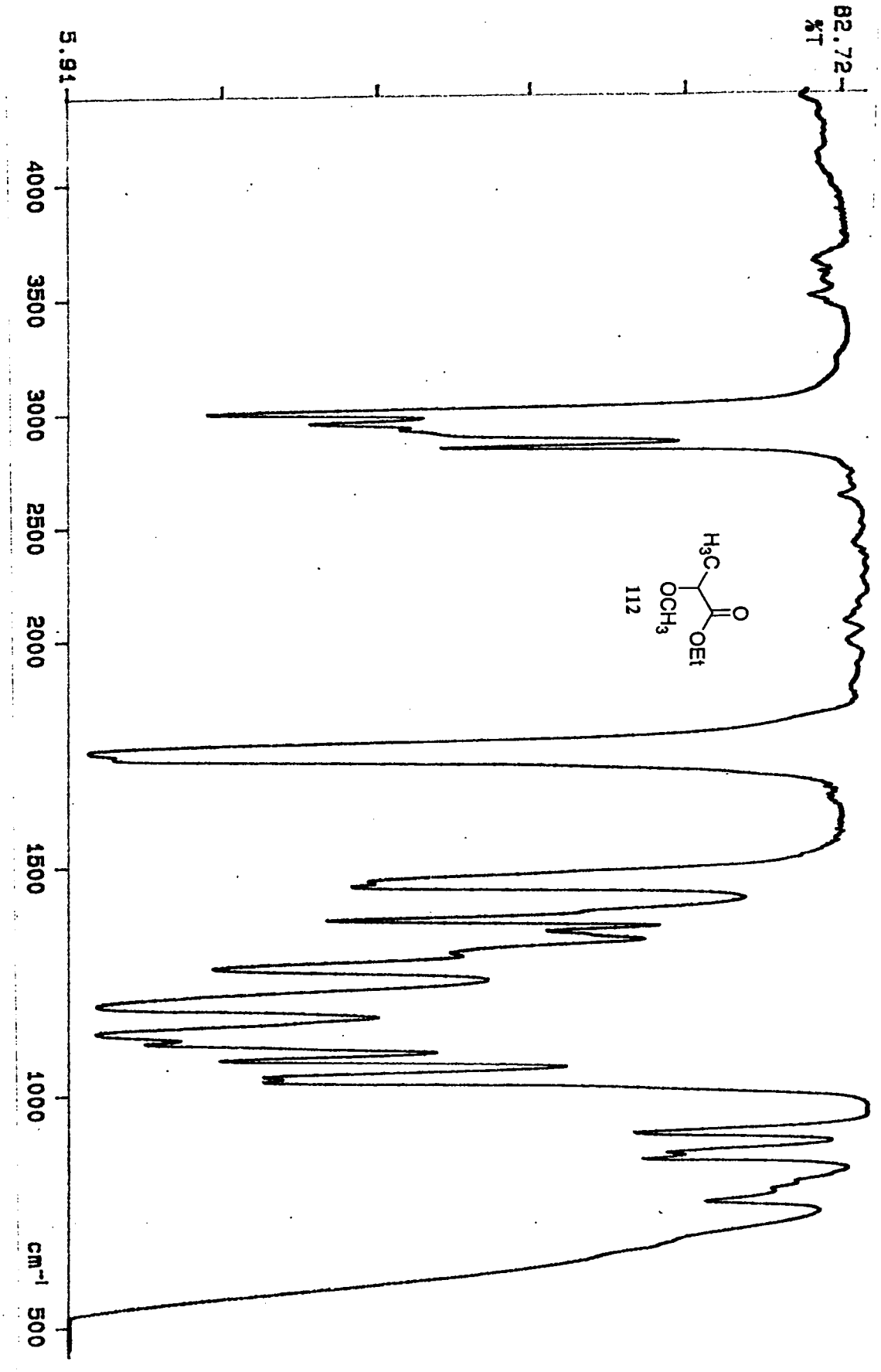

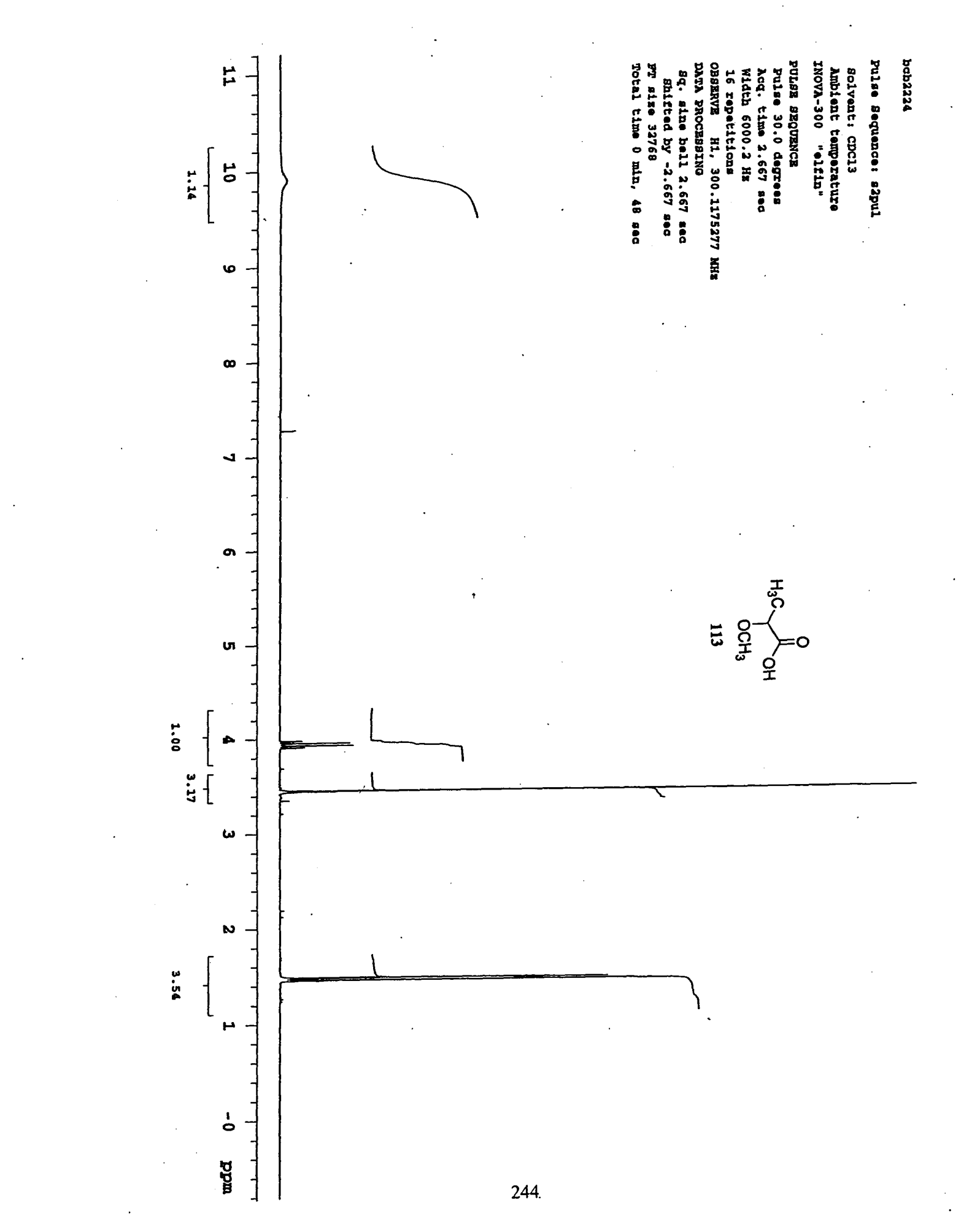

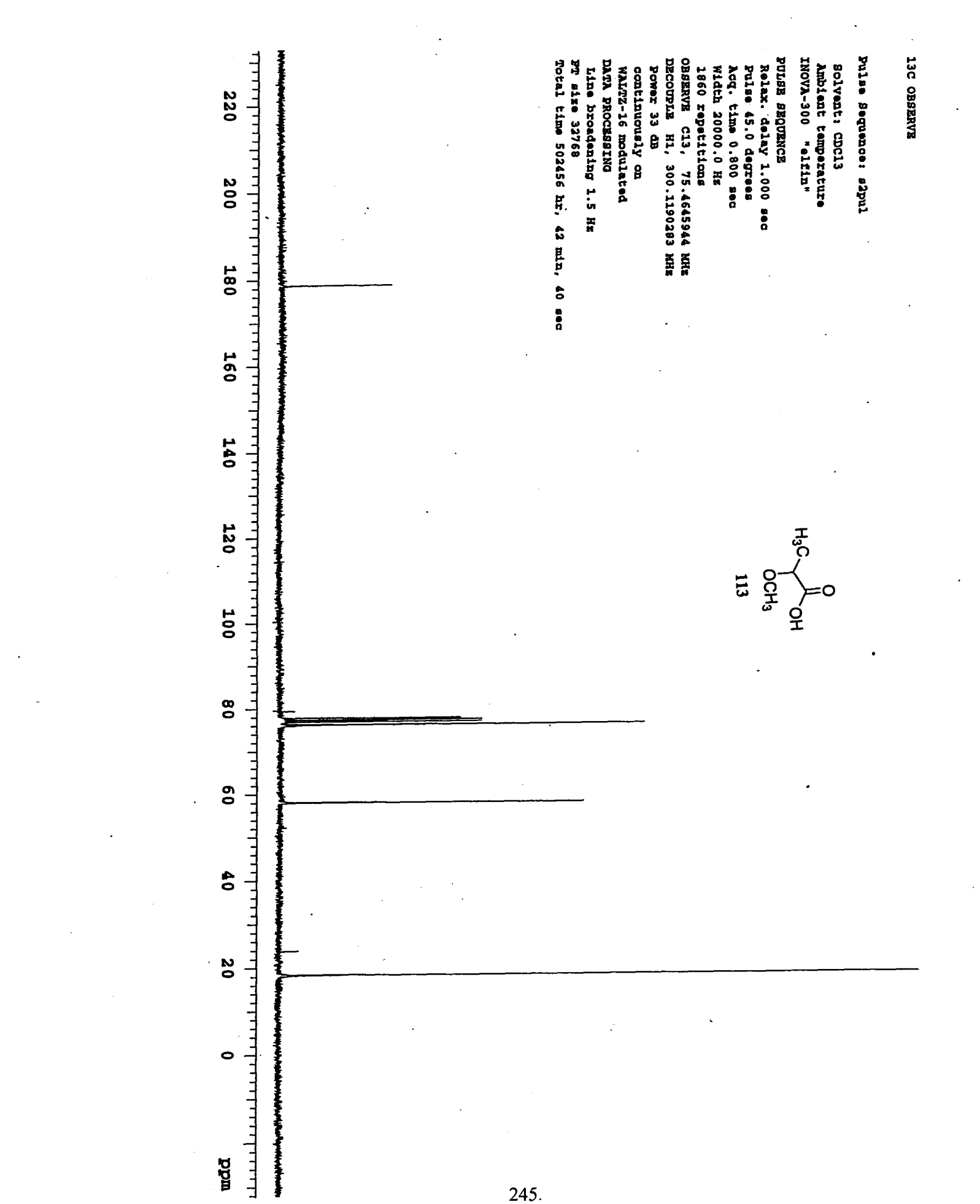

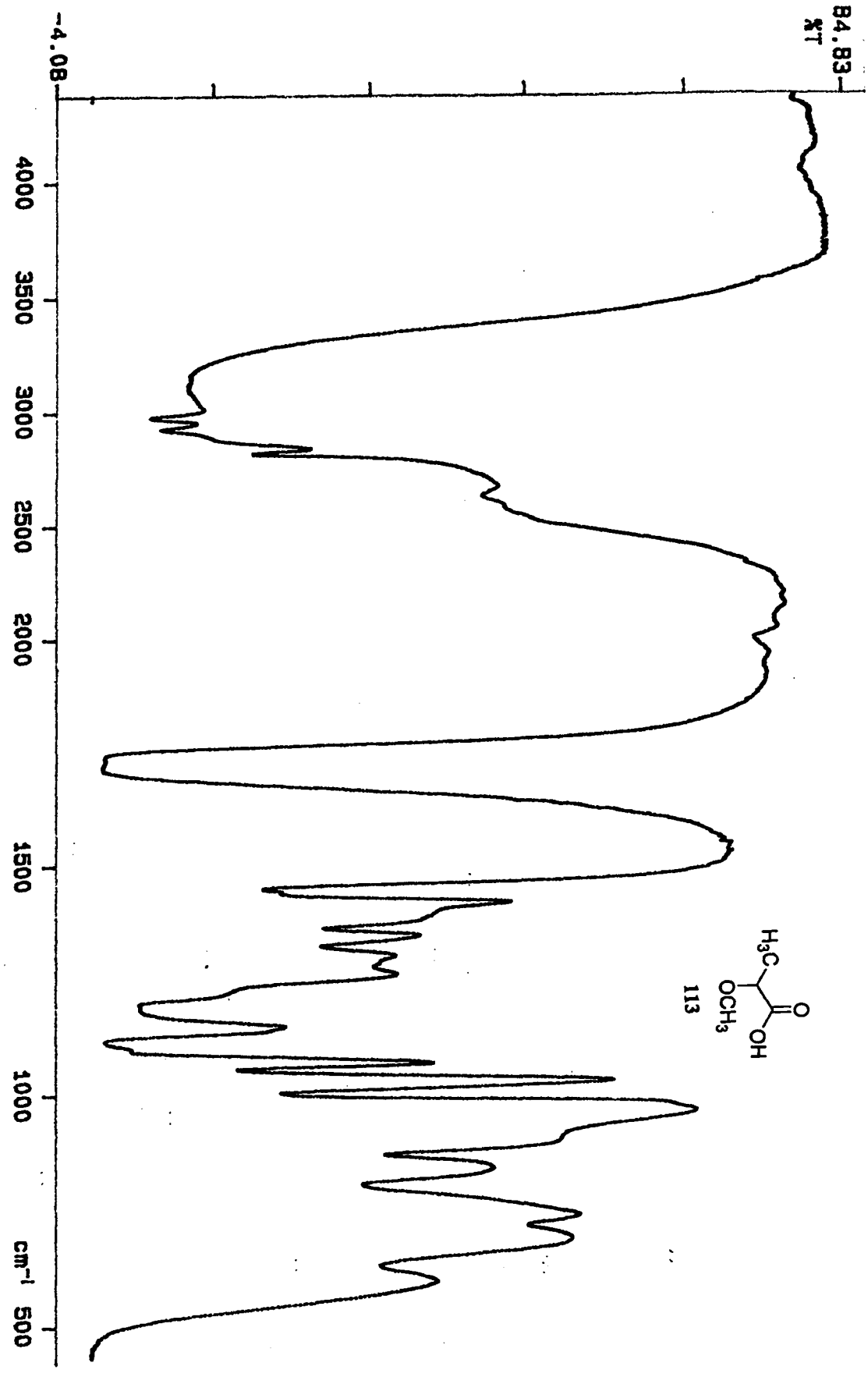

bcb1026

Solvent: CDCl3
Ambient temperature
File: bcb1026
INOVA-500 "greenberg"

PULSE SEQUENCE
Relax. delay 0.000 sec
Pulse 26.0 degrees
Acq. time 2.667 sec
Width 6000.0 Hz
16 repetitions
OBSERVE H1, 300.1559753 MHz
DATA PROCESSING
Gauss apodization 0.896 sec
FT size 32768
Total time 1 minute

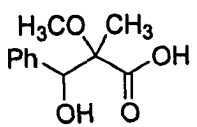

110

bcb1026

Solvent: CDCl3
Ambient temperature
File: bcb1026c13
INOVA-500 "greenberg"

PULSE SEQUENCE
Relax. delay 1.000 sec
Pulse 46.3 degrees
Acq. time 0.696 sec
Width 23000.0 Hz
130 repetitions
OBSERVE C13, 75.4742661 MHz
DECOUPLE H1, 300.1574402 MHz
Power 40 dB
continuously on
WALTZ-16 modulated
DATA PROCESSING
Line broadening 2.0 Hz
FT size 32768
Total time 3 minutes

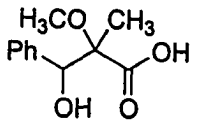

110

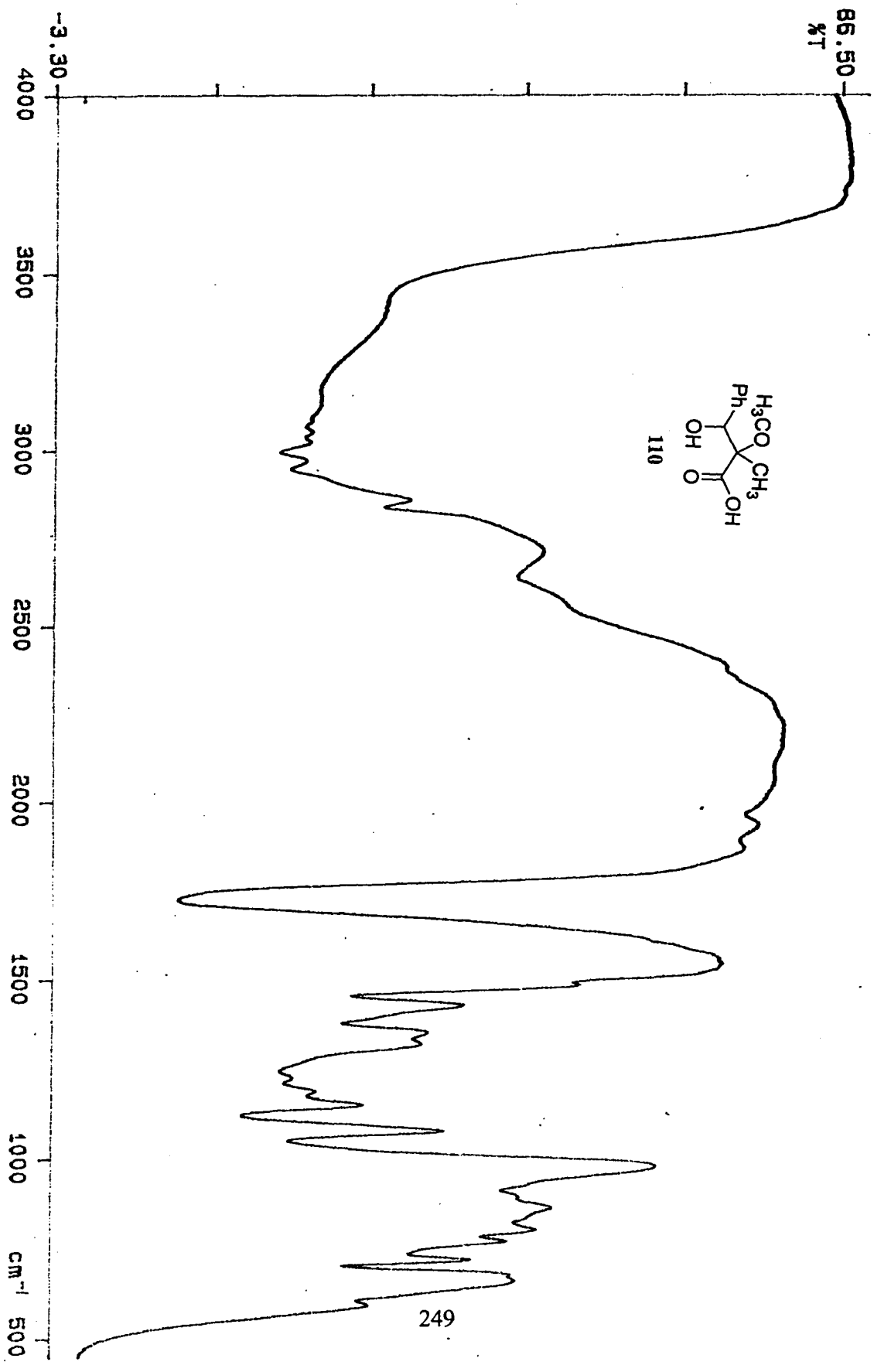

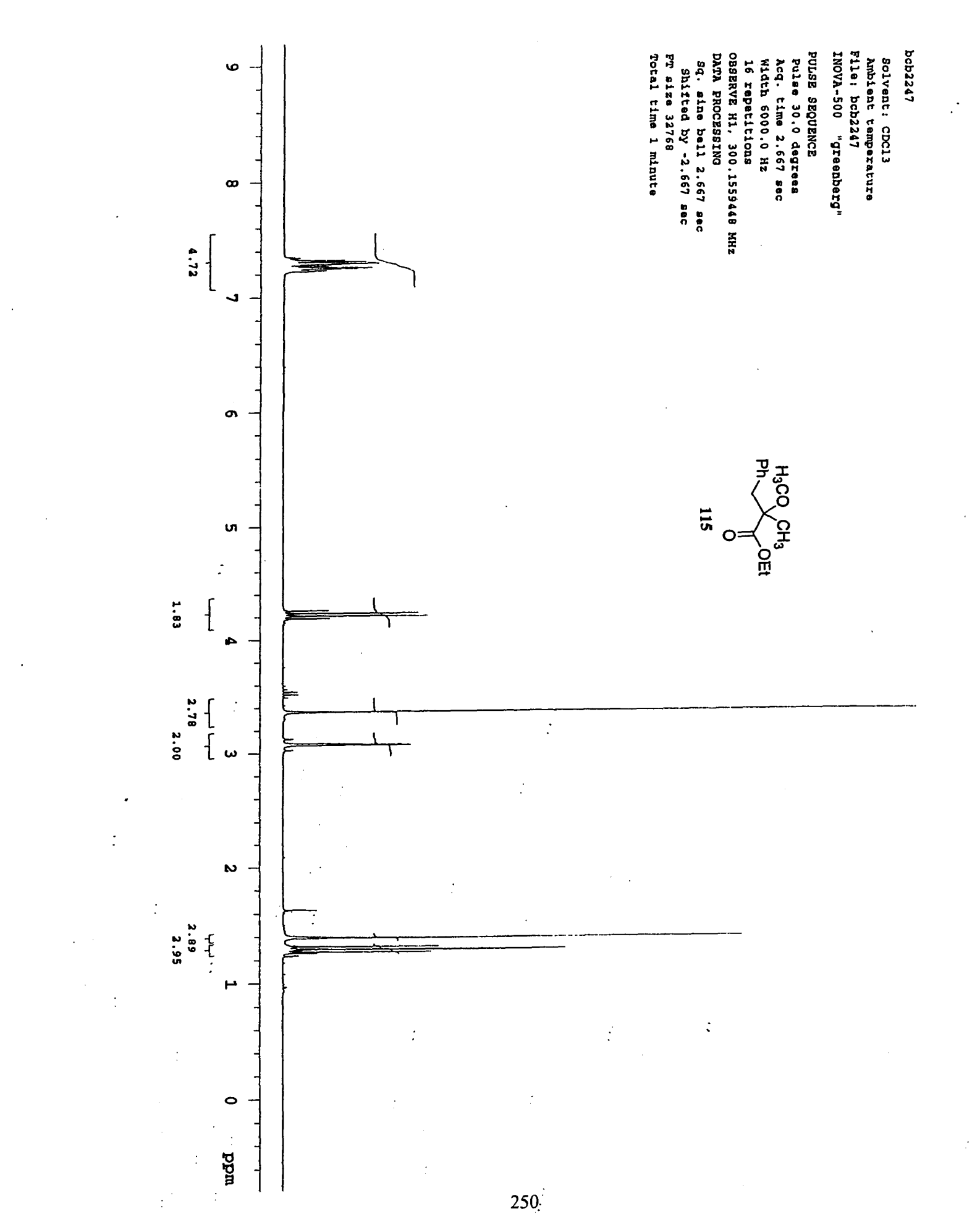

13C OBSERVE

Pulse Sequence: s2pul

Solvent: CDCl3
Ambient temperature
INOVA-300 "elfin"

PULSE SEQUENCE
Relax. delay 1.000 sec
Pulse 45.0 degrees
Acq. time 0.800 sec
Width 20000.0 Hz
378 repetitions
OBSERVE C13, 75.4645944 MHz
DECOUPLE H1, 300.1190283 MHz
Power 33 dB
continuously on
WALTZ-16 modulated
DATA PROCESSING
Line broadening 1.5 Hz
FT size 32768
Total time 502456 hr, 42 min, 40 sec

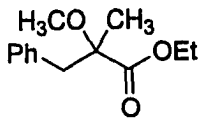

115

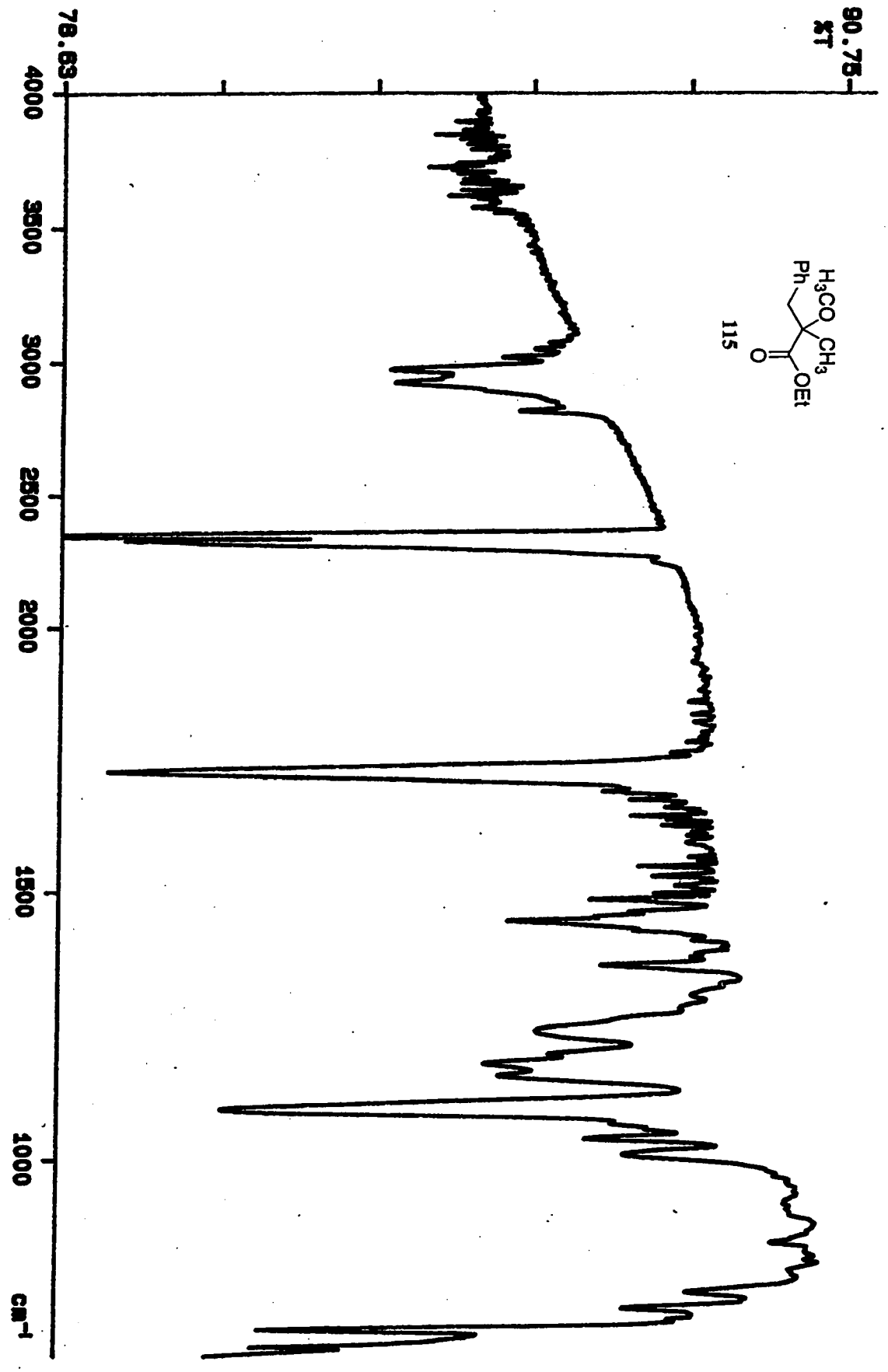

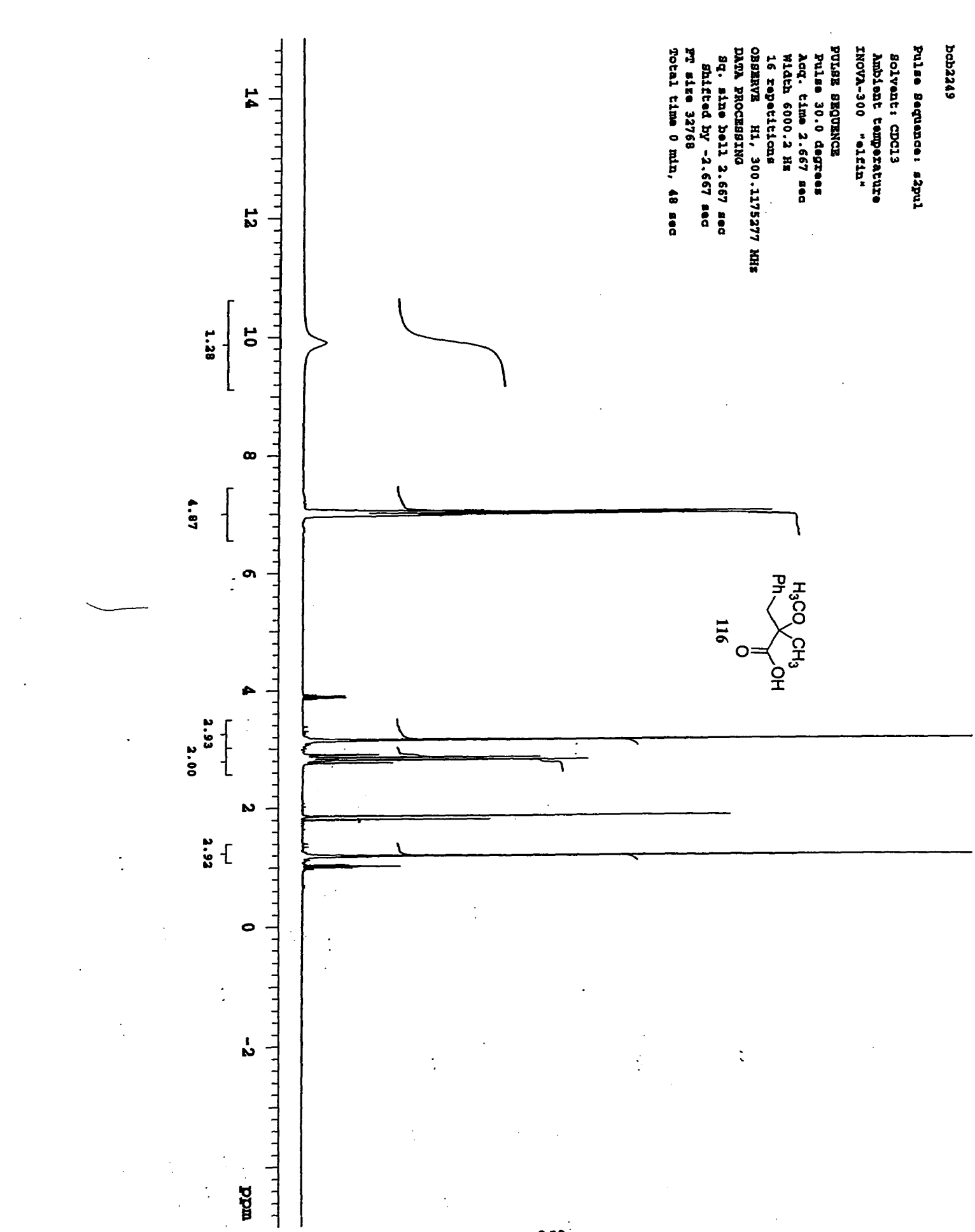

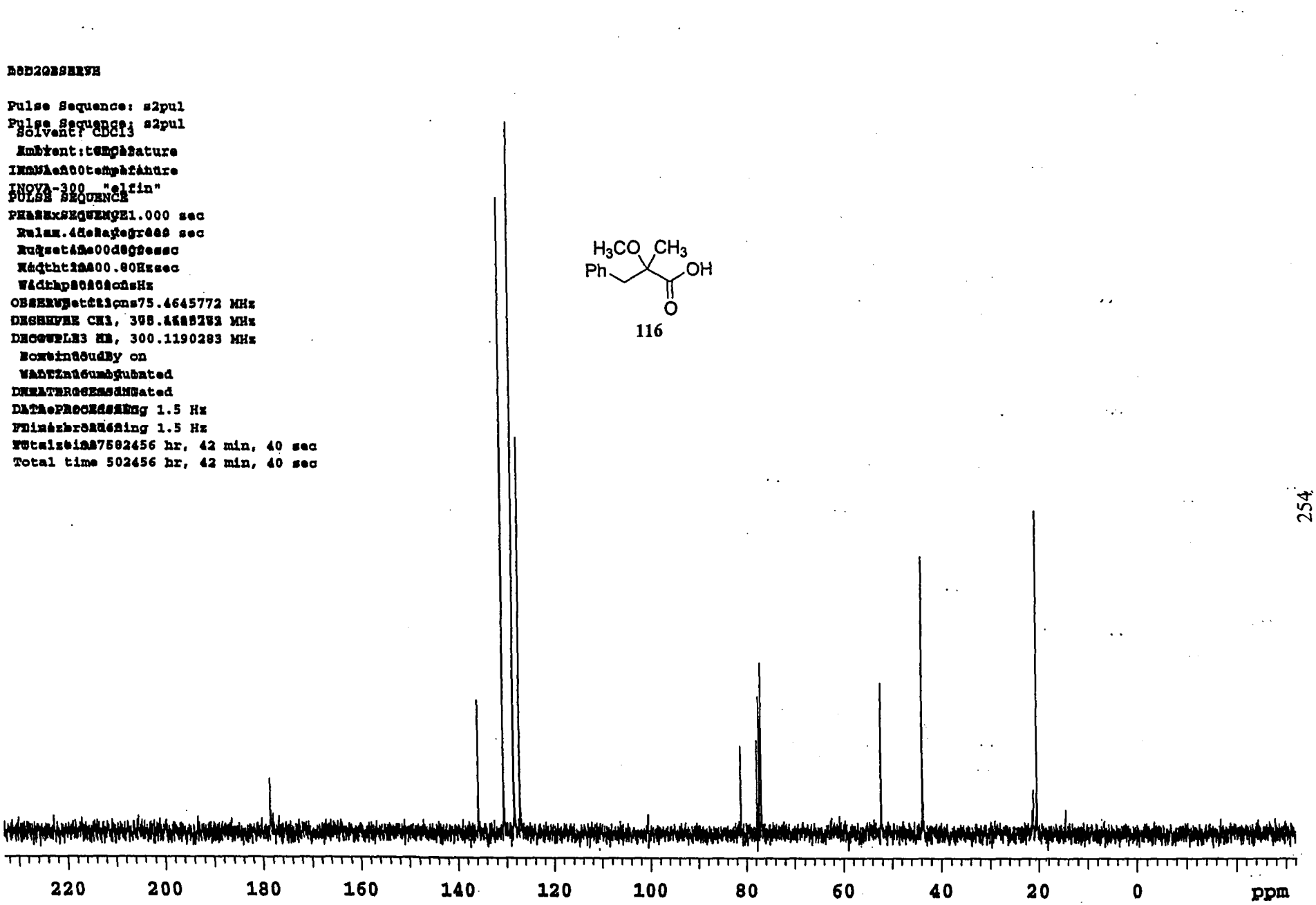

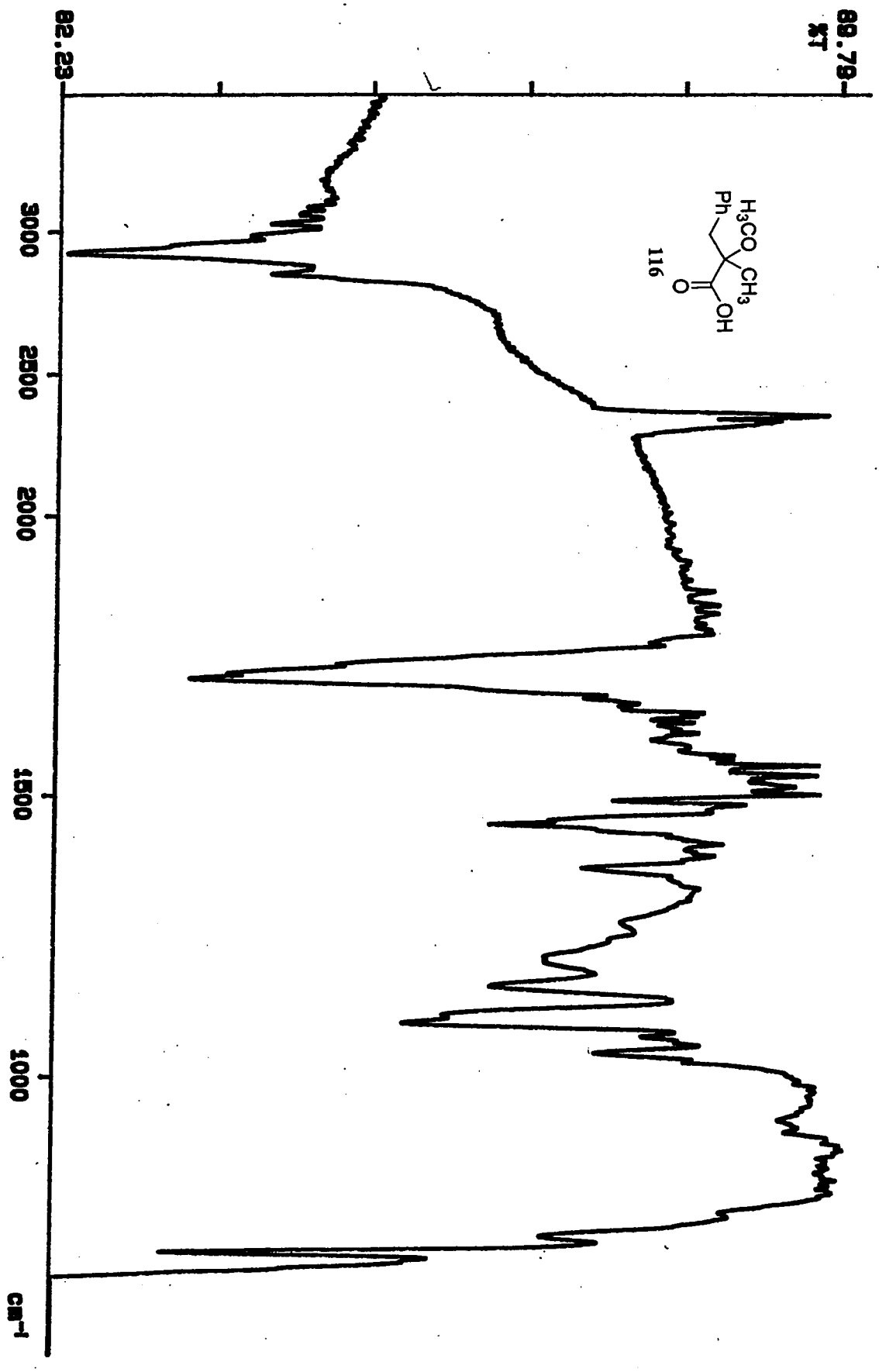

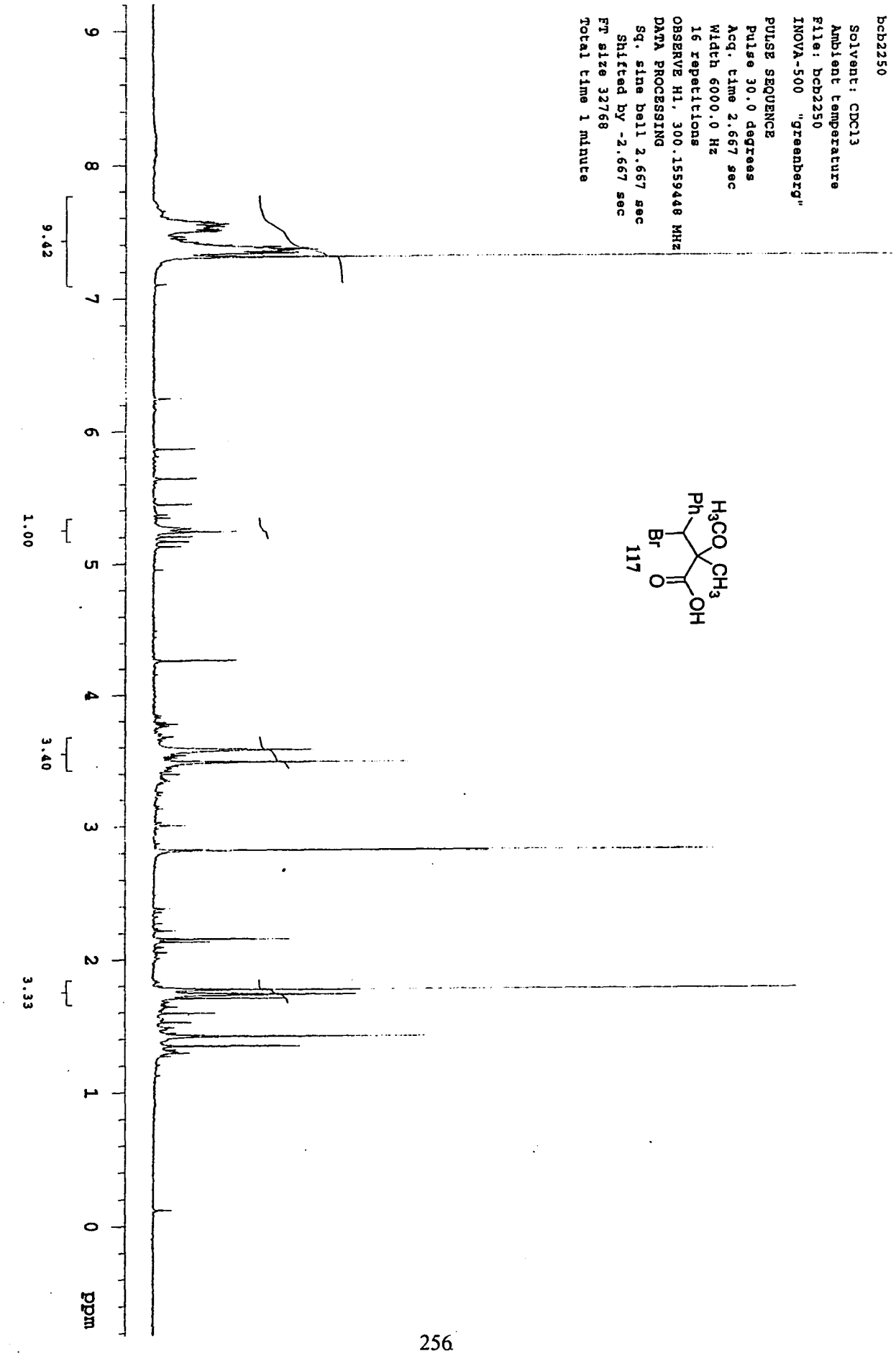

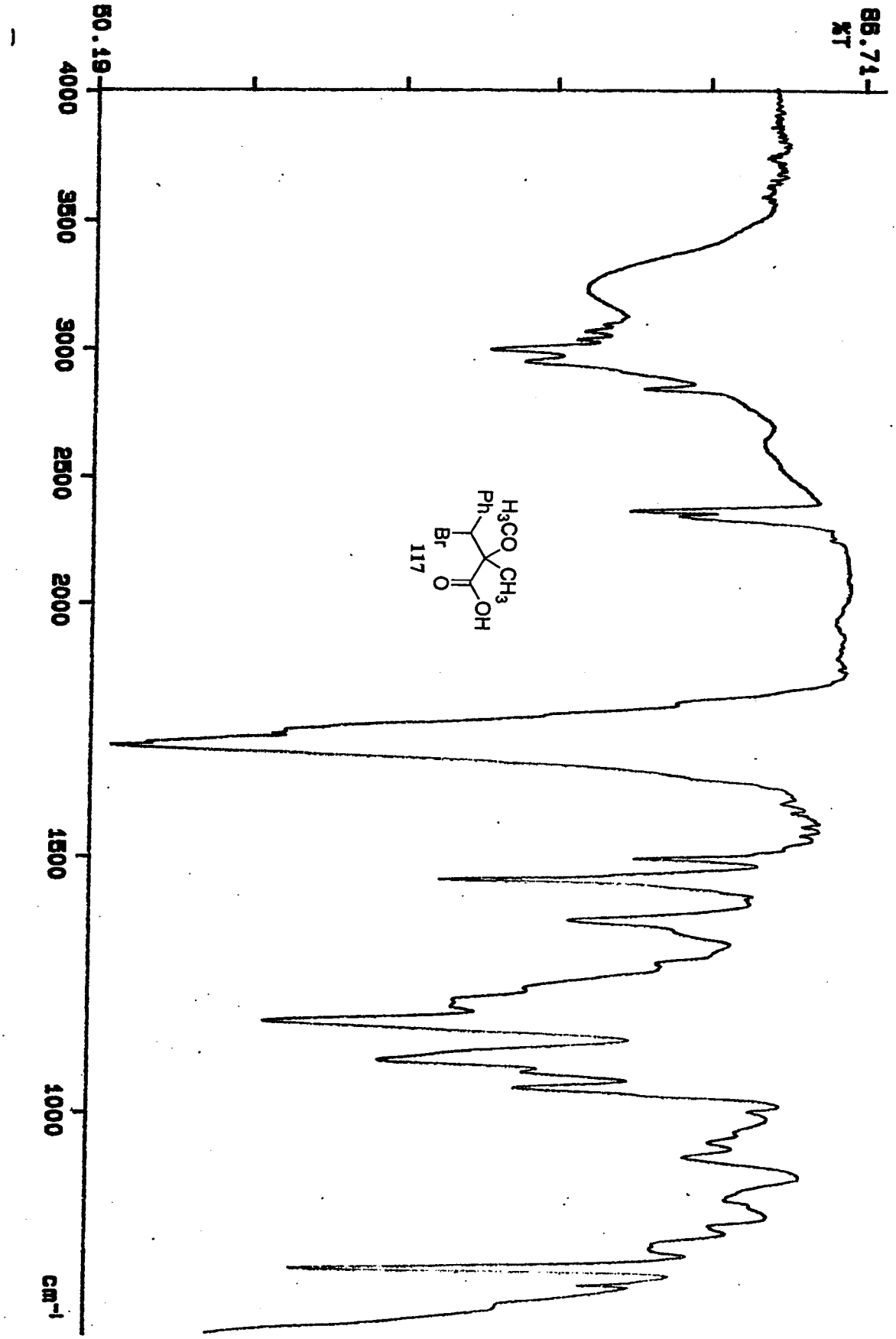

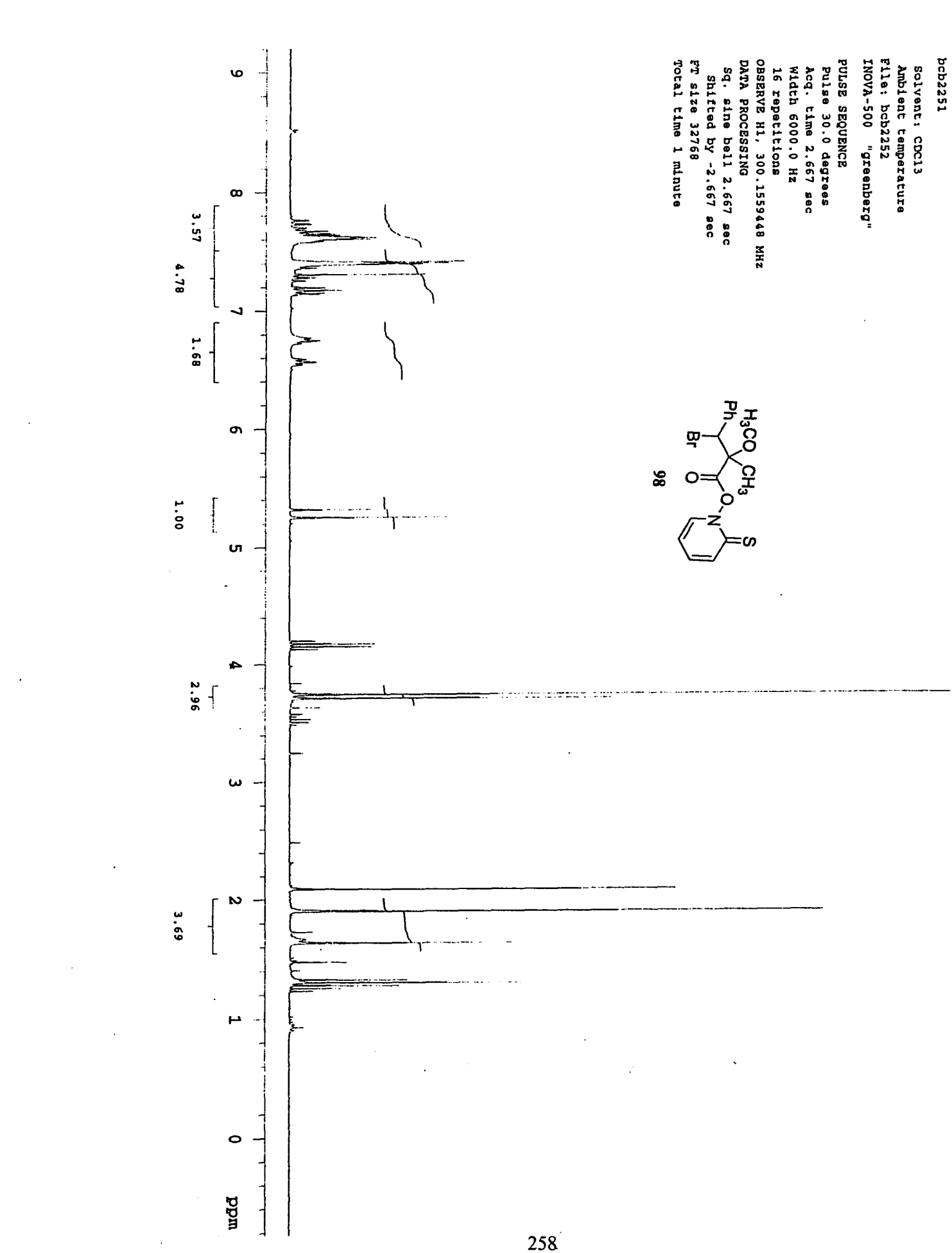

bcb2251c13

Pulse Sequence: s2pul

Solvent: CDCl3
Ambient temperature
File: bcb2251c13
INOVA-300 "elfin"

PULSE SEQUENCE
Relax. delay 1.000 sec
Pulse 45.0 degrees
Acq. time 0.800 sec
Width 20000.0 Hz
2256 repetitions
OBSERVE C13, 75.4645944 MHz
DECOUPLE H1, 300.1190283 MHz
Power 33 dB
continuously on
WALTZ-16 modulated
DATA PROCESSING
Line broadening 1.5 Hz
FT size 32768
Total time 502456 hr, 42 min, 40 sec

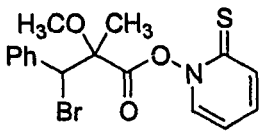

98

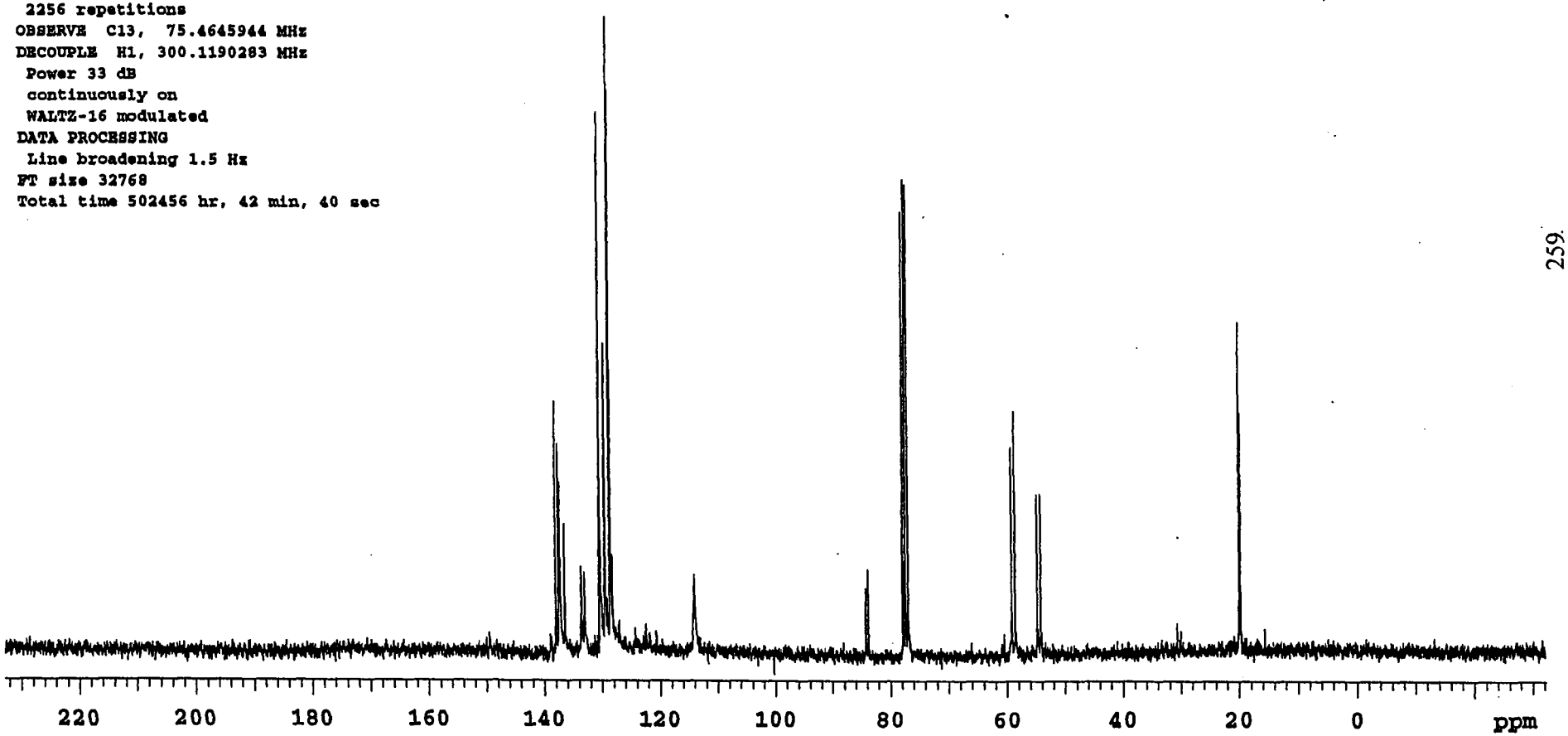

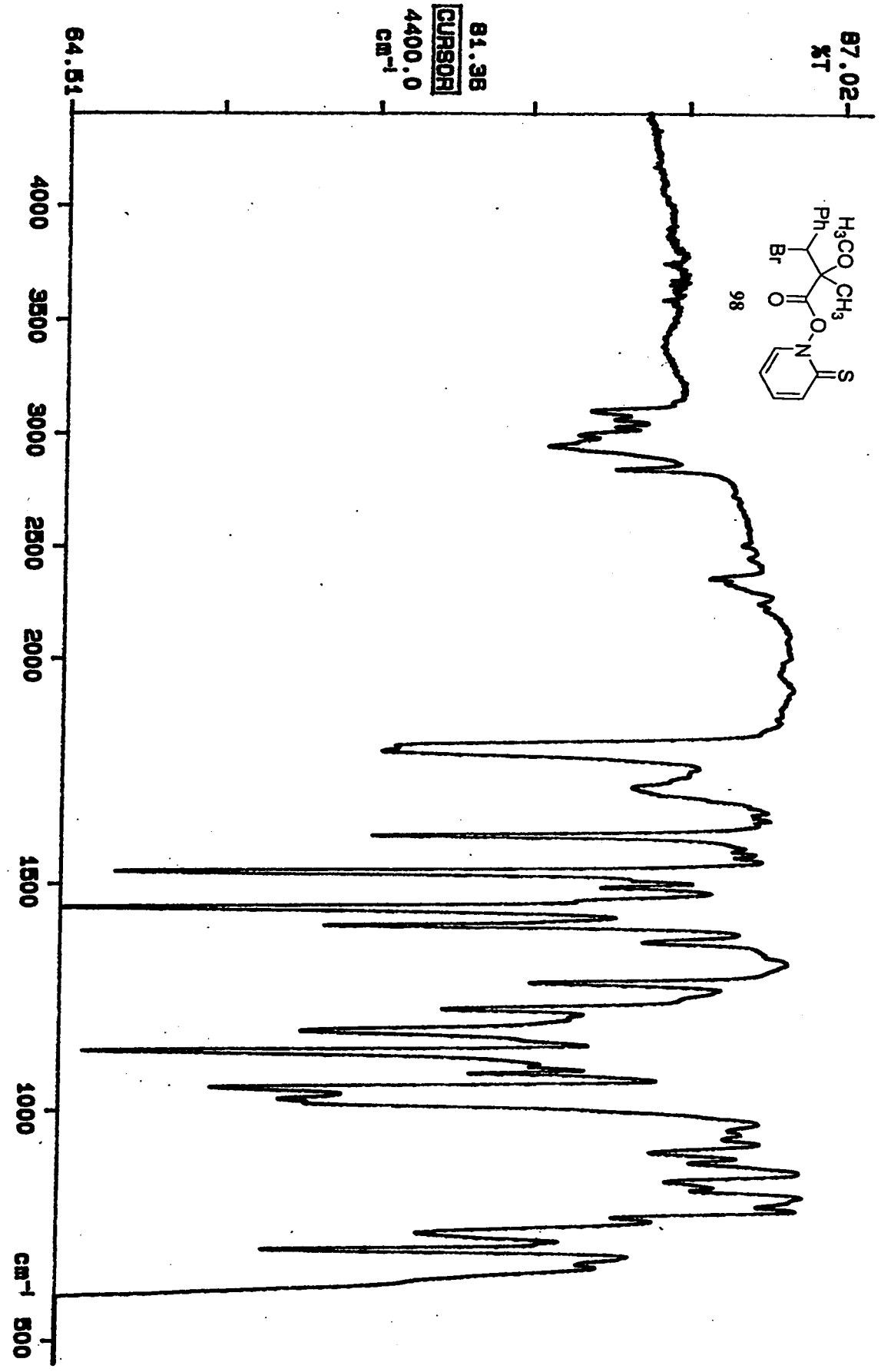

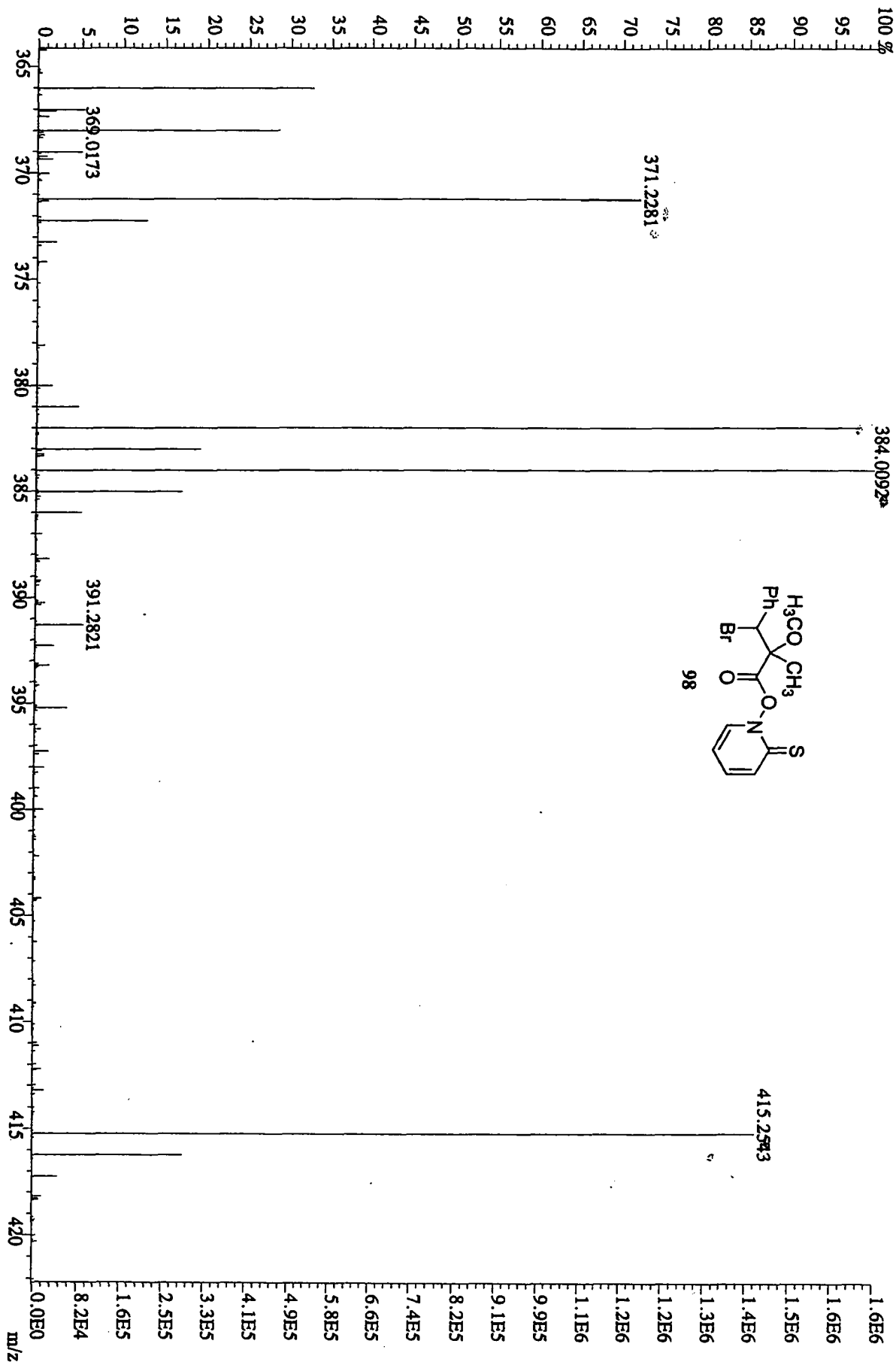

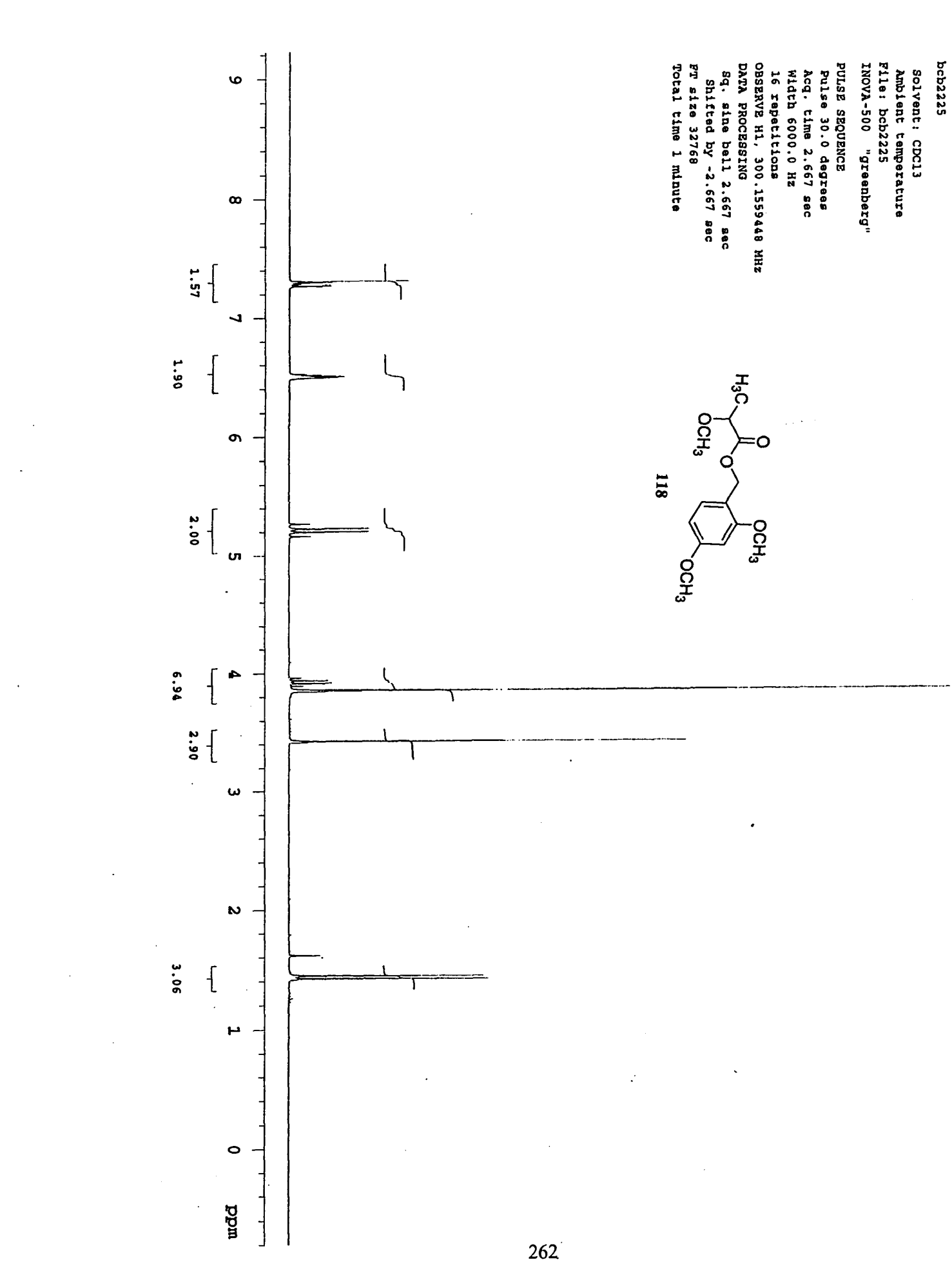

bcb2225c13

Pulse Sequence: s2pul

Solvent: CDCl3
Temp. 22.0 C / 295.1 K
File: bcb2225c13
INOVA-300 "elfin"

PULSE SEQUENCE
Relax. delay 1.000 sec
Pulse 45.0 degrees
Acq. time 0.800 sec
Width 20000.0 Hz
609 repetitions
OBSERVE C13, 75.4645944 MHz
DECOUPLE H1, 300.1190283 MHz
Power 33 dB
continuously on
WALTZ-16 modulated
DATA PROCESSING
Line broadening 1.5 Hz
FT size 32768
Total time 502456 hr, 42 min, 40 sec

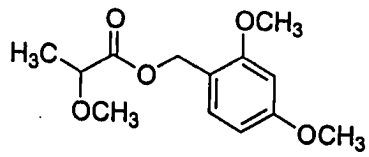

118

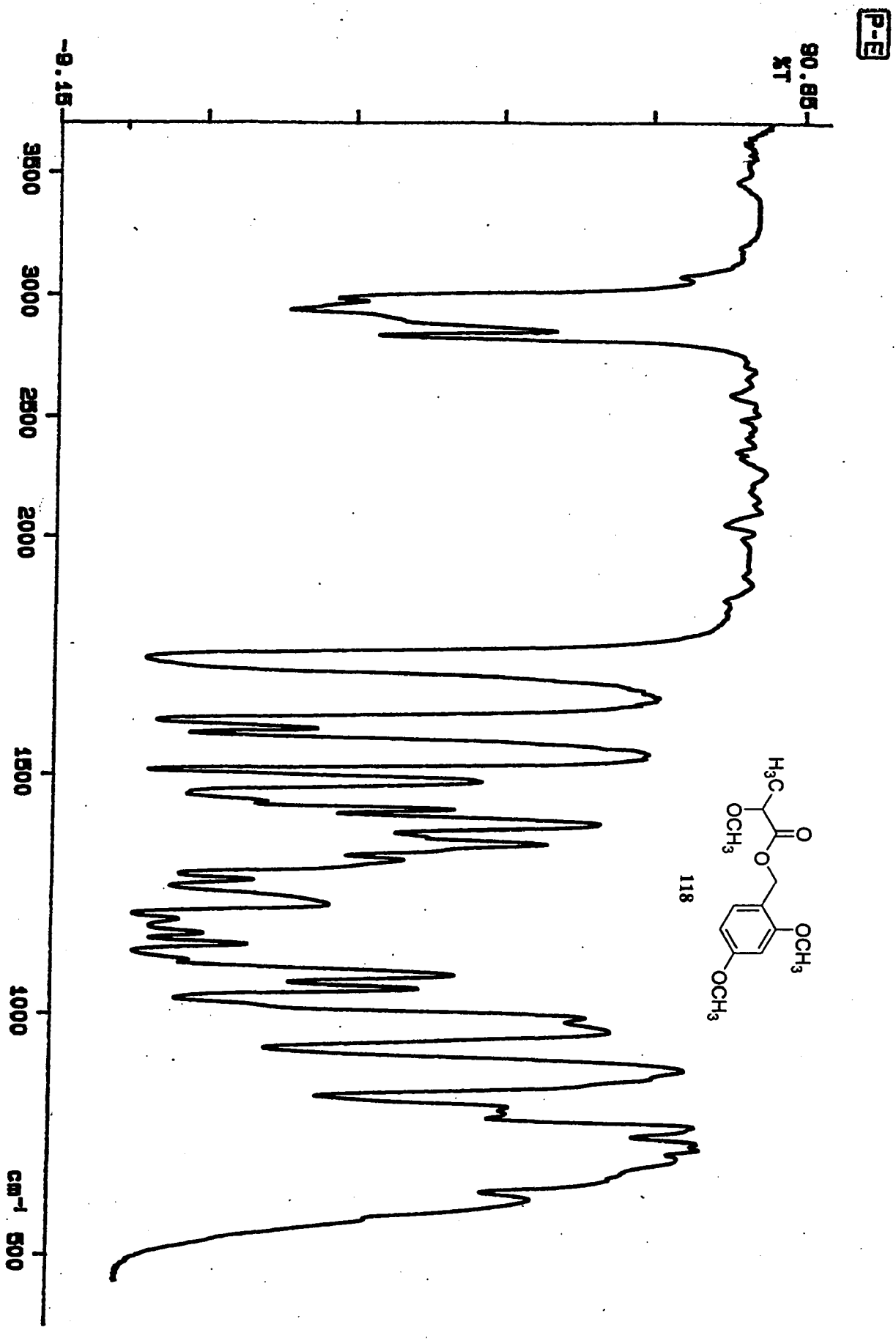

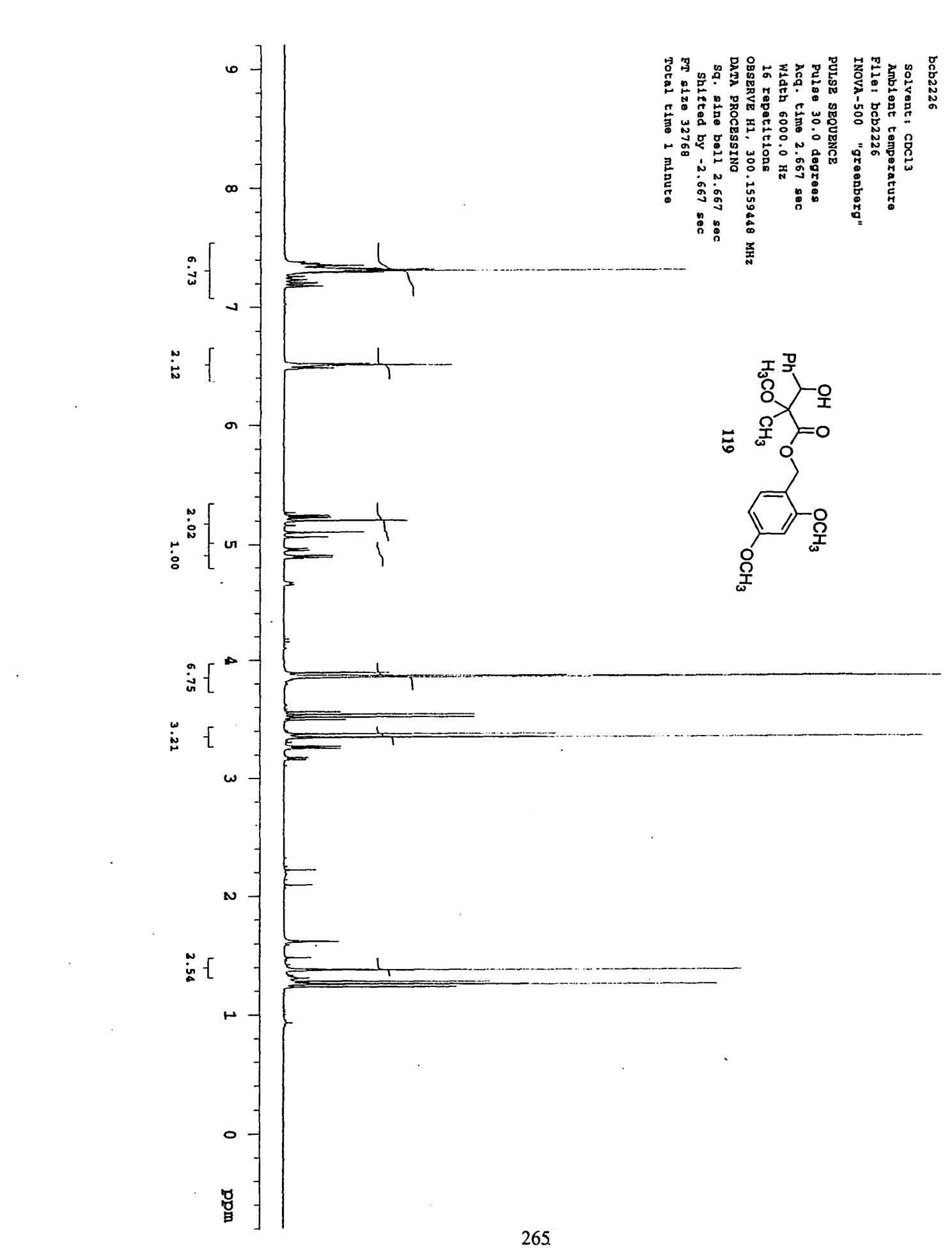

bobhydroxyester
Bg2222
Pulse Sequence: s2pul

Solvent: CDCl3
Ambient temperature
INOVA-300 "elfin"

PULSE SEQUENCE
Relax. delay 1.000 sec
Pulse 45.0 degrees
Acq. time 0.800 sec
Width 20000.0 Hz
3465 repetitions
OBSERVE C13, 75.4645944 MHz
DECOUPLE H1, 300.1190283 MHz
Power 33 dB
continuously on
WALTZ-16 modulated
DATA PROCESSING
Line broadening 1.5 Hz
FT size 32768
Total time 502456 hr, 42 min, 40 sec

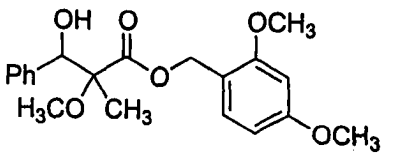

119

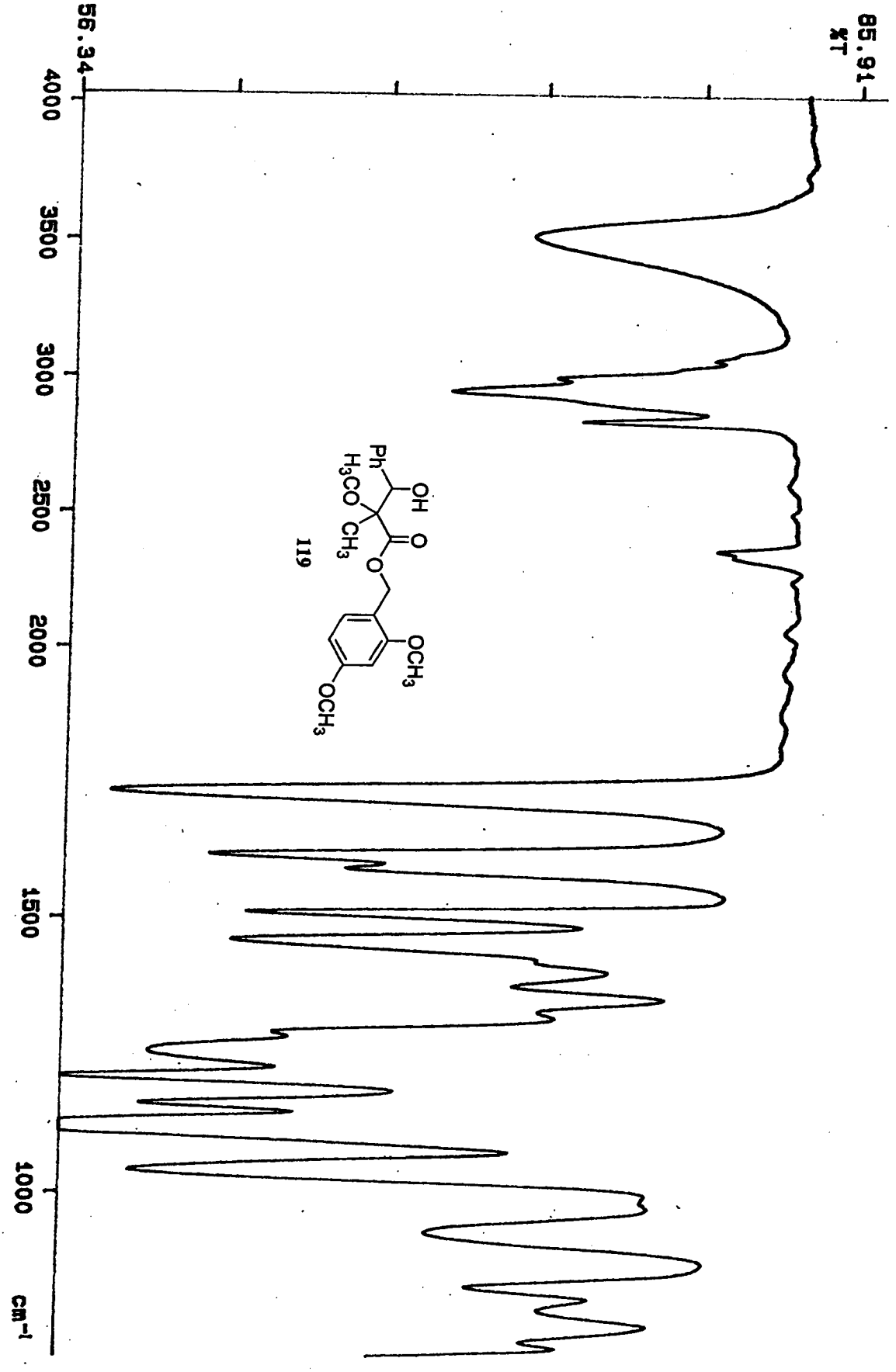

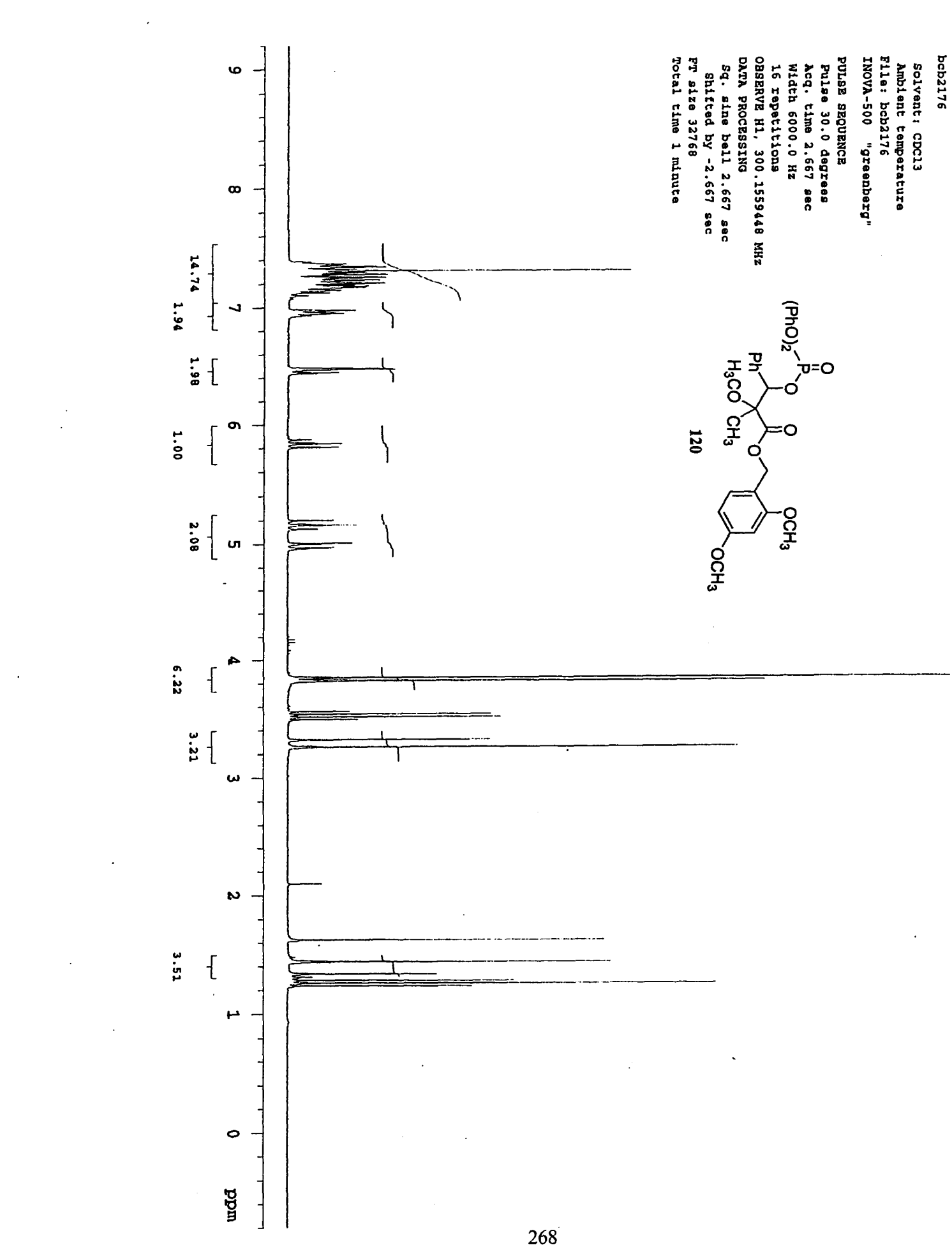

bcb2236c13

Pulse Sequence: s2pul

Solvent: CDCl3
Ambient temperature
INOVA-300 "elfin"

PULSE SEQUENCE
Relax. delay 1.000 sec
Pulse 45.0 degrees
Acq. time 0.800 sec
Width 20000.0 Hz
2891 repetitions
OBSERVE C13, 75.4645944 MHz
DECOUPLE H1, 300.1190283 MHz
Power 33 dB
continuously on
WALTZ-16 modulated
DATA PROCESSING
Line broadening 1.5 Hz
FT size 32768
Total time 502456 hr, 42 min, 40 sec

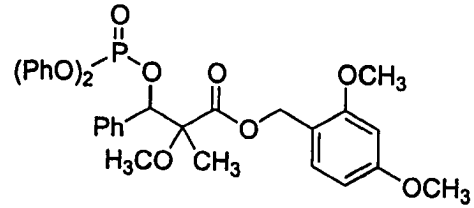

120

bcb2236p31

Pulse Sequence: s2pul

Solvent: CDCl3
Ambient temperature
INOVA-300 "elfin"

PULSE SEQUENCE
Relax. delay 1.000 sec
Pulse 25.0 degrees
Acq. time 0.525 sec
Width 25000.0 Hz
45 repetitions
OBSERVE P31, 121.4897252 MHz
DECOUPLE H1, 300.1190283 MHz
Power 38 dB
continuously on
WALTZ-16 modulated
DATA PROCESSING
Line broadening 1.0 Hz
FT size 32768
Total time 26 min, 13 sec

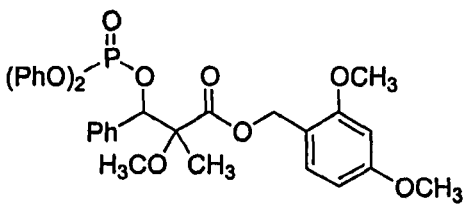

120

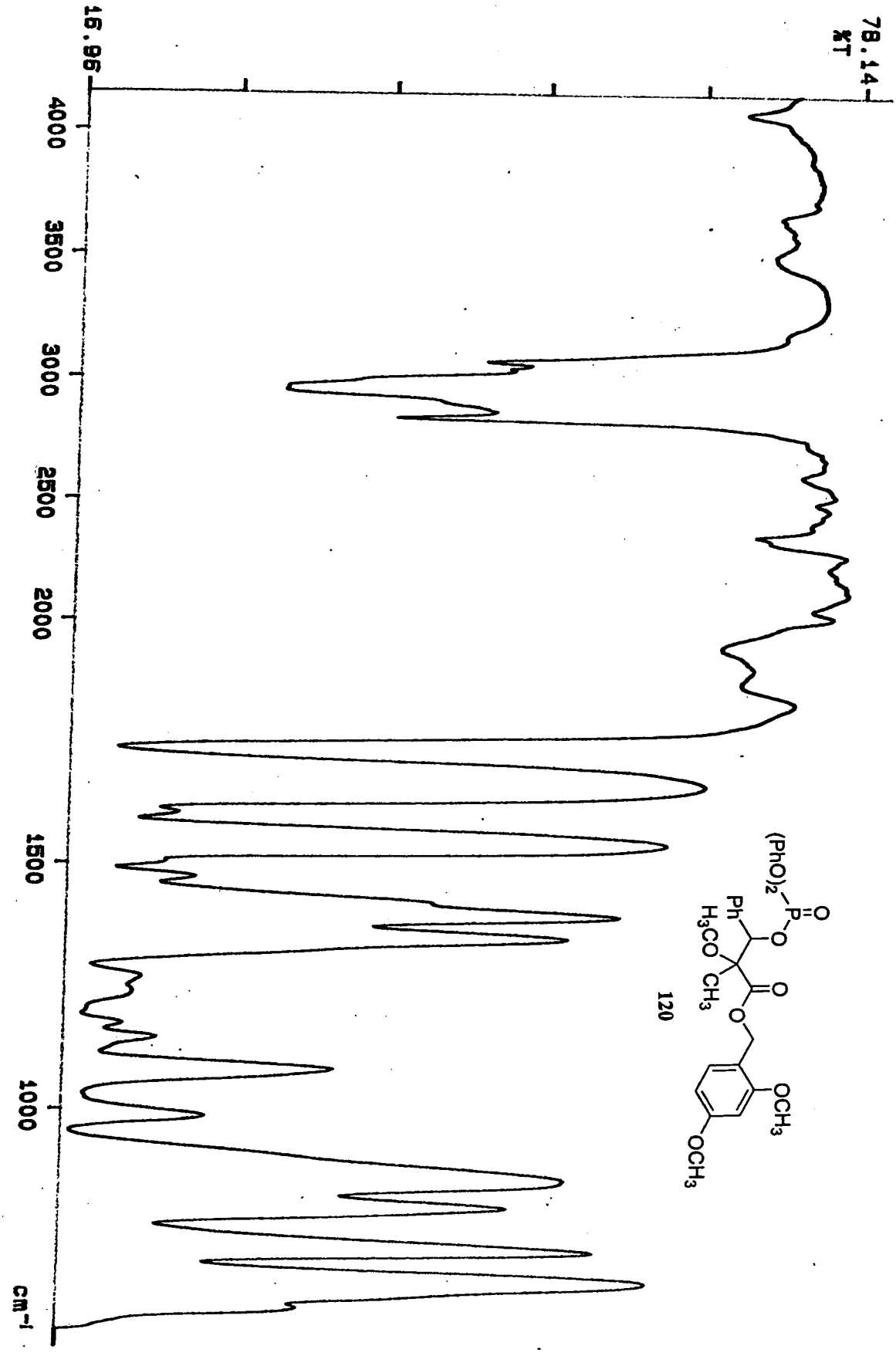

bcb4203

Solvent: CDCl3
Ambient temperature
File: bcb4203
INOVA-500 "greenberg"

PULSE SEQUENCE
Pulse 30.0 degrees
Acq. time 2.667 sec
Width 6000.0 Hz
16 repetitions
OBSERVE H1, 300.1559448 MHz
DATA PROCESSING
Sq. sine bell 2.667 sec
Shifted by -2.667 sec
FT size 32768
Total time 1 minute

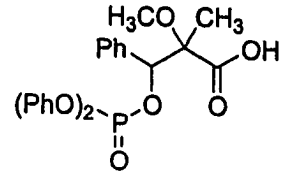

121

bcb4203p31

Solvent: CDCl3
Ambient temperature
File: bcb4203p31
INOVA-500 "greenberg"

PULSE SEQUENCE
Pulse 26.8 degrees
Acq. time 1.600 sec
Width 25000.0 Hz
32 repetitions
OBSERVE P31, 121.5053101 MHz
DECOUPLE H1, 300.1574402 MHz
Power 40 dB
continuously on
WALTZ-16 modulated
DATA PROCESSING
Line broadening 1.0 Hz
FT size 131072
Total time 1 minute

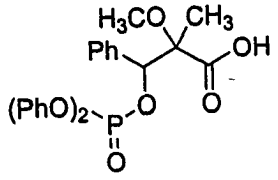

121

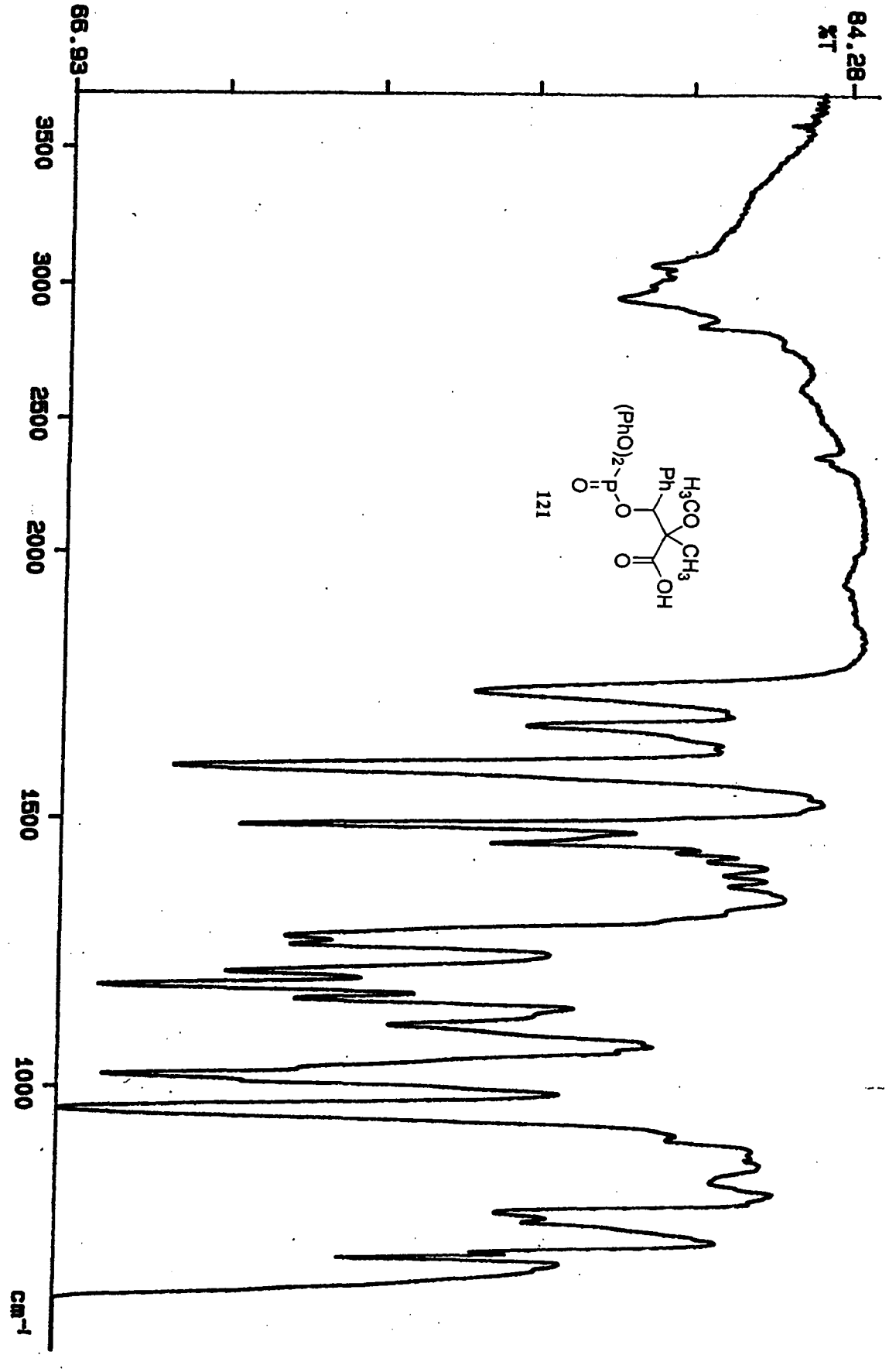

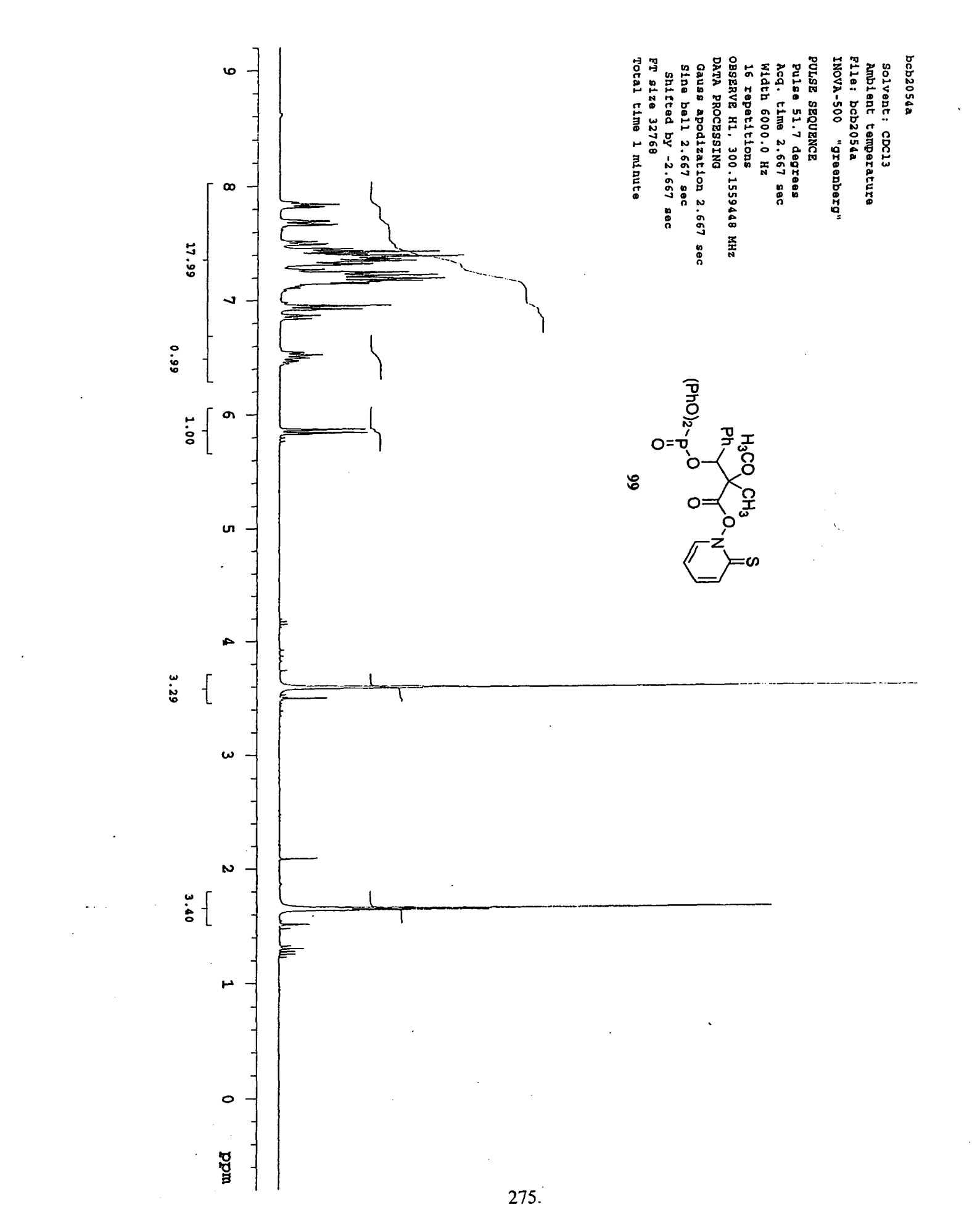

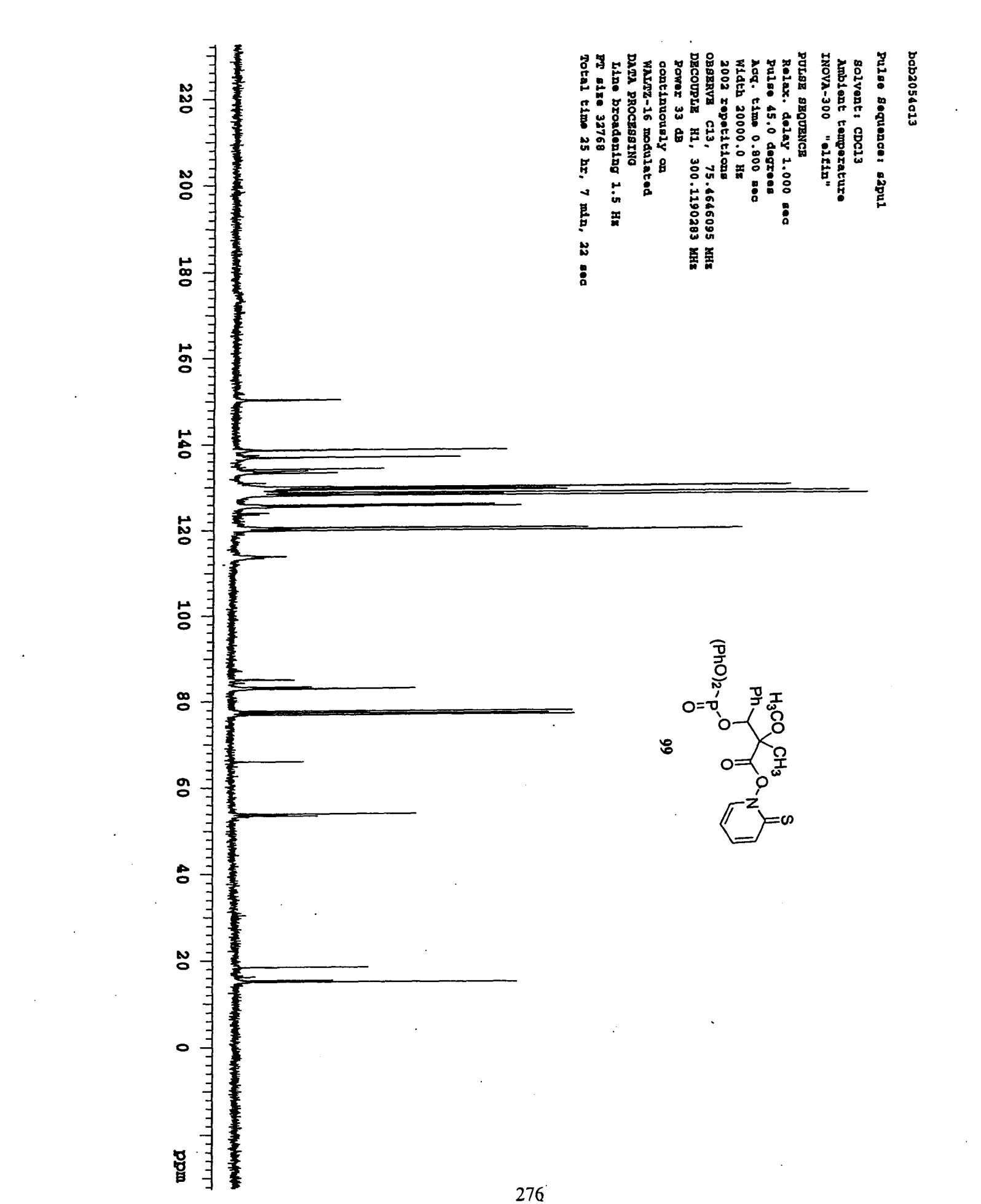

bcb4204p31

Solvent: CDCl3
Ambient temperature
File: bcb4204p31
INOVA-500 "greenberg"

PULSE SEQUENCE
Pulse 26.8 degrees
Acq. time 1.600 sec
Width 25000.0 Hz
32 repetitions
OBSERVE P31, 121.5053101 MHz
DECOUPLE H1, 300.1574402 MHz
Power 40 dB
continuously on
WALTZ-16 modulated
DATA PROCESSING
Line broadening 1.0 Hz
FT size 131072
Total time 1 minute

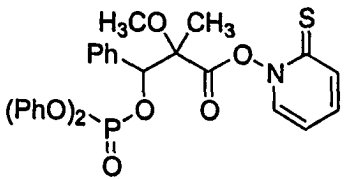

99

277.

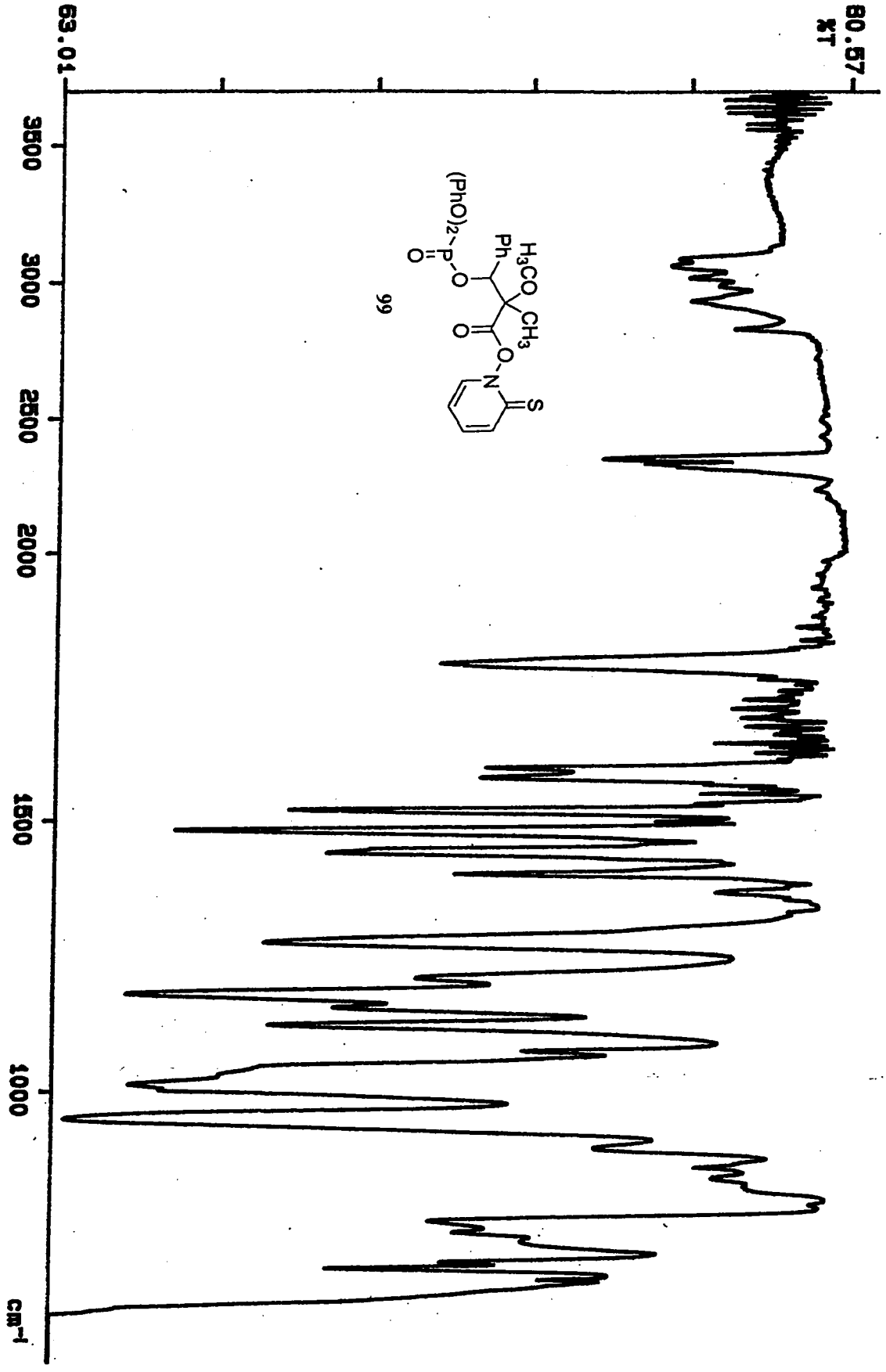

File:MG317 Ident:2_13 SMO(2,5) PKD(5,2,5,0.10%,0.0,33.00%,F,F) SPEC(Heights,Centroid) Acq:16-MAR-1999 10:04:29 +2:34 Ca>
AutoSpecE FAB+ Voltage BpM:547 BpI:406791 TIC:1390468 Flags:NORM
File Text:B. Bales BCB2054

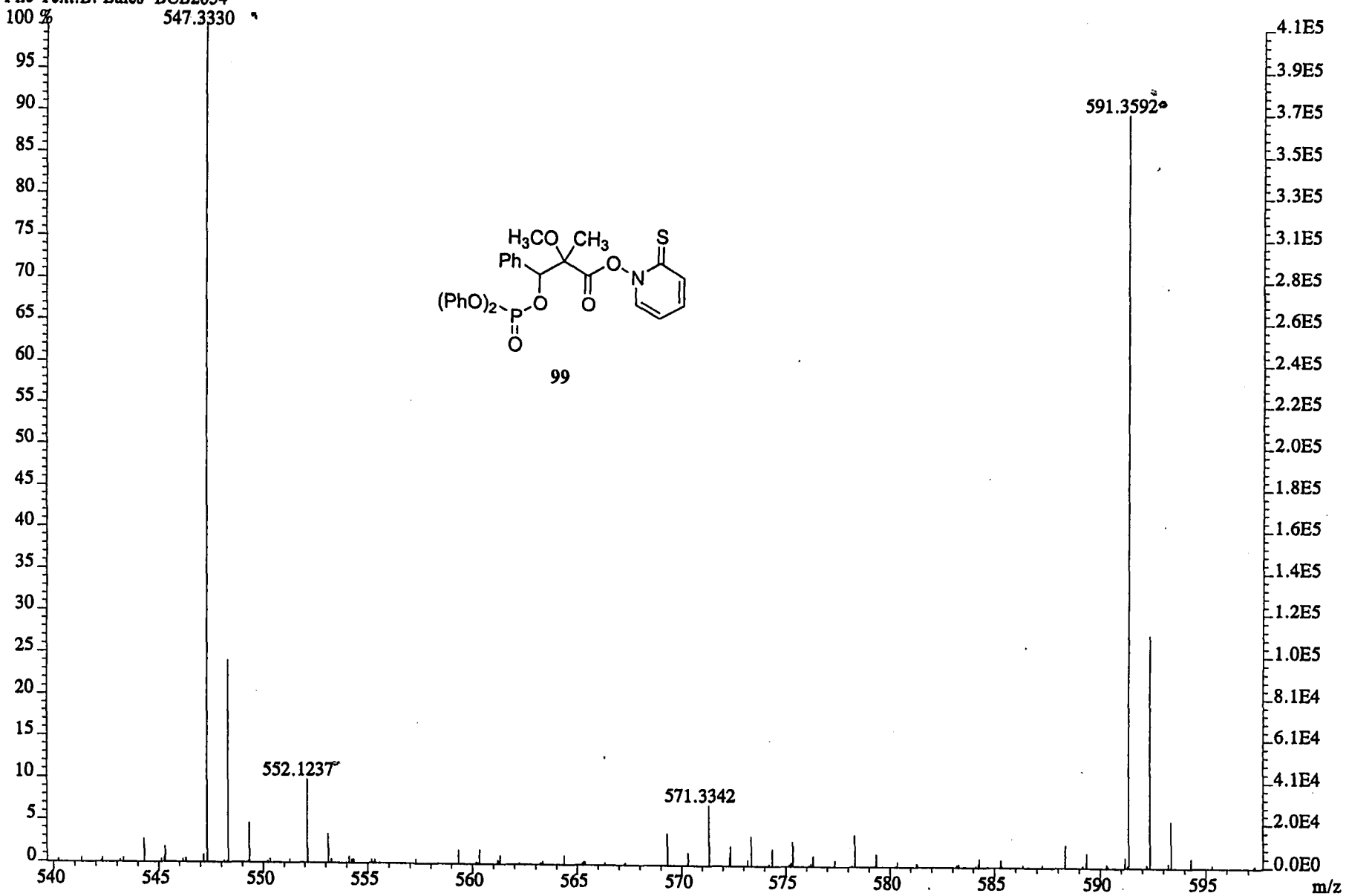

99

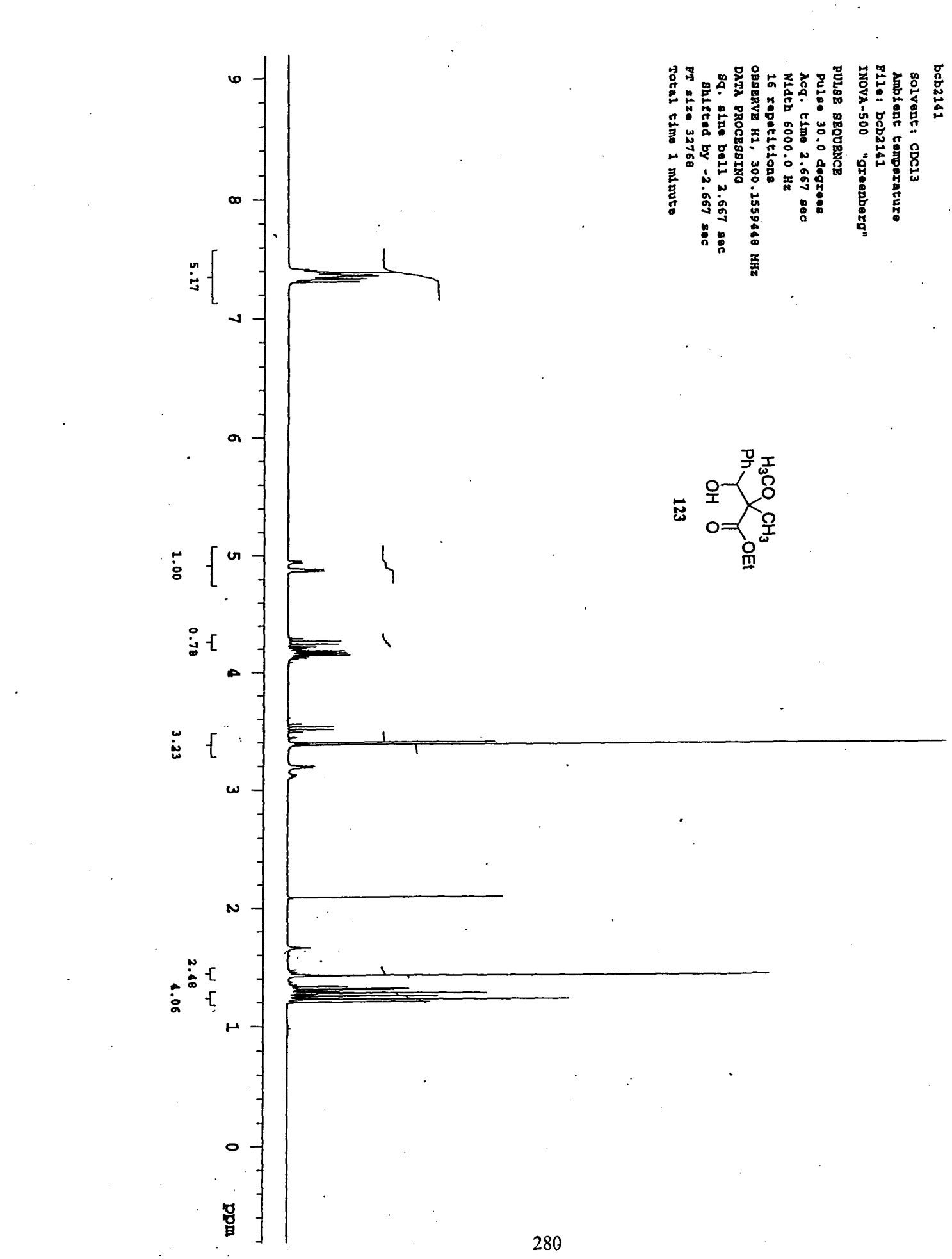

bcb2141c13

exp1 std13c

SAMPLE		DEC. & VT	
date	Sep 25 1999	dfrq	300.157
solvent	CDCl3	dn	H1
file	/usr/people/m-	dpwr	40
mg/vnmrsys/data/bc-		dof	0
	b2141c13	dm	yyy
ACQUISITION		dmm	w
sfrq	75.482	dmf	10540
tn	C13	PROCESSING	
at	0.727	lb	2.00
np	32000	wtfile	
sw	22000.0	proc	lp
fb	12200	fn	not used
bs	8		
tpwr	56	werr	
pw	7.2	wexp	
d1	1.200	wbs	wft
tof	0	wnt	
nt	128		
ct	48		
alock	s		
gain	32		
FLAGS			
il	n		
in	n		
dp	y		
DISPLAY			
sp	-3452.5		
wp	22000.0		
vs	139		
sc	0		
wc	250		
hzmm	1.84		
is	500.00		
rfl	9281.8		
rfp	5829.3		
th	3		
ins	100.000		

nm, pc, ph

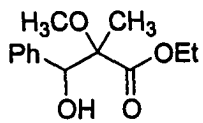

123

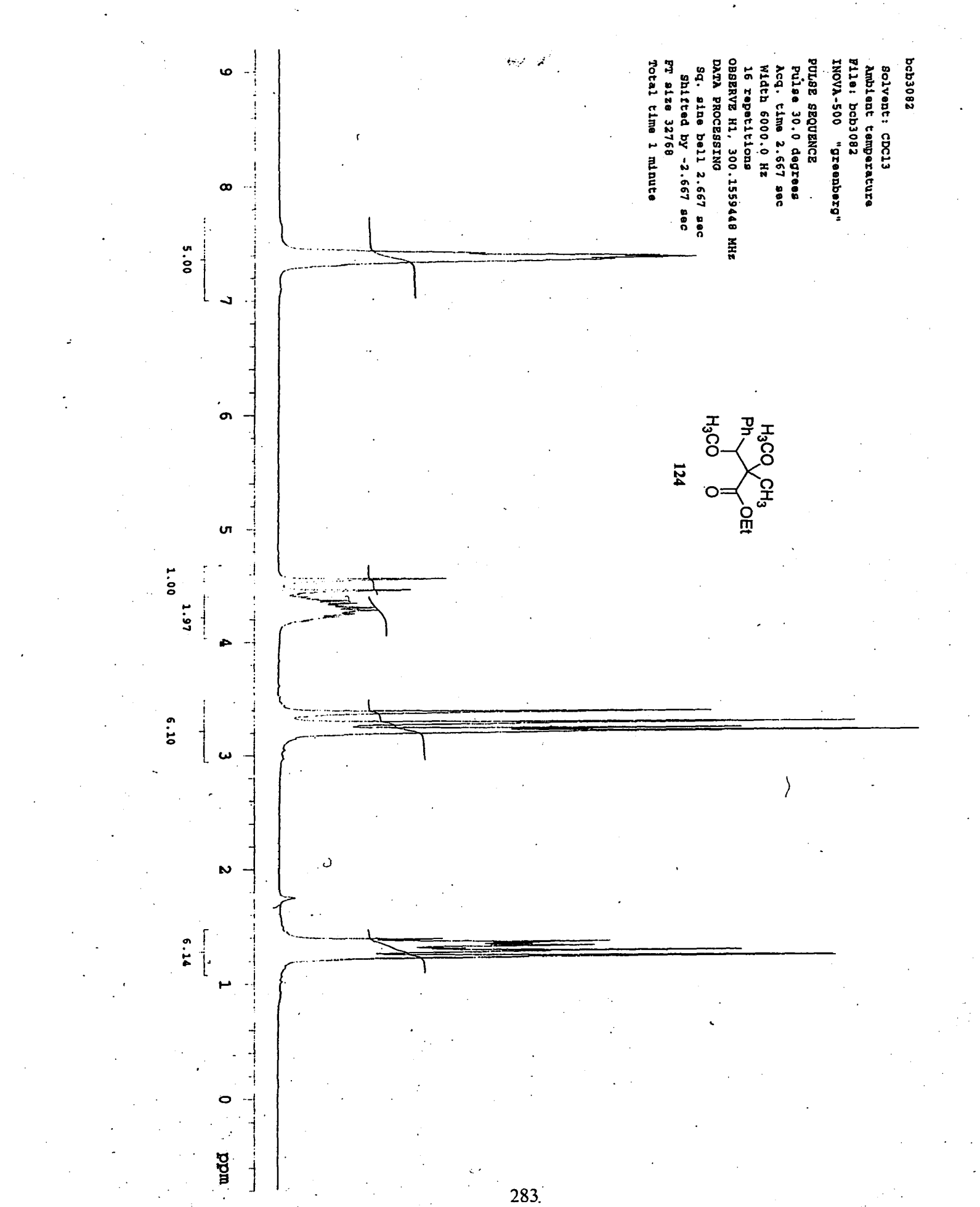

bcb3082c13

Solvent: CDCl3
Ambient temperature
File: bcb3082c13
INOVA-500 "greenberg"

PULSE SEQUENCE
Relax. delay 1.200 sec
Pulse 45.0 degrees
Acq. time 0.727 sec
Width 22000.0 Hz
128 repetitions
OBSERVE C13, 75.4742661 MHz
DECOUPLE H1, 300.1574402 MHz
Power 40 dB
continuously on
WALTZ-16 modulated
DATA PROCESSING
Line broadening 2.0 Hz
FT size 32768
Total time 4 minutes

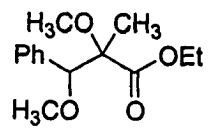

124

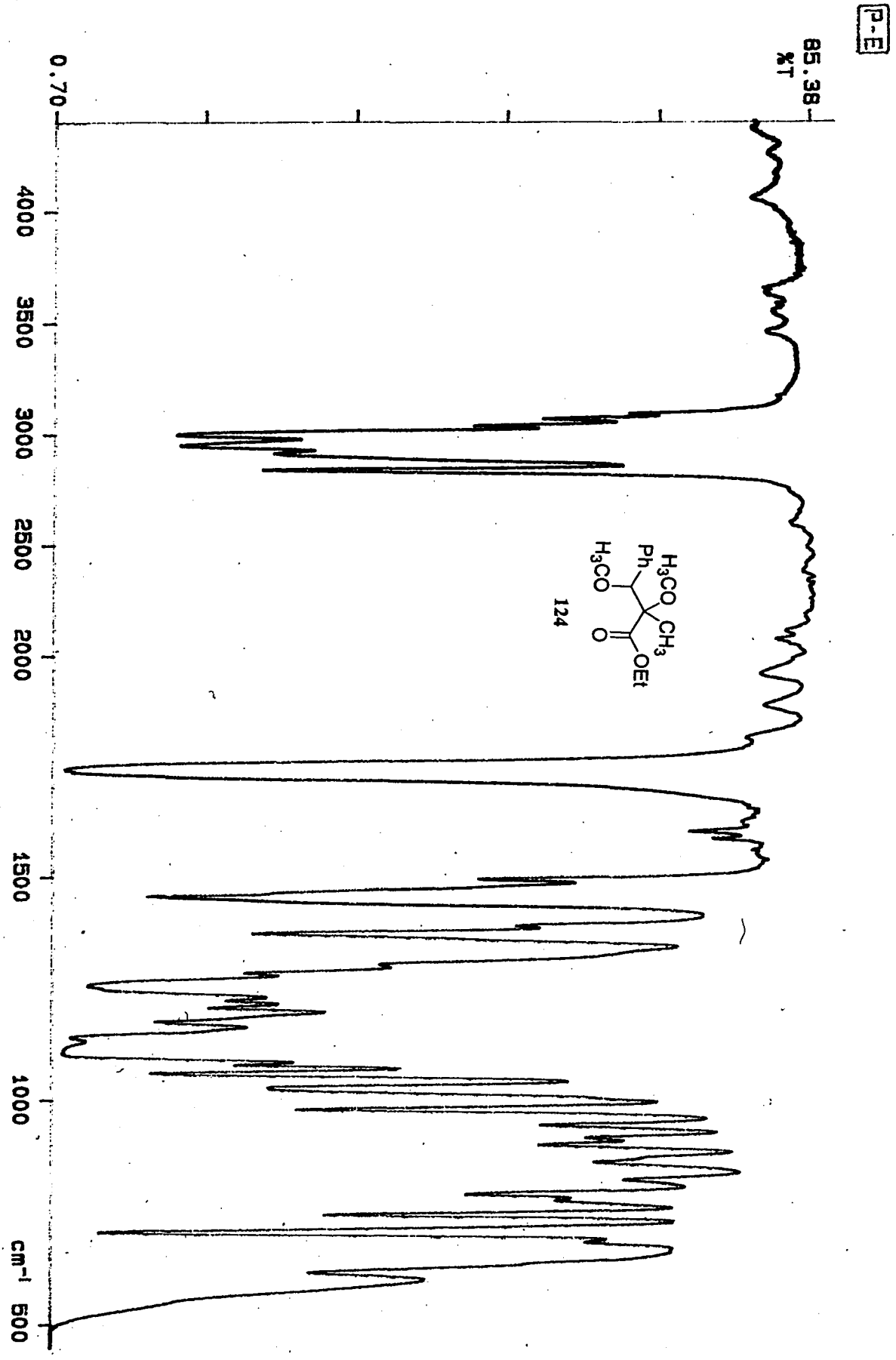

bcb3037

Solvent: CDCl3
Ambient temperature
File: bcb3037
INOVA-500 "greenberg"

PULSE SEQUENCE
Pulse 30.0 degrees
Acq. time 2.667 sec
Width 6000.0 Hz
16 repetitions
OBSERVE H1, 300.1559448 MHz
DATA PROCESSING
Sq. sine bell 2.667 sec
Shifted by -2.667 sec
FT size 32768
Total time 1 minute

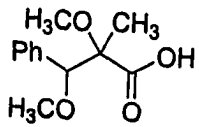

125

286.

bcb3037

Pulse Sequence: s2pul

Solvent: CDCl3
Ambient temperature
File: bcb3037c13
INOVA-300 "elfin"

PULSE SEQUENCE
Relax. delay 1.000 sec
Pulse 45.0 degrees
Acq. time 0.800 sec
Width 20000.0 Hz
247 repetitions
OBSERVE C13, 75.4645997 MHz
DECOUPLE H1, 300.1190283 MHz
Power 33 dB
continuously on
WALTZ-16 modulated
DATA PROCESSING
Line broadening 1.5 Hz
FT size 32768
Total time 502456 hr, 42 min, 40 sec

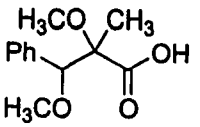

125

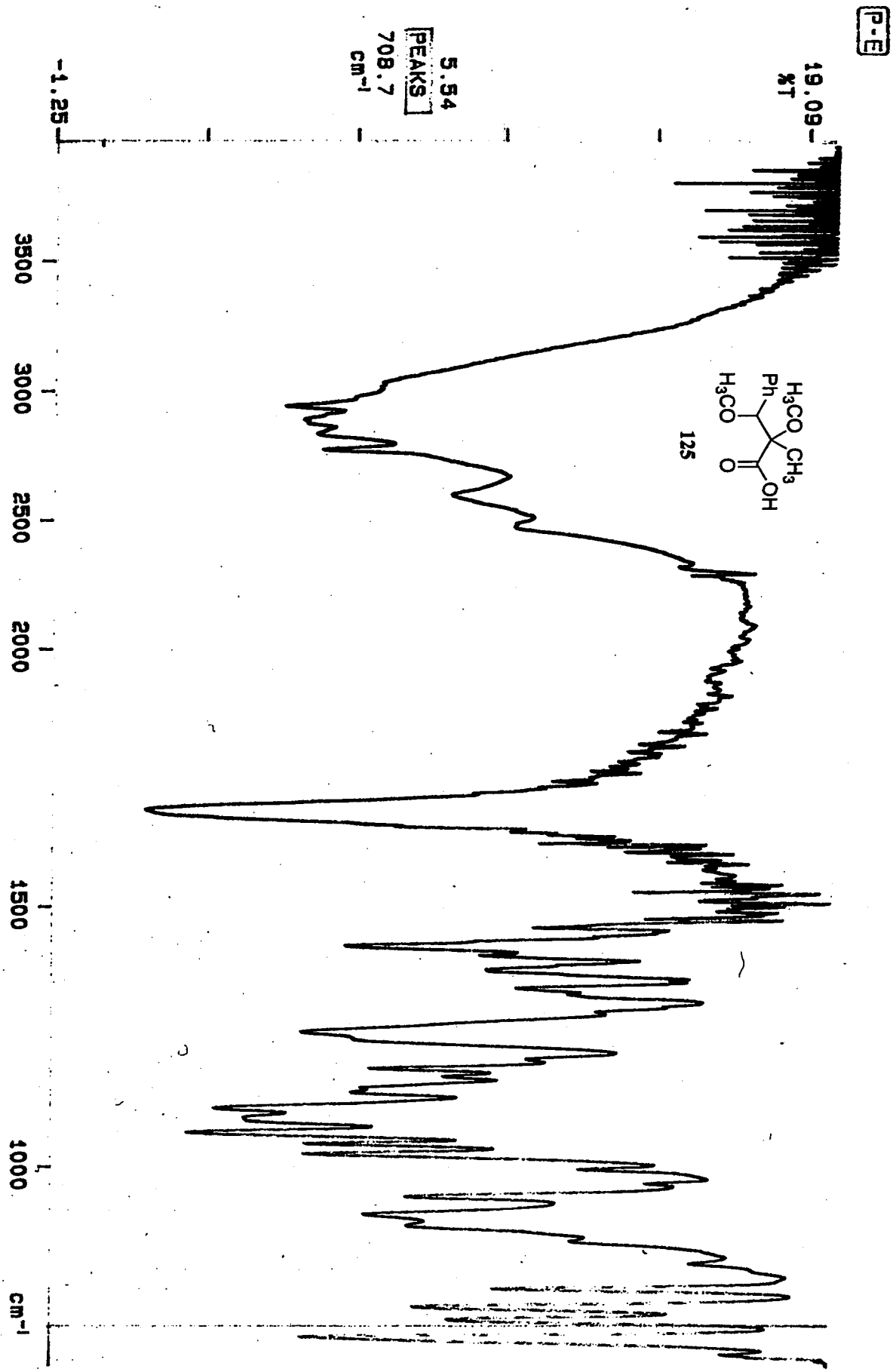

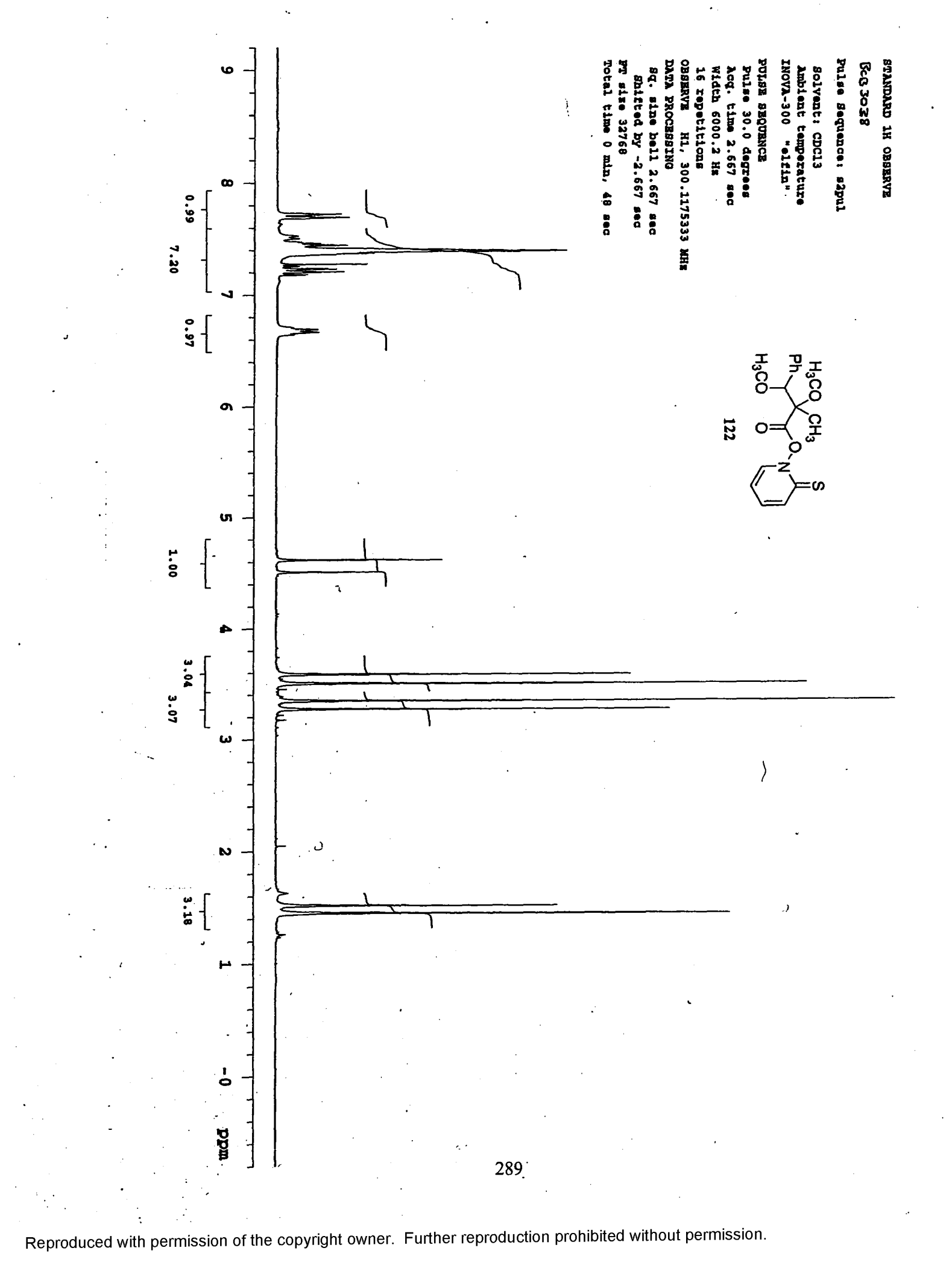

bcb3038

Pulse Sequence: s2pul

Solvent: CDCl3
Ambient temperature
INOVA-300 "elfin"

PULSE SEQUENCE
Relax. delay 1.000 sec
Pulse 45.0 degrees
Acq. time 0.800 sec
Width 20000.0 Hz
439 repetitions
OBSERVE C13, 75.4645997 MHz
DECOUPLE H1, 300.1190283 MHz
Power 33 dB
continuously on
WALTZ-16 modulated
DATA PROCESSING
Line broadening 1.5 Hz
FT size 32768
Total time 502456 hr, 42 min, 40 sec

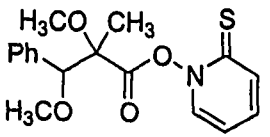

122

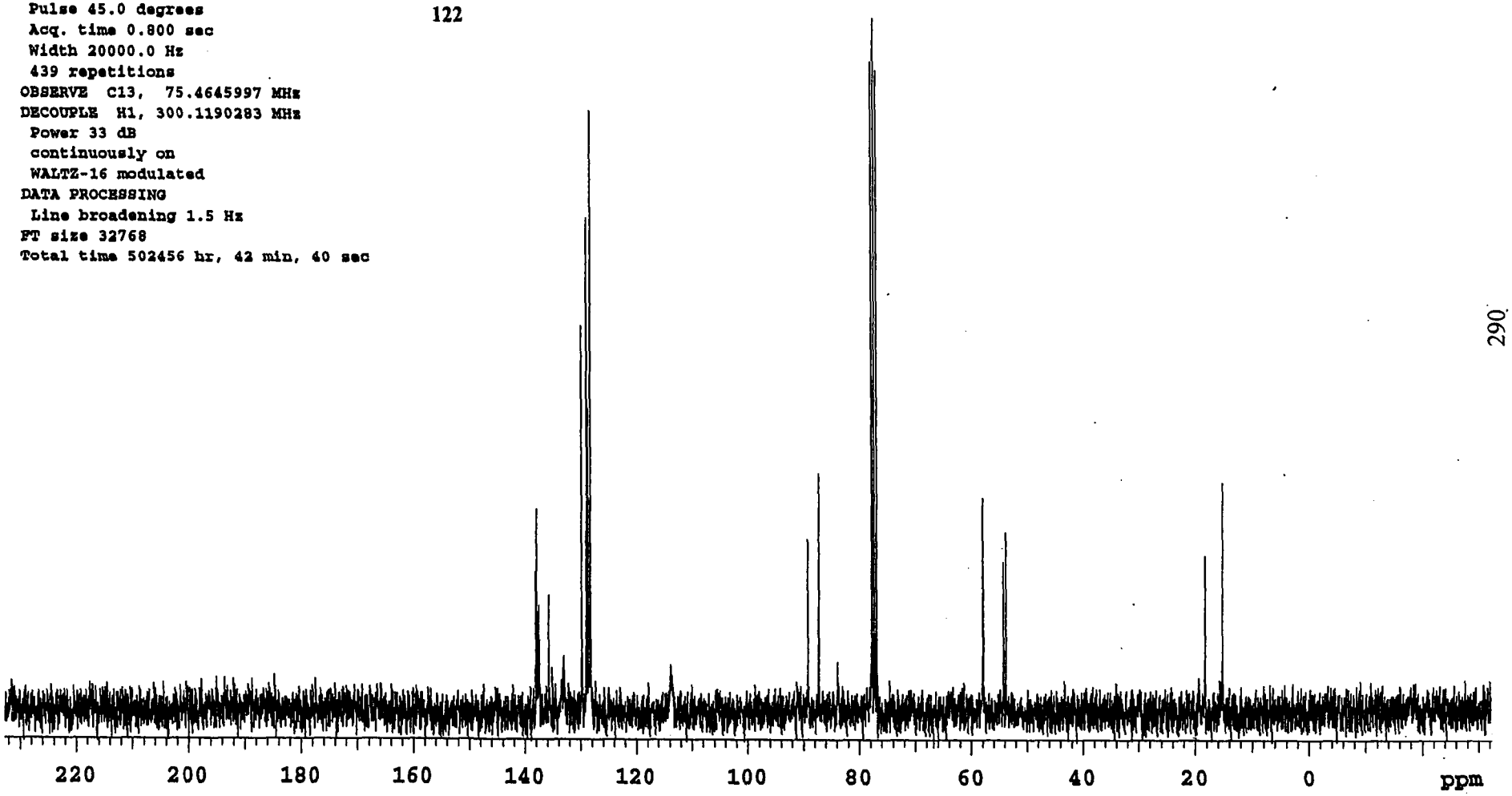

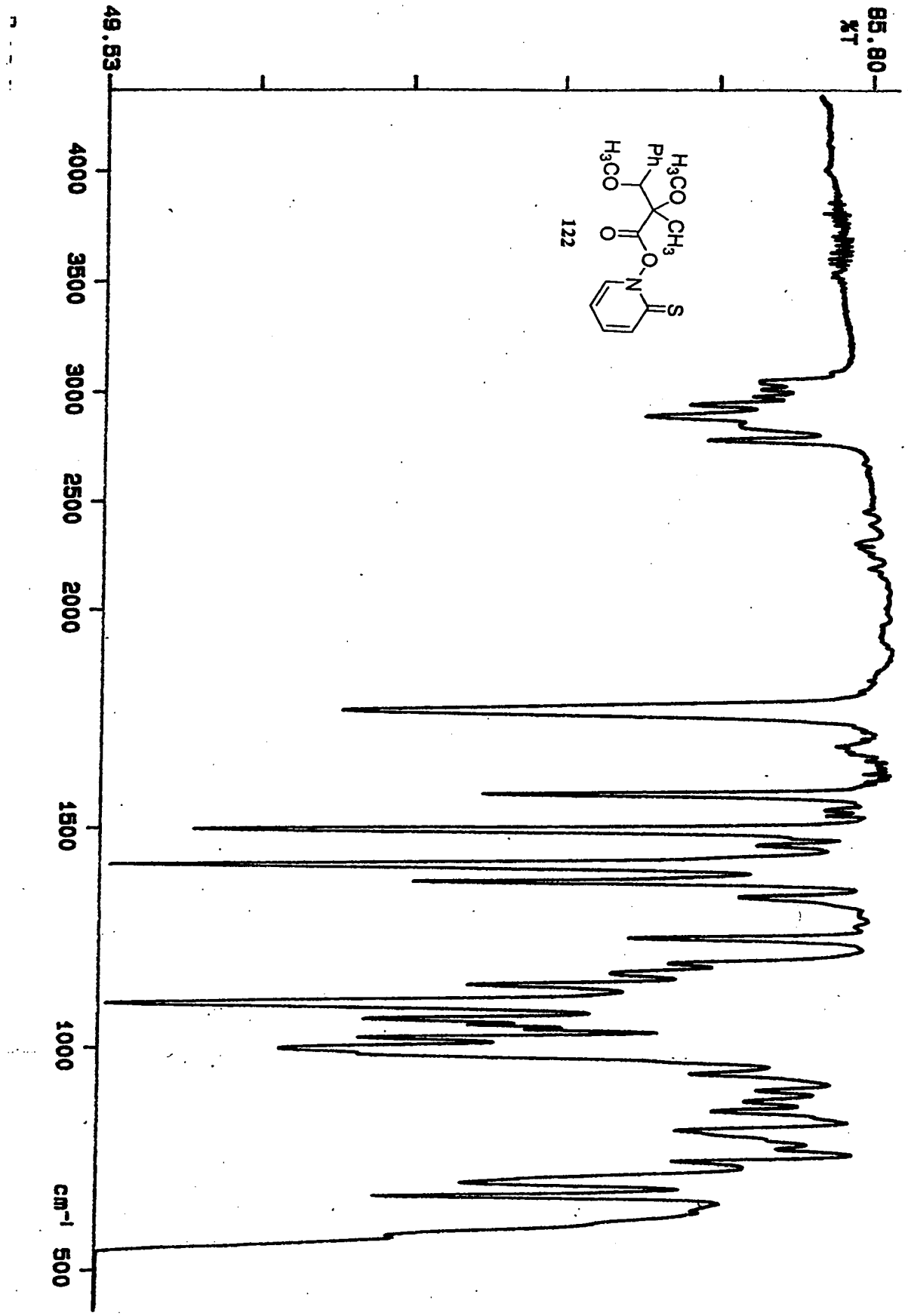

File:MG937 Ident:8_23 SMO(2,5) PKD(5,2,5,0.05%,0.0,33.00%,F,F) SPEC(Heights,Centroid) Acq:14-SEP-1999 15:03:54 +5:30 Ca>
AutoSpecE FAB+ Voltage BpM:327 BpI:2852267 TIC:8173339 Flags:NORM
File Text:B. Bales BCB 3038

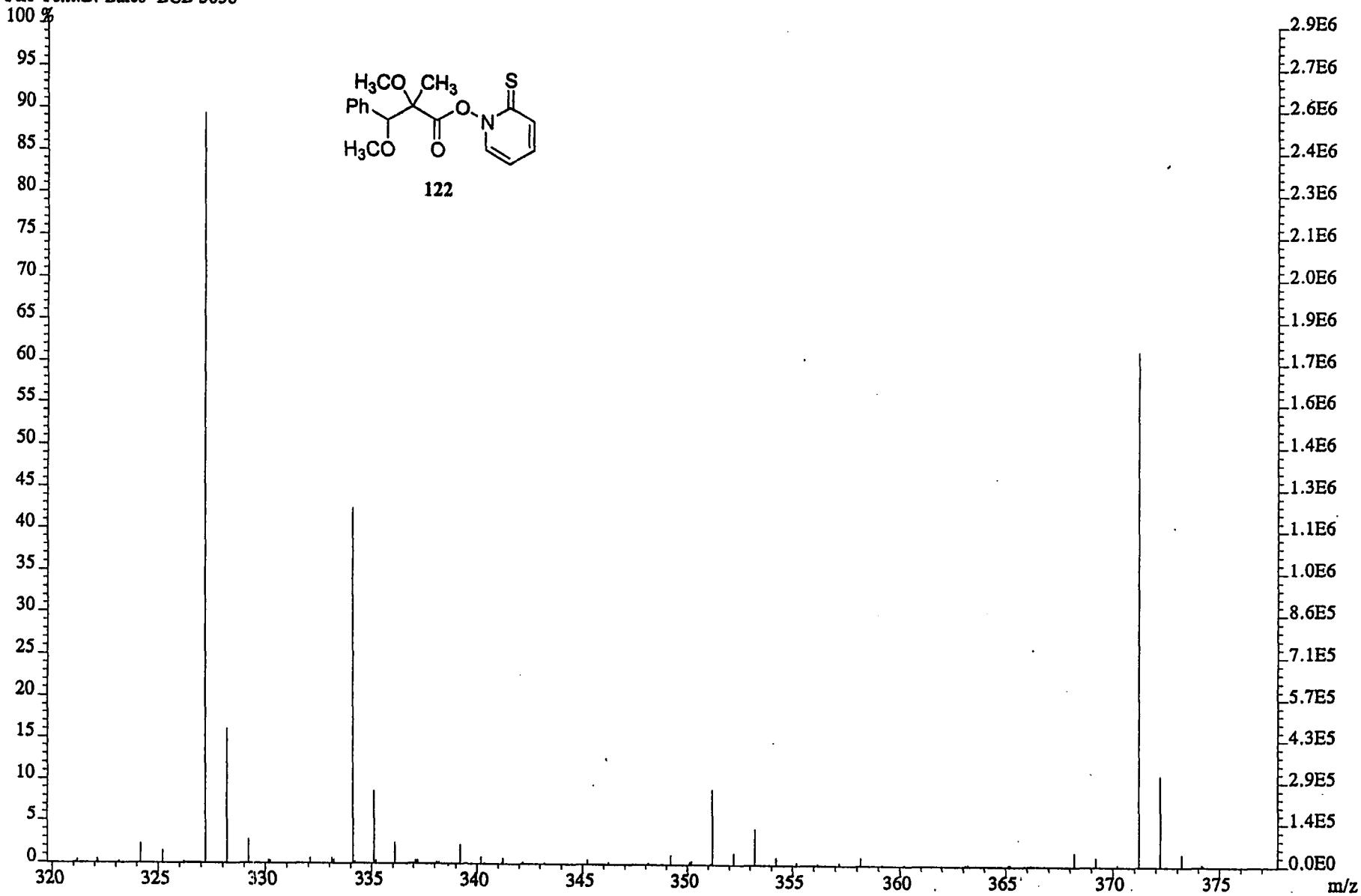

122

bcb3117

Solvent: CDCl3
Ambient temperature
File: bcb3117
INOVA-500 "greenberg"

PULSE SEQUENCE
Pulse 30.0 degrees
Acq. time 2.667 sec
Width 6000.0 Hz
16 repetitions
OBSERVE H1, 300.1559753 MHz
DATA PROCESSING
Sq. sine bell 2.667 sec
Shifted by -2.667 sec
FT size 32768
Total time 1 minute

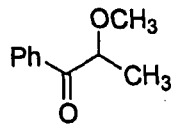

128

bcb3117c13

Solvent: CDCl3
Ambient temperature
File: bcb3117c13
INOVA-500 "greenberg"

PULSE SEQUENCE
Relax. delay 1.200 sec
Pulse 45.0 degrees
Acq. time 0.727 sec
Width 22000.0 Hz
18 repetitions
OBSERVE C13, 75.4742813 MHz
DECOUPLE H1, 300.1574402 MHz
Power 40 dB
continuously on
WALTZ-16 modulated
DATA PROCESSING
Line broadening 2.0 Hz
FT size 32768
Total time 1 minute

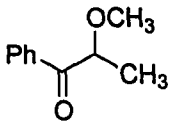

128

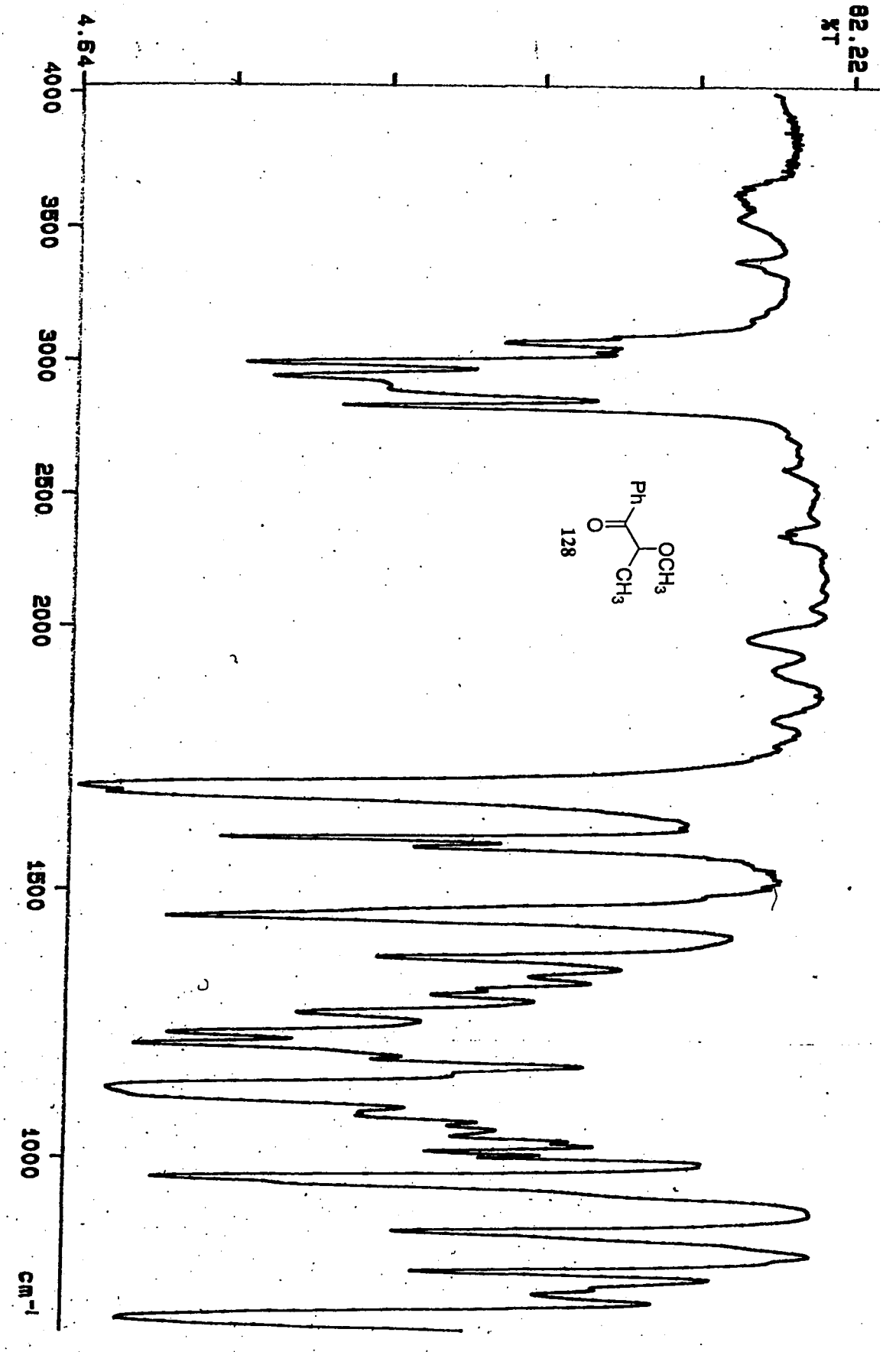

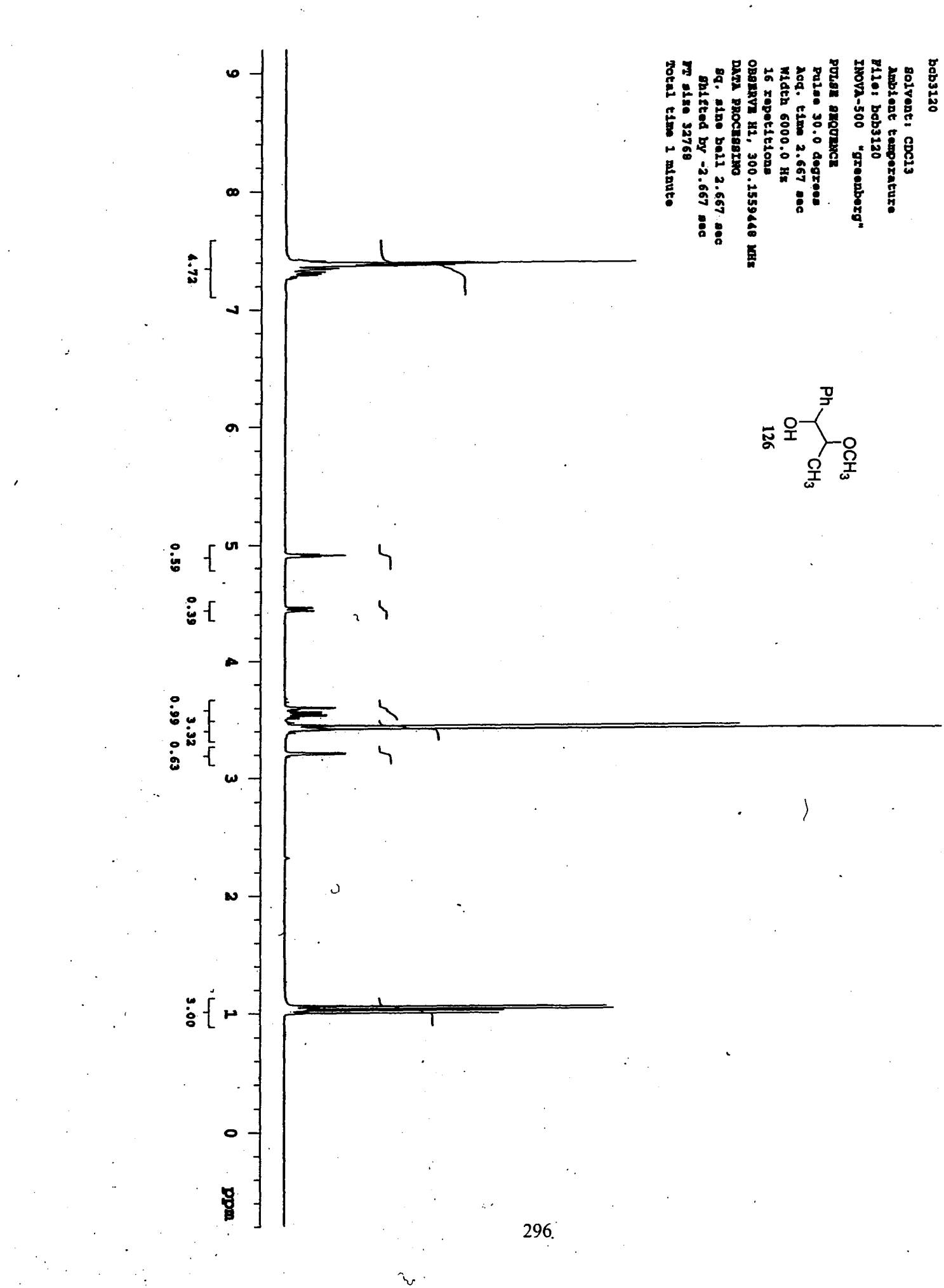

13C OBSERVE

Solvent: CDCl3
Ambient temperature
File: bcb3120c13
INOVA-500 "greenberg"

PULSE SEQUENCE
Relax. delay 1.200 sec
Pulse 45.0 degrees
Acq. time 0.727 sec
Width 22000.0 Hz
39 repetitions
OBSERVE C13, 75.4742813 MHz
DECOUPLE H1, 300.1574402 MHz
Power 40 dB
continuously on
WALTZ-16 modulated
DATA PROCESSING
Line broadening 2.0 Hz
FT size 32768
Total time 1 minute

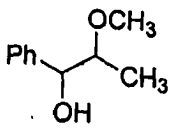

126

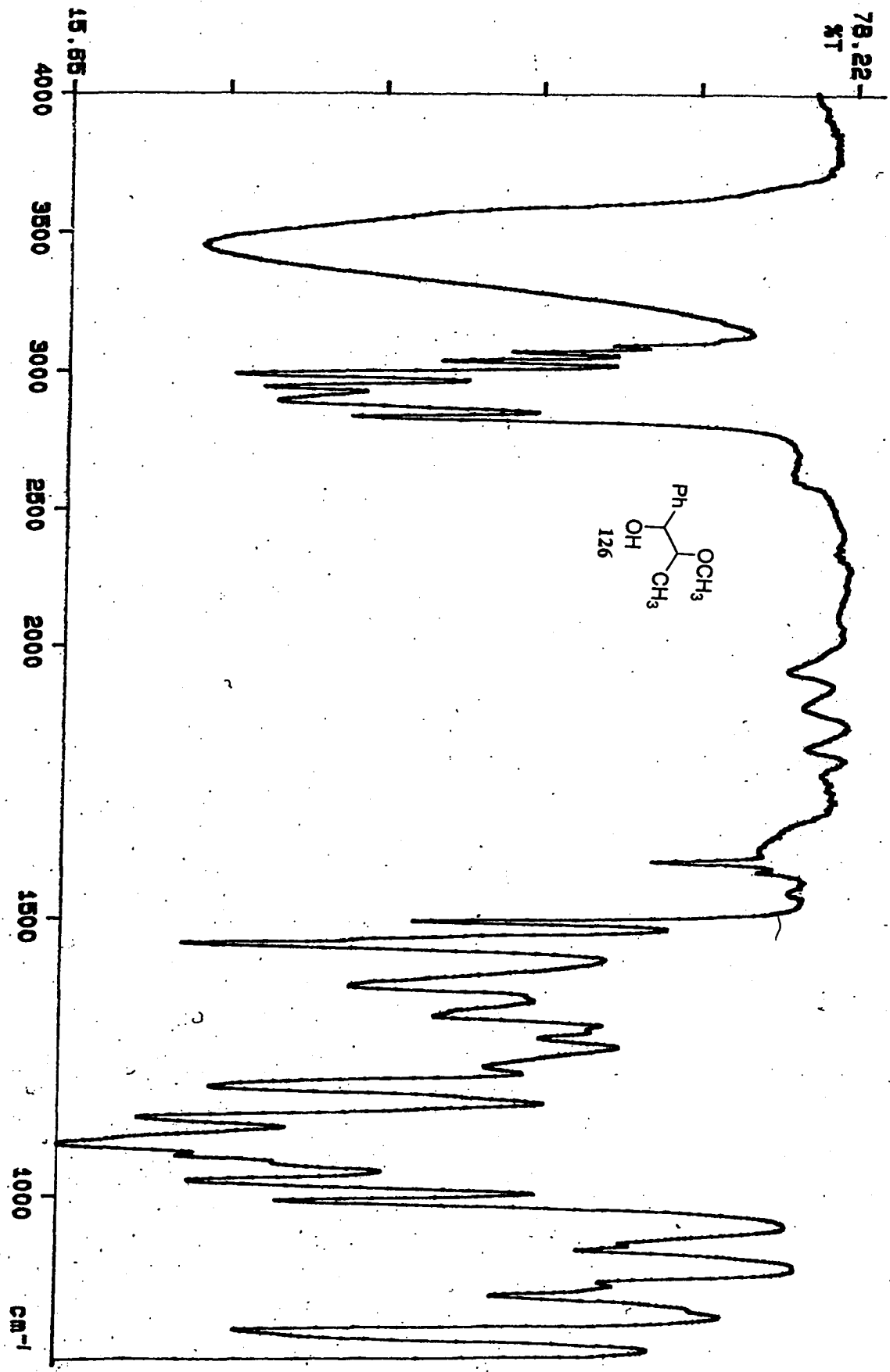

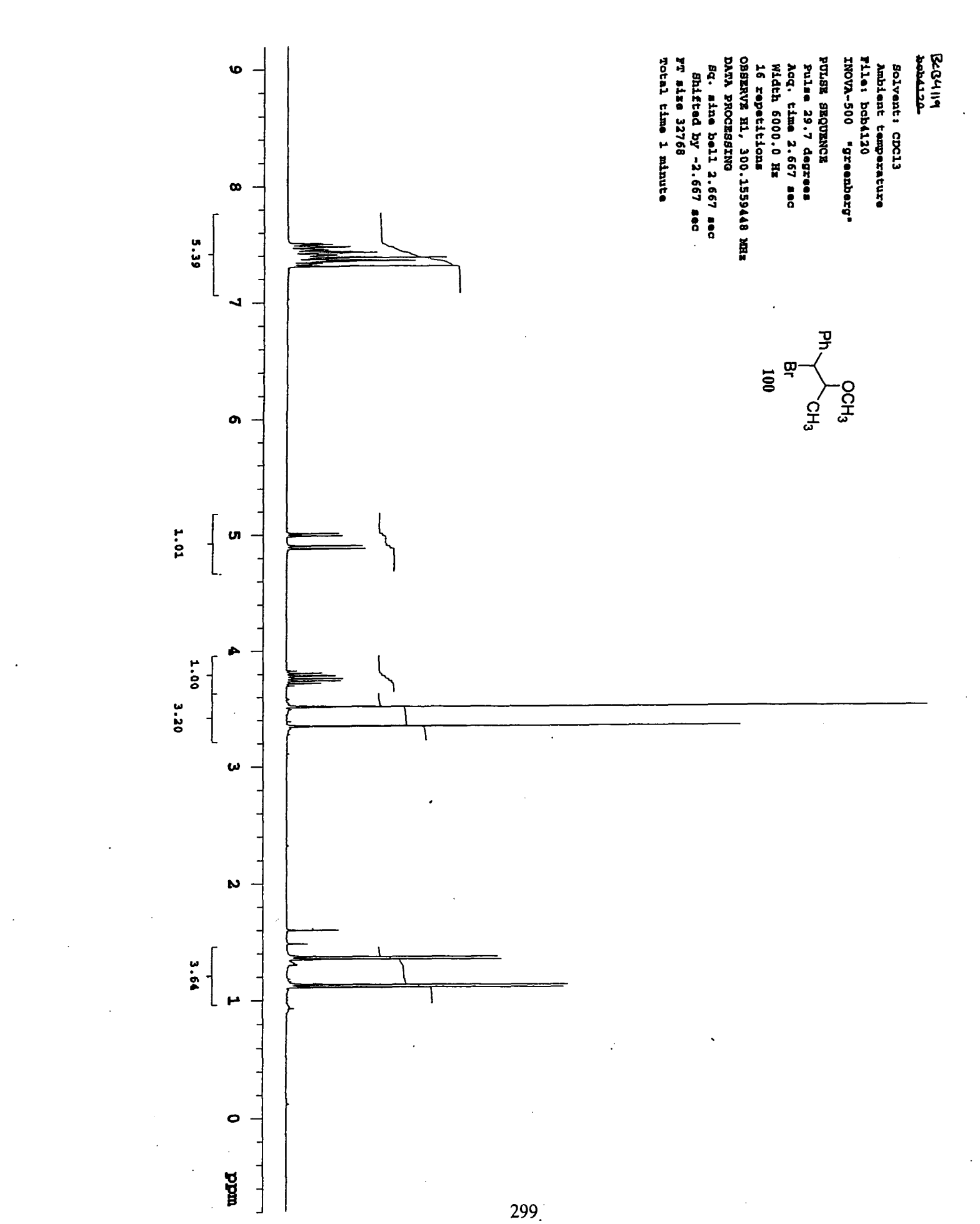

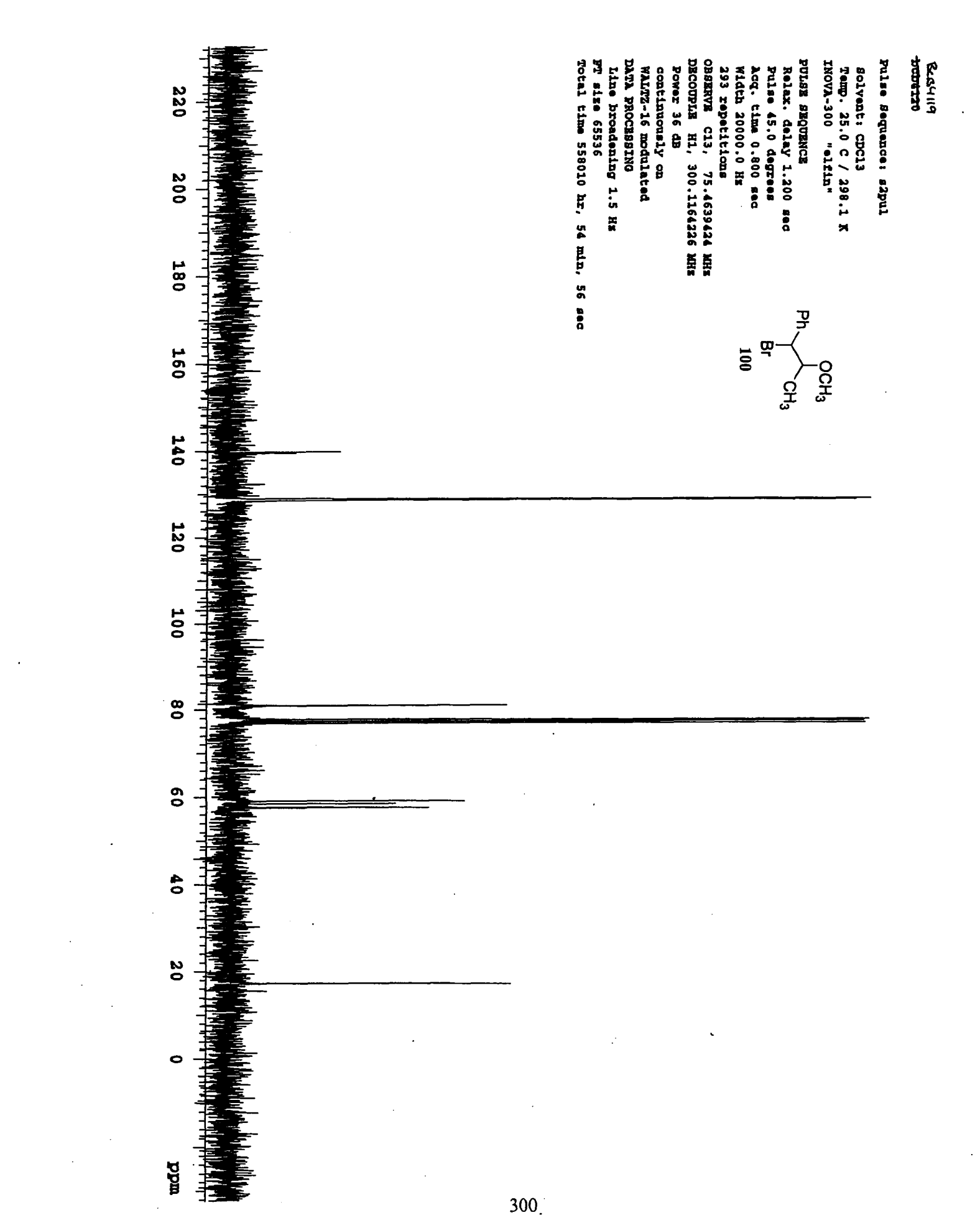

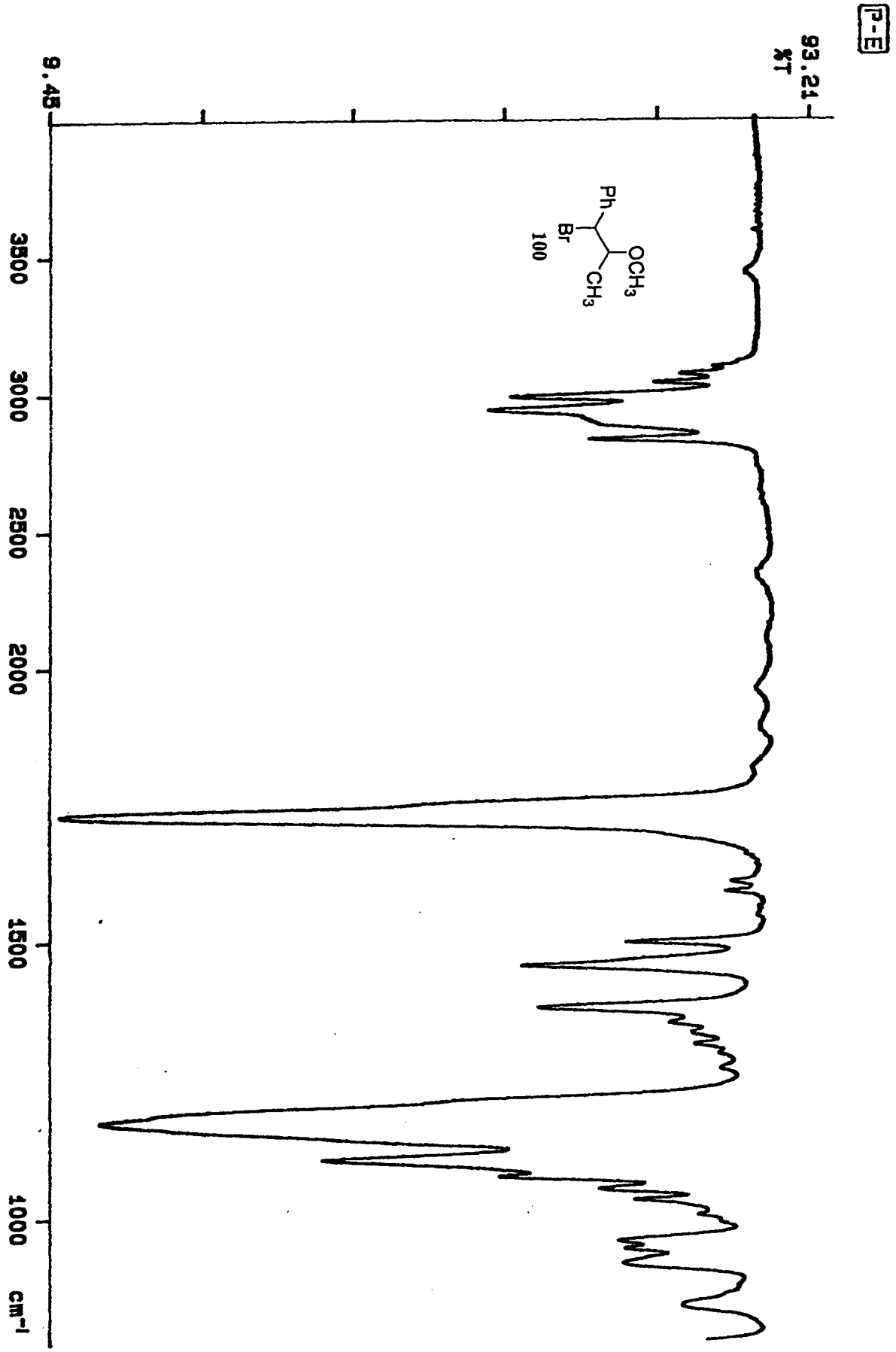

File:MG729 Ident:17 SMO(2,3) PKD(3,2,3,0.01%,0.0,33.00%,F,F) SPEC(Heights,Centroid) Acq:10-JUL-2000 09:59:43 +3:18 Cal:>
AutoSpecE EI+ Voltage BpM:219 BpI:2811647 TIC:17088286 Flags:NORM
File Text:B. Bales BCB 4138

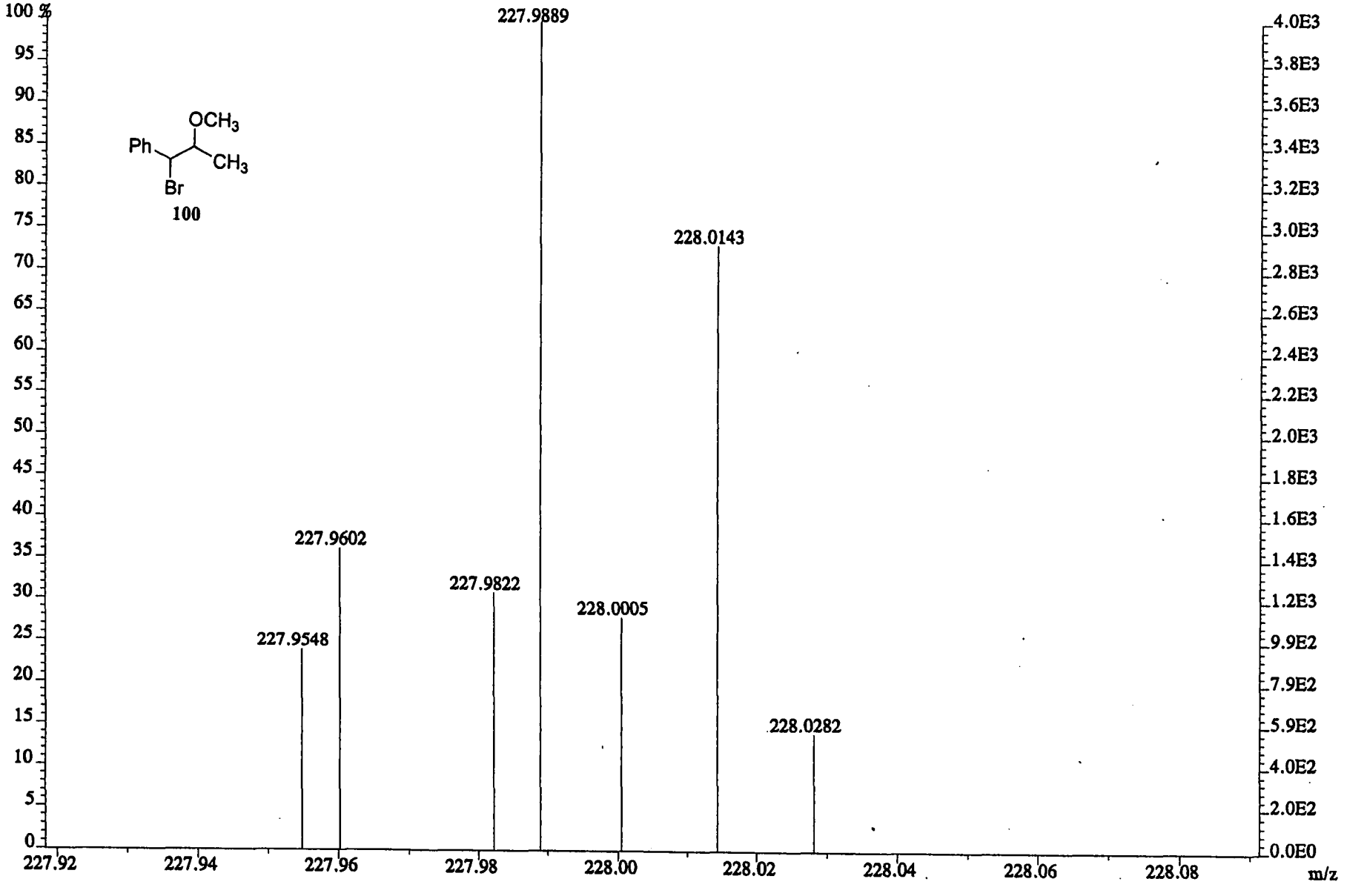

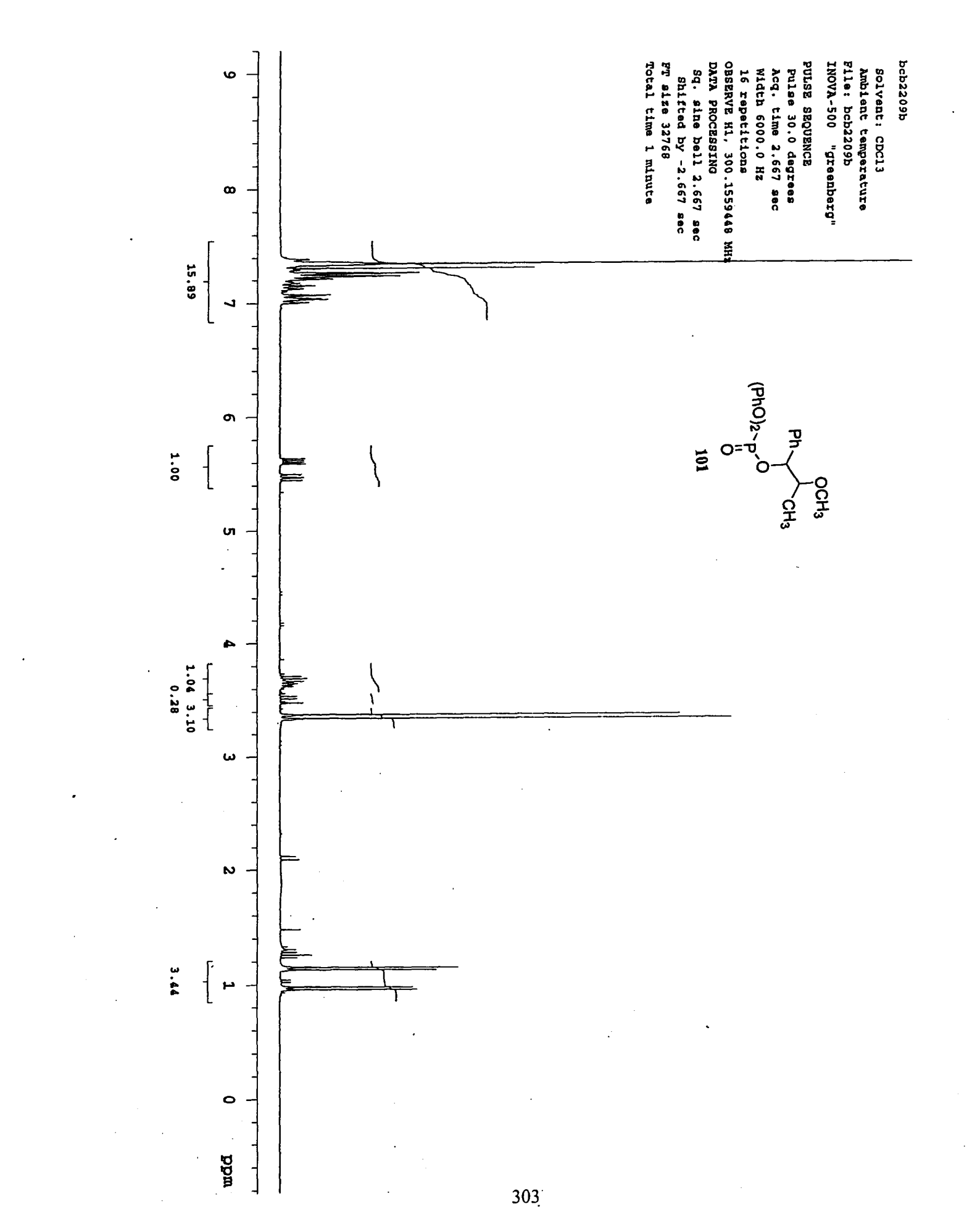

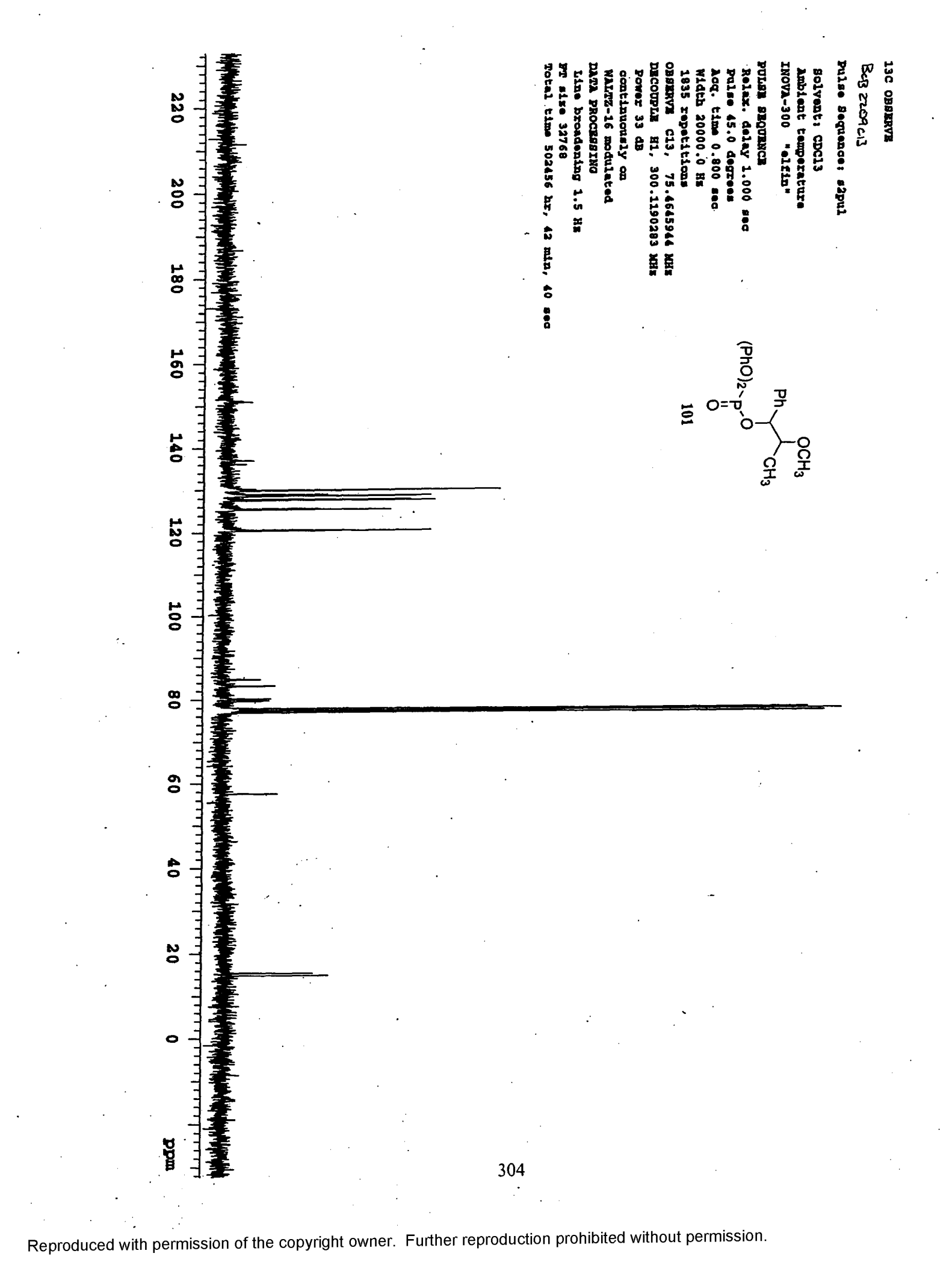

P-31 STANDARD PARAMETERS
PHOSPHATE REGION
BCG2209P31
Pulse Sequence: s2pul

Solvent: CDCl3
Ambient temperature
INOVA-300 "elfin"

PULSE SEQUENCE
Relax. delay 1.000 sec
Pulse 25.0 degrees
Acq. time 0.525 sec
Width 24806.2 Hz
456 repetitions
OBSERVE P31, 121.4897252 MHz
DECOUPLE H1, 300.1190283 MHz
Power 38 dB
continuously on
WALTZ-16 modulated
DATA PROCESSING
Line broadening 1.0 Hz
FT size 32768
Total time 26 min, 13 sec

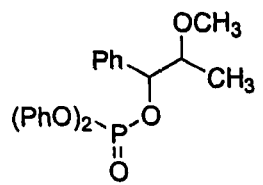

101

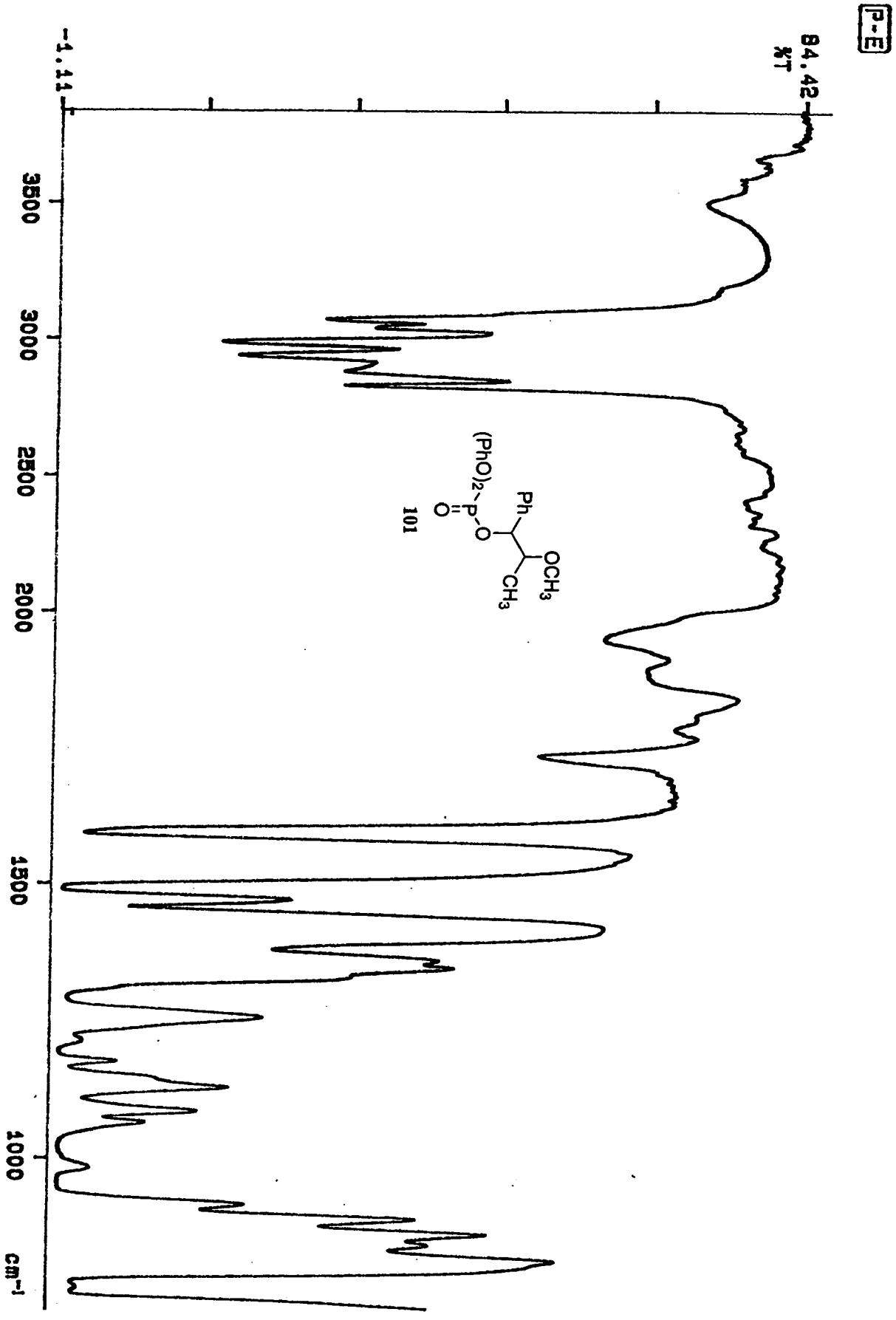

File:MGO11 Ident:2_16 SMO(2,5) PKD(5,2,5,0.05%,0.0,33.00%,F,F) SPEC(Heights,Centroid) Acq:28-SEP-2000 17:03:05 +3:07 Ca>
AutoSpecE EI+ Voltage BpM:150 BpI:36467388 TIC:163496848 Flags:NORM
File Text:B. Bales BCB 1092

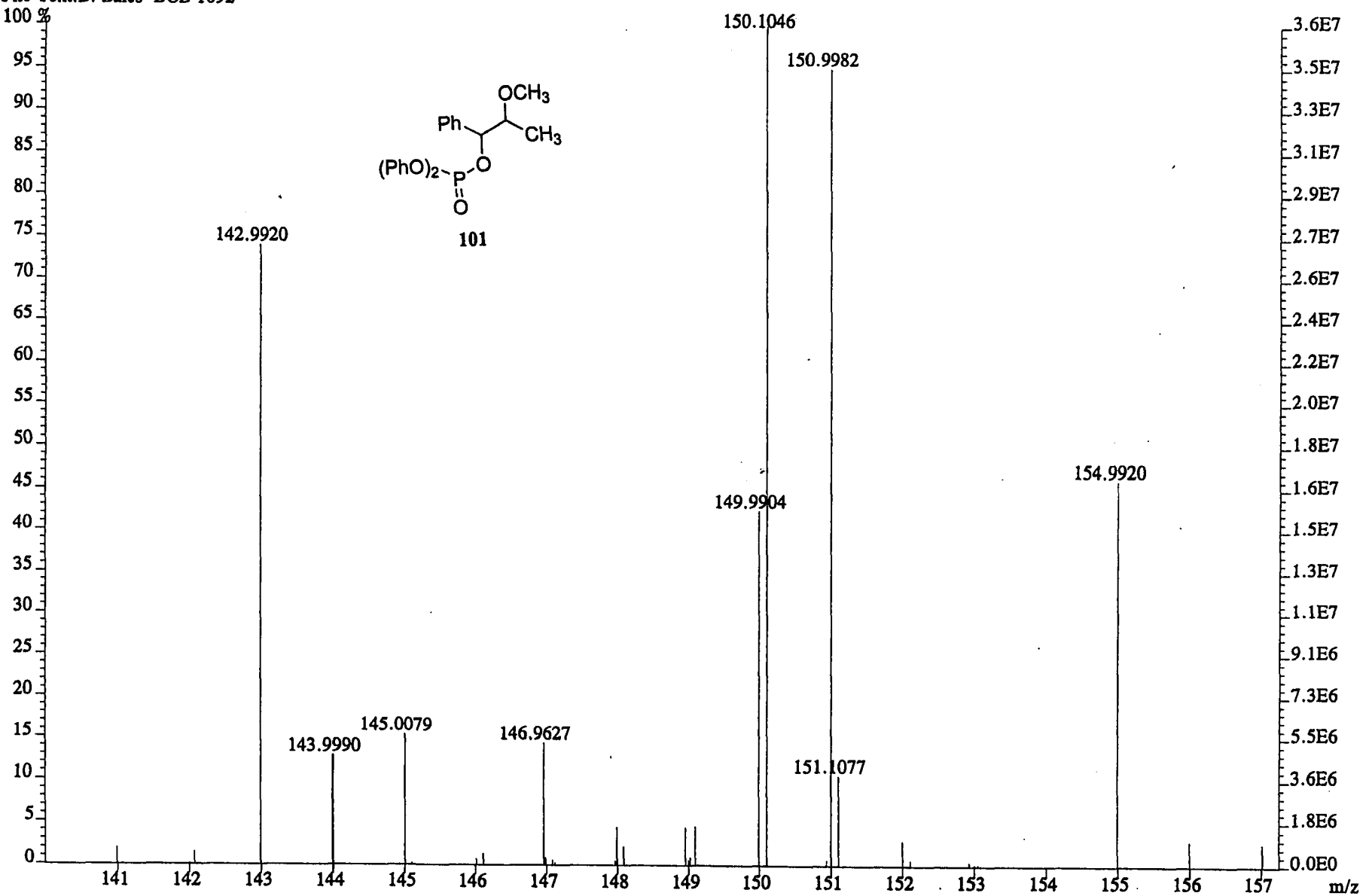

307.

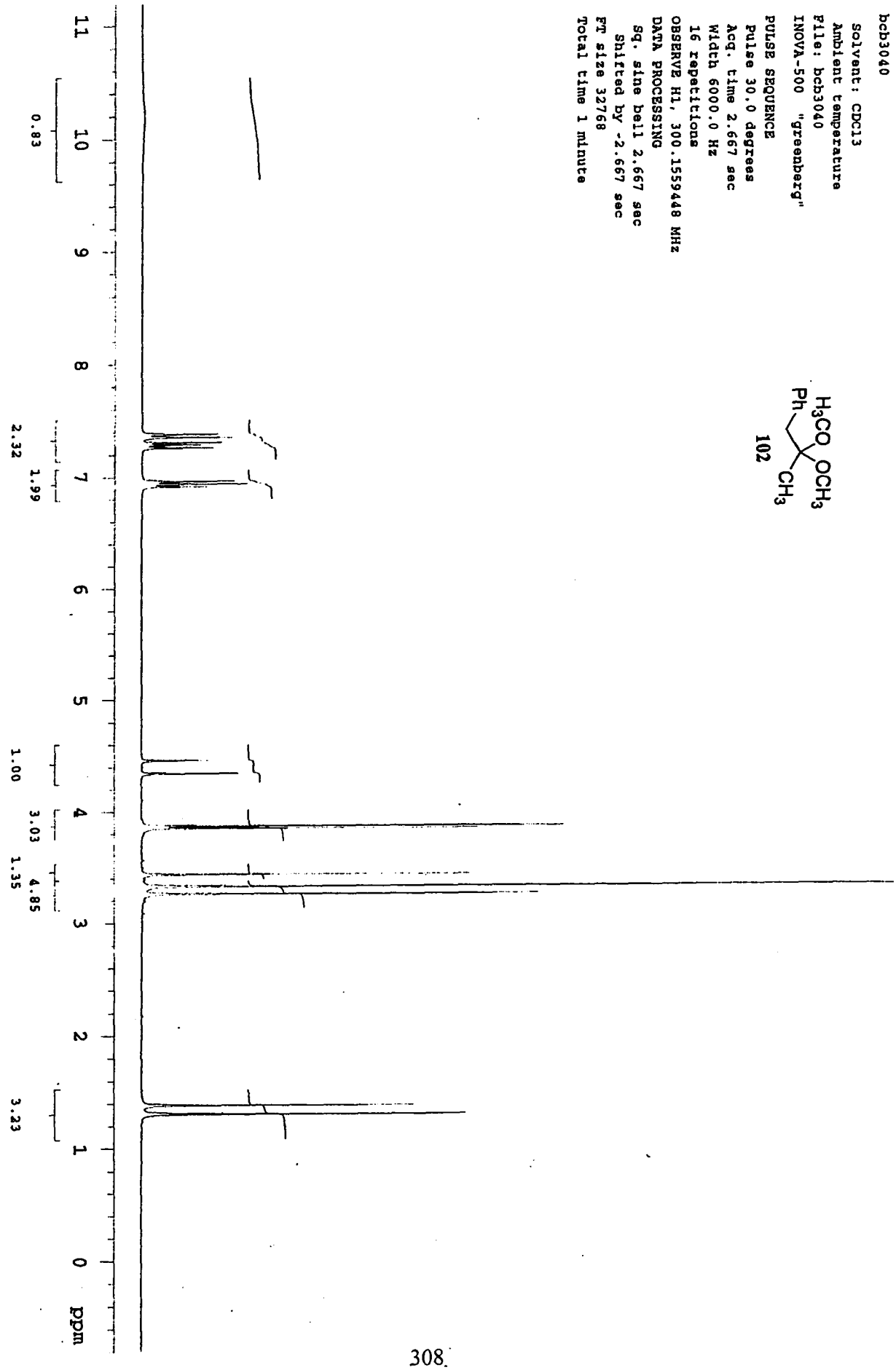

bcb3040c13

Solvent: CDCl3
Ambient temperature
File: bcb3040c13
INOVA-500 "greenberg"

PULSE SEQUENCE
Relax. delay 1.200 sec
Pulse 45.0 degrees
Acq. time 0.727 sec
Width 22000.0 Hz
193 repetitions
OBSERVE C13, 75.4746170 MHz
DECOUPLE H1, 300.1574402 MHz
Power 40 dB
continuously on
WALTZ-16 modulated
DATA PROCESSING
Line broadening 2.0 Hz
FT size 32768
Total_time 6 minutes

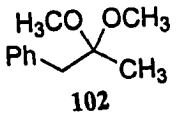

102

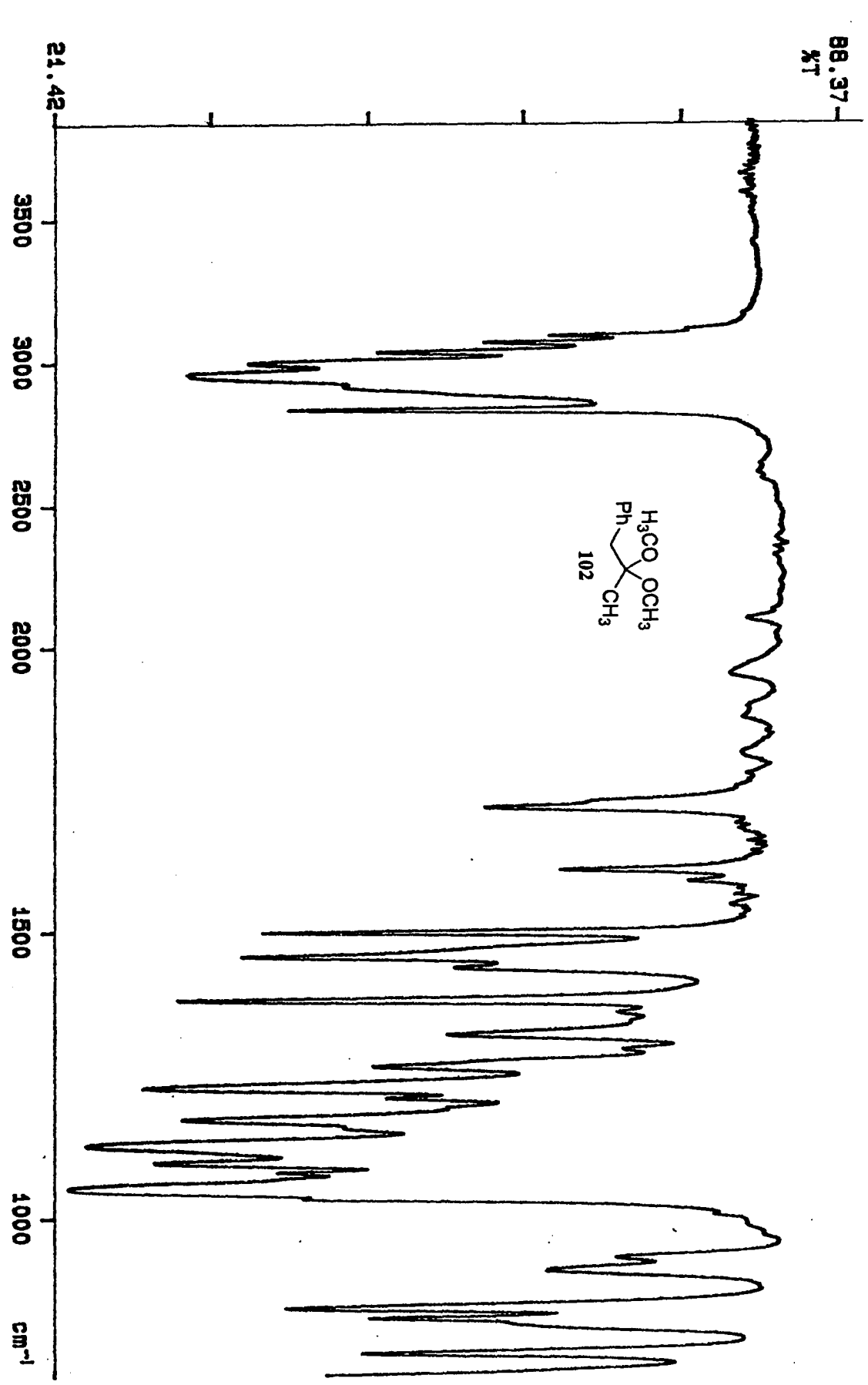

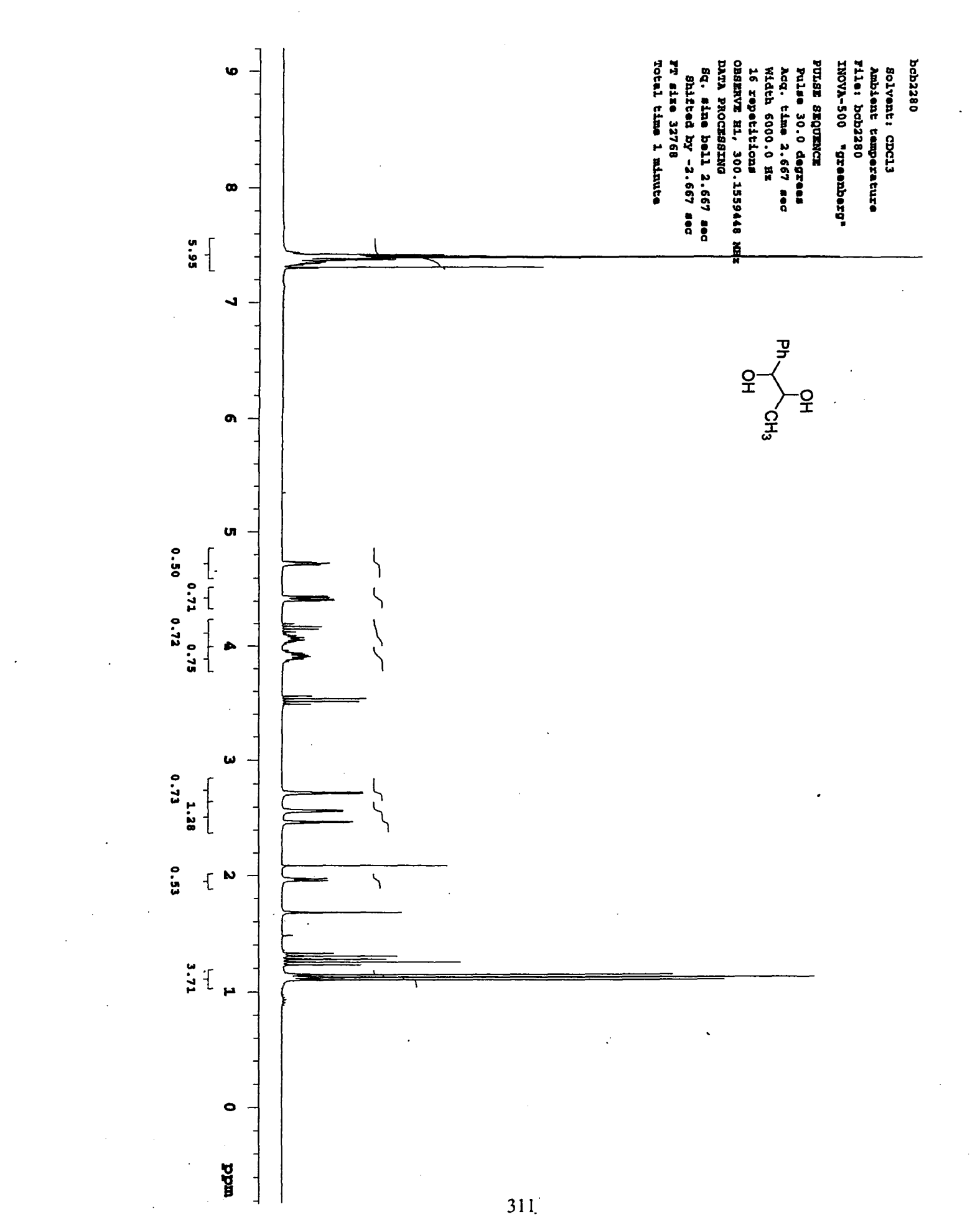

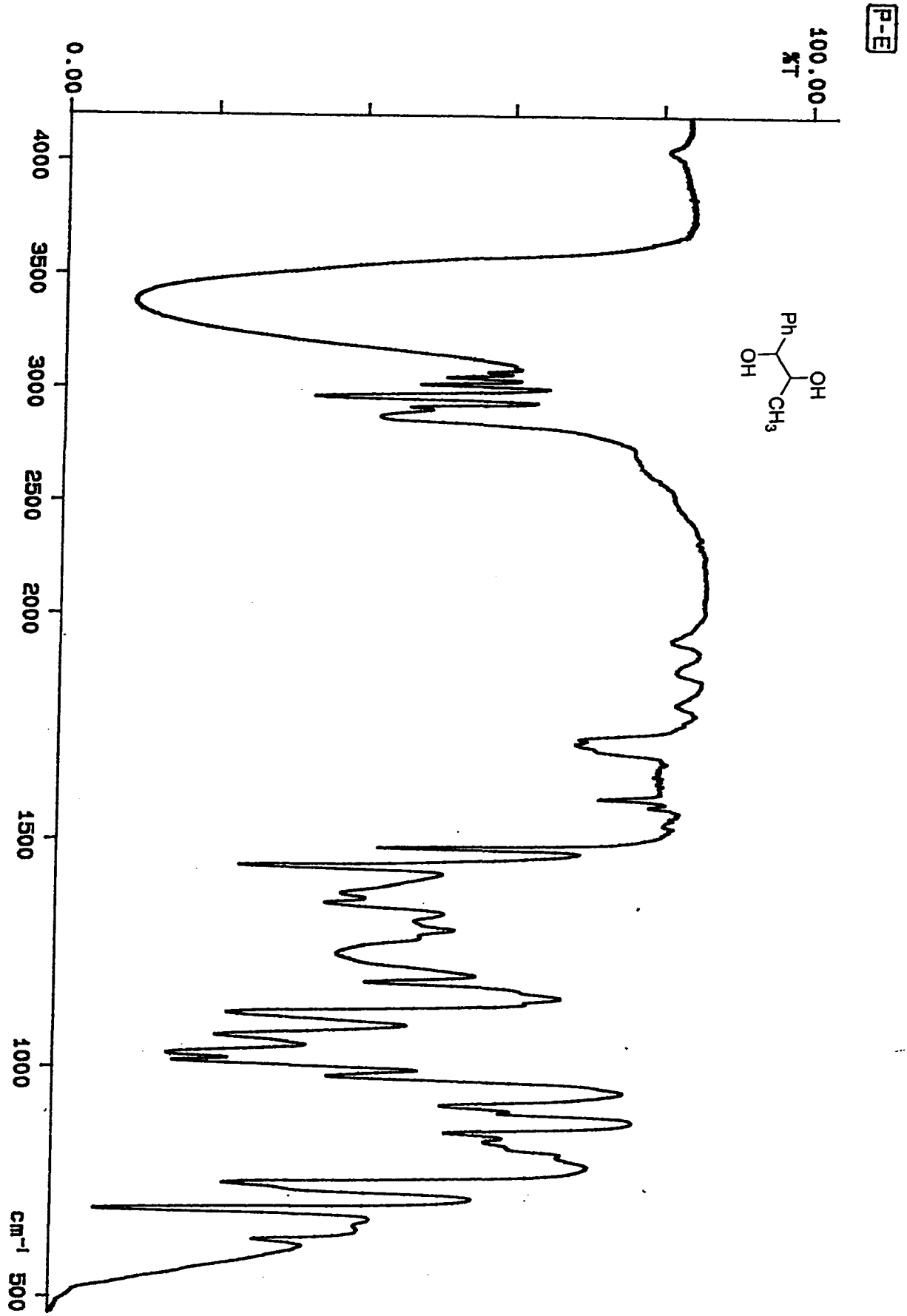

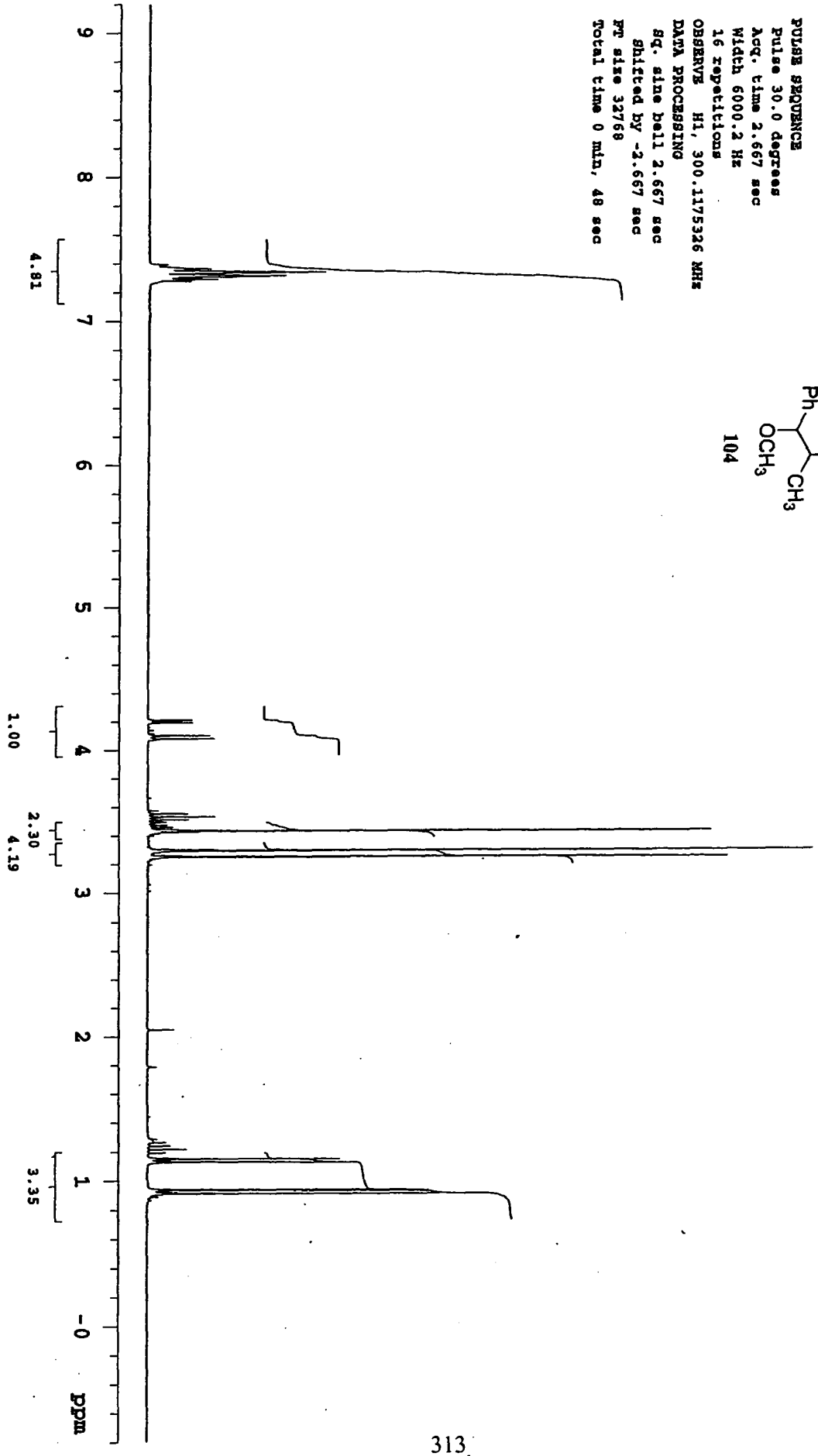

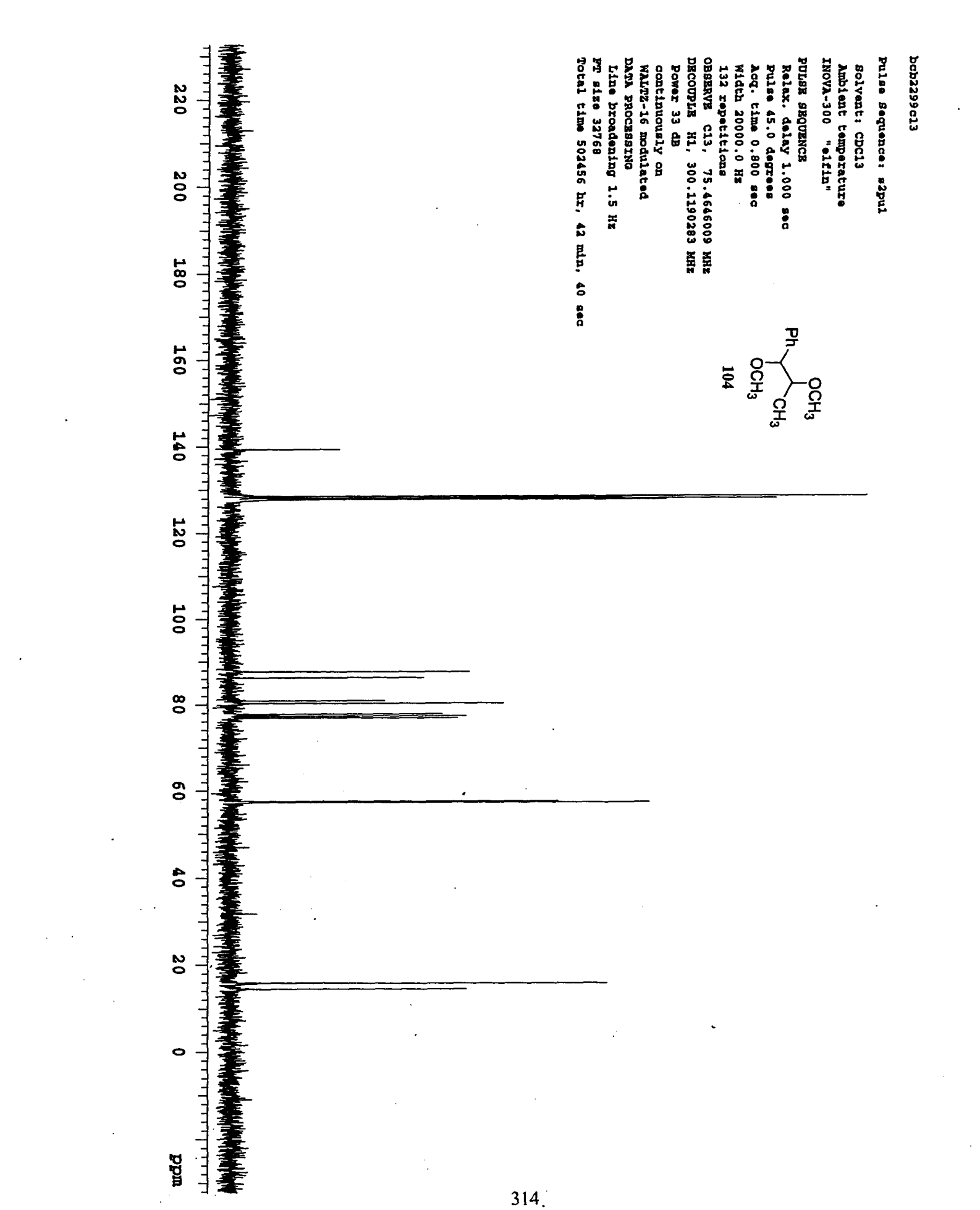

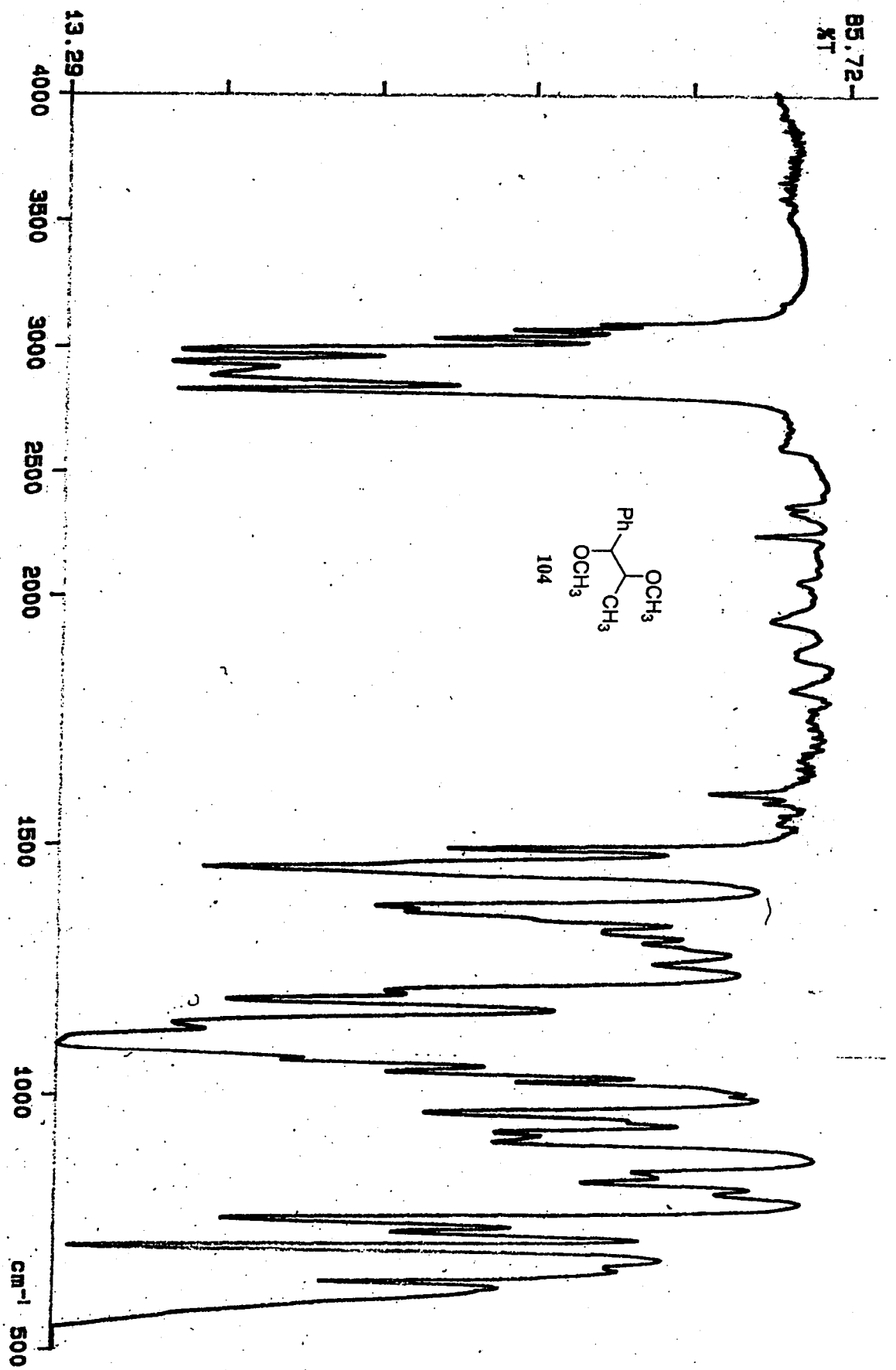

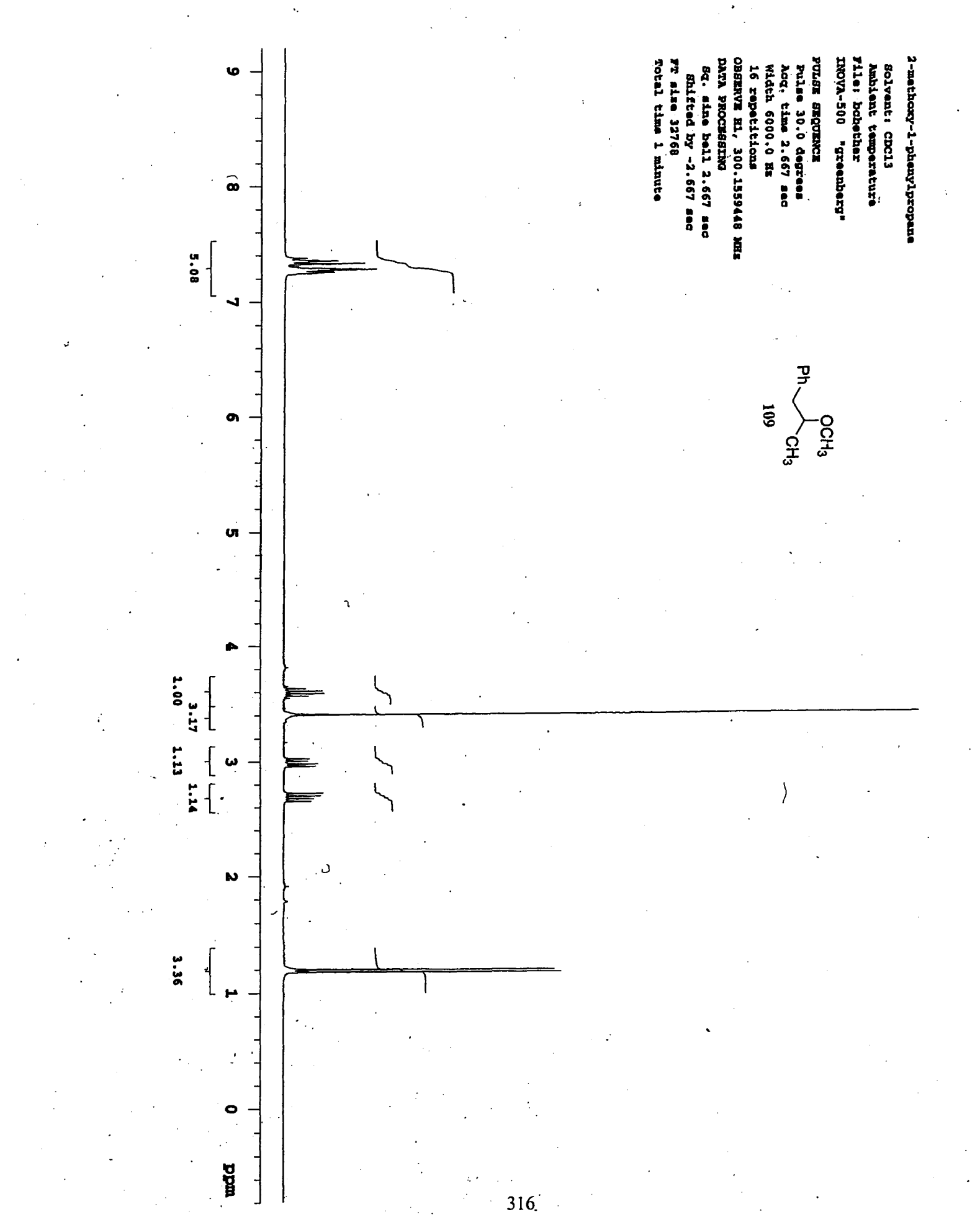

2-methoxy-1-phenylpropane

Solvent: CDCl3
Ambient temperature
File: bcbetherc13
INOVA-500 "greenberg"

PULSE SEQUENCE
Relax. delay 1.200 sec
Pulse 45.0 degrees
Acq. time 0.727 sec
Width 22000.0 Hz
128 repetitions
OBSERVE C13, 75.4742661 MHz
DECOUPLE H1, 300.1574402 MHz
Power 40 dB
continuously on
WALTZ-16 modulated
DATA PROCESSING
Line broadening 2.0 Hz
FT size 32768
Total time 4 minutes

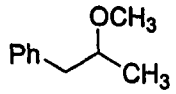

109

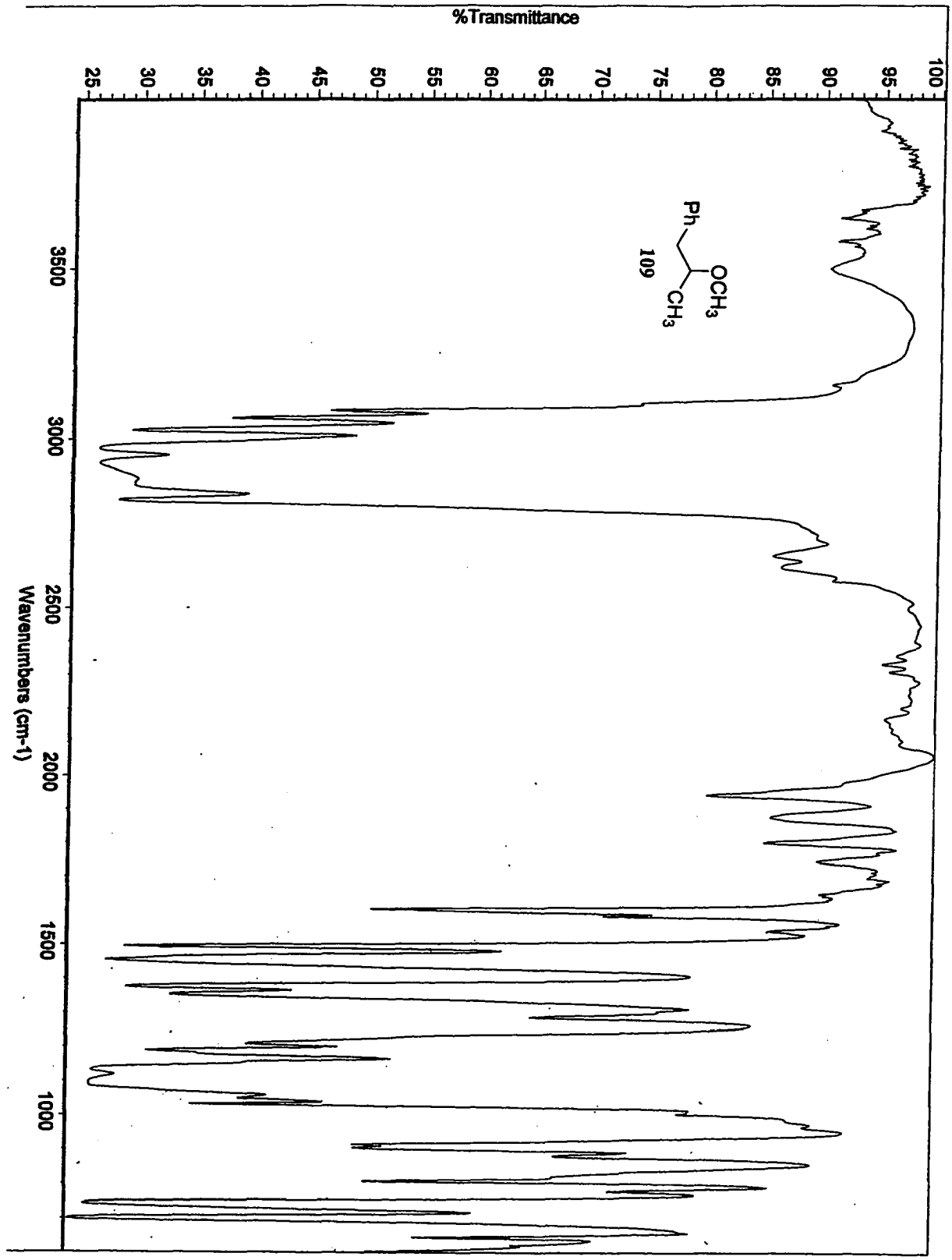

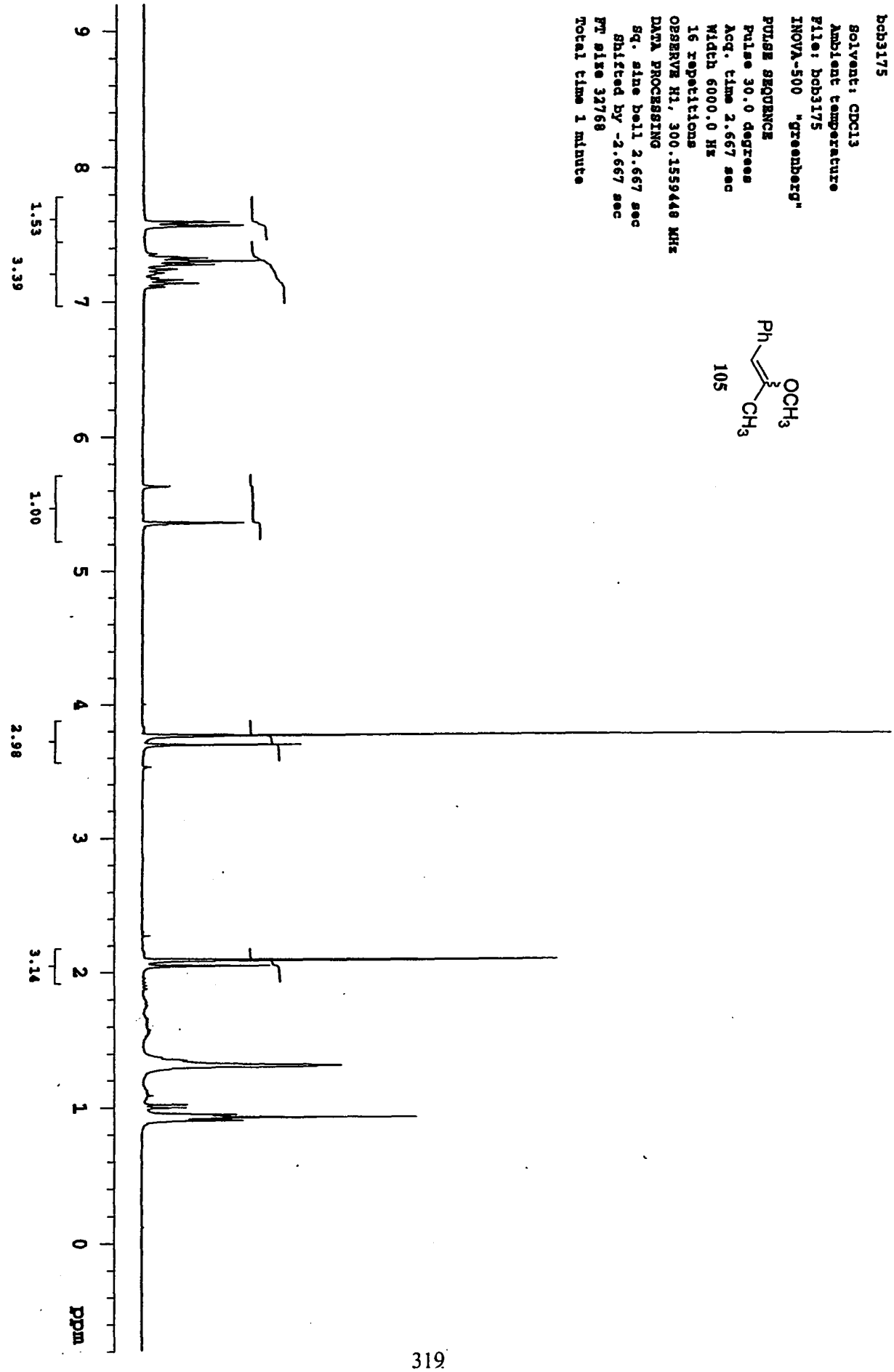

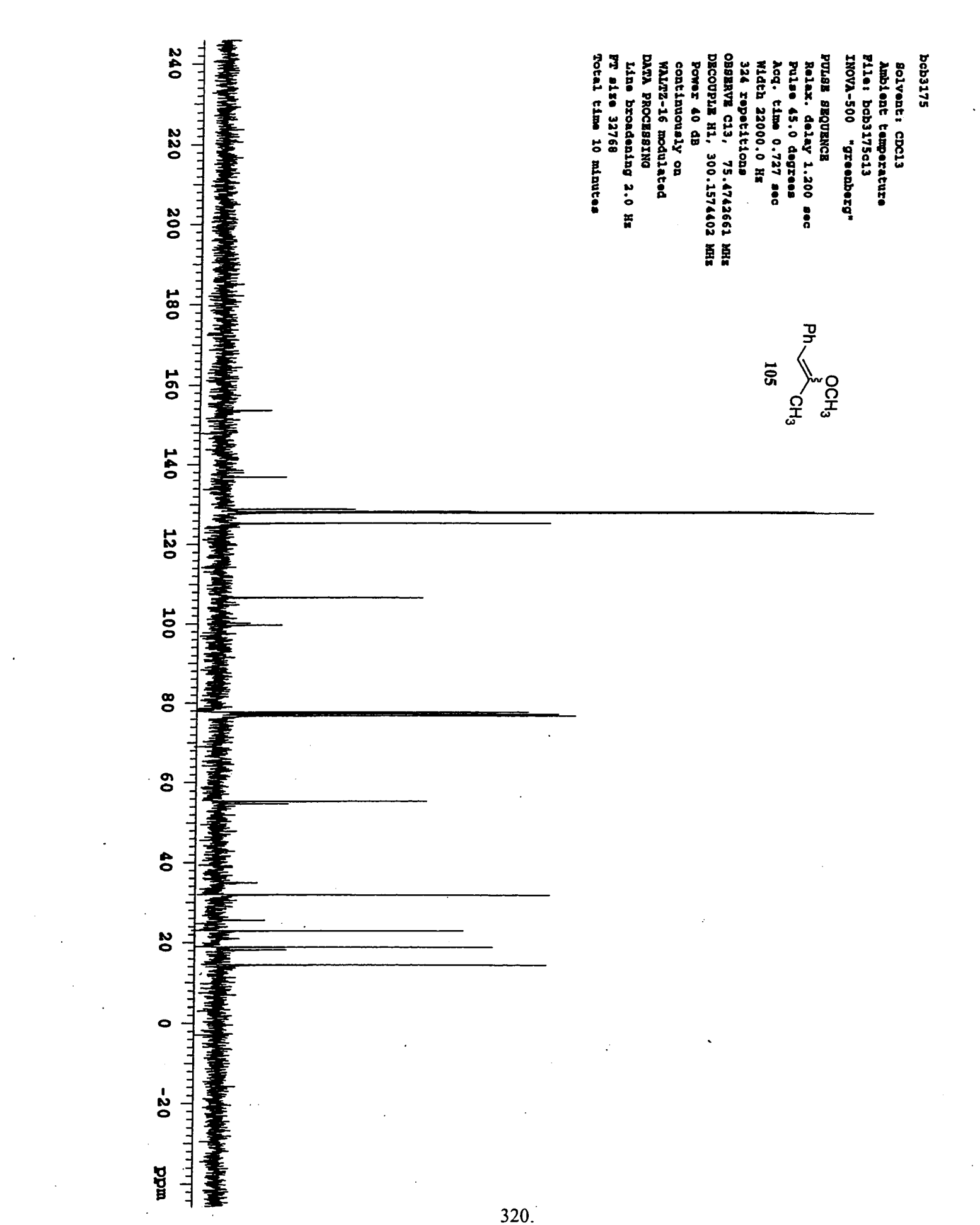

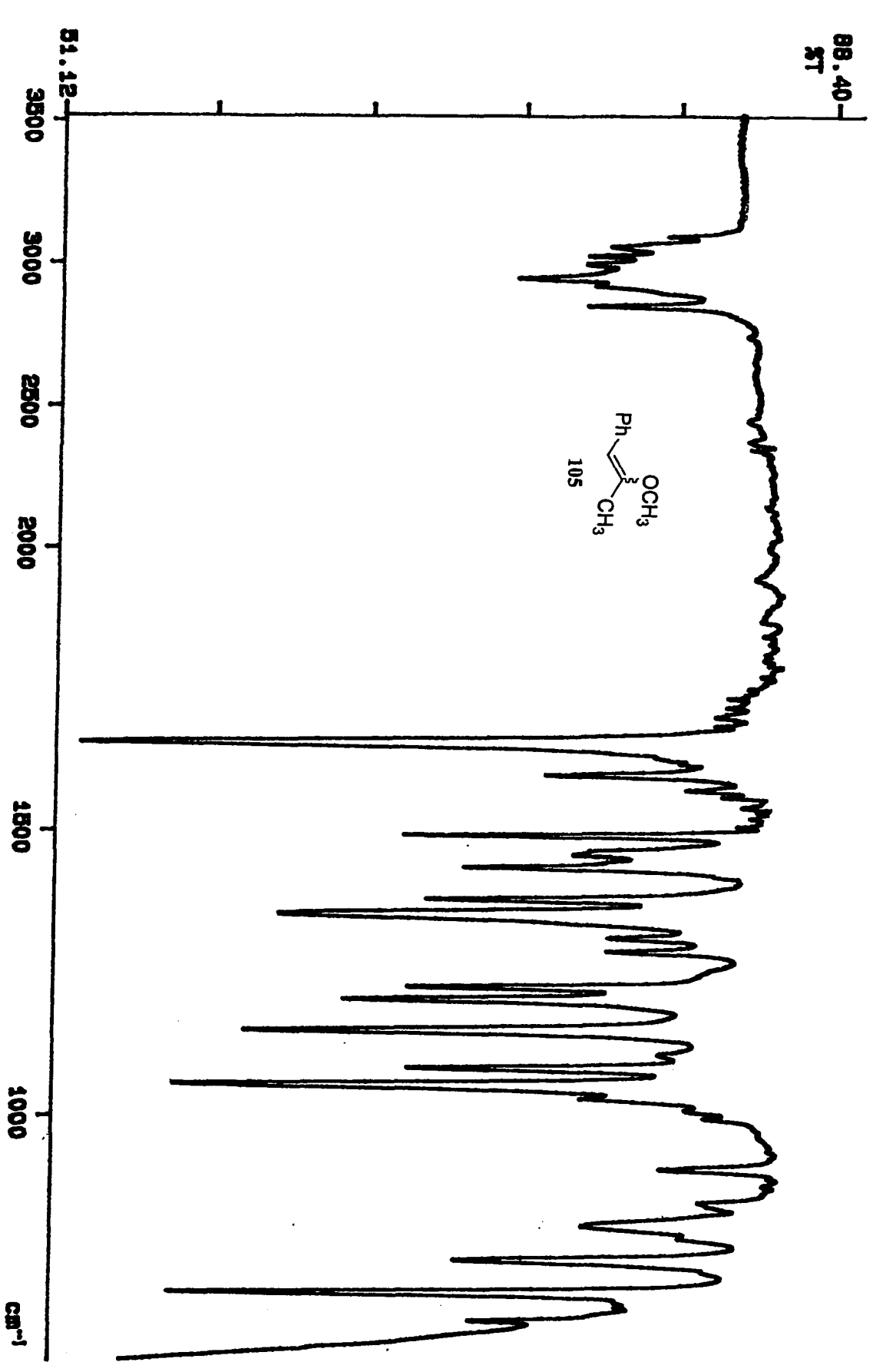

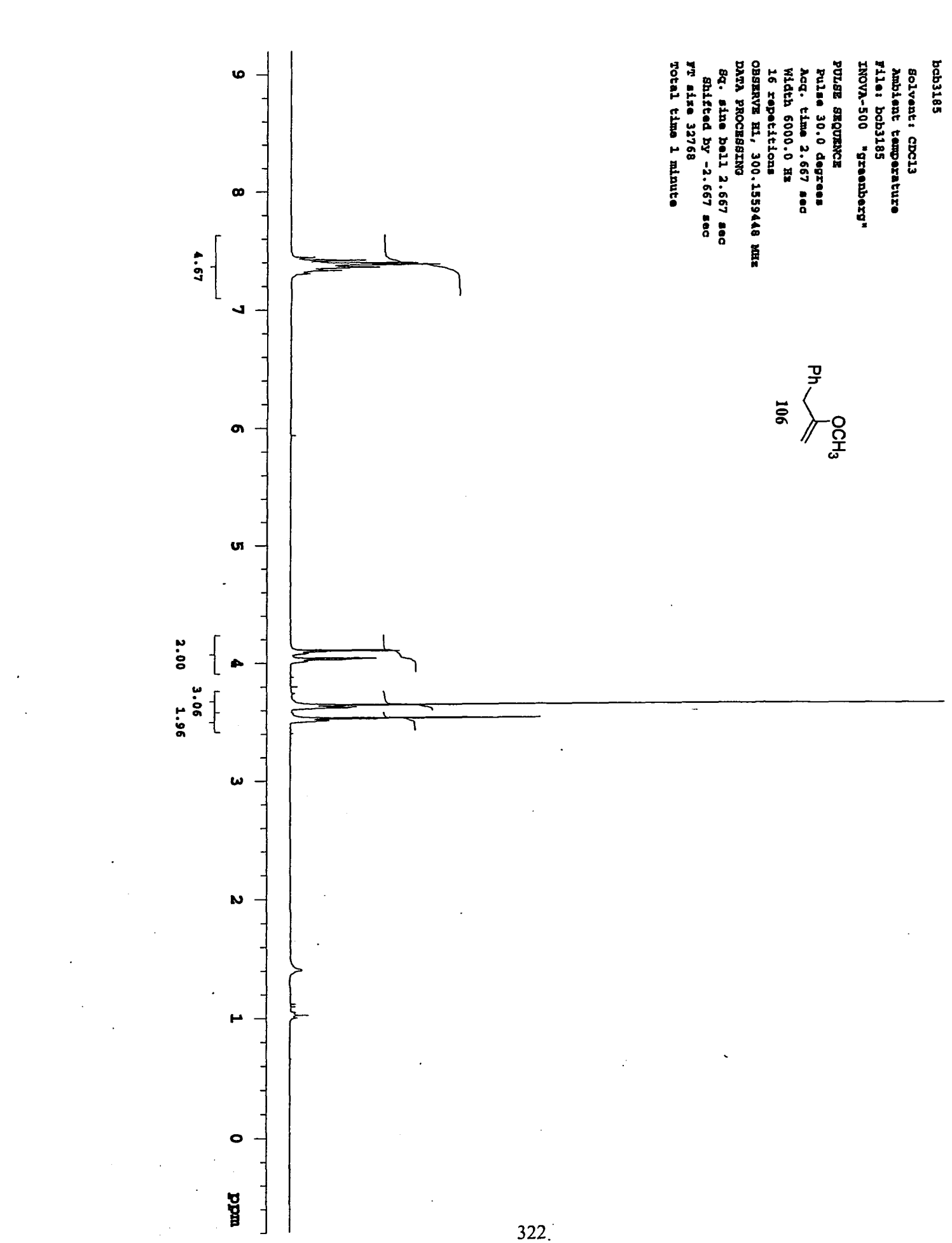

bcb3185c13

Solvent: CDCl3
Ambient temperature
File: bcb3185c13
INOVA-500 "greenberg"

PULSE SEQUENCE
Relax. delay 1.200 sec
Pulse 45.0 degrees
Acq. time 0.727 sec
Width 22000.0 Hz
48 repetitions
OBSERVE C13, 75.4742661 MHz
DECOUPLE H1, 300.1574402 MHz
Power 40 dB
continuously on
WALTZ-16 modulated
DATA PROCESSING
Line broadening 2.0 Hz
FT size 32768
Total time 1 minutes

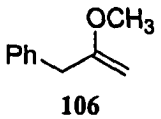

106

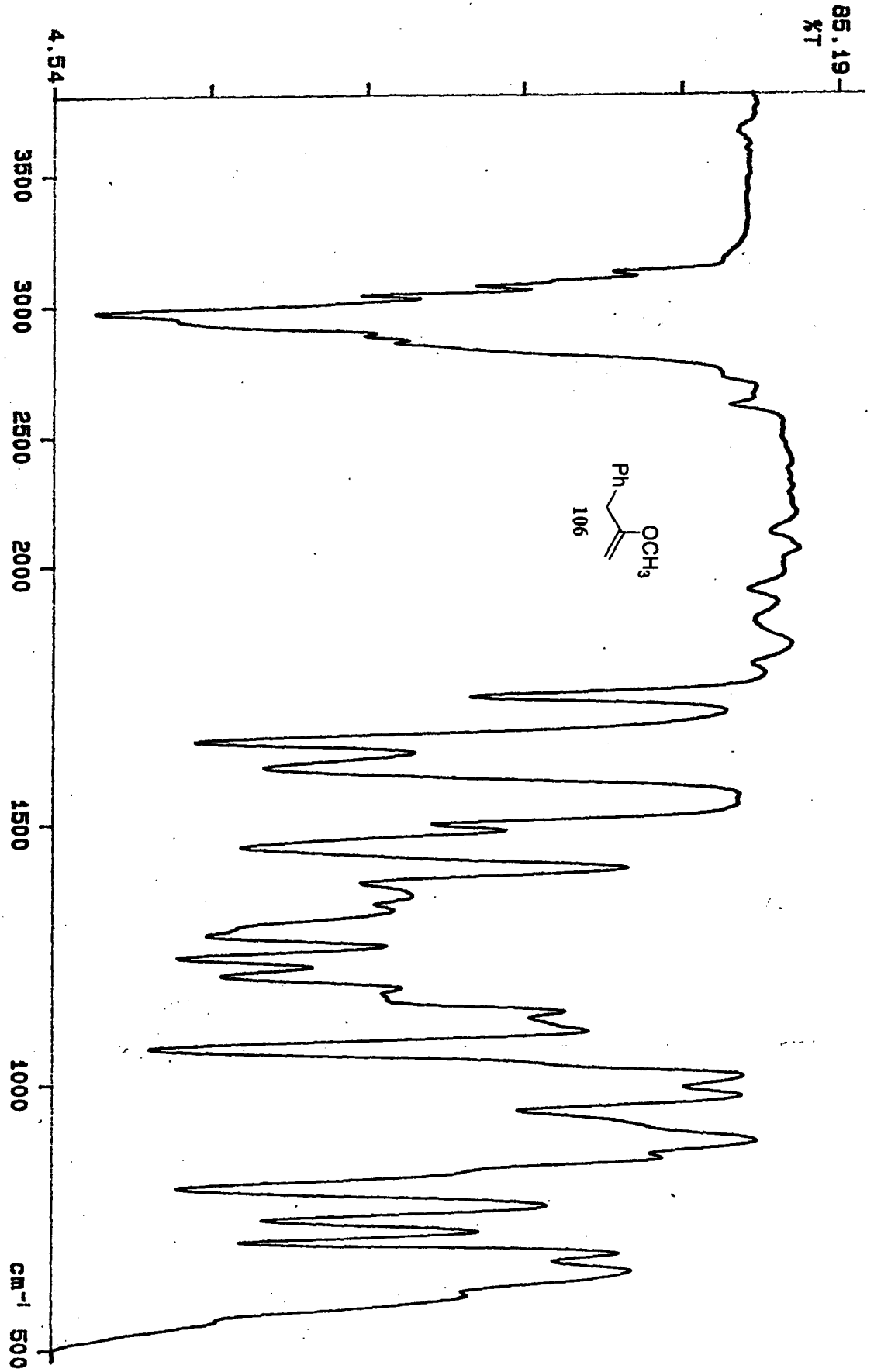

Appendix C:

Typical Autoradiograms

Typical autoradiogram from the measurement of the $Cu(OP)_2$ base enhancement with **57**.

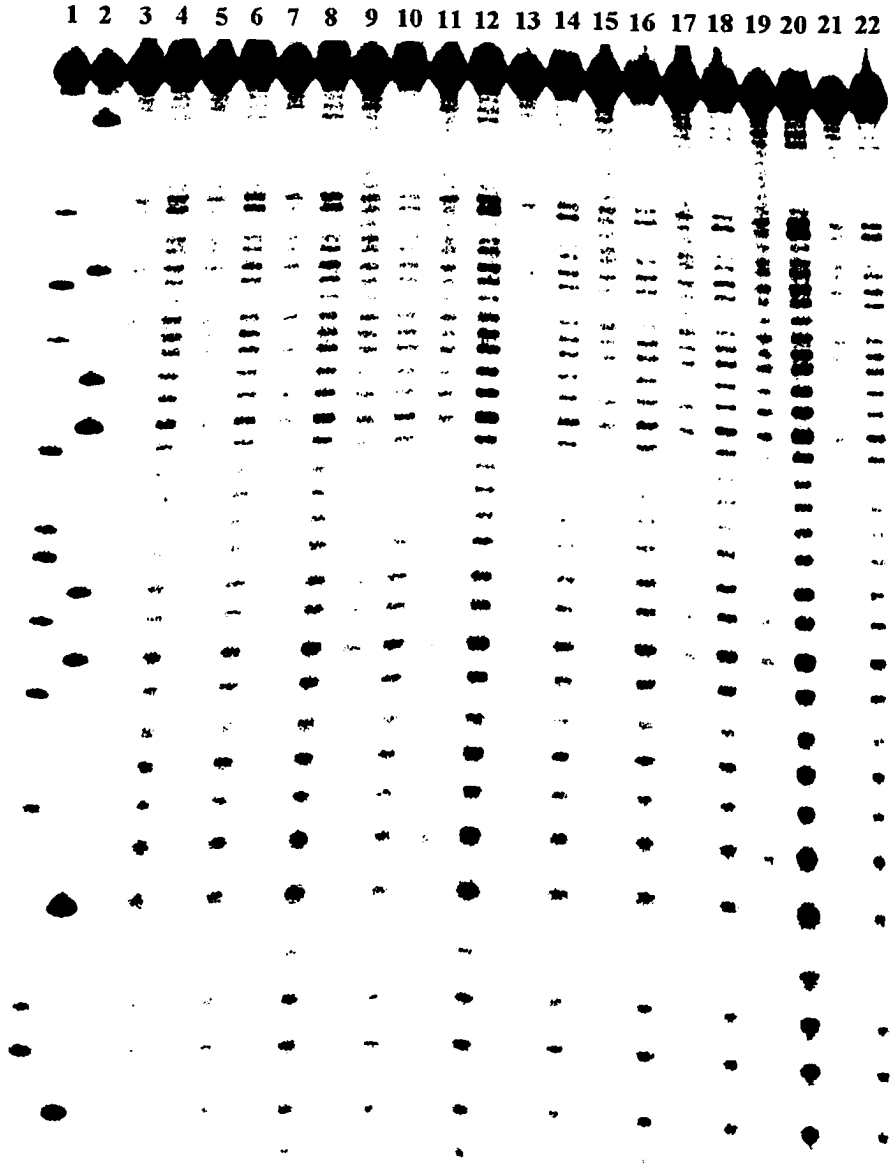

Autoradiogram of **57** treated with $Cu(OP)_2$. Lane 1, dA selective sequencing reaction. Lane 2, dG selective sequencing reaction. Lanes 3-22 contain **57** treated with $Cu(OP)_2$ ($[Cu(OP)_2]$ = 0.96 μM, [**57**] = 58.3 nM, [MPA] = 4.8 mM in 50 mM Tris, pH = 7.5, 37 °C, 15 min: lanes 3,5,7,9,11,13,15,17,19 and 21, no further treatment; lanes 4,6,8,10,12,14,16,18,20, and 22, NaOH (0.1 M), 55 °C, 20 min.

Typical autoradiogram for the reaction of **24** with **59b**.

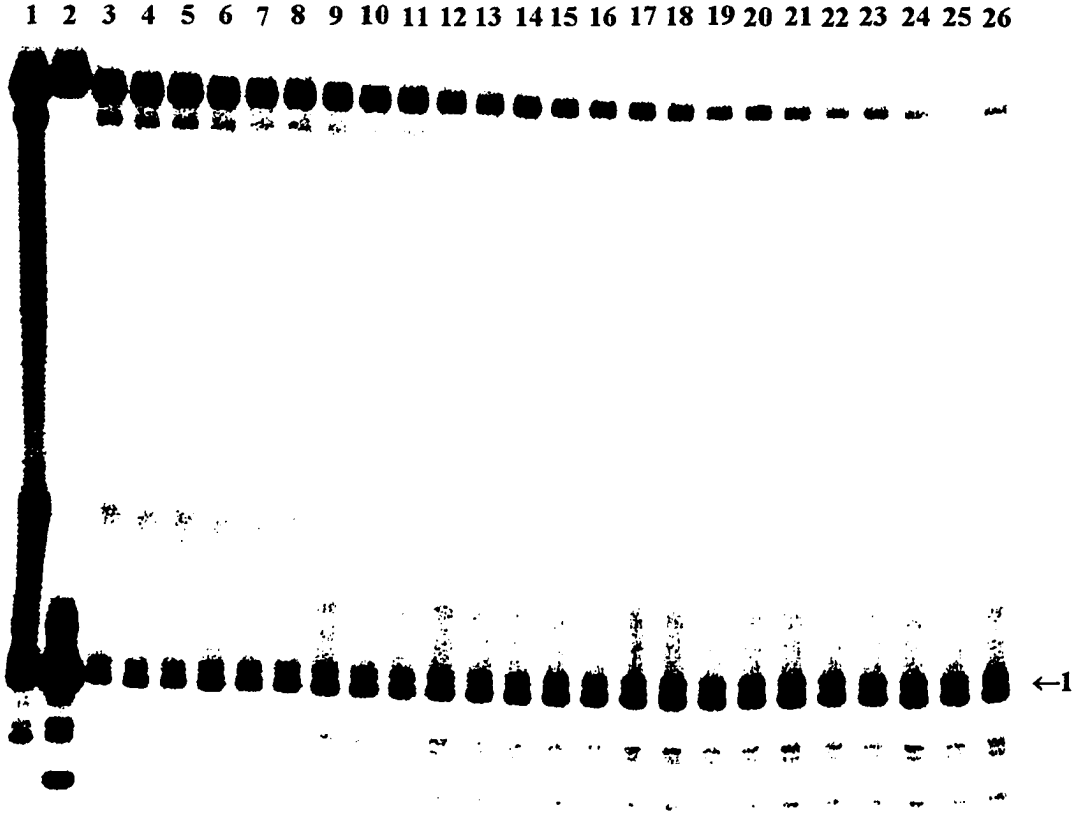

Autoradiogram of **59b** treated with **24** as a function of time. Lanes 1 and 2 contain **59b**: lane 1, no further treatment (t = 0 s); lane 3, NaOH (0.1 M), 20 min, 37 °C. Lanes 3-26 contain **59b** treated with **24** at 37 °C ([**59b**] = 1.0 μM, [**24**] = 10.0 μM, [$CuCl_2$] = 10.0 μM, [MPA] = 2.0 mM in 10.0 mM Tris, pH = 7.0) at the following times: lanes 3-5, 450 s; lanes 6-8, 900 s; lanes 9-11, 1350 s; lanes 12-14, 1800 s; lanes 15-17, 2250 s; lanes 18-20, 2700 s; lanes 21-23, 3150 s; lanes 24-26, 3600 s.

Typical autoradiogram for the reaction of **24** with **58** (direct strand breaks).

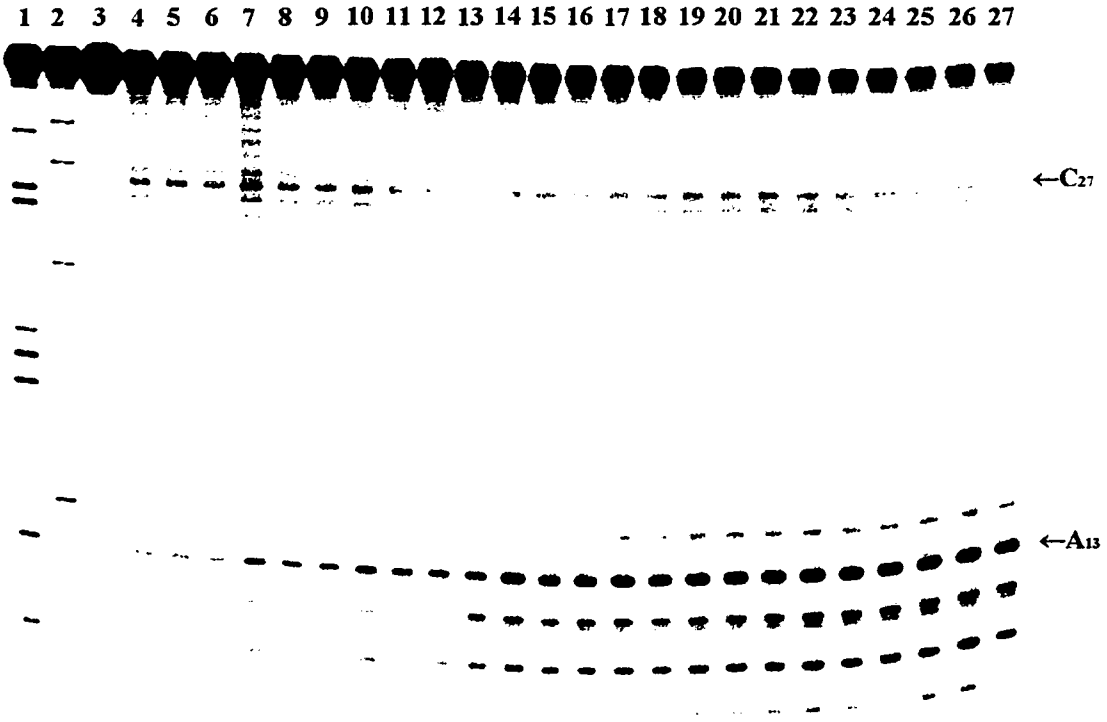

Autoradiogram of **58** treated with **24** as a function of time. Lane 1, dA selective sequencing reaction. Lane 2, dG selective sequencing reaction. Lane 3, **58**. Lanes 4–27 contain **58** treated with **24** at 37 °C ([**58**] = 1.0 μM, [**24**] = 10.0 μM, [$CuCl_2$] = 10.0 μM, [MPA] = 2.0 mM in 10.0 mM Tris, pH = 7.0) at the following times: lanes 4-6, 600 s; lanes 7-9, 1200 s; lanes 10-12, 1800 s; lanes 13-15, 2880 s; lanes 16-18, 3960 s; lanes 19-21, 5040 s; lanes 22-24, 6120 s; lanes 25-27, 7200 s.

Typical autoradiogram for the reaction of **24** with **58** (direct strand breaks + alkali labile lesions).

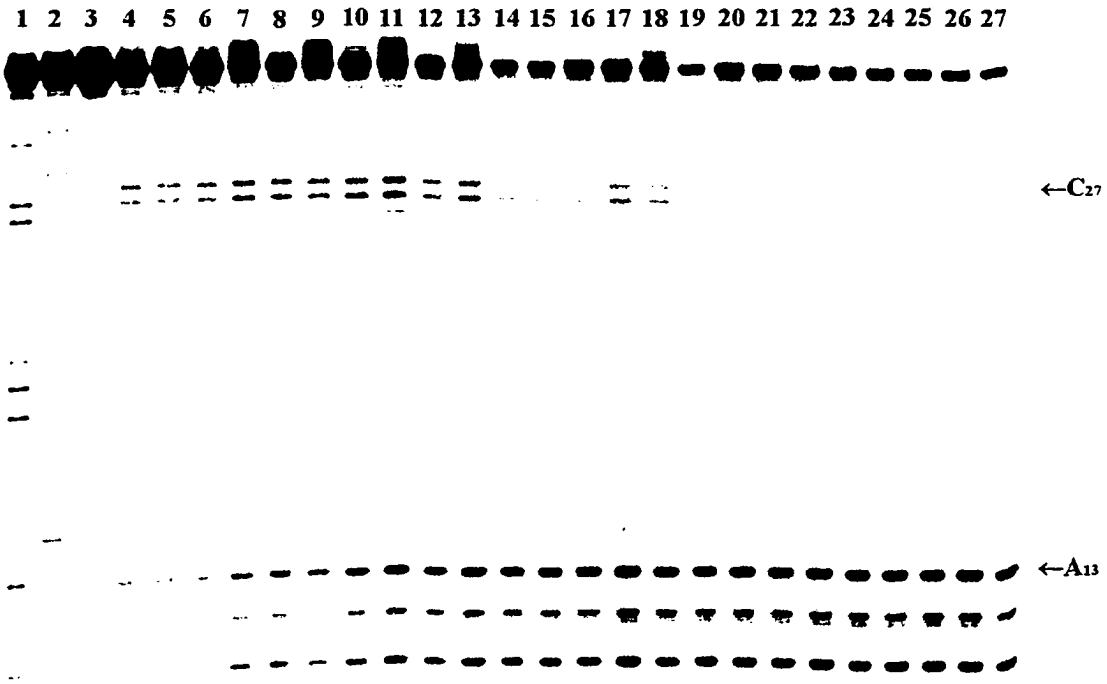

Autoradiogram of **58** treated with **24** as a function of time. Lane 1, dA selective sequencing reaction. Lane 2, dG selective sequencing reaction. Lane 3, **58**. Lanes 4–27 contain **58** treated with **24** at 37 °C ([**58**] = 1.0 μM, [**24**] = 10.0 μM, [$CuCl_2$] = 10.0 μM, [MPA] = 2.0 mM in 10.0 mM Tris, pH = 7.0) followed by NaOH (0.1 M), 20 min, 37 °C, at the following times: lanes 4-6, 600 s; lanes 7-9, 1200 s; lanes 10-12, 1800 s; lanes 13-15, 2880 s; lanes 16-18, 3960 s; lanes 19-21, 5040 s; lanes 22-24, 6120 s; lanes 25-27, 7200 s.

Typical autoradiogram for the reaction of **25** with **58** (direct strand breaks).

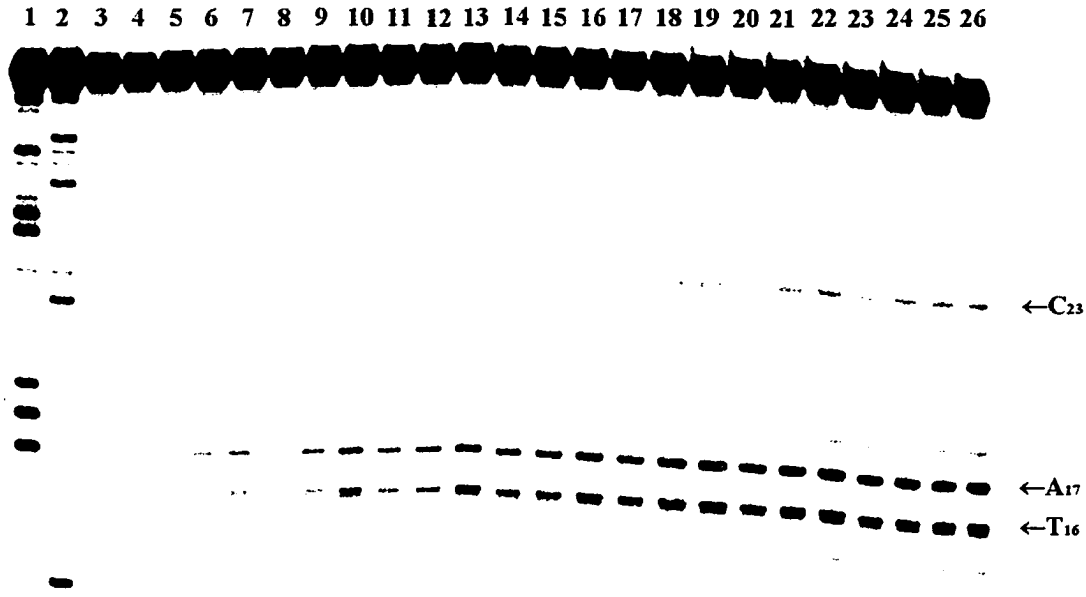

Autoradiogram of **58** treated with **25**. Lane 1, dA selective sequencing reaction. Lane 2, dG selective sequencing reaction. Lanes 3-26 contain **58** treated with **25** at 37 °C ([**25**] = 20.0 μM, [$CuCl_2$] = 20.0 μM, [**58**] = 1.0 μM, [ascorbate] = 200 μM in 10 mM Tris, pH = 7.0), at the following times: lanes 3-5, 1800 s; lanes 6-8, 3600 s; lanes 9-11, 5400 s; lanes 12-14, 7200 s; lanes 15-17, 9000 s; lanes 18-20, 10800 s; lanes 21-23, 12600 s; lanes 24-26, 14400 s.

Typical autoradiogram for the reaction of **25** with **58** (direct strand breaks + alkali labile lesions).

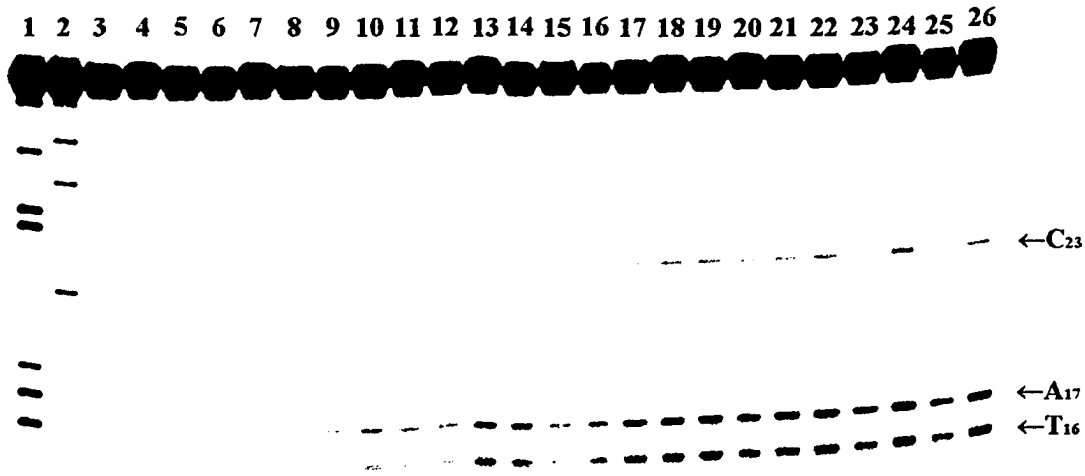

Autoradiogram of **58** treated with **25**. Lane 1, dA selective sequencing reaction. Lane 2, dG selective sequencing reaction. Lanes 3-26 contain **58** treated with **25** at 37 °C ([**25**] = 20.0 μM, [$CuCl_2$] = 20.0 μM, [**58**] = 1.0 μM, [ascorbate] = 200 μM in 10 mM Tris, pH = 7.0) followed by treatment with NaOH (0.1 M), 20 min, 37 °C at the following times: lanes 3-5, 1800 s; lanes 6-8, 3600 s; lanes 9-11, 5400 s; lanes 12-14, 7200 s; lanes 15-17, 9000 s; lanes 18-20, 10800 s; lanes 21-23, 12600 s; lanes 24-26, 14400 s.

Typical autoradiogram for the reaction of **26** with **58** (direct strand breaks).

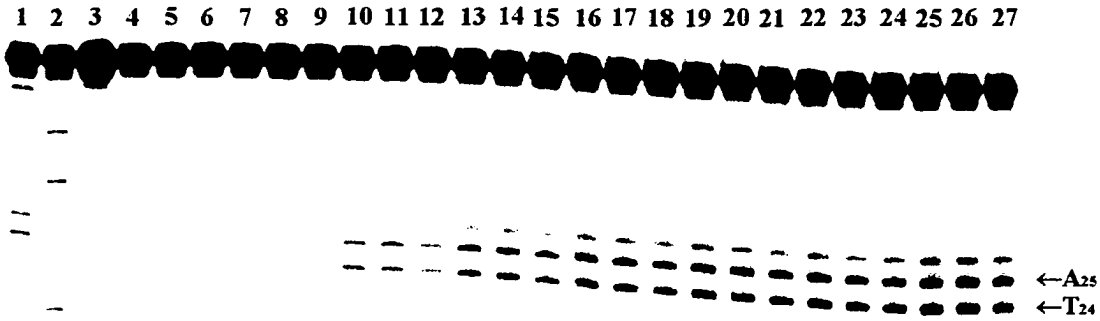

Autoradiogram of **58** treated with **26**. Lane 1, dA selective sequencing reaction. Lane 2, dG selective sequencing reaction. Lane 3, **58**. Lanes 4-27 contain **58** treated with **26** at 37 °C ([**26**] = 20.0 μM, [$CuCl_2$] = 20.0 μM, [**58**] = 1.0 μM, [ascorbate] = 200 μM in 10 mM Tris, pH = 7.0), at the following times: lanes 4-6, 1800 s; lanes 7-9, 3600 s; lanes 10-12, 5400 s; lanes 13-15, 7200 s; lanes 16-18, 9000 s; lanes 19-21, 10800 s; lanes 22-24, 12600 s; lanes 25-27, 14400 s.

Typical autoradiogram for the reaction of **26** with **58** (direct strand breaks + alkali labile lesions).

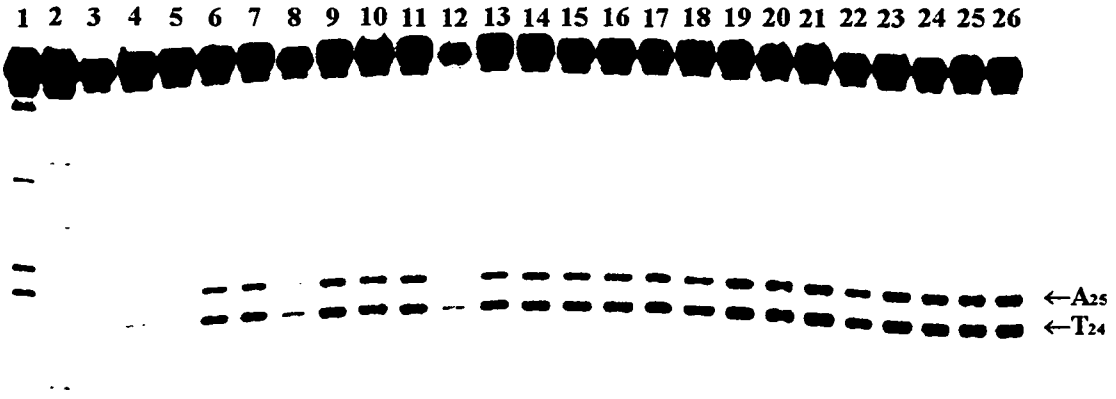

Autoradiogram of **58** treated with **26**. Lane 1, dA selective sequencing reaction. Lane 2, dG selective sequencing reaction. Lanes 3-26 contain **58** treated with **26** at 37 °C ([**26**] = 20.0 μM, [$CuCl_2$] = 20.0 μM, [**58**] = 1.0 μM, [ascorbate] = 200 μM in 10 mM Tris, pH = 7.0) followed by treatment with NaOH (0.1 M), 20 min, 37 °C at the following times: lanes 3-5, 1800 s; lanes 6-8, 3600 s; lanes 9-11, 5400 s; lanes 12-14, 7200 s; lanes 15-17, 9000 s; lanes 18-20, 10800 s; lanes 21-23, 12600 s; lanes 24-26, 14400 s.

Typical autoradiogram for the reaction of E49C-OP with **64b**.

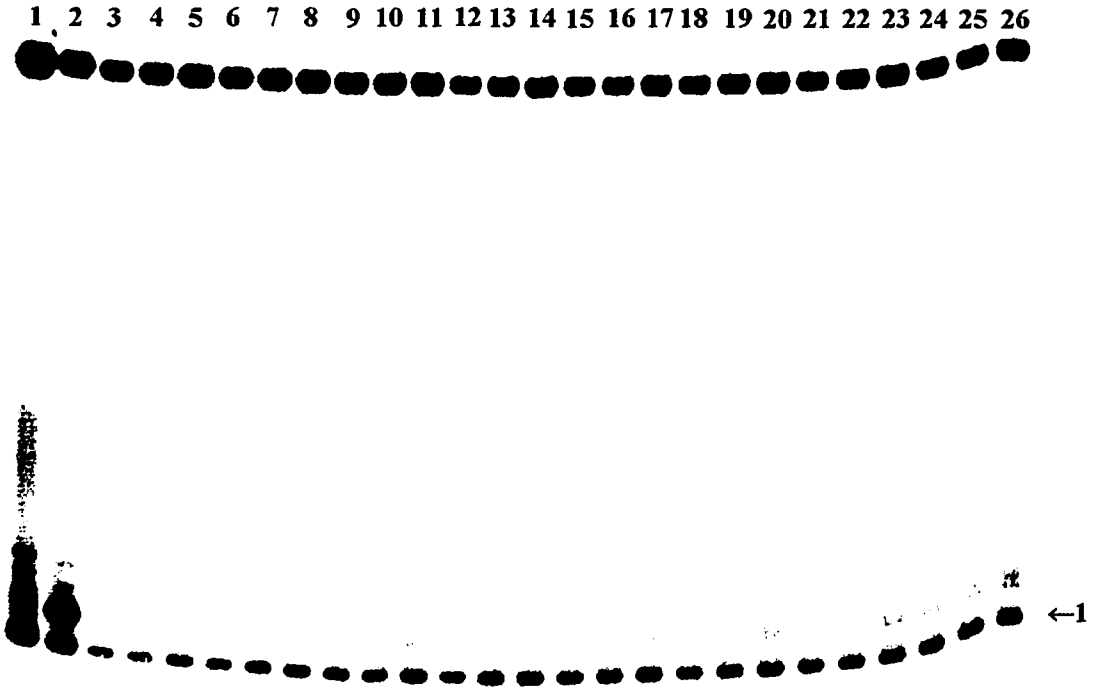

Autoradiogram of **64b** treated with E49C-OP as a function of time. Lanes 1 and 2 contain **64b**: lane 1, no further treatment; lane 2, NaOH (0.1 M), 20 min, 37 °C. Lanes 3-26 contain **64b** treated with E49C-OP at 37 °C ([**64b**] = 50.0 nM, [E49C-OP] = 2.5 μM, [$CuSO_4$] = 5.0 μM, [MPA] = 5.8 mM in 20.0 mM KH_2PO_4, pH = 7.0) at the following times: lanes 3-5, 1125 s; lanes 6-8, 2250 s; lanes 9-11, 3375 s; lanes 12-14, 4500 s; lanes 15-17, 5625 s; lanes 18-20, 6750 s; lanes 21-23, 7875 s; lanes 24-26, 9000 s.

Typical autoradiogram for the reaction of E49C-OP with **57** (direct strand breaks + alkali labile lesions).

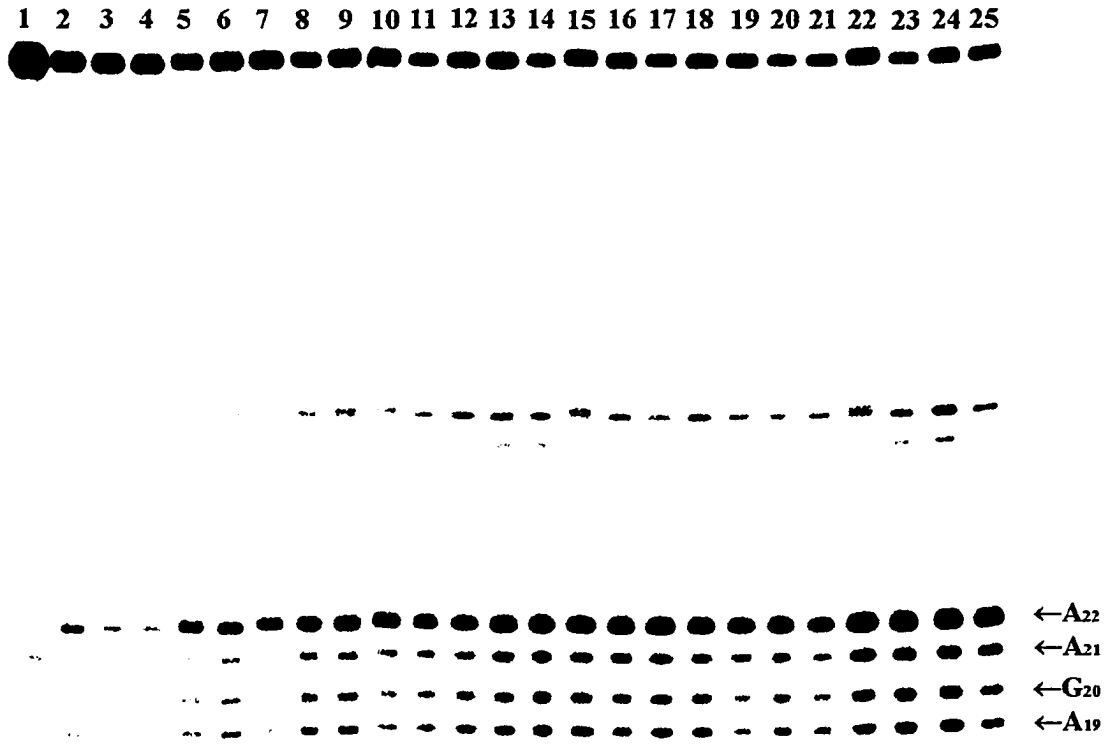

Autoradiogram of **57** treated with E49C-OP as a function of time. Lane 1, dA selective sequencing reaction Lanes 2-25 contain **57** treated with E49C-OP at 37 °C ([**57**] = 50.0 nM, [E49C-OP] = 2.5 μM, [$CuSO_4$] = 5.0 μM, [MPA] = 5.8 mM in 20.0 mM KH_2PO_4, pH = 7.0) followed by NaOH (0.1 M), 20 min, 37 °C at the following times: lanes 2-4, 1125 s; lanes 5-7, 2250 s; lanes 8-10, 3375 s; lanes 11-13, 4500 s; lanes 14-16, 5625 s; lanes 17-19, 6750 s; lanes 20-22, 7875 s; lanes 23-25, 9000 s.

Appendix D:

ES-MS Spectra of Oligonucleotides

D:\Data\Greenberg\MOD\Bcb5110a 12/08/2000 04:35:52 PM BCB5110A

1 RT: 0.00 P: - NL: 4.88E4
T: - p Full ms [450.00-2000.00]

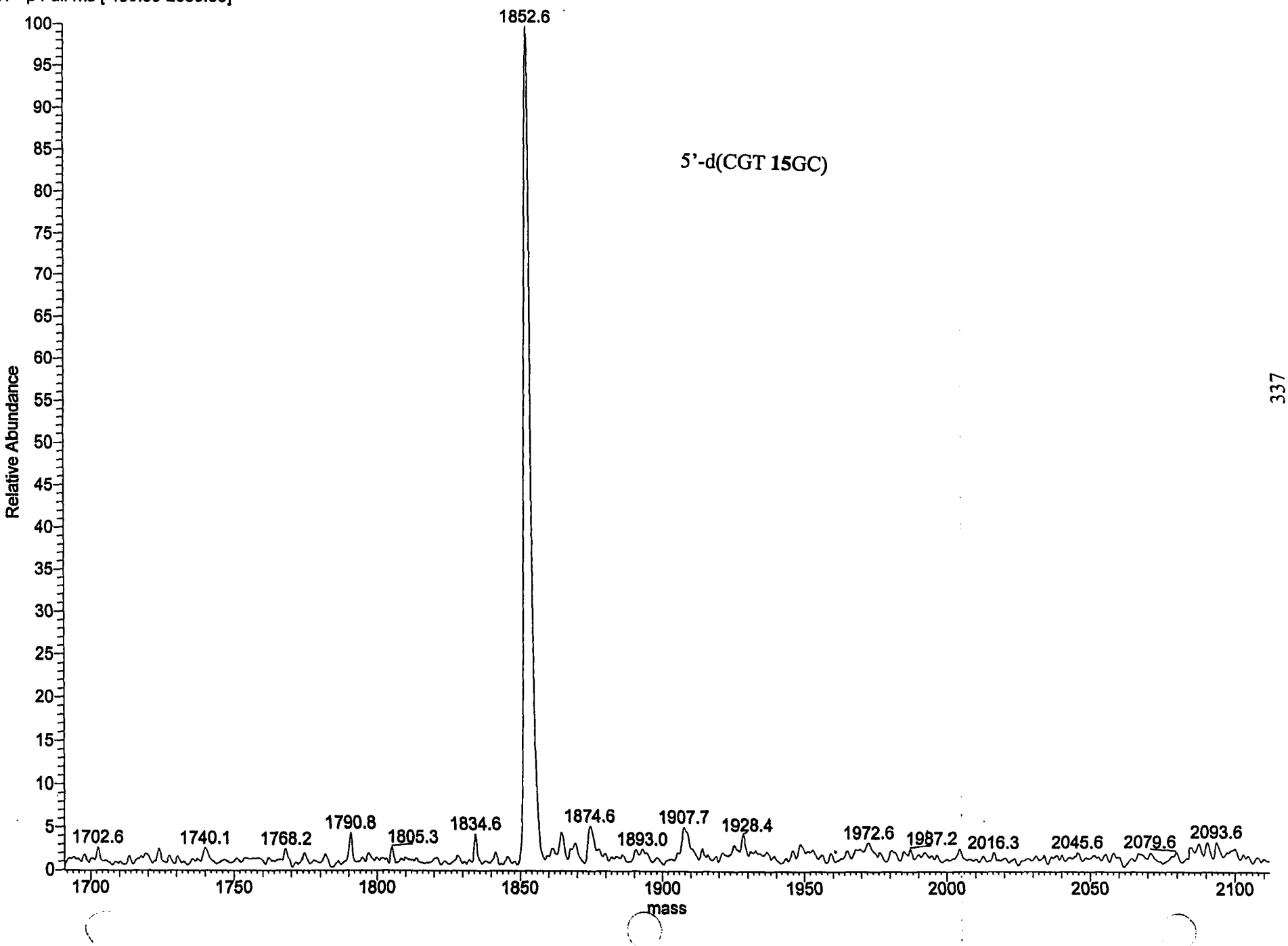

337

B. Bales BCB 5169

MG316Q 1 (1.911) ME [Ev-46771,lt15] (Gs,0.800,410:953,1.00,L33,R33); Sb (0,40.00)

Scan ES-
4.99e7
A: 1672.71±0.03

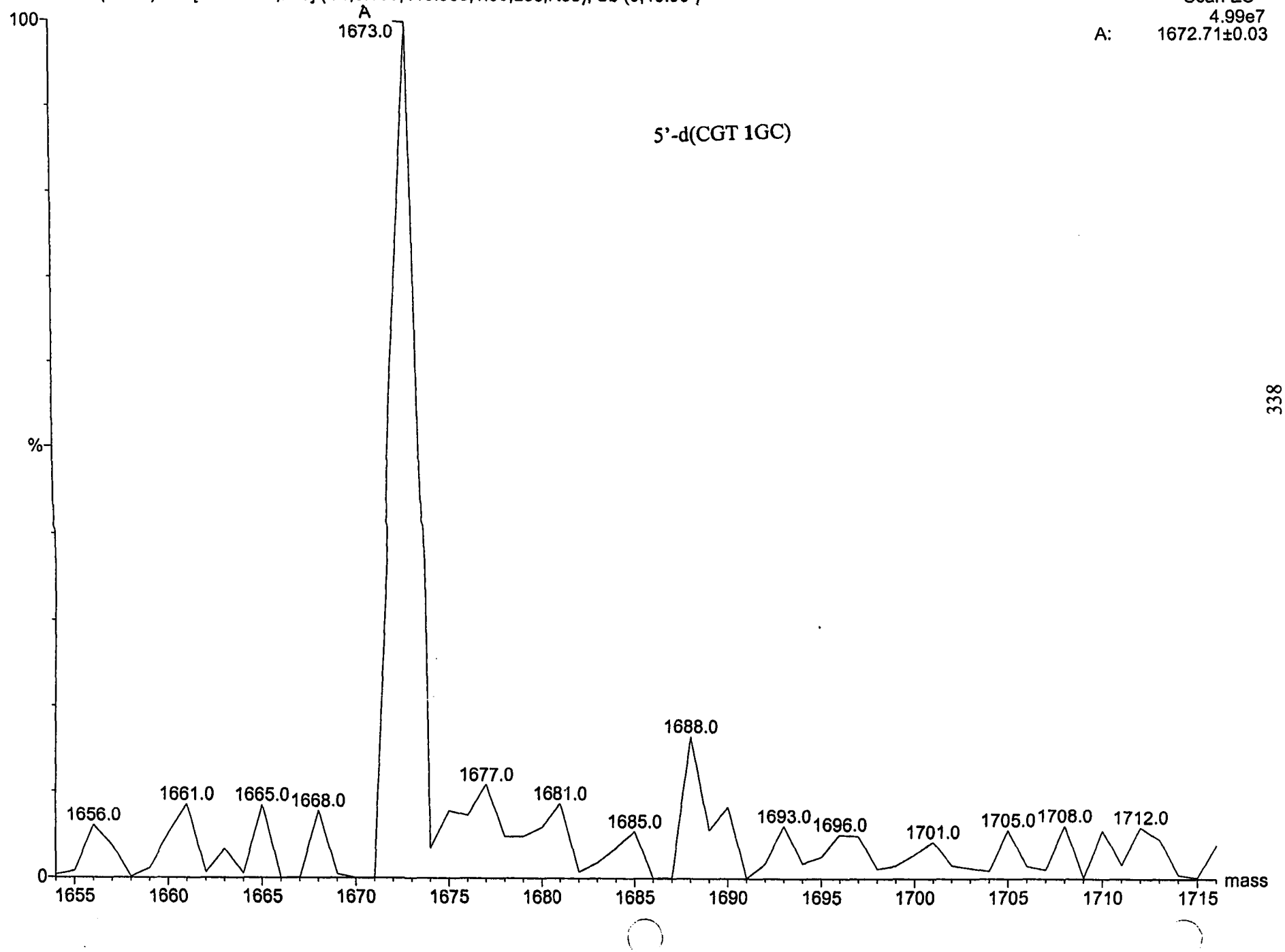

338

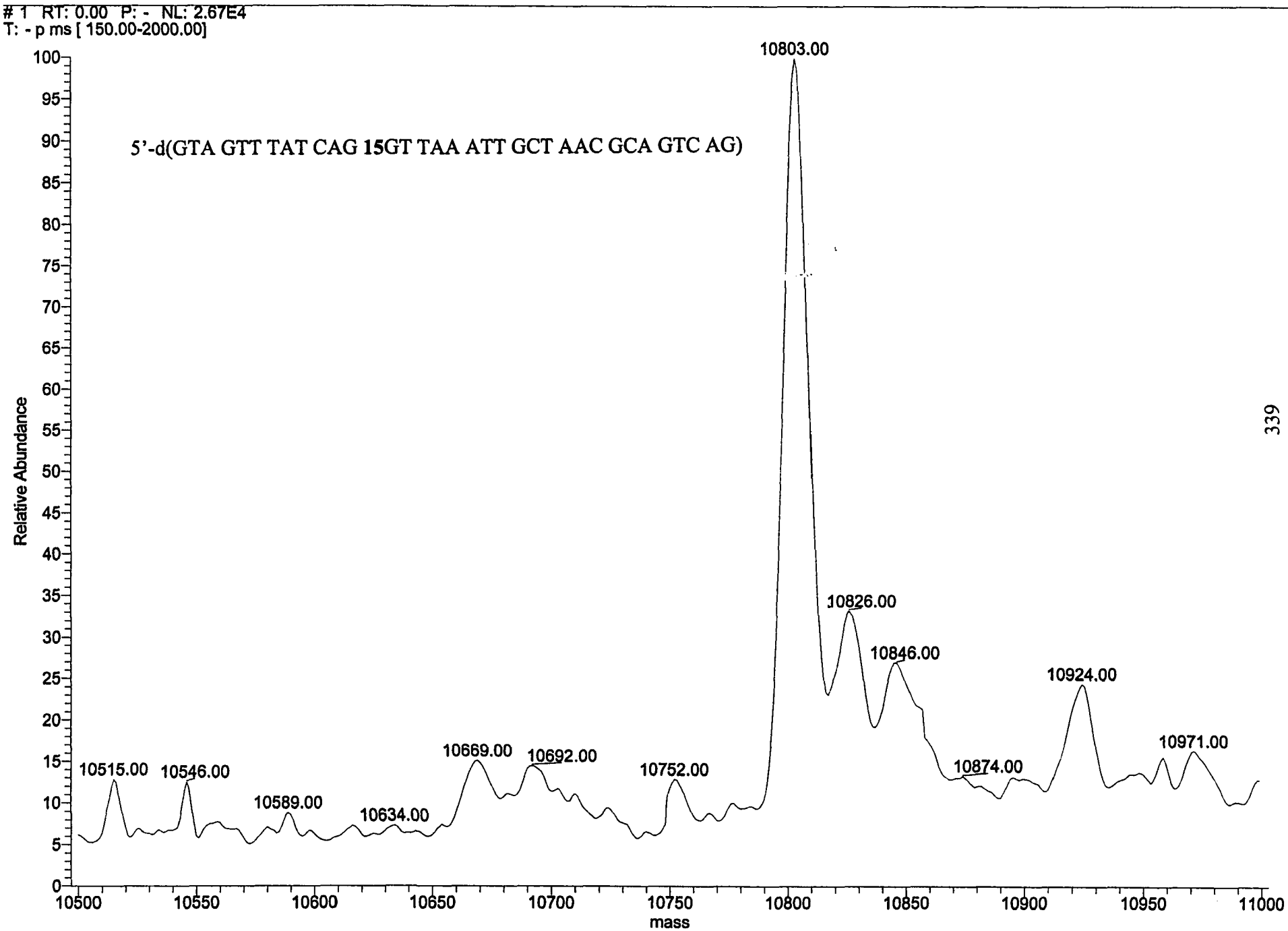

D:\Data\Greenberg\BCB\bcb7278ca 10/23/2001 08:25:12 PM 50-mer Ketone

1 RT: 0.00 P: - NL: 4.09E5
T: - p ms [250.00-2000.00]